Linnaeus University Dissertations
No 170/2014

Jan Oscarsson

Strength grading of structural timber and EWP laminations of Norway spruce – development potentials and industrial applications

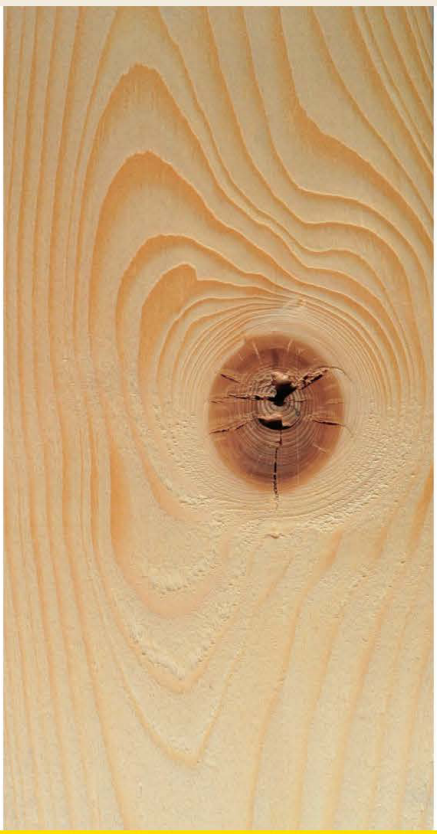

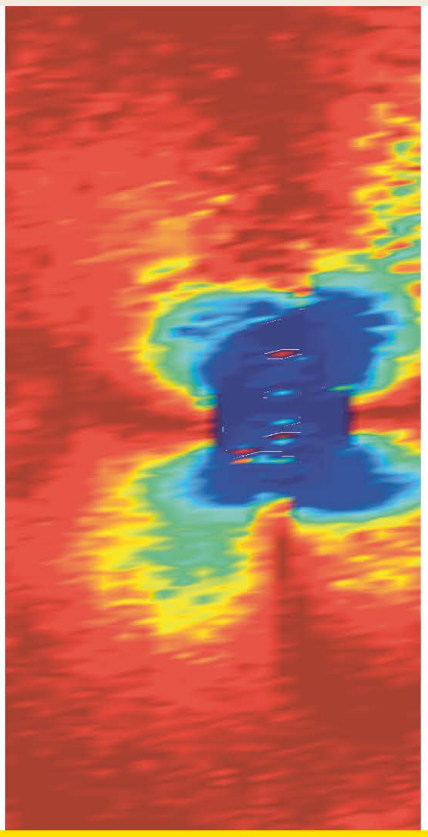

Linnaeus University Press

Jan Oscarsson

Strength grading of structural timber and EWP laminations of Norway spruce – development potentials and industrial applications

Strength grading of structural timber and EWP laminations of Norway spruce – development potentials and industrial applications

Linnaeus University Dissertations
No 170/2014

Strength grading of structural timber and EWP laminations of Norway spruce – development potentials and industrial applications

Jan Oscarsson

Linnaeus University Press

Strength grading of structural timber and EWP laminations of Norway spruce – development potentials and industrial applications
Doctoral dissertation, Department of Building Technology, Linnaeus University, Växjö, Sweden, 2014

ISBN: 978-91-87427-84-8
Published by: Linnaeus University Press, 351 95 Växjö
Printed by: Elanders Sverige AB, 2014

Abstract

Oscarsson, Jan (2014). *Strength grading of structural timber and EWP laminations of Norway spruce – development potentials and industrial applications.* Linnaeus University Dissertations No 170/2014, ISBN: 978-91-87427-84-8. Written in English with a summary in Swedish.

Machine strength grading of structural timber is a sawmill process by which considerable value is added to sawn products. The principle of such grading is that the strength of a timber member is predicted on the basis of a so called indicating property (IP) which, in general, represents an averaged value of the modulus of elasticity (MOE) measured over a board length of about one meter or more.

A limitation of today's grading methods is that the accuracy of strength predictions is often rather poor, which results in a low degree of utilization as regards structural potential of sawn timber. However, it has for many years been well known to researchers that much better strength predictions can be made by using localized MOE values, determined over a very short length, as IP. Still, the determination of such values in a sawmill production environment has been technically very difficult to achieve.

In the research presented in this thesis, dot laser scanning with high resolution was utilized for detection of local fibre orientation on the surfaces of timber members. Since wood is an orthotropic material with superior structural performance in the longitudinal fibre direction, information about fibre orientation was, in combination with beam theory and measured wood material properties, used to determine the bending MOE variation along boards. By application of an IP defined as the lowest bending MOE found along a board, more accurate strength predictions than what is obtained by common commercial grading techniques was attained.

The thesis also involves flatwise wet gluing of Norway spruce side boards into laminated beams. As side boards, being cut from the outer parts of a log, have excellent structural properties it was not surprising to find that the beams had high strength and stiffness, even when laminations of sawfalling quality were used. The possibility of grading boards in a wet state by means of axial dynamic excitation was investigated with a positive result and application of simple grading rules resulted in considerable improvement of beam bending strength. Finally, bending MOE variation determined on the basis of laser scanned fibre directions was used for identification of weak sections in laminations. Elimination of such sections by means of finger jointing showed that average lamination strength of a board sample could be improved by more than 35 percent.

Keywords: fibre angle, grain angle, knots, laser scanning, machine strength grading, modulus of elasticity, side boards, strain, structural timber, wet gluing, wood

Sammanfattning

Hållfasthetssortering av konstruktionsvirke är en sågverksprocess som innebär att värdet av det sågade virket ökar väsentligt. Principen för denna typ av sortering är att styrkan hos ett virkesstycke predikteras med utgångspunkt från en så kallad indikerande egenskap (IP) som oftast representeras av medelvärdet av elasticitetsmodulen (E-modulen) mätt över en sträcka av minst en meter utmed virkesstyckets längd.

De sorteringsmetoder som används idag ger ofta prediktioner med relativt låg noggrannhet, vilket innebär att endast en begränsad del av det sågade virkets konstruktiva potential kan utnyttjas. Det är dock väl känt att avsevärt bättre prediktioner kan erhållas genom att använda en lokal E-modul, uppmätt över en mycket kort sträcka, som IP. I dagsläget saknas dock teknik för att kunna bestämma ett sådant lokalt värde vid produktionshastighet i ett sågverk.

I den forskning som presenteras i denna avhandling har punktlaserskanning med hög upplösning använts för att bestämma fiberriktningens variation på ytorna av virkesstycken. Eftersom trä är ett ortotropt material med högst styvhet och styrka i longitudinell fiberriktning ger skanningsresultaten värdefull information om hur dessa egenskaper varierar längs en planka. Genom att kombinera informationen om fiberriktning med uppmätta virkesegenskaper och klassisk balkteori, kan böjstyvhetens variation utmed en planka beräknas med hög upplösning och därefter omräknas till en E-modul i böjning. Med en IP definierad som det lägsta värdet på nämnda E-modul utmed en planka kan en högre noggrannhet i prediktionen av hållfasthet uppnås, jämfört med vad som kan erhållas med dagens sorteringsmetoder.

Avhandlingen omfattar också limträbalkar tillverkade av sidobräder av gran limmade i rått tillstånd. Eftersom sidobräder sågas från de yttre delarna av en stock har de vanligtvis utmärkta konstruktiva egenskaper. Det var därför inte förvånande att balkarna uppvisade hög styrka och styvhet, även i de fall lamellerna var av sågfallande kvalitet. Möjligheten att med hjälp av axiell dynamisk excitering sortera sidobräder i rått tillstånd undersöktes med positivt resultat och genom att använda sorterade lameller kunde balkarna styrka förbättras avsevärt. Den ovan beskrivna metoden att med utgångspunkt från bl.a. skannade fibervinklar bestämma styvhetens variation längs virkesstycken utnyttjades sedan för att identifiera svaga snitt i lameller av sidobräder. Genom att eliminera sådana snitt med hjälp av fingerskarvning kunde medelhållfastheten för ett stickprov sidobrädor höjas med mer än 35 %.

Nyckelord: elasticitetsmodul, fibervinkel, konstruktionsvirke, kvistar, laserskanning, maskinell hållfasthetssortering, sidobräder, trä, töjning, våtlimning

Acknowledgements

This thesis would not have been brought about without the support and input from a number of people. The first one to be credited is Professor Hans Petersson who bears the main responsibility for me being registered as an industry doctoral candidate at the University in Växjö. HP has been a source of inspiration for almost 35 years, ever since I attended his lectures on the finite element method at Lund Institute of Technology in 1980.

I owe many thanks to my supervisor, Professor Anders Olsson. His knowledge, thoroughness and exactitude have been a great asset throughout the project. A large number of mistakes and less well-reasoned accounts have been avoided in this thesis, thanks to his careful and competent examination of research results, texts and formulations.

What is said about Anders is also true of my co-supervisor Professor Marie Johansson. If you want to improve a paper, provide her with a manuscript and ask for comments!

Together with research engineer Bertil Enquist, I have carried, scanned and broken many boards and planks. I have really enjoyed the long and sometimes late hours that we have spent together around various testing machines and measurement equipments in our joint quest for in-depth understanding of the behaviour of wood.

The research concerning wet gluing of side boards has been carried out within the scope of several projects led by Professor Erik Serrano. His knowledge and assistance concerning, for example, ABAQUS modelling has been very much appreciated.

Contributions have also been made by Professors Bo Källsner, Thomas Thörnqvist, and Charlotte Bengtsson, and Lic. Eng. Rune Ziethén. I am also grateful to my dear friend Senior Lecturer Hans Frisk who, in the course of my studies, has helped me out with some tricky integrals. Stefan Johansson, University IT Support, also deserves to be mentioned. There is not an IT problem to which he has, at least, three completely different solutions.

Regarding co-operation with the industry, I have had the benefit of fruitful collaboration with Södra Timber, Innovativ Vision, Vida Wood, Dynalyse and Derome Timber, and the financial support granted by The Knowledge Foundation, The Swedish Forest Industries Federation, FORMAS, CBBT, The Kempe Foundations, The Bo Rydin Foundation, and my employer SP, is hereby gratefully acknowledged.

Finally, thoughts to my dear family with whom I share both joy and sorrow.…

Växjö, April 2014

Jan Oscarsson

Appended papers

Paper I Jan Oscarsson, Anders Olsson and Bertil Enquist (2012) *Strain fields around knots in Norway spruce specimens exposed to tensile forces*. Wood Science and Technology, 46(4):593-610.

Paper II Anders Olsson, Jan Oscarsson, Erik Serrano, Bo Källsner, Marie Johansson and Bertil Enquist (2013) *Prediction of timber bending strength and in-member cross-sectional stiffness variation on the basis of local wood fibre orientation.* European Journal of Wood and Wood Products, 71(3):319-333.

Paper III Jan Oscarsson, Anders Olsson and Bertil Enquist (2014) *Localized modulus of elasticity in timber and its significance for the accuracy of machine strength grading*. Submitted to Wood and Fiber Science.

Paper IV Jan Oscarsson, Anders Olsson, Marie Johansson, Bertil Enquist and Erik Serrano (2011) *Strength grading of narrow dimension Norway spruce side boards in the wet state using first axial resonance frequency.* International Wood Products Journal, 2(2):108-114.

Paper V Erik Serrano, Jan Oscarsson, Magdalena Sterley and Bertil Enquist (2014) *Green-glued products for structural applications*. In: S. Aicher *et al.* (eds.), *Materials and Joints in Timber Structures*, RILEM Bookseries 9, DOI: 10.1007/978-94-007-7811-5_4, pp. 45-55. Included by courtesy of RILEM.

Paper VI Jan Oscarsson, Anders Olsson and Bertil Enquist (2014) *Improving strength of glulam laminations of Norway spruce side boards by removal of weak sections using optimized finger jointing*. In: S. Aicher *et al.* (eds.), *Materials and Joints in Timber Structures*, RILEM Bookseries 9, DOI: 10.1007/978-94-007-7811-5_71, pp. 801-811. Included by courtesy of RILEM.

Contents

1 INTRODUCTION

1.1 Structural timber – a product by nature

Wood is a material that is basically manufactured by nature itself. Whereas the mechanical properties of construction materials such as concrete, steel or aluminium could be varied by, for example, modifying concrete mix proportions, changing the reinforcement ratio in concrete elements, adjusting the quantity of different alloying materials in steel or aluminium mixtures or changing process parameters such as temperature or pressure, the possibility of influencing material properties in growing trees are, in comparison, rather limited. Säll (2002) claimed that wood properties of individual trees of Norway spruce (*Picea abies*) are dependent on genetic heritage, silvicultural measures and growth conditions. Examples of the latter are stand density, social standing of a tree within a stand and site characteristics, including climate, topography of the terrain and also texture and nutritional status of the ground.

An increase of stand density will have a positive effect on several wood material parameters that, in turn, will improve the performance of sawn timber for structural purposes. For example, a high stand density will as a rule lead to a decrease of both branch diameters in trees (*e.g.* Mäkinen and Hein 2006) and

Figure 1. Typical fractures initiated at knots in structural timber subjected to bending load.

knot diameter in sawn timber. This will improve the timber quality with respect to strength and stiffness, since these properties are dependent on occurrence and size of knots (*e.g.* Johansson 2003). Figure 1 on the previous page exhibits typical fractures of structural timber exposed to bending load. A low growth-rate, as obtained in stands with a high stand density, will also contribute to decreasing annual ring width (*e.g.* Herman *et al.* 1998), which will, in general, have a similar positive effect on strength and stiffness as a reduction of knot size (*e.g.* Hoffmeyer 1995; Kliger *et al.* 1995; Lundgren *et al.* 2007), however not as evident. Spiral grain, *i.e.* the inclination of the wood fibres in relation to the longitudinal direction of the log, is another characteristic that is important for the performance of sawn timber. According to Säll (2002), Norway spruce stands that are dense and free of gaps, will probably result in wood with relatively low risk of obtaining large grain angle and subsequent shape distortion in the form of twist in sawn timber. In a recent investigation of Norway spruce (Högberg *et al.* 2013), a relationship between genetic characteristics and grain angle was revealed. The fibre orientation in a board, *i.e.* the inclination of the fibres in relation to the longitudinal board direction, affects strength and stiffness of a piece of timber, since the performance of these properties is much higher in the fibre direction than in directions perpendicular to the fibres (Dinwoodie 2000, after Baumann 1922).

A silvicultural treatment that will contribute to a reduction of knot size in structural timber is pruning, *i.e.* removal of branches on standing trees. As a tree continues to grow after such a measure, knot-free clear wood with, in most cases, excellent structural properties will develop outside the removed branches. However, in Sweden this method is rarely applied on Norway spruce due to the risk for development of rot at the pruned branches (Thörnqvist 2011), whereas experiences from *e.g.* Germany are more positive (Metzler 1997).

Assessment of wood properties of standing trees has, according to Wang *et al.* (2007a), traditionally been carried out on the basis of simple physical measurements, *e.g.* height, diameter and taper, and visual inspection of stem surface characteristics such as size and distribution of knots and other defects. The spiral grain can be quantified on a trunk or log surface the bark of which has been peeled off (Säll 2002). A scribed line following the direction of the wood fibres is drawn on the debarked surface and the angle between this line and the longitudinal direction of the trunk can then be measured using a simple angle measurement device. However, it is also established that stiffness properties of standing trees can be estimated using acoustic measurement methods. For example, it has been found that there is a relationship between acoustic wave velocity measured between a transmitter probe and a receiver probe inserted into the sapwood of butt log parts of trees in stands of Radiata pine (*Pinus radiata*) and the modulus of elasticity (MOE) of core samples

from the butt logs of the measured trees (Wang *et al.* 2007a; Wang *et al.* 2007b). The wave velocity was measured on the basis of acoustic energy introduced into the tree through a hammer impact on the transmitter probe, see Figure 2. However, acoustic measurements on lower parts of standing trees do not provide information about the stiffness variation over the entire length (or height) of a tree. Such variation has been found by, for example, Kliger *et al.* (1995), who investigated the difference in, *inter alia*, bending stiffness between timber pieces cut from the cores of butt logs and top logs, respectively, of fast grown Norway spruce trees. They found that the stiffness was significantly higher in the top log pieces, which was, according to the authors, explained by smaller annual ring width and higher density in the core pieces cut from the top logs. Xu and Walker (2004) found a similar stiffness relationship between top logs and butt logs from trees taken from a stand of 27-year-old Radiata pine (*Pinus radiata*). However, an investigation of structural timber originating from a 70-year-old stand of Douglas-fir (*Pseudotsuga menziesii)* gave quite opposite results (Wang *et al.* 2013), *i.e.* decreasing stiffness with increasing vertical position. A high proportion of juvenile wood in the crown of Douglas-fir was suggested as a possible explanation.

Regarding application of the acoustic measurement techniques described in the previous paragraph, Huang *et al.* (2003) claimed that such methods can be used to identify trees that, due to poor stiffness properties, are appropriate to be removed at thinning operations, *i.e.* at the selective removal of certain trees in a stand carried out to increase the growth-rate of the remaining trees and to enhance the profit of a future final cutting.

Figure 2. Stiffness property determination on standing trees using acoustic wave velocity measurement. Photos by courtesy of Fibre-gen, Inc., New Zealand.

After harvesting a stand that has been subjected to measurements and silvicultural treatments such as those described above, the knowledge about the structural wood properties of the harvested timber is, however, still limited. This is mainly due to the enormous variability of the material in general, both between and within logs. The property variation is explained by both the occurrence of local defects such as knots, cracks, top ruptures and compression wood, and the anisotropy of the material, *i.e.* the mechanical properties being different in longitudinal, radial and tangential directions, respectively, of the annual ring pattern of a log or a timber member. To be able to use wood as raw material for development and manufacturing of structural products intended for load bearing applications, the mentioned variability has to be managed and controlled in the sense that mechanical properties of manufactured products have to be predictable. This can be achieved by means of two fundamentally different methods; either by non-destructive strength grading of logs and solid sawn timber, or by dismembering wood into *e.g.* chips, strands, veneers or sawn laminations and then glue or by other means join the disintegrated parts together, under influence of heat and pressure, into structural members such as beams, columns or panels.

Logs are usually sorted according to diameter and species, but quality sorting with respect to outer log shape and wood characteristics such as density, spiral grain and knot volume is gradually becoming more frequent. Such log sorting is, in most cases, carried out using optical or X-ray scanners and it enables sawmills to classify logs according to specific material properties. The value yield of the sawn timber could then be increased by sawing each log into dimensions that optimize the utilization of the quality class of the log (Skog *et al.* 2010).

Regarding sawn timber, it has been shown that strength and stiffness of such pieces can be estimated already at log level, *i.e.* before the actual sawing operation, using techniques such as X-ray scanning (*e.g.* Källsner *et al.* 2002; Oja *et al.* 2005), resonance frequency techniques (*e.g.* Kliger *et al*. 2003), ultrasonic measurements (Sandoz 1996), or such acoustic methods as described above. Rais *et al.* (2014) investigated the possibility of increasing the yield of strength graded structural timber by means of pre-grading of logs on the basis of axial resonance frequency. Rejection of logs of low quality resulted in an increase in yield of about 10 %. However, the application of the described measurement techniques on logs is surrounded by certain limitations. For example, Lycken *et al.* (2009) found that X-ray scanning of Norway spruce logs gives predictions with rather low accuracy and that resonance frequency measurement gives unreliable results when the technique is used on frozen logs. Furthermore, Brännström (2009) asserted that application of ultrasonic methods requires a reduction of the grading speed, since contact between sensors and the measured object is needed. Such contact

is also required as regards measurement of acoustic wave velocity (see Figure 2). It is also likely that both ultrasonic and acoustic measurements are affected by logs being frozen. Thus, the described limitations of log grading imply that prediction of strength and stiffness of solid sawn structural timber, typically cut from the centre parts of a log, requires strength grading of individual timber members after sawing. Such grading is carried out on the basis of either visual inspection or application of certified grading machines. General requirements regarding both visual grading and machine grading are stated in the European Standard EN 14081-1. Visual grading is based upon visible defects being smaller than limits stipulated in a large number of visual grading standards listed in the European Standard EN 1912. Machine strength grading means that certain properties of a piece of timber are non-destructively measured as the piece passes through or by a grading machine. Statistical relationships between the measured properties and bending strength are subsequently applied for prediction of the latter. However, machine graded timber must also fulfill certain so called *visual override requirements* regarding defects that machines in general are unable to detect, but the existence of which are reason for downgrading. According to EN 14081-1, this concerns fissures, warp, wane, rot, insect damage and abnormal defects such as compression wood and top ruptures. Thus, even if machine strength grading is applied, visual inspection is still required to a certain degree. Yet, it should be emphasized that the visual override can be carried out either manually or by machinery in the form of optical scanners.

As regards the method of property control based on gluing of disintegrated wood pieces into load bearing components such as beams or panels, a major benefit of the disintegration is that local defects in logs and timber pieces are also being dismembered. The subsequent joining of the disintegrated parts means that the defects are disseminated, resulting in products with high shape stability and predictable and homogeneous mechanical properties with high performance and low variability. Structural wood products manufactured on the basis of disintegration and subsequent gluing are by definition called *Engineered Wood Products*, abbreviated *EWP*. An example of such a product is *Laminated Veneer Lumber* (*LVL*), see Figure 3 (left), which consists of several layers of veneer sheets about 3 mm thick, glued together and cut into prismatic structural members with the grains in all the veneers running parallel with the longitudinal axis of the product. Another typical EWP is *Parallel Strand Lumber* (*PSL*), manufactured from veneer strands with approximate dimensions 3×19×2400 mm (Lam and Prion 2003). Similar to LVL products, the grain in a PSL strand are oriented in the same direction as the PSL member's main axis. Examples of EWP panels are *plywood*, consisting of several layers of veneer sheets with orthogonally oriented grain directions in adjacent layers, and *Oriented Strand Board* (*OSB*), which are made of rectangular wooden flakes of approximate dimensions 0.8×13×100 mm (Lam

and Prion 2003) glued into sheets. A typical OSB includes three such sheets with different main orientation of the flakes in face and core layers, respectively (Lam and Prion 2003). A further and widely used EWP is *Glued-laminated timber*, or *glulam*, made up of strength graded laminations that are glued in the flatwise direction into structural elements with rectangular cross-section (Figure 3, right). Utilized laminations are typically strength graded structural timber with thickness of 30-45 mm, *i.e.* the same kind of products that are used as solid load bearing studs and joists in timber framed structures. However, split centre cuts with thickness down to approximately 20 mm are also used, *e.g.* in service class 3 or in curved beams. Within the scope of this industry doctoral candidate project it has been shown (see attached Paper V) that glulam products with excellent structural properties can be achieved from wet glued laminations of strength graded Norway spruce side boards of narrow dimensions (thickness ≤ 25 mm). Thus, glulam products are composed of laminations that are graded using the same techniques as applied for strength grading of structural timber. In this respect, glulam can be considered as products that combine the concepts of EWP and strength grading of solid timber members. Such strength grading, *i.e.* grading of structural timber and EWP laminations, is what this thesis is about.

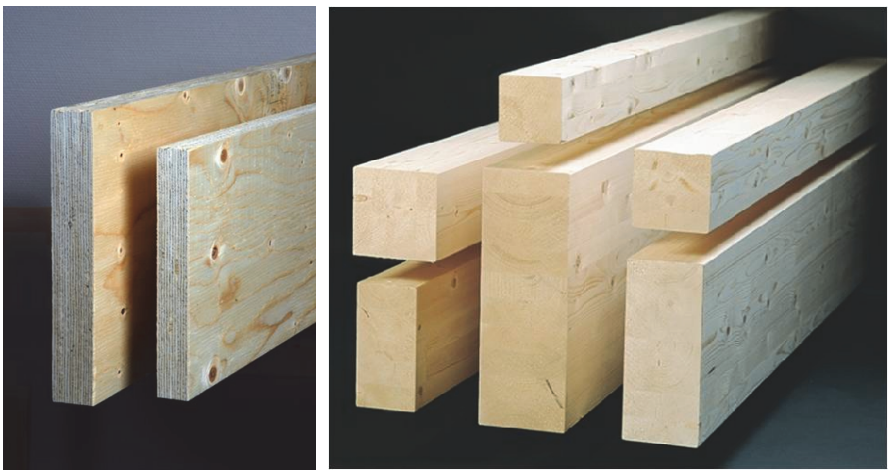

Figure 3. Engineered wood products: Laminated veneer lumber, LVL (left), and glulam beams (right). Photos by courtesy of Moelven Töreboda AB.

1.2 Research idea, objectives and realization

Strength grading of structural timber means that timber is graded either by visual inspection or machine strength grading (see section 1.1) into strength classes, or strength grades, to which characteristic and mean values of structural properties are allocated. In the European Standard EN 338, a system

of strength classes intended for use in structural codes is established. According to this standard, timber is allocated to a certain strength class on the basis of requirements regarding characteristic bending strength, stiffness in terms of mean MOE in bending, and characteristic density. According to EN 14081-2, these properties are defined as *grade determining properties*. The property values that are presented in EN 338 refer to timber having a moisture content that corresponds to a standard environment of 20 °C and 65 % relative humidity. For Norway spruce, this climate is consistent with an equilibrium moisture ratio of about 12 %.

For softwood species, the grades defined in EN 338 are indicated by the capital letter *C* followed by two digits that represent the characteristic bending strength of timber pieces graded into the class in question. The characteristic value corresponds to the 5-percentile bending strength of all pieces graded into the class, which actually means that five percent of the pieces in a certain class may be weaker than the strength indicated by the class designation. Likewise, the requirements in EN 338 regarding density also refer to a characteristic 5-percentile value.

The first grading machines were introduced around 1960 in USA and Australia (Glos 1995). Before that, strength grading of timber was based entirely on visual inspection. Such grading is still frequently applied in many countries, but during the last 10 to 15 years, there has been a strong development as regards utilization of machine grading. In 2012, the quantity of machine graded timber in Sweden had reached a volume of about 1.92 million m^3 (Hansson 2014), whereas the volume of visually graded timber had decreased correspondingly. For the latter, the volume of 2012 is not available, but in 2011 it amounted to about 0.1 million m^3 (Stenman 2012).

Machine strength grading is, as described in section 1.1, in general based on statistical relationships between bending strength and measured timber properties, the latter also called *indicating properties* (IPs). According to EN 14081-2, an IP is defined as a measurement or a combination of measurements that is a) made by a grading machine, and b) closely related to one or more of the grade determining properties. Timber characteristics that are most frequently used as IPs are stiffness in terms of MOE, knot measures and density.

The machine grading techniques that are used today are, in general, based on relationships between applied IPs and bending strength that are rather weak. The most important consequence of this is that strength predictions on the basis of measured IPs are associated with some degree of uncertainty, resulting in downgrading of many timber pieces into strength classes with characteristic bending strength that is much lower than the actual strength of the pieces. Another consequence is that grading of timber to strength classes of C40 and better results in very low yield. Thus, to avoid unnecessary

downgrading and to be able to utilize the structural potential of timber with high stiffness and strength, better grading methods are needed.

The primary purpose of this industry doctoral candidate project was to initiate development of new strength grading procedures for accurate and efficient grading of timber in terms of both stiffness and strength. Tools and theories identified to be of use in such a process were, for example, optical and laser surface scanning of timber members, determination of timber stiffness properties by means of static tests and dynamic excitation, beam theory, finite element modeling and theories of fracture mechanics. From the outset of the research, it was well known that image analysis of pictures obtained from a WoodEye scanner available at Linnæus University, see Figure 4, can be applied for determination of wood properties such as spiral grain, local grain deviations and occurrence of knots and other defects on the surfaces of a board or a plank. The basic research idea was that such information, combined with timber stiffness measures, could be used as a basis for development of beam models of timber members, or parts of such members, to be applied for prediction of stiffness and strength. As regards the latter, the possibility of using theories of fracture mechanics was initially considered as an option to be investigated.

Figure 4. WoodEye scanner of model v4 for optical and laser scanning of timber pieces.

The objectives that were formulated from the outset of the research were, first, to develop a method by which internal structural properties such as stiffness variation in a timber piece could be described and, second, that information about such variations should then be included in a beam model to be utilized for prediction of timber strength.

Being employed at an industry research institute as the SP Technical Research Institute of Sweden, and at the same time being registered as a doctoral candidate at Linnæus University where the main part of the research concerning timber engineering is carried out in close co-operation with the industry, there is a danger, or a possibility, that the doctoral student becomes involved in time-consuming industry related research projects. The content of such projects will, to a considerable extent, reflect demands articulated by participating companies from which there is also an expectation that achieved results should be possible to implement within a rather short time. Doctoral candidate participation in projects of this type will, with pros and cons, influence the scope and the time frame of the doctoral candidate project. The described course of event is, to some extent, what happened in this case. Paper I, dealing with local strain fields around knots in timber members exposed to tensile forces, Paper II, describing a new strength grading method based on scanned information about local fibre orientation along board surfaces, and Paper III, which concerns the relationship between grading accuracy and the degree of localization of measured MOE, the latter partly evaluated by means of tensile strain fields, can be considered as being in line with the original research plan. However, Paper IV, dealing with strength grading of narrow side boards in a wet state, and Paper V, which describes the development of laminated wet-glued beams manufactured from Norway spruce side boards of narrow dimensions, means that the scope of the doctoral candidate project has, in the course of time, been widened to comprise also issues regarding strength grading of EWP laminations and development of EWPs. Yet, in the last paper, Paper VI, the primary purpose concerning new strength grading procedures is combined with EWP development; the grading method described in Paper II is applied for identification of weak sections to be eliminated in side board laminations by means of finger jointing. Thus, the common denominator of the six papers is that they deal with development potentials for strength grading and strength improvement of structural timber and EWP laminations of Norway spruce. All papers, except Paper I, are the results of two long-term research and development efforts carried out in close co-operation with industrial partners.

One objective of both Paper I and III was to achieve a more thorough understanding of the development of strain fields around knots in timber members under load. Knowledge about such characteristics is of importance for development of more efficient grading methods, since strength and stiffness properties are, as mentioned in section 1.1, strongly dependent on the presence, location and size of knots in timber members. The strain field information can also be valuable for comparison with and calibration of models designed for prediction of stiffness and strength.

1.3 Scientific methods

As described in section 1.2, the overall purpose of this doctoral candidate project was to initiate a development of a new strength grading procedure that is more accurate and efficient than those applied on the market today. The scientific method that was utilized could possibly be described as *hypothetico-deductive* in the sense that the purpose might be formulated in terms of hypotheses related to the performance of various grading procedures. Although the scope of the project was gradually widened to include also EWP development based on strength grading of laminations, the same scientific method was applied. However, a more *inductive* approach was utilized in parts of Paper I, *i.e.* conclusions were drawn on the basis of observed measurement results.

1.4 Theories, measurements, materials and limitations

Machine strength grading of timber is in general based on application of theory of linear-elastic mechanics of materials. The main part of the research carried out in this project has also been based on Bernoulli-Euler beam theory which rests on the assumption that plane beam cross-sections that are perpendicular to the longitudinal direction of the beam before it is subjected to bending remain plane and perpendicular to the said beam direction during deformation. Grading procedures are also dependent on statistical theories applied to express relationships between strength and different measureable timber properties. Such relationships are described in terms of *regression analysis*.

Methods utilized in the research involved laboratory testing and post-processing of measurement results, analytical calculations, numerical calculations using the finite element method, optimization algorithms and regression analysis. The laboratory testing included optical contact-free deformation measurements based on white-light digital image correlation, determination of resonance frequencies corresponding to longitudinal modes of vibration induced into timber pieces by axial excitation, measurement of dimension and weight and subsequent determination of density of investigated pieces, measurement of fibre angle variation in the pieces using optical scanning of board surfaces illuminated by laser dots, determination of flatwise static bending stiffness utilizing a flatwise bending machine, and determination of strength and stiffness of pieces exposed to static edgewise bending test and static tension test, respectively. Finger jointing of side-board laminations and gluing of glulam beams in a wet as well as in a dried state was carried out in an industrial environment. Principles for axial resonance frequency determination, and static bending tests in edgewise and flatwise

directions, respectively, are described in section 2.2.2.1. The contact-free deformation measurements are presented in section 4.1.2, and a description of the optical dot laser scanning is found in section 4.1.3. Also, further accounts of the experimental methods are found in the appended papers, respectively.

Methods for post processing of measurement results, numerical calculations, analytical calculations and applied optimization principles are described in those appended papers in which each method or technique is utilized, respectively. Concerning regression analysis, the most frequently used types in connection with machine strength grading of structural timber are *simple* and *multiple linear regression*, respectively. The former is described in more detail in section 2.1.

As regards materials, four different samples of Norway spruce timber were investigated in the research presented in the appended papers. The first one, which was used in the research presented in Paper I, included only two test pieces of dimensions 45×70×700 mm and 41×50×700 mm, respectively, each one displaying a traversing knot. The second sample, applied in Papers II and III, consisted of 105 boards with a plank dimension (45×145×3600 mm) that is common for structural timber. The third one was used in Papers III and IV and originally included 58 side boards of dimension 25×120×3900 mm, which were subsequently split and cross-cut into 116 boards of dimension 25×56×3000 mm. The fourth and last sample, which was investigated in Paper VI, was initially made up of 51 side boards of dimension 25×125×4800 mm, but later split, finger jointed, planed and cross-cut into 102 boards of dimension 21×57×3885 mm. The characteristics and treatments of the different samples are described in the papers, respectively, in which they are utilized. The research also comprised 128 glulam beams with cross-sectional dimension 50×300 mm and length either 4900 mm (40 beams) or 5400 mm (88) beams. The research in which these beams were investigated is presented in Paper V. The main part, 113 beams, were manufactured from side board laminations glued in a wet state, whereas the remaining 15 beams were made up of side boards that were dried before gluing. Laminations of three different thicknesses were used; 21 mm, 21.5 mm and 25 mm.

Limitations of this thesis are that all investigations and measurements were based on application of Norway spruce timber from sawmills located in the south of Sweden, and that investigated development potentials only concern machine strength grading techniques. The presentation mainly concerns conditions that are predominant in Europe, but comparisons with present state of circumstances in North America are occasionally made.

2 INDICATING PROPERTIES – STATISTICS AND MATERIAL CHARACTERISTICS

2.1 Basic statistics for machine strength grading

The fundamentals of machine strength grading of timber are the statistical relationships that exist between strength and various non-destructively measured wood properties. Statistical models that are utilized are based on the application of *regression analysis* by which the relationship between a *response variable Y*, *i.e.* the strength, and one or several *predictor variables* X_i, *i.e.* certain measurable wood properties, can be evaluated. In statistics textbooks, response variables are also denoted *dependent variables*, whereas predictor variables are also referred to as *independent variables* or *regressor variables*, see *e.g.* Montgomery (2009). A predictor variable is, as mentioned in section 1.2, denoted *indicating property* (IP) when regression analysis is applied in connection with strength grading of timber.

Linear regression analysis is most frequently used. It can be either *simple* or *multiple*, depending on the make of the applied grading machine. As indicated by the designations, *simple* regression involves only one predictor variable / indicating property, whereas two or several of such properties are included in *multiple* regression. In the account below, the principles of linear regression are described on the basis of the simple case. An introduction to the basic concepts of multiple linear regression is found in *e.g.* Montgomery (2009).

To carry out a simple linear regression analysis of structural timber, a sample of timber pieces is needed. For each piece, the response variable, *i.e.* the strength, and an IP, in most cases either a local or an average MOE value, are determined, often on the basis of measurement methods described in the European Standard EN 408. Applicable IP measures can also be determined using measurement techniques implemented in grading machines. Strength and IP for each timber piece represent pair of observations which can be

plotted in a scatter diagram, see example in Figure 5. The result of the regression analysis is a regression model that describes the linear relationship between strength and IP. The model is mathematically expressed as a regression line, see Figure 5, according to the equation

$$Y = \beta_0 + \beta_1 X \tag{1}$$

including the response variable Y, the predictor variable X, and the parameters β_0 and β_1 representing, respectively, the interception between the regression line and the y-axis, and the inclination of the regression line. The line represents expected strength values (or long-run average strength values) as a function of IP values and it is determined on the basis of the method of least squares applied on errors ε, see Figure 5. The errors, or residuals, are equivalent with the difference between a particular strength observation and the strength value obtained from Equation (1) using the observed IP value that corresponds with the strength observation in question. Thus, the values of β_0 and β_1 are chosen in order to minimize the sum of the squares of the errors ε.

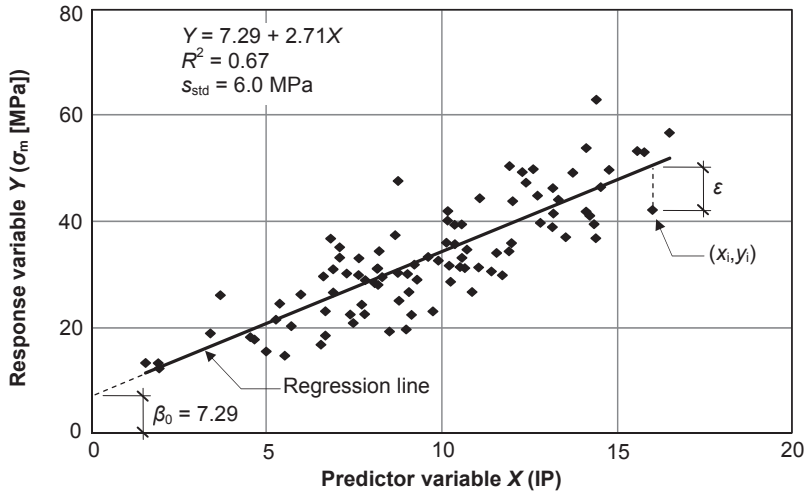

Figure 5. Scatter diagram showing the relationship between an IP and bending strength (σ_m) for a sample of structural timber pieces.

To evaluate to what extent a regression model could be used to predict the strength on the basis of a measured IP, the *coefficient of correlation*, denoted R, and the *coefficient of determination*, denoted R^2, are determined. For a sample of n pair of observations of variables X and Y, the coefficient of correlation is calculated as

$$R = \frac{\mathrm{cov}(x,y)}{s_x \cdot s_y} = \frac{n\sum_{i=1}^{n} x_i y_i - \sum_{i=1}^{n} x_i \sum_{i=1}^{n} y_i}{\sqrt{n\sum_{i=1}^{n} x_i^2 - (\sum_{i=1}^{n} x_i)^2}\sqrt{n\sum_{i=1}^{n} y_i^2 - (\sum_{i=1}^{n} y_i)^2}} \quad (2)$$

where x_i and y_i are the values of each pair of observations (see Figure 5), cov(x,y) is the sample covariance and s_x and s_y are the sample standard deviations of the variables X and Y, respectively. For a sample of structural timber, R provides information about the degree of linearity in the relationship between IP and strength. The value of R is in the interval $-1 \leq R \leq 1$. Values close to zero means that there is no linear relationship, whereas values of −1 or +1 means that there is a linear relationship that is either perfectly positive (R = +1, *i.e.* Y increases when X increases) or perfectly negative ($R = -1$, *i.e.* Y decreases when X increases).

Regarding the coefficient of determination, R^2, it is interpreted as the proportion of strength variation that is explained by the linearity between strength and IP. It could be determined either by squaring the R value calculated from Equation (2), or by applying

$$R^2 = \frac{\sum_{i=1}^{n} (y_i' - \bar{y})^2}{\sum_{i=1}^{n} (y_i - \bar{y})^2} \quad (3)$$

where y_i is an observed value of variable Y, y_i' is the predicted Y value calculated from Equation (1) using the observed value x_i that corresponds with y_i, and $\bar{y}$ is the mean of all the observations of Y in the sample. Values of R^2 range between 0 and 1. For $R^2 = 1$, the entire variation of strength would be explained by variation of IP, whereas $R^2 = 0$ would mean that IP variation has no influence on variation of strength.

A further statistical quantity by which the accuracy of a simple linear regression model can be assessed is the *standard error of the estimate*, denoted s_{est} and given by

$$s_{est} = \sqrt{\frac{\sum_{i=1}^{n} (y_i - y_i')^2}{n-2}} \quad (4)$$

This measure is an estimator of the standard deviation of the errors, or residuals, $\varepsilon = y_i - y_i'$ (Blom 1970).

2.2 Wood material characteristics

2.2.1 Wood features

Development of methods for strength grading of structural timber requires a wide knowledge about the relationships between, on one hand, different wood material characteristics and, on the other hand, structural properties that are to be predicted. For clear wood, *i.e.* wood void of any defects, it is well known from research carried out by, for example, Foslie (1971) that both MOE and the bending strength in the direction of the grain are dependent on the clear wood density. Foslie's investigation was carried out on small pieces of Norway spruce, and by application of regression analysis he found an R^2 between MOE and density of 0.64. The corresponding relationships between density and strength were 0.66 in bending and 0.51 in tension, respectively, and an R^2 as strong as 0.76 was obtained between MOE and bending strength. For wood including defects such as knots, cracks, compression wood and top ruptures, the described relationships are weaker, see Table 1, but they are nevertheless utilized for strength predictions of structural timber.

An important feature of wood is that several characteristics which influence the structural properties vary considerably in the radial direction, *i.e.* from pith to bark. For example, the MOE of Norway spruce increases significantly, sometimes by a factor of two, from the pith and outwards (*e.g.* Wormuth 1993; Dahlblom *et al.* 1999) and similar observations, but less pronounced, have also been made for density (*e.g.* Steffen *et al.* 1997; Dahlblom *et al.* 1999). Another characteristic that varies in the same direction is the spiral grain. Close to the pith, fibres in Norway spruce trees are inclined slightly to the left, usually at its largest between annual rings number four and eight (Säll 2002). On the basis of measurements of 309 logs, Säll found that the maximum grain angle was, on average, 3.1° with a standard deviation of 1.3°. Outwards, in the radial direction, the grain angle normally decreases linearly and the fibres close to the bark in trees older than 40-70 years are, according to Säll, in most cases inclined to the right. For some spruce trees, the leftward inclination increases throughout, to the bark. A further characteristic showing variation in the radial direction is the annual ring width. According *e.g.* to Perstorper *et.al.* (1995) and Herman *et al.* (1998), it is often larger in early years, but decreases towards the bark. It could be manipulated by silvicultural measures such as thinning, but after an increase of growth rate in the years following such a treatment, the ring width decreases again.

2.2.2 Strength and stiffness determining properties

2.2.2.1 Modulus of elasticity

As described in section 2.1, machine strength grading of structural timber is based upon statistical relationships between timber strength and various non-

destructively measured wood properties. A number of such relationships are exhibited in Table 1 which is an extract from a table originally presented by Hoffmeyer (1995). That table is often referred to in publications regarding strength grading of structural timber.

Table 1. Statistical relationships, in terms of coefficient of determination (R^2), between strength of Norway spruce timber and various non-destructively measured wood properties (Hoffmeyer 1995). The investigations referred to are 1. Johansson et al. (1992), 2. Hoffmeyer (1984), 3. Hoffmeyer (1990), 4. Lackner and Foslie (1988), 5. Glos and Heimeshoff (1982), and 6. Johansson (1976).

Non-destructively measured wood properties	**Coefficient of determination (R^2)**						
	Bending strength				**Tensile strength**		
Source:	**1**	**2**	**3**	**4**	**1**	**5**	**6**
Knots	0.27	0.20	0.16	0.25	0.36	0.42	0.30
Annual ring width	0.21	0.27	0.20	0.44	0.36	0.33	0.28
Density	0.16	0.30	0.16	0.40	0.38	0.29	0.38
MOE, bending or tension	0.72	0.53	0.55	0.56	0.70	0.69	0.58
MOE, flatwise bending, short span	0.52				0.65		0.74
Knots + annual ring width	0.37	0.42	0.39		0.49		0.48
Knots + density	0.38		0.38		0.55	0.61	0.64
Knots + MOE	0.73	0.58	0.64		0.70	0.76	0.78

From the R^2 values presented in Table 1, it is evident that the best single predictor, or indicating property, of both bending and tensile strength is the stiffness expressed in terms of different MOEs. The values exhibited on row 4 refer to relationships between strength and more or less locally determined MOE in either edgewise bending or tension. However, regarding the values exhibited it is important to underline that R^2 values obtained from different investigations are *not* directly comparable, since different samples and different test set-ups were used.

As mentioned in section 1.2, a strength class intended for use in structural codes is, according to EN 338, indicated by the capital letter *C* followed by two digits representing the characteristic bending strength of the timber graded into the class. Structural timber is in general rectangular in shape, and the bending strength of a class is applicable for bending in both the edgewise and flatwise direction. However, even if structural timber is more or less exclusively exposed to bending in the edgewise direction when it is utilized as horizontally oriented load bearing components, the bulk of grading machines and grading methods that are available on the market are based upon MOE measures being determined on the basis of either dynamic excitation in the axial direction or static bending over a certain width of span in the flatwise direction. Thus, even if MOE is a material property that varies in both longitudinal and lateral directions of a timber piece, the MOEs that are determined by grading techniques of today actually reflect MOE variation

over a certain length. Different values will be obtained depending on which type of load case or MOE measurement technique that is applied. Table 2 exhibits mean value, standard deviation and relationship with bending strength (σ_m) in terms of coefficient of determination (R^2) for five different MOE measures determined for a sample of 105 Norway spruce boards of plank dimensions 45×145×3600 mm. The first three of these measures were utilized in the research presented in the attached Paper II, the first four were applied in an investigation in which timber bending strength was predicted on the basis of resonance frequencies corresponding to edgewise bending modes of vibration (Olsson *et al.* 2012), and all five measures were applied in the investigations described in Paper III.

Table 2. Mean value, standard deviation and relationship to bending strength (σ_m) in terms of (R^2) for five different MOE measures obtained from investigating 105 boards of Norway spruce with nominal plank dimensions 45×145×3600 mm (see Olsson et al. (2012) and Papers II and III). Reported values are based on actual dimensions of 104 boards (one board disregarded due to a major crack).

Method for assessment of MOE	Symbol	Mean value [GPa]	Standard deviation [GPa]	R^2 between MOE and σ_m
Local static edgewise bending (EN 408)	$E_{m,loc}$	11.0	2.8	0.73
Global static edgewise bending (EN 408)	$E_{m,glob}$	10.9	2.3	0.72
Axial dynamic excitation[1]	$E_{a,1}$	12.4	2.6	0.60
Edgewise dynamic excitation[2]	$E_{b,1}$	12.7	2.7	0.66
Local static flatwise bending	E_{flat}	9.7	1.9	0.62

1. First axial mode of vibration.
2. First transversal (edgewise) mode of vibration.

For the boards referred to in Table 2, both local and global static MOE and bending strength were determined in the edgewise direction by means of bending tests carried out on the basis of test procedures specified in EN 408. The test set-up is exhibited in Figure 6. The testing machine was of make Lorentzen & Wettre, type Alwetron TCT100 equipped with a 100 kN load cell and with the loading applied to the test pieces from underneath. The critical section at which failure was expected to occur was selected in each piece by means of visual inspection. As stipulated in the European Standard EN 384 (clause 5.2), this section was positioned between the two point loads and the tension edge of each piece was chosen at random after the critical section had been decided upon. To be able to determine local and global static edgewise MOE, respectively, two different deformations, denoted *v* and *w* in Figure 6, were measured. The local deformation, *v*, includes deformation due to bending only, since there are no shear forces in the mid span between the two loads. The global deformation, *w*, includes shear but also local effects, such as indentation perpendicular to the grain at the supports.

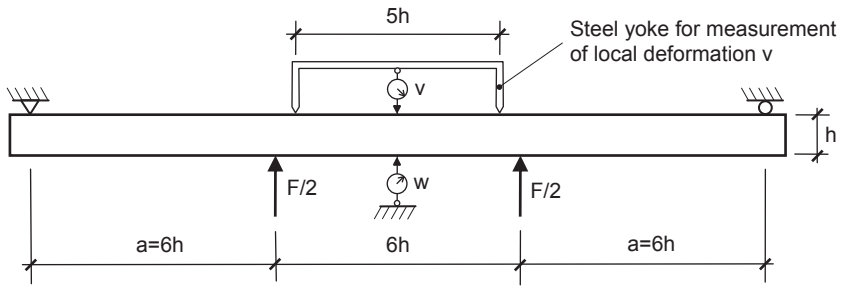

Figure 6. Test set-up based on EN 408 for determination of static edgewise bending stiffness, locally ($E_{m,loc}$) as well as globally ($E_{m,glob}$), and bending strength (σ_m).

In EN 408, it is specified that the local edgewise bending MOE shall be determined on the basis of local deformation measured within the mid span and over a gauge length of five times the depth of the timber piece (see Figure 6). It is also specified that this deformation shall be taken as the average of measurements on both wide faces at the neutral axis. However, an accurate value of local MOE is easier to achieve if the measurement of local deformation v is performed at the tension edge than on both wide faces. Thus, the values referring to local static edgewise bending MOE in Table 2 are based on local deformations v that were measured using a steel yoke installed at the tension edge. According to Källsner and Ormarsson (1999) this set-up results in a local MOE that is about 1 % lower than if the deformations had been measured at the neutral axis.

The local static edgewise MOE was calculated as

$$E_{m,loc} = \frac{al^2(F_2 - F_1)}{16I(v_2 - v_1)} \tag{5}$$

in which a is the distance between one of the point loads and the nearest support, l is the length (equal to $5h$) of the steel yoke over which the local deformation v is measured, I is the second moment of inertia, F_2-F_1 is the increment of load (*i.e.* the increment of the sum of the two point loads) measured between two points on the straight portion of the load-deformation graph, and v_2-v_1 is the increment of deformation corresponding to F_2-F_1.

The global static edgewise MOE was calculated from the expression

$$E_{m,glob} = \frac{L^3(F_2 - F_1)}{bh^3(w_2 - w_1)}\left[\left(\frac{3a}{4L}\right) - \left(\frac{a}{L}\right)^3\right] \tag{6}$$

where a and F_2-F_1 are the same as in Equation (5), h is the depth of the board, b is the board thickness and L is the total span in bending, *i.e.* $L=18h$ according to Figure 6. An equivalent expression for determination of $E_{m,glob}$ is found in a recently presented final draft of a worldwide (ISO) standard

providing requirements for testing of structural properties of sawn timber (Anon 2014a).

Axial dynamic MOEs were calculated for ideal free-free boundary conditions, meaning that the beam has no supports, (*e.g.* Hearmon 1966; Ohlsson and Perstorper 1992) as

$$E_{a,n} = 4\rho\left(\frac{f_{a,n} \cdot L_{tot}}{n}\right)^2 \tag{7}$$

where $f_{a,n}$ is the axial resonance frequency that corresponds with the n^{th} axial mode of vibration, ρ is the board density at the time of measurement of axial resonance frequency, and L_{tot} is the total length of the board. The axial dynamic MOE value that is presented in Table 2, and there denoted $E_{a,1}$, was calculated on the basis of the first axial resonance frequency. The vibrations were excited from a blow of an impulse hammer at one end of the board and measured by an accelerometer that was fastened using wax at the other end.

The determination of MOE using resonance frequencies for edgewise bending modes of vibration is more complicated compared to MOE determination using axial resonance frequencies, since transversal vibrations include shear, which means that the shear modulus, G, also should be regarded, in general. In the investigation presented by Olsson *et al*. (2012), the six lowest resonance frequencies of edgewise bending modes were measured for the 105 boards in a similar way as for the axial modes, apart from the fact that the vibrations were excited from a hammer blow at the narrow edge at one end of each board, and that the accelerometer at the other end was fastened on the same edge. The bending resonance frequencies were denoted $f_{b,n}$ where n refers to the n^{th} resonance frequency. Corresponding MOEs, represented as $E_{b,n}$, were calculated for each board on the basis of an assumed shear modulus G=700 MPa, a measured board density, Timoshenko beam theory by which shear deformations are taken into account, and a finite element board model utilized for modeling the stiffness of each board. In Table 2, the mean value and the standard deviation for $E_{b,1}$, *i.e.* the MOE corresponding to the resonance frequency of the first edgewise bending mode, is exhibited. For clarity, it should be noted that G has a limited influence on resonance frequencies of lower bending modes. According to the Bernoulli-Euler beam theory, in which shear deformations are neglected, the edgewise MOE for ideal free-free boundary conditions is determined as

$$E_{b,n} = \frac{4mL_{tot}^4 f_{b,n}^2}{\gamma_n^2 \pi^2 I} \tag{8}$$

where

$$\gamma_n = \left[n + \left(\frac{1}{2} \right) \right]^2 \tag{9}$$

and n is the number of the mode of vibration, m is the mass per length unit, I is the second moment of inertia in the edgewise direction and h is the depth of the board, see Figure 6. Thus, application of Equation (8) means that $E_{b,1}$ can be estimated from

$$E_{b,1} = \frac{4mL_{tot}^4 f_{b,1}^2}{\gamma_1^2 \pi^2 I} \approx 0.96 \frac{\rho L_{tot}^4 f_{b,1}^2}{h^2} \tag{10}$$

which is the equation applied in the research presented in Paper III. An approximation in accordance with Equation (10) will result in an underestimation of dynamic edgewise bending MOE by a few percent.

The local static MOE in flatwise bending, denoted E_{flat}, was determined using a three-point bending machine of make Cook-Bolinder, see Figure 7 (left). The boards were fed through the machine at a feed speed of 40 m.p.s., which was the lowest speed possible to set. A low feed speed reduces the board vibrations, which, in turn, contributes to more stable and reliable measurements. As a board is passed through the machine, it is exposed to a flatwise three-point bending at which the board is supported by two fixed rollers located at a distance of 900 mm, see Figure 7. A pre-determined deflection δ of 5.6 mm is applied and the corresponding load needed to achieve this deflection is registered by a load cell at a measurement interval of one (1) cm between measurement points along the board's length. To account for possible initial bow, each board is fed through the machine twice with

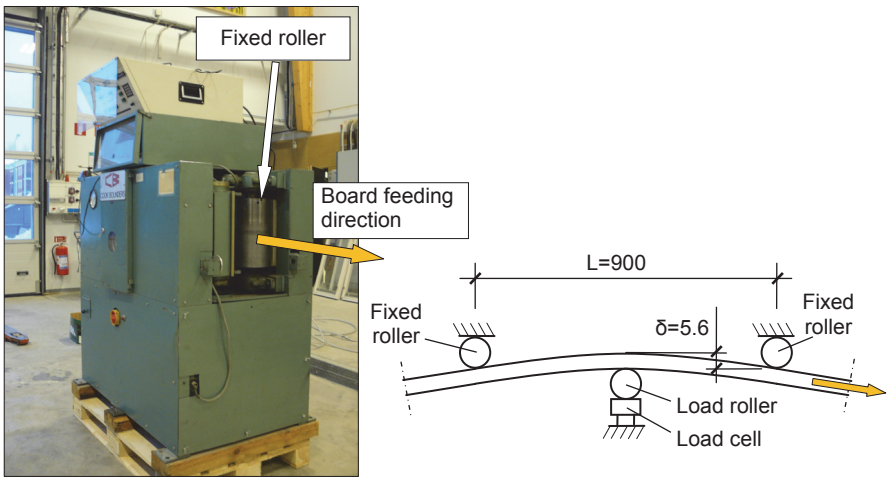

Figure 7. Measurement principle (right) for Cook-Bolinder strength grading machine (left).

opposite bending directions and the average load at every measurement point is calculated. The corresponding $E_{flat,local}$ values are calculated as

$$E_{flat,local} = \frac{P_{average} \cdot L_{flat}^3}{48I\delta} \quad (11)$$

where $P_{average}$ is the average load at every measurement point, L_{flat} is the distance between the fixed rollers and I is the second moment of inertia in the flatwise direction. Moving average MOE values for intervals of ten cm along the length of a board were then calculated and the lowest of these average values was chosen as the board's E_{flat} value, *i.e.* the local static MOE in flatwise bending. Regarding the Cook-Bolinder measurements, it might be considered as somewhat misleading to characterize E_{flat} as a *static* MOE, due to the vibrations that occur in a board on its way through the machine. The MOE value is *static* in comparison with $E_{a,n}$ and $E_{b,n}$, but as a consequence of the vibrations, *quasi-static* might be a more appropriate term.

The relationships in terms of R^2 presented in Table 2 between different MOEs and bending strength (σ_{m}) are based on strength values determined on the basis of EN 408 (see Figure 6), *i.e.*

$$\sigma_m = \frac{3Fa}{bh^2} \quad (12)$$

The results presented in Table 2 show that MOE values determined using dynamic excitation ($E_{a,1}$ and $E_{b,1}$) are higher than corresponding values obtained from static bending in both edgewise ($E_{m,loc}$ and $E_{m,glob}$) and flatwise (E_{flat}) directions. It is also shown that E_{flat} is the MOE measure that gives the lowest MOE value. The described differences between the MOE measures could be explained by various combinations of interacting factors.

There are at least two reasons why $E_{a,1}$ and $E_{b,1}$ are higher than $E_{m,loc}$. Firstly, the two dynamically determined MOEs both reflect average MOE values for entire boards, whereas the $E_{m,loc}$ is measured locally over the assumed weakest section. Secondly, the two "dynamic" MOEs are determined on the basis of resonance frequencies that are measured instantaneously, whereas the local static edgewise MOE is based upon deformations that are measured over a certain period of time and, thus, allowing for creep deformations to develop (*e.g.* Larsson *et al.* 1998).

The global static MOE, $E_{m,glob}$, is also assumed to be affected by creep since it is measured over the same period of time as $E_{m,loc}$, see Figure 6, but unlike $E_{m,loc}$, it represents, just as the two dynamically determined MOEs, an average MOE for the entire board. Nonetheless, the achieved $E_{m,glob}$ exhibited in Table 2 was even somewhat lower than $E_{m,loc}$, a relationship that also could be found in other investigations, *e.g.* Källsner and Ormarsson (1999). According to their research, one reason why $E_{m,glob}$ determined on the basis of

EN 408 results in low MOE values is that vertical compression perpendicular to the grain occurs at the supports when load is applied. Consequently, an increase of the global deformation, *i.e.* the deformation denoted *w* in Figure 6, is measured. A further enlargement of this deformation is, according to Källsner and Ormarsson (1999), observed for tested boards that are initially twisted. At the start of a bending test, such shape distortion results in lack of full contact between the supports and the edge surface of the boards. When load is gradually applied the area of contact is increased due to rotation of the board ends but this rotation also results in an increase of the measured mid span deformation. Another factor that contributes to an underrating of $E_{m,glob}$ in relation to $E_{m,loc}$ is that the former includes shear deformations (Boström 1999). Thus, of the two edgewise bending MOEs that are determined statically, the one that is measured locally is the one that is most appropriate as indicating property for determination of strength class.

Finally, the E_{flat} value, which was the lowest MOE value achieved for the 105 boards, was, just as the $E_{m,loc}$ value, determined locally at a critical board section, but on the basis of a somewhat different span and load case (900 mm, see Figure 7). However, the creep that is assumed to affect $E_{m,loc}$ is not reflected in E_{flat}, since the measurement of applied load in the flatwise bending machine is done instantly and continuously along a board as it is fed through the machine. Still, the E_{flat} value was 12 % lower than $E_{m,loc}$, which actually indicates that the creep effect on deformations used for determination of $E_{m,loc}$ and $E_{m,glob}$ is probably rather limited. The relationship between E_{flat} and $E_{m,loc}$ has previously been investigated by, for example, Steffen *et al.* (1997) who found that the local flatwise MOE, determined using a Cook-Bolinder strength grading machine, was considerably lower than the local edgewise static MOE determined from bending test according to EN 408. This was explained by two main factors. Firstly, E_{flat}, being determined on the basis of three-point bending tests, includes shear deformations which accounts for about half the difference between E_{flat} and $E_{m,loc}$. Secondly, the natural variation of MOE over the cross section of a piece of structural timber cut from the centre of a log contributes to an increase of $E_{m,loc}$. This can be explained by reference to Figure 8, which shows an example of a sawing pattern, a so called 2X-log pattern, which is frequently used in sawmill operations. As described in section 2.2.1, MOE increases in the radial direction of a tree, *i.e.* from the pith and outwards. The ratio between MOE measured for mature wood close to the bark and MOE measured for juvenile wood close to the pith could be as high as two, see Figure 8 (right). When boards such as those shown in Figure 8 are bent in the edgewise direction, the MOE distribution over the cross section is favourable, since the fibres with the highest MOE values are located in the parts of the cross section where the largest strains occur. This will, in turn, contribute to a higher $E_{m,loc}$ value. On the other hand, when the boards are

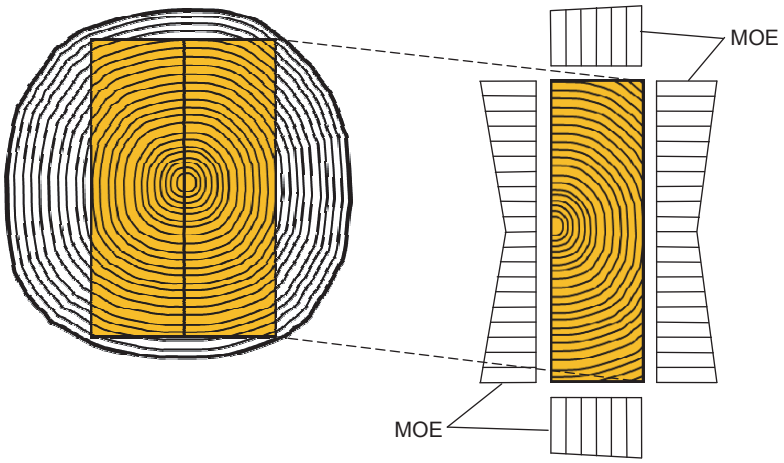

Figure 8. 2X-log sawing pattern (left) and variation of MOE along the edges of a board sawn from such a pattern (right).

bent in the flatwise direction, parts of the largest strains will be obtained in the juvenile wood which will result in a comparatively low E_{flat}.

2.2.2.2 Knots

It is well known that strength of structural timber is reduced when the ratio of knot area in the cross-section of a board is increased, but from simple linear regression analysis, using strength as response variable and different measures reflecting the occurrence of knots as a single predictor variable, limited relationships in terms of coefficient of determination are actually found. The R^2 values reported in Table 1 between tensile strength and applied knot measures varied between 0.30 and 0.42, and R^2 between knots and bending strength was even lower; between 0.16 and 0.27.

The knot measures that were included in the six investigations referred to in Table 1 were determined on the basis of visual inspection. In total, more than ten different knot measures were applied. A common denominator of the investigations was that various so called *knot area ratios* (KAR) were applied in all of them. Two such ratios widely used also in other research (*e.g.* Lam *et al.* 2004) are *total knot area ratio* (TKAR) and *margin knot area ratio* (MKAR). Both are defined in the British Standard BS 4978, the former as *ratio of the sum of the total projected cross-sectional areas of all knots intersected by any cross-section to the total cross-sectional area of the piece* and the latter as *ratio of the sum of the projected cross-sectional areas of all knots or portions of knots in a margin intersected at any cross-section, to the cross-sectional area of margin*. These definitions are visualized in Figure 9. According to BS 4978, different knots shall be included as part of the same

cross-section if any part of the knots or the grain disturbances around them overlap along the length of the timber piece. In that way, the effect of knot clusters could be regarded. The *margin* is understood as one of the outer quarters of the width of the piece. Thus, application of MKAR means that the position of the knots within a cross-section is taken into consideration. It should be noted that there are other definitions of both TKAR and MKAR than the ones presented in BS 4978. For example, Isaksson (1999) calculated MKAR as the sum of the projected cross-sectional knot areas in *both* outer quarters of the cross-section of a timber piece, divided by half the cross-sectional area. He also determined TKAR and MKAR on the basis of the sum of the projected knot areas of knots located within a longitudinal "window" of 150 mm length, see Figure 9. Similar "windows" were also applied in two of the investigations (no. 1 and no. 5) referred to in Table 1.

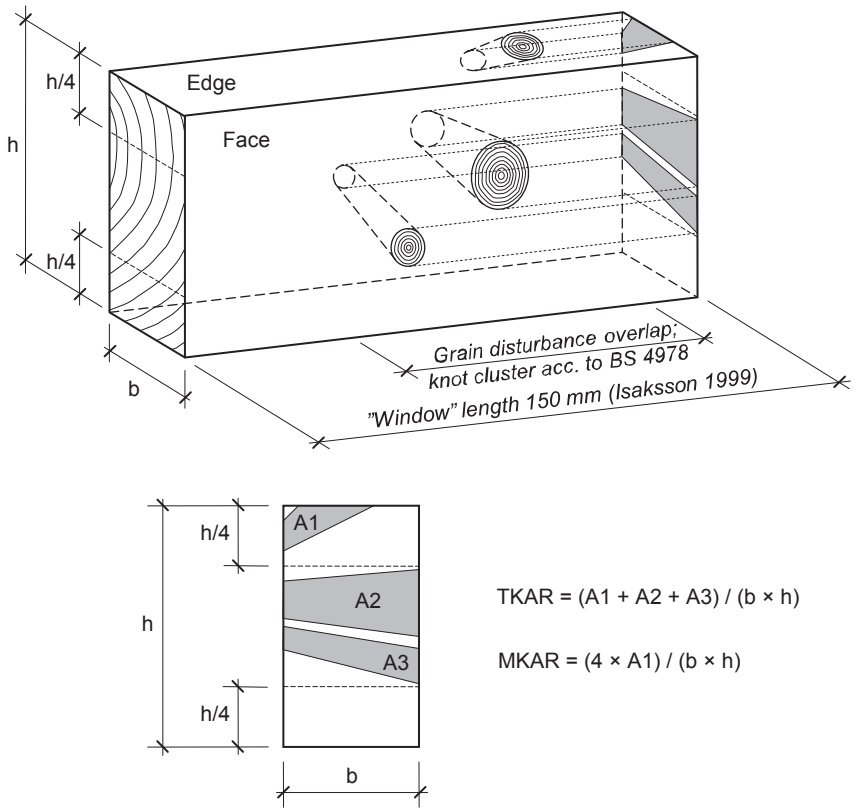

Figure 9. Definition of knot area ratios TKAR and MKAR. Top: Knot projection on a cross-sectional plane according to BS 4978, and "window" length defined by Isaksson (1999) for calculation of KAR values of knot clusters. Bottom: Projected cross-sectional areas of knots, and equations for determination of TKAR and MKAR, respectively, according to BS 4978.

The results of the investigations referred to in Table 1 showed that the relationship between strength and occurrence of knots could be improved if knot positions within a cross-section were regarded, but the relationship was still limited. Similar weak correlations between bending strength and position related knot measures were also found by Isaksson (1999) and Ziethén (2006).

The results in Table 1 also show that the relationship between knots and board strength could be improved using *multiple linear regression analysis*. When MOE measures and knots measures were applied together as indicating properties, the multiple linear regression resulted in R^2 values as high as 0.73 with respect to bending strength, and 0.78 with respect to tensile strength. However, these high R^2 were mainly due to strong relationship between strength and MOE.

When knot measures were combined with density or annual ring width, a considerable increase of R^2 between such IP combinations and bending strength were achieved, see Table 1, in comparison with what was obtained when a knot measure was used as indicating property alone.

From the results presented in this section, it can be concluded that knot measures as suggested and defined in the research referred to above do not alone provide a firm ground for strength grading. At the same time it is well known that the presence of knots has a large influence on the initiation of fractures in structural timber (see for example Figure 1). Attention should also be called to the fact that the design of visual strength grading rules, such as those stated in the Inter-Nordic standard INSTA 142, in general implies that the occurrence, location and size of knots are crucial for the grading. In an investigation concerning visual strength grading carried out by Johansson *et al.* (1998) it was found that about 65 % of the boards graded in the investigation were downgraded due to the presence of knots or knot clusters. Further evaluation of the results showed that the presence of knots was the cause of fracture for 91 % of the tested boards (Johansson 2003).

As a consequence of what has been related above, two somewhat contradictory conclusion that can be drawn regarding knots are that they, on one hand, have a very strong influence on the load bearing capacity of a board, but the usefulness of various knot measures as regards prediction of bending strength is, on the other hand, rather poor when knots are used as single indicating properties. However, when a knot measure and an MOE measure are used together as IPs in multiple linear regression, the knot measure may contribute to stronger relationships between strength and IPs (see investigations 2, 3, 5 and 6 in Table 1). Nevertheless, establishment of theories and models that could provide more reliable descriptions of the relationship between knots and bending strength would offer opportunities for development of more accurate strength grading methods.

In the sawmill production process, detection and assessment of knots has traditionally been carried out by means of visual inspection, but application of

techniques such as optical and X-ray scanning, respectively, is gradually increasing. On the basis of image analysis of camera pictures obtained from optical scanners such as the one exhibited in Figure 4, it is possible to determine size and position of knots on surfaces of timber members. Density variation within timber can be estimated by means of X-ray scanning (*e.g.* Schajer 2001), and since knot density is about twice as high as clear wood density (Schajer 2001), volume and position of knots within scanned timber can be determined.

2.2.2.3 Spiral grain and other fibre angle deviations

Spiral grain is a further wood characteristic that is important not only, as mentioned in section 1.1, for shape stability of structural timber, but also for the strength and stiffness. Since these latter properties are far better in the longitudinal direction of the grain than in the perpendicular directions, an increase of the grain angle in relation to the longitudinal direction of a timber member implies a decrease of the member's structural performance. This also holds for local grain disturbances occurring, for example, close to knots, at top ruptures and in areas where cross-grained wood is found.

Research concerning the relationship between grain angle and strength of timber was carried out already in the early 1920s. Relationships between grain direction and strength in tension, compression and bending, respectively, were presented, see Figure 10 (Dinwoodie 2000, after Baumann 1922), and an empirical formula for the relationship between varying grain angle and compression strength of spruce was introduced (Hankinson 1921). In the latter research it was also found that the formula was valid when applied to other

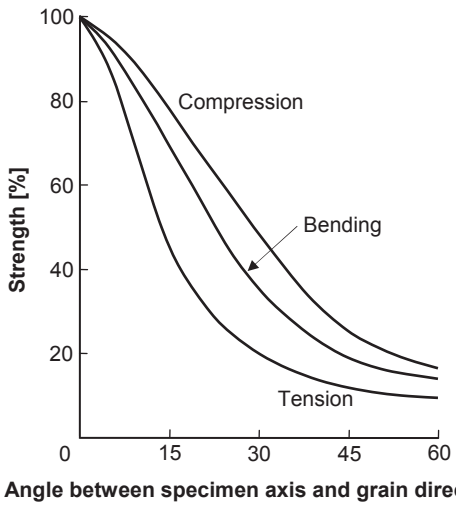

Figure 10. Effect of grain angle on tensile, bending and compression strength of timber (Dinwoodie 2000, after Baumann 1922).

wood species as well. On the basis of further research (Kollman and Côté 1968), the original formula was modified to include also tensile and bending strength. In this developed form, it can be written as

$$f_\theta = \frac{f_0 \cdot f_{90}}{f_0 \sin^n \theta + f_{90} \cos^n \theta} \tag{13}$$

where f_θ is the strength at angle θ from the grain direction, f_0 is the strength parallel to the grain, f_{90} is the strength perpendicular to the grain, and n is an empirically determined constant that is dependent on the load being applied in either tension, compression or bending.

Hatayama (1984), investigating four different wood species, found that the grain angle distribution in the vicinity of traversing wide-face knots could be described by an empirical function expressed as

$$\theta = \frac{15 \cdot \sqrt{N^\phi \cdot \phi}}{\sqrt{x}} - \frac{\phi}{2} - 5 \tag{14}$$

in which θ is the three-dimensional grain inclination (degrees), $\varnothing$ is the diameter of the knot (cm) defined as the average of the knot diameters measured on opposite wide-faces, x is a horizontal distance (cm) from the knot (see Figure 11), and N is an empirically determined constant the variation of which ($0.9 \leq N \leq 1.3$) is dependent on the species and whether the knot is dead or intergrown. Grain angle functions established for various combinations of loading, species and type of knots were used by Hatayama for determination of the corresponding constants n in Hankinson's formula. For this purpose, strength in tension and compression were experimentally determined for different strips cut from boards containing single wide-face knots (see Figure 11). The n values for the different combinations of load, species and knots were achieved on the basis of finding a good fit between the experimentally obtained strength of the strips and corresponding strength calculated using Hankinson's formula. Finally, tensile, compression and bending strength were experimentally determined for three samples of knotted boards (one sample for each testing mode) with cross section dimensions varying from 15×95 mm to 40×235 mm. Each sample included pieces of all four species and the total numbers of investigated boards calculated as the sum of all four species were 55 in tension, 121 in compression and 57 in bending. The strength of the boards was also predicted using the described expressions of Hankinson's formula, including the fitted n values. The relationships between experimentally measured and calculated (predicted) strengths were *not* presented in terms of correlation (R) or coefficient of determination (R^2), but such value could be calculated using the results presented in Hatayama's paper. The R^2 values, calculated as average of the investigated species, were

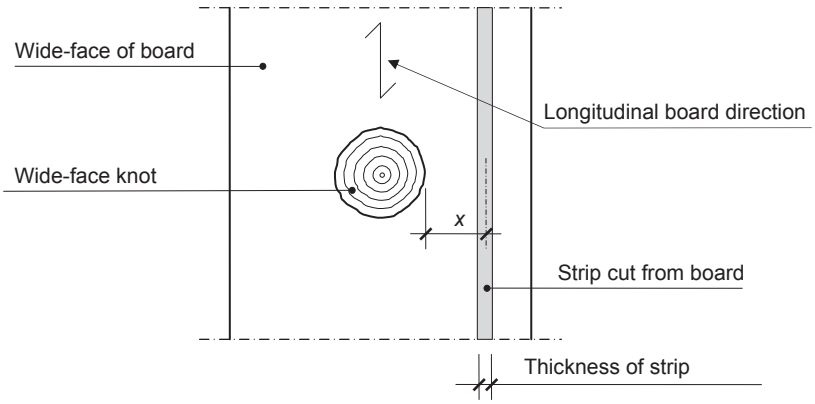

Figure 11. Strips cut at different distances x from wide-face knots for determination of the relationship between three-dimensional grain angle and strength in tension and compression, respectively (Hatayama 1984).

found to be about 0.8 for compression and bending and even somewhat higher for tension.

Hatayama also showed that Hankinson's formula could be used for prediction of MOE in tension and that this MOE value decreases rapidly with increasing grain angle. The latter has also been established in research carried out by Ormarsson (1999).

Even if the applicability of Hatayama's grain angle function according to Equation (14) is limited since it is developed only for traversing wide-face knots, it shows that knowledge about grain disturbances around knots could be utilized for the purpose of achieving accurate predictions of strength properties. For an even more detailed discussion concerning the findings of Hatayama (1984), see Foley (2003).

The variation of grain angle on the surface of a timber piece can be determined on the basis of tracheid effect scanning (*e.g.* Petersson 2010; Nyström 2003). This effect can be observed when a beam of highly concentrated light, such as laser light, strikes a wood surface. A part of the light will be reflected at the surface but some of it penetrates the outermost fibres and scatters within the wood. The scattering is larger in the fibre direction than in the direction perpendicular to the fibres. Scattered light that is reflected back to the surface will take the shape of an ellipse oriented in parallel with the fibre direction.

The direction of the grain can also be determined by dielectric scanning (Bechtel and Allen 1987) and the possibility of using microwaves for the same purpose has been investigated by *e.g.* Schajer and Bahar Orhan (2006) and Denzler *et al.* (2013).

2.2.2.4 Density

As mentioned in the first paragraph of section 2.2.1, the correlation between clear wood density and strength is rather strong in both tension and bending, whereas these relationships are weaker when determined for timber, *i.e.* for boards and planks of full size.

Timber density is one of the three wood characteristics that are referred to as *grade determining properties* for structural timber assigned to strength classes of EN 338. As mentioned in the first paragraph of section 1.2, the characteristic and mean densities given in EN 338 refer to timber with a moisture ratio of about 12 %.

Results from investigations concerning the relationship between timber density and strength in bending as well as in tension are shown in Table 1. In bending, the R^2 values vary between 0.16 and 0.40, and in tension they are, on average, somewhat higher ($0.29 \leq R^2 \leq 0.38$). However, and as asserted in the paragraph immediately after Table 1, this difference may to some extent be explained by the fact that different samples and different test set-ups were used in the investigations referred to in Table 1. It is also important to note that oven-dry density (0 % moisture ratio) was applied in investigations no. 1 and no. 3-6. As regards the remaining investigation (no. 2), it is not quite clear what density measure that was applied.

For the sample of 105 boards (with dimension 45×145×3600 mm) that was used in the investigation described in Papers II and III and discussed in section 2.2.2.1 (see Table 2), the coefficient of determination between bending strength and density at 12 % moisture ratio (ρ_{12}) was 0.27, which is similar to the corresponding values presented in Table 1. However, the research presented in Paper IV concerned 116 boards with dimension 25×56×3000 mm tested in tension, and the relationship between tension strength and density (ρ_{12}) was for this sample as low as R^2=0.12, *i.e.* a much lower value than what was found in the tension tests exhibited in Table 1. The reason for this is most likely related to the very narrow dimensions of the boards described in Paper IV, which make both strength and stiffness very sensitive to occurrence of large knots, and, as a consequence, less dependent on properties such as density.

From the R^2 values presented in the two last paragraphs, it is evident that the relationship between density and strength of a timber piece is moderate. At the same time the relationship between density and MOE can be rather strong (*e.g.* Olsson *et al.* 2012). This implies that the benefit of applying density as a second indicating property, *i.e.* to be used in combination with MOE for prediction of strength, is often rather limited.

The main reason why density is elevated to the status of *grade determining property* can be referred to the relationship between density and the load-bearing capacity of fasteners such as nails, bolts and dowels installed in connections of timber structures. The characteristic strength of such fasteners

are calculated according to formulas in Eurocode 5 (EN 1995) and these strengths, and formulas, are most often dependent on the characteristic timber density as defined in EN 338. Accurate information about the density is also crucial for accurate determination of axial dynamic MOE of a piece of timber, see Equation (7).

Different techniques can be applied for wood density determination. As mentioned in section 2.2.2.2, X-ray scanning is one option. Microwaves, which can be used for determination of grain angle (see section 2.2.2.3), can also be utilized for the purpose of measuring both density and moisture content (*e.g.* Johansson *et al.* 2003; Aichholzer *et al.* 2013). It deserves to be noted that by application of microwaves, the mentioned properties (grain angle, density and moisture content) can be identified simultaneously. In sawmill operations in which the boards are transported in transversal direction, weight and length can be measured at production speed, and density can then be calculated using nominal cross-sectional dimensions.

2.2.2.5 Annual ring width

When strength grading is carried out on the basis of visual rules such as those included in BS 4978, the German standard DIN 4074-1 or the Nordic rules INSTA 142, all referred to in EN 1912, it is not possible to predict the board density *directly*. Instead, visual grading standards include limits concerning maximum annual ring width. By such requirements, density is *indirectly* regarded (Hoffmeyer 1984), which is explained by the fact that the density in late wood is much higher than in early wood. When the annual ring width decreases, the part of the board cross section that is covered by the heavier late wood increases, which also results in an increase of the density. However, the correlation between annual ring width and density that has been found in previous research is modest. In investigations presented by Hoffmeyer (1990), Johansson *et al.* (1992) and Johansson *et al.* (1998), the R^2 values varied from 0.18 to 0.38. Consequently, to use annual ring width as a substitute for density in visual grading might be questioned. On the other hand, the relationship between strength and annual ring width is on a similar level as R^2 between strength and density, see Table 1, which indicates that annual ring width criteria may contribute to more accurate visual grading results.

Regarding the machine strength grading techniques of today, measures of annual ring width are actually not applied as grading parameters. As mentioned in section 1.1, general requirements regarding both visual and machine grading are included in the European Standard EN 14081-1, and the parts that are applicable for machine grading are void of limitations concerning annual ring width.

In sawmill production, the traditional technique applied for determination of annual ring width has been visual inspection, but today scanning of board ends can be carried out by means of optical measurement systems.

2.2.2.6 Top ruptures

This kind of defect is caused by the top of a tree being broken by *e.g.* browsing game or load of heavy snow or wind. When such damage occurs, one of the branches just below the rupture of the stem bends upwards and takes the place as leading shoot. As the tree continues to grow, the grain disturbances caused by the top rupture are overgrown and the damage could later in the life time of the tree be observed as a crook on the stem. On boards cut from logs that contain top ruptures, the grain disturbances appear in different ways depending on the orientation of the saw cuts. When the plane of these cuts are parallel with the plane of the crook in the stem, as shown in Figure 12, the grains are oriented in a pattern that corresponds with the crook. However, when the saw cut plane is perpendicular to the plane of the stem crook, the damage is more difficult to observe since the top rupture produces a so called *diving angle*, also denoted *out-of-plane angle*, between the fibre direction and the observed face of the board.

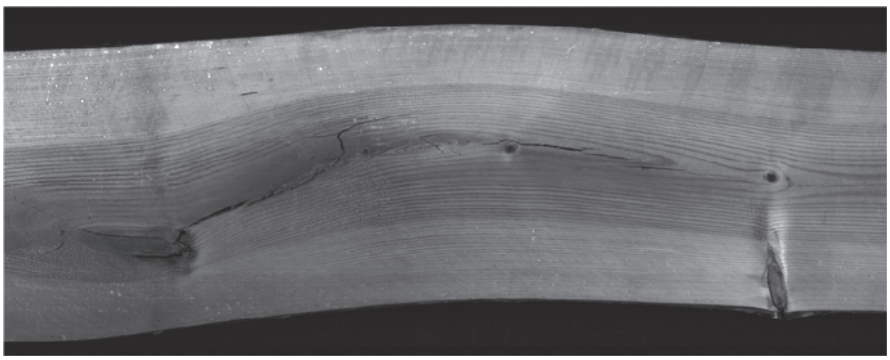

Figure 12. Top rupture in sawlog of Scots pine (Skog et al. 2011).

Top ruptures have a serious effect on the strength and stiffness of boards and planks. In an investigation of about 500 timber pieces of Norway spruce (Johansson *et al.* 1992), *i.e.* investigation no. 1 in Table 1), the point with the lowest flatwise bending stiffness was located in each piece. In almost all of them it coincided with either knots or top ruptures.

To the knowledge of the author of this thesis, none of the strength grading machines that are available on the market today include detection of top ruptures. This also holds for optical scanners that are utilized for visual override, but occasionally, when such scanning is applied, grain deviations caused by top ruptures are identified as cross-grained wood (Svensson 2012). To be able to identify actual top ruptures in the industrial process of strength grading, manual inspection still has to be relied upon. However, a method for identification of top ruptures by means of polarized microwave radiation has recently been presented by Denzler and Weidenhiller (2014).

Regarding identification of top ruptures on logs, Skog *et al.* (2011) investigated the possibility of using the sharpness of the crook of sawlogs as indicator. Outer shape and heartwood shape of logs of Scots pine (*Pinus sylvestris*) was determined on the basis of data from an optical three-dimensional log scanner and an X-ray scanner, respectively. The research showed that both shapes can be applied for detection of top ruptures.

2.2.2.7 Compression wood

When a tree is exposed to eccentric load caused by *e.g.* snow load, wind load or stem inclination induced by the tree growing on sloping ground, so called *reaction wood* is formed as a means for the stem to re-erect itself and to retain vertical growth (Säll 2002). In softwoods, this kind of wood is called *compression wood* since it is formed on the compression side of the stem. In hardwoods, the formation takes place on the opposite side and the wood is, consequently, called *tension wood*.

Compression wood is characterized by a higher late wood proportion in the annual rings (Isaksson 1999). This is, in turn, due to the walls of late wood fibres being thicker in compression wood than in normal wood (Johansson 2003), which also implies a higher density in the former type of wood (Isaksson 1999). The thickness of early wood fibres in compression wood is, however, about the same as in normal wood (Ormarsson 1999).

Other differences between compression wood and normal wood are found within the cell wall. In normal wood of Norway spruce, it includes a primary wall and a secondary wall, the latter divided into three layers denoted S_1, S_2 and S_3, respectively. In compression wood, the S_3 layer is missing and the inclination of the microfibrils in the S_2 layer is much larger than the corresponding inclination in the S_2 layer of normal wood (Côté *et al.* 1967). The latter implies a considerable reduction of the longitudinal MOE (Johansson 2003) and an increased shrinkage in compression wood (Dinwoodie 2000).

Regarding load bearing capacity of compression wood, it is found that tensile strength is lower and compression strength is higher than that of normal wood (Dinwoodie 2000). Thus, due to high density, low tensile strength and low longitudinal MOE, density is a very poor indicating property for strength of compression wood (Foley 2003). It is also well known that tensile failure in compression wood often is brittle, see Figure 13.

In visual inspection of timber, compression wood is identified as areas with darker brownish colour. According to the visual override requirements in EN 14081-1, it is characterized as an abnormal defect (Brundin 2011), which could be accepted as long as the reduction in strength that is caused by it is obviously less than what is caused by other defects to which visual override requirements are applicable. Rules that are somewhat more adapted to practical use are found in *e.g.* INSTA 142 in which the occurrence of

Figure 13. Brittle tensile fractures in compression wood. Left: Lamination fracture in wet glued beam (dim. 50×300×5400 mm) with laminations of Norway spruce side boards. The exhibited beam was tested as part of the research presented in Paper V. Right: Structural timber (dim. 45×145×3600 mm) included in the tests presented in Papers II and III.

compression wood is, *inter alia*, limited to 10 % of the cross sectional area of timber pieces graded to strength classes C18, C24 and C30.

Most grading machines on the European market utilize average board MOEs as indicating property. Consequently, it can be presumed that such measures at least partly include the effect of low MOE in compression wood. When it comes to visual override requirements, the colour of compression wood can be identified and evaluated manually or by means of optical scanning, but it may be difficult to discern, particularly on flatwise surfaces of timber pieces, since its colour may resemble the colour of both rot and pith. The possibility of detecting compression wood using different scanning techniques has been investigated by Nyström (2002), who found that a combination of colour detection and tracheid effect scanning was the most promising method for industrial implementation. The tracheid effect is dependent on the wood density, implying that scattering of light in compression wood is less evident compared with the scattering in clear wood, due to the larger cell wall thickness in compression wood.

For further reading about compression and tension wood, respectively, an extensive literature survey has recently been presented by Wimmer and Johansson (2014).

2.2.2.8 Wood decay

Wood decay is a serious defect caused by different kinds of rot fungi that attack and degrade the walls in wood fibres. The growth of such funguses is dependent on temperature. They can, according to Nylinder and Fryk (2011), grow at a temperature in the range of 0-40 °C with an optimum between 25 to 32 °C. They also need access to free water in the wood cells, *i.e.* a moisture content (MC) that exceeds the fibre saturation point, which for Norway spruce

normally occurs at about 30 % MC. The growth is at its largest at 40-80 % MC (Nylinder and Fryk 2011).

Root rot is a defect that is caused by funguses attacking root systems, primarily via stumps from recently felled trees. Also root damages caused by forestry machines applied at thinning operations imply a risk for root rot infestation (Nylinder and Fryk 2011).

Decay may also occur in sawlogs. Immediately after the cutting of a stand, the MC in the saw logs is in most cases far too high for the funguses to develop. However, in the summer the MC could quickly decrease to levels at which growth conditions are favourable. Accordingly, the development of rot in sawlogs could be avoided by retaining a high MC. This could be achieved by wet storing, which means that water is sprinkled over log piles (Nylinder and Fryk 2011).

In an early stage of the decay process, discoloration of the wood will occur simultaneously as water is produced, resulting in an increase of the density (Skog 2013). Further decay development results in disintegration of the cell wall structure and subsequent fast reduction of strength, mass, volume and density (McGovern *et al.* 2010).

Limitations regarding occurrence of rot is included in the visual override requirements in EN 14081-1. *Soft rot*, *i.e.* rot that has reached an advanced stage of development at which the strength of the wood cells is strongly reduced, is not permitted in timber members graded to *any* strength class. *Dote*, also called *firm rot*, is on the other hand accepted in strength classes C18 and below, since this concept refers to rot at an early stage at which strength has not changed to any appreciable extent.

Following an attack of most of the existing rot fungi, the colour of the wood turns brownish, which means that this kind of defect might be detected by use of optical colour scanners. However, and as mentioned in section 2.2.2.7, the colour of the attacked wood cells is sometimes similar to that of pith or compression wood, implying a certain degree of limitation as regards optical rot detection. Rot may also be identified on the basis of either ultrasonic measurements (Beall 2002) or acoustic methods (Råberg *et al.* 2005), but application of these techniques require, as mentioned in section 1.1, contact between sensors and measured logs or timber pieces. The contact requirement also applies to Pilodyn needle penetration by which wood density can be evaluated. Pilodyn is a handheld device which fires a pin into the wood at a determined force, and the density is indicated by the depth of penetration. Thaler *et al.* (2012) carried out Pilodyn measurements on Norway spruce and found a clear correlation between needle penetration and mass loss due to brown rot decay. A further option for detection of severe rot is X-Ray computed tomography (CT), since the considerable loss of density that occurs during the process of decay can be measured by means of CT scanning (McGovern *et al.* 2010; Skog 2013). Still, it can be concluded that manual

visual inspection is, as yet, the most common method for identification of wood decay.

3 STRENGTH GRADING – MACHINES, TECHNIQUES AND STANDARDS

3.1 Strength grading in the past

Ever since man in a far distant past began to use wood as material for building of shelters and making of tools, it is most likely that knowledge about the difference in properties between both various kinds of species and different wood pieces has been available and utilized. Tradition and craftsmanship was the basis for timber sorting until some 150 years ago. In Sweden, the first actual rules for quality sorting of sawn timber were introduced in the second half of the 19th century. They concerned *appearance grading* based on visual inspection and they were implemented on a local basis in various districts along the coast of northern Sweden (Eliasson 2005). The concept of *appearance grading* refers to grading of sawn timber for which the visual appearance is of importance. Such grading is still applied and on the European market of today it follows the rules laid down in the European Standard EN 1611-1.

The first detailed rules concerning visual strength grading of structural timber were introduced in the USA in the beginning of the 1920s (Glos 1995) and an American standard laying down principles for such grading was published in 1927 (Madsen 1992). During the following decades, similar rules were implemented in European countries. For example, strength grading based on visual inspection was standardized in Germany in 1939 (Glos and Heimeshoff 1982) and in Sweden the first edition of the so called *T-rules* for visual grading and marking of *T-timber* were published in 1951 (Anon 1981).

The shortcomings of visual grading is rather obvious since only visible defects such as knots, cross-grained wood and compression wood can be regarded, whereas intrinsic timber properties such as density and various measures of MOE can not. As shown in Table 1, the MOE is the timber property that is by far the one that is best correlated with strength. The idea of

applying this relationship as a basis for strength grading of timber was presented in USA, Australia and the UK in the late 1950s (Fewell 1982; Madsen 1992). The MOE was determined on the basis of three-point bending in the flatwise board direction, *i.e.* the same principle as the one exhibited in Figure 7. One of the first commercial grading machines (the *Microstress Grading Machine*) was introduced in Australia (Galligan and McDonald 2000) around 1960 and approval of two further machines (the *CLT Continuous Lumber Tester* and the *Stress-O-Matic Grading Machine*) was granted in USA in 1962 (Anon 2014b). Later on, in 1969, machine strength grading was introduced on the UK market (Fewell 1982). In Sweden, the first grading machine was approved in 1974 (Johansson *et al.* 1992).

The possibility of using vibrational parameters of timber as indicating properties for machine grading was investigated already in the mid-1960s by researchers in USA, UK and Canada (*e.g.* Pellerin 1965; Hearmon 1966; Müller 1968). The main focus in those days was on dynamic properties measured in the transversal board direction, but grading techniques based on such characteristics have not had any significant impact on the market.

3.2 Strength grading of today

On the European market, there is a diversity of existing visual strength grading rules in use in different countries (Stapel and van de Kuilen 2014). This is a consequence of differences in species, geographic origin, dimensional requirements, quality of available material, historic influences and traditions, and varying requirements for different uses (EN 14081-1). Many of the current visual rules were introduced more than half a century ago, most of them having been further developed since then. As an example, a revised version of the Swedish *T-rules* is today embodied in the previously mentioned Inter-Nordic standard INSTA 142. Many nationally applied visual grades are, on the basis of EN 1912, assigned to the common European strength classes defined as *C-classes* in EN 338.

As regards machine strength grading, the three-point flatwise bending type of machines which were introduced in the beginning of the 1960s dominated the market for almost 40 years. On a world-wide basis, such machines are still widely used. For example, the *CLT Model 7200 HCLT*, from Metriguard Inc, USA, and exhibited in Figure 14, are installed in many planer mills throughout North America, Australia, New Zealand and Japan. About 50 % of all grading units utilized in North America are of this type (Kurle 2014). Compared with the Cook-Bolinder grading machine shown in Figure 7, in which the boards are fed twice with opposite flatwise bending directions to account for initial bow, the CLT machine includes two successive bending sections which bend the timber pieces in opposite directions. Thus, two different bending forces are registered at every measurement points along a board and the local MOE is

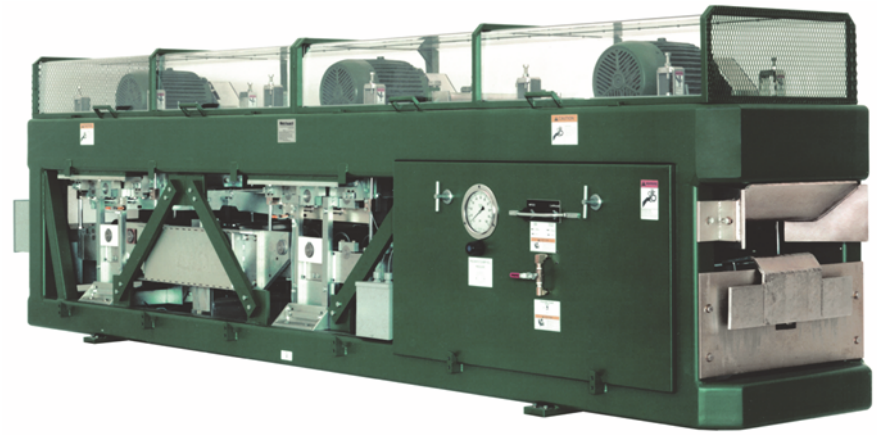

Figure 14. The dual flatwise bending machine CLT Model 7200 HCLT. Photo by courtesy of Metriguard Inc., USA.

determined on the basis of the average of these two forces. The *CLT Model 7200 HCLT* can be described as a developed version of the *CLT Continuous Lumber Tester* which was approved in 1962 (Kurle 2014).

Even if flatwise bending machines are still used, a paradigmatic shift was begun in the late 1980s and early 1990s when the possibility of using axial dynamic excitation for grading purposes was investigated (Görlacher 1990; Ohlsson and Perstorper 1992; Blass and Gard 1994). Machines based on this technique were introduced on the market in the late 1990s. A longitudinal vibration is generated in a board by a hammer blow at one of the board ends and information about the induced vibrations is captured by a microphone, a laser vibrometer or an accelerometer. The first device measures the "sound" of the board and the two latter ones capture the axial oscillation of one of the board ends. On the basis of measured vibrations and by application of so called *Fast Fourier Transform* (FFT), resonance frequencies corresponding to axial modes of vibration are determined. In combination with measured length and determined density, such frequencies can be utilized for calculation of a mean axial dynamic MOE of a board using Equation (7).

Application of the axial dynamic technique is gradually increasing. At the time of writing, more than 25 models of different makes of grading machines are approved for grading on the European market, and axial dynamic excitation is applied in about 60 % of them. In North America, the flatwise bending machines still hold a strong position, but the application of axial dynamic grading machines is gradually increasing. What is particularly attractive about this technique is that the equipment needed is installed in production lines where the timber is transported transversely, which means that the grading is carried out at a moderate feed speed. Furthermore, the equipment is fairly simple and the space needed for its installation is limited.

Attention should also be brought to the fact that even if the described method only delivers the mean MOE of a board, the accuracy of the predicted strength is in many cases the same as what is obtained from bending machines (see for example Table 2 and Betzhold 1999), despite the latter type being able to deliver information about MOE variation along a piece of timber.

Two grading machines that are based on axial dynamic excitation are the Dynagrade and the Precigrader (the latter one shown in Figure 15), both developed and marketed by the Swedish company Dynalyse AB. The main difference between these machines is that the Dynagrade applies an average density for a certain species, whereas the Precigrader measures the weight and calculates the density of each board to be graded. Since the first of these machines was introduced in 1997, they have gained large market shares and are today sold on the markets of *e.g.* Scandinavia, Russia, USA and Australia.

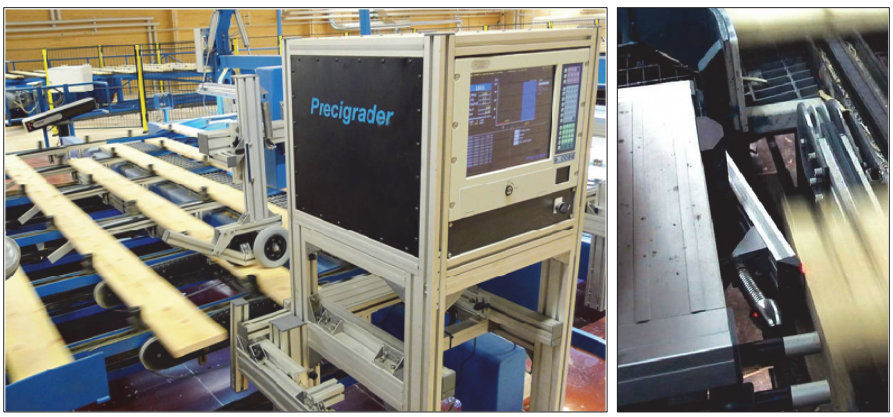

Figure 15. Precigrader grading machine in a sawmill production line with a length measuring device at the opposite side of the line (left), and dynamic excitation hammer (right). Photos by courtesy of Dynalyse AB, Sweden.

The simplicity of the axial dynamic excitation technique is underlined by the fact that a handheld and wireless measuring instrument called Timber Grader MTG from the Dutch company Brookhuis is approved for strength grading of structural timber intended for the European market. In addition to the actual axial dynamic grader (Figure 16, left), a grading set (Figure 16, right) includes a balance and a computer in which relevant software is installed. Such a set was utilized in the research presented in Papers II-IV and VI. A more detailed description of the MTG grading equipment is found in Paper IV.

In the last paragraph of section 3.1 it was mentioned that the possibility of using grading techniques based on transversal dynamic excitation was investigated already in the 1960s, but that their impact on the market have been very small. At the time of writing, there are a few makes of such

Figure 16. Timber Grader MTG (left) and grading set including grader, balance and computer with applicable software (right).

machines that are approved for grading in Europe and North America, respectively, but their share of the market is very limited. However, one of these machines, the *Metriguard Model 340 E-Computer*, is a portable test system frequently used by third-party inspection agencies in North America to certify production-line strength grading equipment, to verify production, and to test samples of timber, panels and composite materials. There are also a couple of small North American glulam manufacturers who use the *Model 340E* for their grading operations (Kurle 2013).

In section 2.1 it was described that machine strength grading can be based on linear regression that is either simple or multiple, the latter meaning that at least two indicating properties (IPs) are used simultaneously. Thus, by combining, for example, axial dynamic MOE with other IPs, the grading accuracy can be improved. One machine that combines this kind of MOE with information obtained from X-ray scanning is *Goldeneye 706* from the Italian company *Microtec*, see Figure 17. The X-ray scanning provides information about the density of a piece of timber and since there is a density difference between knots and clear wood, the scanning also gives information about knot size and knot position. When knot measures determined on the basis of X-ray scanning of a sample of timber was combined with axial dynamic MOE, a coefficient of determination as high as 0.69 was achieved between indicating properties and tensile strength (Bacher 2008). When, for the same sample, the axial dynamic MOE was used as single IP, a relationship of $R^2 = 0.58$ was reported.

On the market there are also other measurement techniques than those described above that could be utilized for machine strength grading. For example, the stiffness can be determined on the basis of a relationship between MOE and ultrasonic wave velocity, knots are detected by microwaves, density is determined from attenuation of γ-rays or microwaves and, as described in section 2.2.2.3, grain angle deviation can be measured using either microwaves or the tracheid effect achieved when a board surface is illuminated by a dot laser.

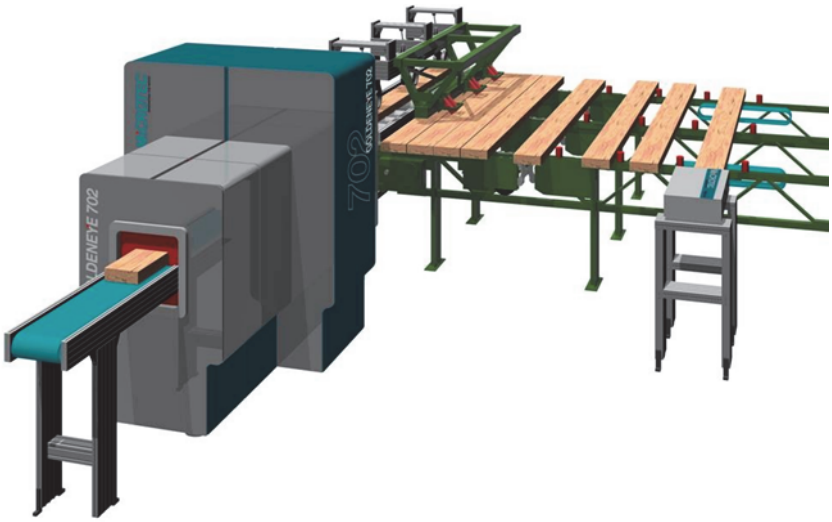

Figure 17. Set-up for GoldenEye 706 including axial dynamic excitation (right) and X-ray scanning left). Picture by courtesy of Microtec GmbH/srl, Italy.

A grading method that is not applied in Europe today is so called *proof-loading*, which means that a board is loaded up to a stress level equal to the strength required for the intended strength class. If the board stands the test, it is accepted for structural use and classified accordingly. Ziethén (2006), who investigated different aspects of this method, claimed that it is mainly in Australia that proof loading is presently applied for strength grading.

A further conceivable grading method would be to use a combination of visual and machine strength grading techniques. In an investigation carried out by Blass and Frese (2004) machine grading based on axial dynamic excitation was combined with visual grading requirements according to the German standard DIN 4074-1. It was found that grading results were improved when visual requirements were added to those applied for machine grading. However, to the knowledge of this author, no commercial strength grading is carried out on the basis of similar combinations.

3.3 European standards and approval of grading machines

3.3.1 Standards

Regulations for strength grading of structural timber intended to be put on the European market is found in a number of interrelated European standards most of which has already been referred to. The core standard is *EN 14081 Timber*

structures – Strength graded structural timber with rectangular cross section which consists of four parts:

- Part 1 – General requirements, (EN 14081-1),
- Part 2 – Machine grading; additional requirements for initial type testing (EN 14081-2),
- Part 3 – Machine grading; additional requirements for factory production control (EN 14081-3), and
- Part 4 – Machine grading – Grading machine settings for machine controlled systems (EN 14081-4).

The general requirements laid down in EN 14081-1 comprise, as mentioned in section 1.1, both visual and machine strength grading, the latter also including visual override requirements. The rules concerning machine strength grading apply to grading systems that are either *machine controlled* or *output controlled*. Both types are based on so called *machine settings* which are determined on the basis of different procedures depending on which control system that is applied. The concept of settings, as defined in EN 14081-2, refers to values of parameters that are used to set a machine to grade timber. They are mathematically related to indicating properties which, in turn, are related to one or several of the grade determining properties of the C-classes defined in EN 338, *i.e.* bending strength, MOE and density. Settings for a certain machine type define boundaries between different strength classes to be graded simultaneously by one machine in one production pass. Thus, the relationship between indicating properties measured for individual timber pieces and the settings for a machine determines to which strength class an individual piece shall be assigned. For some machine types, values of indicating properties are directly applied as settings, without the need of any further parameters.

The settings of a machine are dependent on species, grade, grade combinations, board dimensions and geographic origin of the timber to be graded. If, for example, several species are to be graded by a certain grading machine, different settings are required.

Machine control means that the grading is controlled only by the grading machine's settings which are derived on the basis of a rather comprehensive initial type testing (ITT) procedure laid down in EN 14081-2 and described in section 3.3.2 below. The results of such a procedure carried out for a specific machine type are evaluated by a technical group (TG1) set up under a technical committee (TC 124) within the European Committee for Standardization. Settings that are accepted by TG1 for a certain machine controlled system are constant for all machines of the same type and they cannot be influenced by neither sawmills nor grading machine manufacturers. Also for grading systems based on output control, settings are determined on the basis of initial type testing, but in this case they are considered as being

merely *initial* since they can be adjusted in the run of sawmill production. The basis for such adjustments is proof-loading of pieces sampled on a daily basis from the sawmill production output. The consequence of the adjustment possibilities is twofold. First, the extent of testing required for determination of initial settings is much less than for determination of settings for machine controlled systems. Second, different output controlled machines of the same type can have different settings. Machine control systems are predominant on the European market, whereas output control is mainly used in North America, Australia and New Zealand.

The requirements in EN 14081-3 concern operation, calibration and maintenance of grading machines in current use, and EN 14081-4 contains grading machine settings that are accepted by TG1 for various machine controlled systems. However, the procedure of publishing machine settings in a European Standard was replaced in 2009 by a course of action implying that new machines or added settings can be introduced on the market as soon as acceptance has been obtained by TG1 and an ITT report has been issued. In a current proposal for a revised version of EN 14081, Part 4 is repealed.

Other important standards that are linked up with EN 14081 are

- *EN 338 Structural timber – Strength classes* (referred to in sections 1.2, 2.2.2.1, 2.2.2.4, 3.2, 3.3.1, 3.3.2.4 and 3.3.2.7),
- *EN 384 Structural timber – Determination of characteristic values of mechanical properties and density* (referred to in section 2.2.2.1 and 3.3.2.4),
- *EN 408 Timber structures – Structural timber and glued laminated timber – Determination of some physical and mechanical properties* (referred to in sections 2.1, 2.2.2.1, 3.3.2.4, 4.1.2.3, 4.1.4.3, 4.1.4.4, 4.2.4 and 4.2.5), and
- *EN 1912 Structural timber – Strength classes – Assignment of visual grades and species* (referred to in sections 1.1, 2.2.2.5, and 3.2).

3.3.2 Settings for machine controlled grading systems

3.3.2.1 Initial type testing

In the Introduction of EN 14081-2, it is stated that

> *The acceptability of grading machines and the derivation of settings rely on statistical procedures and the results will therefore depend on the method used. For this reason this document gives appropriate statistical procedures.*

These procedures are part of the initial type testing (ITT) that is described in the quoted standard. The settings accepted by TG1 for a specific type of machine refer to a single strength class or a combination of strength classes to

be graded simultaneously in one production pass. The application of the settings is also limited by specified timber dimensions cut from trees of a certain species grown within a defined geographic area. One such area for which common settings often are applied consists of Sweden, Norway, Finland, Estonia, Latvia and northern parts of Russia west of the Urals. Another geographic area is Germany, Austria and the Czech Republic.

The ITT procedure for determination of settings can be divided into five main consecutive parts; sampling, grading, testing, determination of settings, and verification of settings.

3.3.2.2 Sampling

To derive machine settings that are valid for a new machine type, a minimum total number of 900 timber pieces originating from at least four different sub-samples shall, according to EN 14081-2, clause 6.2.2, be sampled. However, the number of sub-samples required by TG1 as basis for settings derivation is often much larger. A number of eight is frequently applied (Ziethén 2012). Each sub-sample shall consist of at least 100 pieces, it shall, in general, be sampled in full from one single sawmill, and it can include several board dimensions. The quality of the pieces shall be sawfalling, *i.e.* they must not be pre-graded. The sub-samples shall be distributed over the chosen geographic area with the purpose of reflecting the variation of growth conditions. The principles on which this distribution is based are, however, not laid down in detail in the standard, which may be regarded as a lack of transparency in the ITT procedure. To remedy this state of affairs, sampling guidelines has been issued by TG1 (Anon 2012).

It is in most cases sufficient to test three different board dimensions with varying width and thickness. The range of board sizes permitted to be graded on the basis of derived settings is ±10 % of the tested sizes. As an example, if a total sample of 900 boards includes the dimensions 35×150, 50×77 and 65×230 mm (see Table 3), the derived settings will be applicable for timber with dimensions ranging from 32×70 mm to 70×250 mm.

Table 3. Example of dimensions (marked with an "X") tested in an initial type testing resulting in settings valid for board sizes ranging from 32×70 mm to 70×250 mm.

Thickness [mm]	Depth / Width [mm]		
	77	150	230
35		X	
50	X		
65			X

According to EN 14081-2, it shall be ensured that strength reducing characteristics that are not detected neither by the grading machine nor by the visual override inspection shall be present in the total sample in the same

proportions as will exist in the sawmill grading. This may be relevant for characteristics such as top ruptures, rot and compression wood when optical scanners are applied for the visual override.

3.3.2.3 Grading

All pieces in the total sample are passed through the grading machine and the value of the indicating property (or properties) is recorded for each piece. Pieces that have defects that would be rejected by visual override inspection shall not be included in neither the total sample nor in any of the sub-samples (Anon 2012).

3.3.2.4 Testing – Determination of grade determining properties

The grade determining properties, *i.e.* bending strength, density and MOE, are determined at a selected critical section of each timber piece on the basis of tests and procedures described in EN 408 and EN 384, respectively. The section is "critical" in the sense that it is assumed to be the weakest section along the piece. In four point bending tests, the critical section shall, according to EN 384, clause 5.2, be positioned between the loads (see Figure 6). In the same clause it is also stated that the tension edge in bending shall be selected at random and that the grade of the piece shall be deemed to be the grade of the critical section. The MOE for this section is determined on the basis of a globally measured MOE, see Equation (6), that is subsequently adjusted to compensate for support indentation and shear deformations (see EN 384, clause 5.3.2). Density shall be determined from a small board section cut as close as possible to the fracture obtained at a strength test (EN 408, clause 7).

For timber of Norway spruce, measured values of MOE and density are adjusted to a moisture ratio of 12 % (EN 384, clause 5.3.4.2), since the characteristic and mean property values of the C-classes in EN 338 are defined for a climate that corresponds to an equilibrium moisture ratio of 12 % in Norway spruce. A similar adjustment of the bending strength is, however, not required. The bending strength is adjusted to a reference board depth (or width) of 150 mm (EN 384, clause 5.3.4.3), since the strength of structural timber is size dependent; the larger the depth, the lower the strength.

3.3.2.5 Determination of settings and assigned grades

The next step of the ITT procedure concerns development of mathematical models that describe the relationships between measured IPs and the values of the grade determining properties obtained from EN 408 tests. In general, one model is needed for each grade determining property. For example, simple regression models can be applied to describe the relationship between bending strength, σ_m, and an IP that represents *e.g.* an average axial dynamic MOE. According to Equation (1), such models will follow the formula

$$\sigma_m = \beta_0 + \beta_1 \cdot IP. \tag{15}$$

For a bending strength model as the one presented by Equation (15), settings in terms of IP values shall be determined for each grade to be graded together such that the required grade determining property, in this case σ_m, is achieved for each grade. The procedure for setting determination is rather comprehensive, but the principle is visualized in the scatter diagram shown in Figure 18 in which the setting for a grade combination of C24 and reject is exhibited. The setting value for C24, S_{C24}, is determined such that all pieces in the total sample with an IP larger than S_{C24} are assigned to C24, whereas pieces with a lower IP are assigned to reject. Grades determined in this way are called *assigned grades* and they reflect the performance of the investigated machine. Note that the setting value is chosen such that 5 % of the boards assigned to C24 do not fulfil the required strength of 24 MPa.

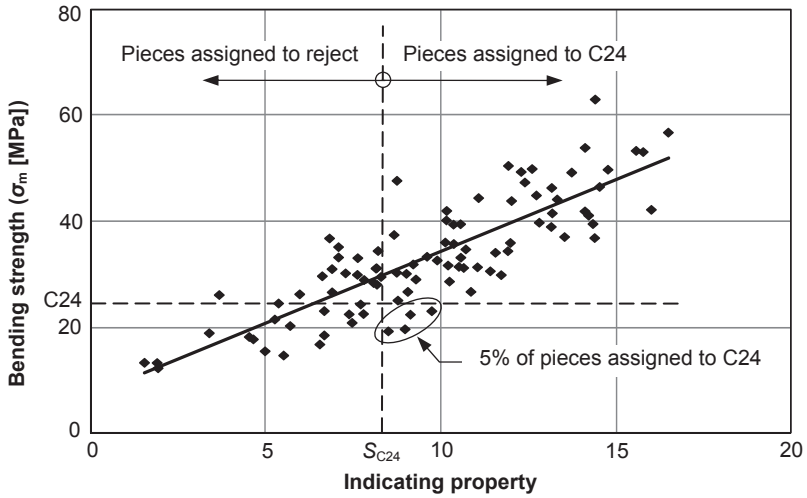

Figure 18. Determination of setting value, S_{C24}, and assignment of grades for a grade combination of C24 and reject.

3.3.2.6 Optimum grades and verification of settings

Verification of models and settings could be described as a course of actions in which the performance of the investigated grading machine is compared with an imaginary machine that is able to perform a perfect grading resulting in each timber piece being graded to its *optimum grade*, *i.e.* the highest possible grade of those for which settings are required. The optimum grade is determined on the basis of the results of the tests described in section 3.3.2.4. This means that the true values of the grade determining properties of each board shall equal or exceed the corresponding characteristic values (*i.e.* 5-percentile values of bending strength and density, respectively, and mean MOE) of the highest possible grade (see EN 338, clause 6.2.2).

Each board in the total sample is arranged in a *Size matrix*, see example in Table 4, which shows to what extent boards are either wrongly up- or wrongly downgraded. The figures in the table indicate the number of boards arranged into each cell of the matrix.

Table 4. Example: Size matrix for a total sample of 900 boards graded to strength classes C30 and C18, and also reject.

Optimum grade	Assigned grade		
	C30	**C18**	**Reject**
C30	300	60	2
C18	16	429	8
Reject	8	12	65

Finally, the numbers of the Size matrix are divided by the total number of pieces in the assigned grade in question and multiplied with weighting factors that are pre-set in EN 14081-2 and dependent on the pieces being either wrongly upgraded or wrongly downgraded. The factors applicable to the former group are more severe than those applied for the latter one, since a wrongly upgraded board may jeopardize the strength of the structure in which it is installed, whereas the consequences of using wrongly downgraded boards are limited to the fact that larger dimensions than necessary are used. The results of the described divisions and multiplications are presented in a *Global cost matrix*. The one achieved on the basis of the Size matrix in Table 4 is exhibited in Table 5.

For settings to be accepted, a number of requirements stated in EN 14081-2 must be fulfilled. A crucial one is that none of the values in the cells of the Global cost matrix that reflect wrongly upgraded pieces must exceed 0.2. In Table 5, these values are shown in ***bold italics*** type. Another requirement is that characteristic values of the grade determining properties of the boards graded to a certain assigned grade shall fulfill the required values for that grade. If requirements are not met, the settings have to be adjusted and the assignment of grades and the procedure of verification of settings repeated. Even if there are no restrictions in EN 14081-2 regarding the cost matrix values representing wrongly downgraded boards (values shown in *italics* in Table 5) they should still be calculated since they represent an indication of the accuracy of the machine.

Table 5. Example: Global cost matrix obtained from the Size matrix shown in Table 4.

Optimum grade	Assigned grade		
	C30	**C18**	**Reject**
C30	0	*0.12*	*0.06*
C18	***0.11***	0	*0.12*
Reject	***0.10***	***0.03***	0

3.3.2.7 Grading of one or several strength classes in a pass: Difference in setting values

According to EN 338, a strength class is defined by 5-percentile and mean values of different stiffness and strength properties and density. The application of 5-percentiles for the grade determining properties bending strength and density means that 5 % of the timber pieces assigned to a certain strength class do not have to fulfill the characteristic values of the class. This means that the setting, or IP value, for a certain class graded by a certain machine type vary depending on whether the class is graded as a single class or if it is graded together with other classes in the same production pass. In Figure 19, the setting/IP for boards graded to C24 as single class is illustrated. All boards for which the IP is larger than the setting, the latter denoted $S_{C24,single}$, are graded to C24. Figure 20 shows settings for C24 and C30 when these classes are graded together. All boards with IP larger than the indicated setting $S_{C30,combi}$ are graded to C30, whereas all boards with IP between $S_{C24,combi}$ and $S_{C30,combi}$ are graded to C24. It is evident that the setting for C24 is more rigorous when C24 is graded together with C30 in comparison with the setting when C24 is graded as single class. This is an effect of the requirement that 95 % of the boards graded to a class have to fulfill the required 5-percentile values. It is also evident that the number of rejects is larger when several strength classes are graded together.

3.3.2.8 ITT-procedure – Improvement potentials

In section 3.3.2.2 it is asserted that there is what may be regarded as a lack of transparency in the ITT procedure as regards the principles of sampling and geographic distribution of sub-samples. A part of the problem could possibly be explained by the terminology that is used in the interrelated standards as regards origin of timber. A number of partly overlapping terms (*e.g.* timber source, source, timber population, source country, source of production, growth area and accepted region) are used. Some of them are defined, but some are not. To understand the difference between many of them is, at least for researchers and engineers not involved in the work of TG1, difficult.

Another example of an issue that deserves to be highlighted is that the concept of settings is given two non-identical definitions; one in EN 14081-1 and another one in EN 14081-2. The terminology applied in the former definition refers to *variable controls*, whereas the latter one lay stress upon the relationship between settings and indicating properties.

As regards the number of sub-samples in a total sample, it is mentioned in section 3.3.2.2 that at least four different sub-samples shall be sampled for derivation of settings for a new machine type, whereas the number required by TG1 is often much larger. On what grounds the required number is determined is, however, not fully transparent. In this context, it should be mentioned that work concerning revision of EN 14081 is ongoing.

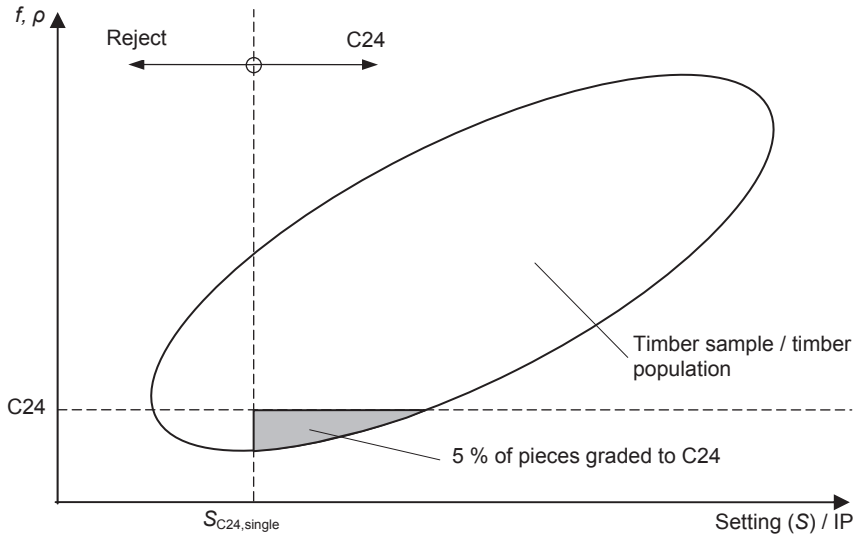

Figure 19. Setting when C24 is graded as single class.

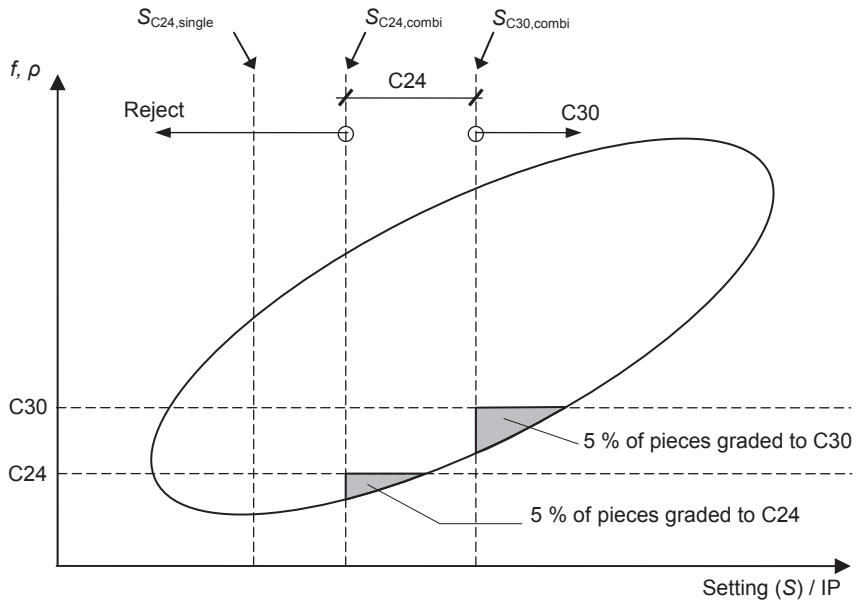

Figure 20. Settings when C24 and C30 are graded together in one pass.

3.4 Grading standards and organizations in USA

In the United States, the *American Softwood Lumber Standard* (ALS 2010) serves a similar purpose as the one of the EN 14081 standard on the European market as regards both visual and machine strength grading, respectively, of sawn timber. In this context, it should be noted that according to the ALS, clause 2.14, *lumber* is defined as *a manufactured product derived from a log through sawing or planing*, which, according to European terminology, is equivalent with *sawn timber*.

The ALS is part of a Voluntary Product Standards Program, which means that it is developed under procedures published by the US Department of Commerce. The purposes of such voluntary standards are to *establish nationally recognized requirements for products and provide all concerned interests with a basis for common understanding of the characteristics of the products* (ALS 2010). The mentioned Standards Program is administered by the National Institute of Standards and Technology (NIST) which acts as unbiased coordinator in the development of the voluntary standards, provides secretarial functions for each committee appointed under the procedures of the Program, and publishes the standards as public documents (ALS 2010).

The committee appointed for development and maintenance of the ALS is the *American Lumber Standard Committee* (ALSC) the membership of which is appointed by the US Secretary of Commerce to constitute a proper balance among producers, distributors and consumers of softwood sawn timber (ALS 2010). The ALCS also approves by-laws and establishes policies under which an affiliated body, the *Board of Review* (Board), function under the ALS. The Board is responsible for *e.g.*

- approval and certification of machines used for machine grading (ALS clause 6.3.2.2),
- accreditation of agencies to supervise production of machine graded timber/lumber, (ALS, clause 10.5), and
- accreditation of rules-writing agencies (ALS, clause 10.5) and certification of grading rules published by such agencies (ALS, clause 10.4).

A rules-writing agency formulates, publishes and maintains grading rules that are suitable for designated wood species under the responsibility of the agency in question (ALS, clause 9.3.1). The various species and conditions prevailing in various parts of North America are covered by the following seven sets of grading rules (publishing agency between brackets):

1. Standard grading rules for Northeastern lumber (Northeastern Lumber Manufacturers Association, NeLMA),
2. Standard grading rules (Northern Softwood Lumber Bureau, NSLB),

3. Standard specifications for grades of California Redwood lumber (Redwood Inspection Service, RIS),
4. Standard grading rules for Southern pine (Southern Pine Inspection Bureau, SPIB),
5. Standard grading rules for West Coast lumber (West Coast Lumber Inspection Bureau, WCLIB),
6. Western lumber grading rules (Western Wood Products Association, WWPA), and
7. Standard grading rules for Canadian lumber (National Lumber Grades Authority, NLGA, Canada).

4 CONTRIBUTIONS OF PRESENT RESEARCH

4.1 Strength grading based on localized stiffness

4.1.1 Relationship between strength and occurrence of knots

From previous research and the results presented in appended Papers II-IV and VI, it is evident that strength of timber pieces is, in general, dependent on the presence of knots. Results from bending tests of structural timber referred to in sections 1.1 and 2.2.2.2 have shown that more than 90 % of fractures in test pieces can be related to the occurrence of knots (Johansson 2003). In consideration of this, it may be found somewhat surprising that the relationship in terms of simple linear regression between strength and various indicating properties based on size and location of knots (*e.g.* TKAR and MKAR as defined in Figure 9) is rather weak.

The inherent contradiction between, on one hand, fractures being dependent on the presence of knots and, on the other hand, the knot measures used up to now being poor predictors of strength can be explained by the fact that a fracture in a timber members is in most cases *not* initiated precisely at an actual knot, but in wood fibres at some distance from it (*e.g.* Nagai *et al.* 2011). During the tests of the sample of timber of nominal dimensions 45×145×3600 mm used in the research presented in Papers II and III, two typical but different failure modes were observed. For stronger members, the first sign of failure appeared as localized compression buckling of fibres close to the compression edge (Figure 21, left). As load increased, these buckling zones grew towards the neutral layer. However, the final failure was most often caused by a tensile failure initiated at inclining fibres close to a knot at the tensile edge. This failure mode, which is rather ductile, is characterized by a splintered appearance on the tensile side of the member with several cracks extended in the longitudinal member direction. A typical example is exhibited in Figure 21 (right). For the sample of 105 boards investigated in Papers II and III, this ductile failure mode was observed in about 20 % of the boards. For weaker members, the failure was often initiated at inclining fibres at a corner

Figure 21. Typical buckling of fibres at compression edge of a board bent in the upward direction (left), and typical subsequent splintered tensile failure (right).

(see Figure 22, left) from which a tensile crack developed, resulting in a rather brittle failure (see Figure 22, right). The two described modes were also observed and analyzed by Boughton (1994).

A common feature of the two modes is that tensile failure is initiated in fibres with an orientation that deviates considerably from the longitudinal direction of the piece. Thus, application of new IPs that not only take account of size and location of knots themselves, but also include effects exerted by surrounding clear wood fibres on structural properties of a timber piece, would be very useful for development of more accurate strength grading models. To be able to define such new IPs, detailed information about both fibre directions around knots and the joint structural behaviour of knots and surrounding fibres is needed. In this doctoral candidate project, two different measurement techniques was applied with the purpose of achieving such information; contact-free deformation measurements and laser scanning of fibre angles.

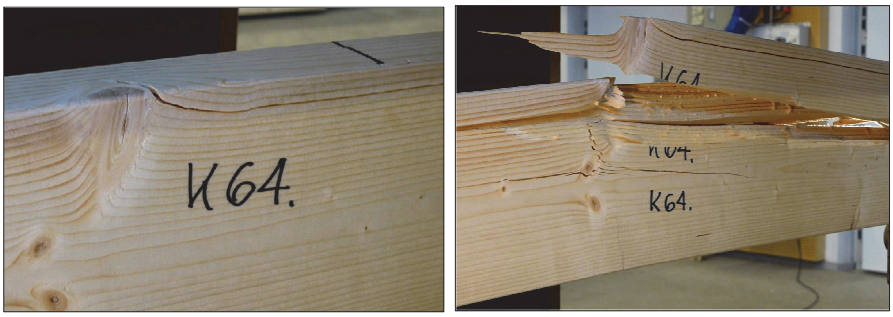

Figure 22. Typical initiation of bending fracture at an outbound arris knot (left) and fully developed fracture (right) in a timber piece of dimension 45×145×3600 mm bent in the upward direction.

4.1.2 Contact-free deformation measurements

4.1.2.1 DIC technique

A contact-free deformation measurement system based on white-light digital image correlation (DIC) was used in this doctoral project. The system was of make ARAMIS^{TM} from GOM mbH, Germany. The technique implies that strain fields occurring on a surface of a timber piece are calculated on the basis of displacements measured at a large number of pre-defined measuring points distributed over the surface. The strains fields, *i.e.* strains in lateral and longitudinal board directions and in shear, are determined and visualized as function of load level. In this research, DIC measurements were applied for determination of strain fields on both local and global level in timber pieces.

4.1.2.2 Strain fields around knots

Local tensile strain fields were determined around knots in a number of boards and test pieces. One such piece of dimensions 45×70×700 mm is shown in Figure 23 (left). It includes a traversing edge knot which is shown in more detail in the bottom row of Figure 24.

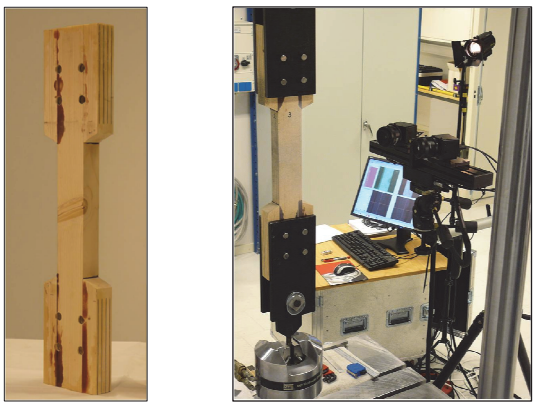

Figure 23. Test piece of dimension 45×70×700 mm with traversing edge knot (left) and test set-up for contact-free deformation measurements (right).

The strains occurring under load on the four surfaces of the piece are visualized in Figure 24 by means of two ARAMIS post-processing tools denoted *contour plots* and *section diagrams*. A *contour plot* means that the strain distribution that occurs in longitudinal or lateral board direction or in shear over a measured surface is visualized, for a certain load stage, on the basis of a defined colour scaling. An example of longitudinal strains determined for the piece in question is shown in the top row of Figure 24. By means of the *section diagrams* tool, more detailed strain information can be obtained on a local scale. A section is defined as a line with fixed coordinates

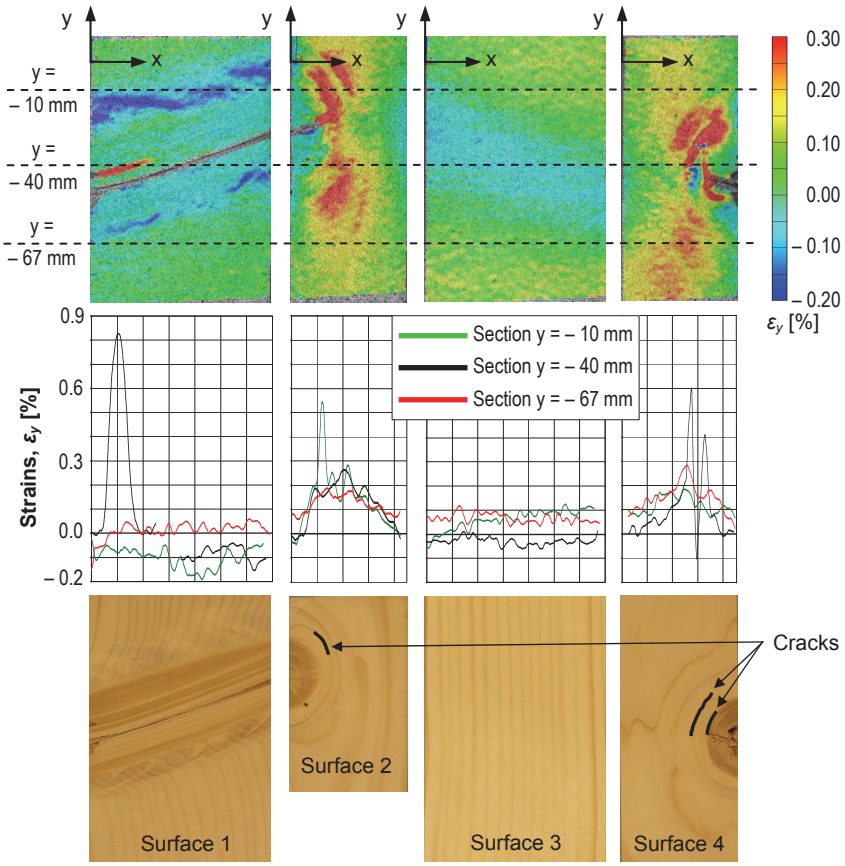

Figure 24. Longitudinal tensile strains (ε_y) in edge knot piece. Top row: Strain fields. Middle row: Strains along defined sections (dashed lines in top row). Bottom Row: Identified cracks.

in camera images and the strains and displacements along such lines can be exhibited in section diagrams.

The strains shown in Figure 24 correspond to a tension load of 30 kN. In the top row, three defined sections are exhibited as dashed lines and the strains along these are displayed in the diagrams of the middle row. Three distinct tensile peaks are found on Surfaces 2 and 4 and they correspond to cracks indicated in the bottom row. In strength testing, such cracks will most likely serve as indications of fracture. They were identified by use of a pocket lens since they could not be seen by the naked eye. The strain peak in the diagram of Surface 1 was caused by displacements at a crack within the knot, visible even before the testing was begun. It is shown as a thick red stripe in the top row of Figure 24. Furthermore, in the contour plots it can also be seen that the largest tensile strains arose in fibres just outside the knot, *i.e.* in those fibres

where, according to the account in section 4.1.1, the failure is expected to be initiated.

The strain fields exhibited in the contour plots were compared with those obtained from finite element (FE) calculations. The correspondence was surprisingly good, in spite of the fact that the utilized FE models were fairly simple.

4.1.2.3 Strains along narrow side boards

Tensile strain fields occurring along flat surfaces of nine of the split side boards included in the third sample described in section 1.4 were investigated, see Paper III. The total length of each of these boards was 3000 mm, but since 750 mm at each end were hidden by the grips of the tensile testing machine, the strain fields were only measured over the remaining 1500 mm. The cross-sectional dimension of the boards was 25×56 mm and boards with similar dimensions were utilized as laminations in the research concerning wet-gluing of laminated beams presented in Papers IV and V. Results from one of the tested boards, board no. 28B, are exhibited in Figure 25. It is clearly shown to what extent the presence of knots affect the behaviour of the board. The most conspicuous observation is that the reduction of longitudinal stiffness at a knot is very local. According to Figure 25d, the length of reduction can be estimated to about 50 mm for the board in question, in which the maximum knot size was 15 mm. An interesting comparison can be made with the required length over which a local tensile stiffness in terms of MOE parallel to the grain shall be measured according to EN 408. The stipulated length is five times the board's width, which for the board shown in Figure 25a corresponds to a measurement length of 280 mm. Thus, it can be concluded that a local MOE measured in accordance with EN 408 will overestimate the localized stiffness at critical knots in narrow boards, since the measurement length will include parts of the board in which the stiffness is unaffected by the presence of the critical defect. In previous research works, it has been shown that a similar overestimation of localized MOE also occurs for timber of typical structural dimensions that is tested in bending (*e.g.* Foschi 1987). Furthermore, since stiffness in terms of MOE is correlated with strength, it is well known that such overestimation has a negative influence on the correlation, whereas, as a consequence, the relationship will be improved if MOEs determined on a very local scale is applied (*e.g.* Boughton 1994).

Another observation made from the measurement results displayed in Figure 25c is that displacements perpendicular to the direction of applied load occur, revealing an uneven stress distribution over the board cross-section. The displacements were clearly visible with the naked eye. The maximum edgewise displacement was about 1.5 mm, see Figure 25c, and distinct peaks or irregularities coinciding with knots can be observed on the displacement curves.

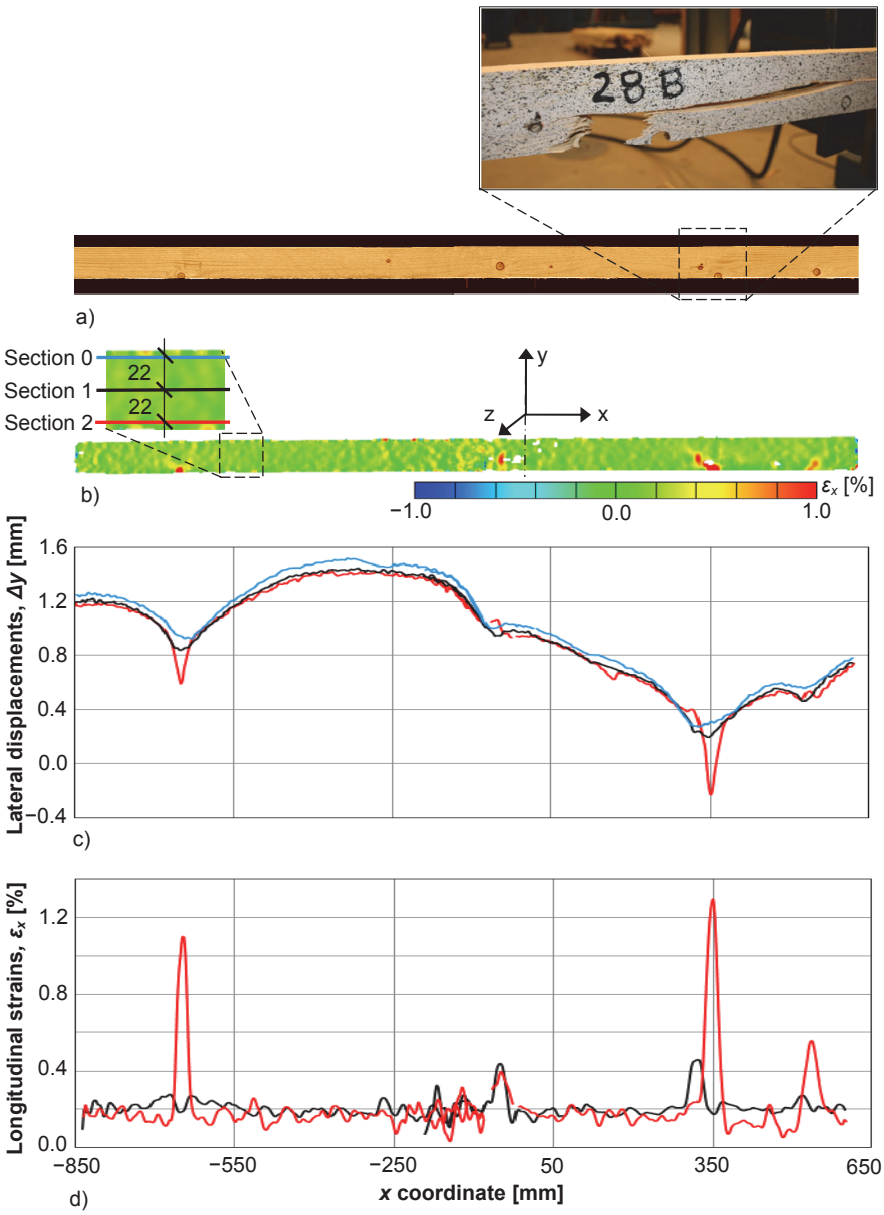

Figure 25. Displacements and tensile strains in a board of dimension 25×56 mm: a) measured flat surface and board fracture, b) longitudinal strains, ε_x, sections and origin of coordinate system, c) lateral displacements, Δy, in edgewise board direction along sections 0-2, and d) longitudinal strains, ε_x, along sections 1-2 (see Paper III).

4.1.3 Laser scanning of fibre angles

The relationship between grain deviating from the longitudinal direction of a timber piece and structural properties of the same piece has been discussed in section 2.2.2.3. Fibre inclination implies that the structural performance is severely impaired which is the reason why bending and tensile fractures, respectively, in timber members are frequently initiated in fibres oriented in a direction that deviates from the longitudinal direction of the piece. From the research referred to in section 2.2.2.3, it is evident that information about local grain angles measured with high resolution has a great potential as regards development of more accurate strength grading methods.

Detailed information about the variation of fibre directions on the surface of a timber piece can be obtained by application of dot laser illumination and simultaneous tracheid effect scanning. A WoodEye scanner, see Figure 4, was utilized for this purpose. By application of four sets of dot lasers and cameras, fibre angles projected on the four longitudinal surfaces of scanned timber pieces applied in the research presented in Papers II-IV and VI were measured. The scanning resolution varied somewhat between the samples. On average, the longitudinal resolution was about 1 mm, whereas the lateral was about 4 mm. Detailed scanning information is found in the papers referred to. The mentioned fibre angle projection on the surface means that the diving angle, *i.e.* the angle between the board surface and the direction of the wood fibres, is not regarded.

A typical result of tracheid scanning is shown in Figure 26. Each dash indicates the two-dimensional direction of the major axis of a measured laser dot, which, due to the tracheid effect, has adopted an elliptic shape. It can also be observed that the dashes within the knot are randomly directed, due to the fact that the fibre direction within the knot in reality is more or less perpendicular to the displayed surface.

The direction of each dash and its coordinates in both longitudinal and lateral board direction are identified in coordinate systems that are defined in the camera images taken by the WoodEye cameras. The directions and coordinates are subsequently documented in text files that can be obtained from the Wood Eye scanner.

4.1.4 New machine grading method based on localized MOE

4.1.4.1 Determination of localized MOE: Previous research

Ever since the first grading machines based on flatwise bending over span lengths of about 0.9 to 1.2 meters were introduced during the first half of the 1960s, it has been well known to researchers that the correlation between strength and measured MOE is dependent on the length over which MOE is determined. One of the first papers in which this state of things was discussed was presented by Corder (1965), who had found that a minimum localized

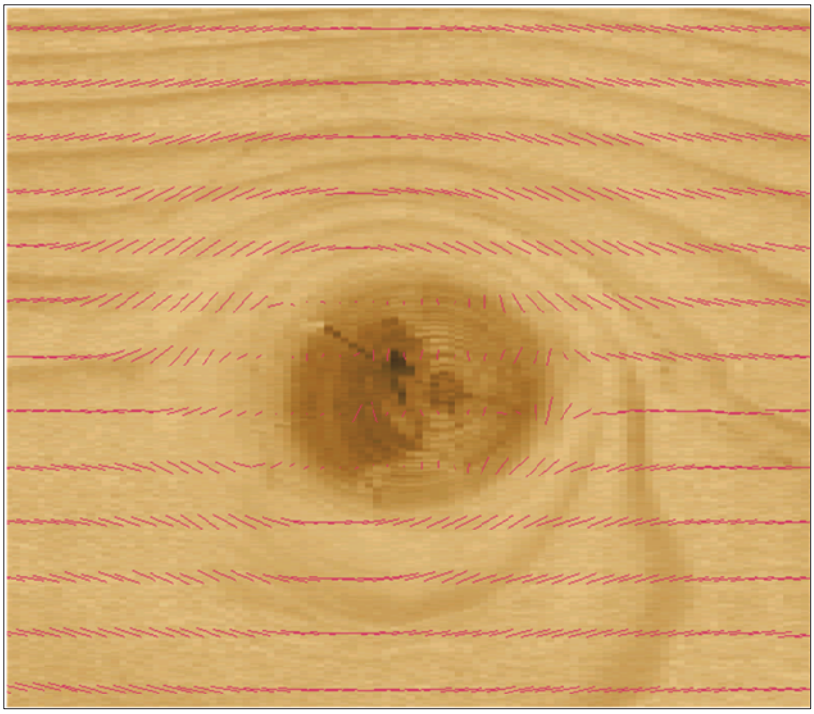

Figure 26. Fibre directions, measured on the basis of dot laser illumination and tracheid effect scanning, around a traversing knot (ϕ=16 mm) in a board of dimension 19×95 mm.

MOE correlated more closely with bending strength than did MOE determined on the basis of four-point bending over the entire length of investigated members. The reason for this is that MOE, when determined as an averaged or smoothed value over a certain span, is higher than the lowest localized value found within the same span. This issue was discussed in section 4.1.2.3.

Over the years, large research efforts have been made to develop methods and techniques for the purpose of determining high-resolution MOE distribution along timber members. Parts of this extensive work are described in Paper III. Yet, to the knowledge of this author, none of the investigated techniques has found its way to the market, mainly due to the fact that MOE determination over very short spans is dependent on accurate measurement of deformations that are small, which means that they tend to be biased by measurement noise (*e.g.* Foschi 1987).

4.1.4.2 New machine grading method

The results obtained from DIC measurement and tracheid effect scanning described in sections 4.1.2 and 4.1.3, respectively, have been utilized in the development of a new method for machine strength grading based on the

relationship between localized MOE with very high resolution and bending strength. The method, in which Bernoulli-Euler beam theory is utilized, is described in detail in Paper II. Like most of the machines described in section 3.2, it includes application of average longitudinal MOE values determined on the basis of axial dynamic excitations, board density and board length. It is, however, different from today's grading techniques in important aspects. It takes account of local fibre direction detected on the surfaces of a timber piece and measured using the scanning technique described in section 4.1.3. By combining information about average axial MOE and fibre direction, local MOE on the surfaces of a timber piece can be calculated with a resolution that corresponds to the tracheid effect measurements shown in Figure 26. On the basis of a model for integration over cross-sections, stiffness variation in terms of edgewise bending (*EI*) and axial stiffness (*EA*), respectively, can then be determined along the board. New IPs can be defined as the lowest bending MOE and the lowest axial MOE, respectively, found along the piece. The IP based on edgewise bending stiffness is calculated as

$$IP_{E,edgewise} = \frac{EI \cdot 12}{b \cdot h^3} \tag{16}$$

and the IP based on axial stiffness is equal to

$$IP_{E,axial} = \frac{EA}{b \cdot h}. \tag{17}$$

It should be mentioned that the application of the new grading method is protected by a national Swedish patent (Innovativ Vision AB 2014).

4.1.4.3 Application of the new grading method on two homogeneous samples

The novel IPs presented in Equations (16-17) were applied to the second and third samples of timber described in section 1.4, *i.e.* the sample of 105 boards of plank dimension 45×145×3600 mm (called the plank sample in the following), and the sample of side boards which were split and cut into 116 boards of dimension 25×56×3000 mm. Strength and local stiffness of both samples were determined according to EN 408, but for different load cases. The planks were tested in edgewise bending, whereas the side boards were tested in tension. An important issue was on what local scale the new IPs should be determined. For both samples, the spatial resolution of scanned fibre angles was 0.8 mm in the longitudinal direction of the members, which meant that the IPs could be calculated with corresponding resolution. However, since critical knots or groups of knots have an extension in the longitudinal direction of a piece, moving average values of bending and axial MOE, respectively, were also calculated over different length intervals along the pieces.

The results of the application of the IPs on the plank sample are presented in Figure 27. The strongest coefficient of determination, amounting to R^2=0.68, between stiffness and bending strength was achieved for the IP represented by a moving average of the lowest bending MOE determined over an interval of about 90 mm. The highest R^2 value between lowest axial MOE and bending strength was 0.65 obtained for an interval of about 70-75 mm, see Figure 27, which is equivalent with half the width (or depth) of the planks.

Another important observation made on the basis of Figure 27 is that the R^2 value achieved for a moving average interval of 725 mm, *i.e.* a length equivalent with five times the board width which is the length over which local MOE in bending shall be determined according to EN 408, is considerably lower than the maximum R^2 value exhibited in the figure. This is in agreement with the discussions in sections 4.1.2.3 and 4.1.4.1 regarding the decrease of correlation between strength and MOE that occurs when a localized MOE is replaced by an MOE averaged over a certain length.

For comparison, the frequently applied coefficient of determination between axial *dynamic* MOE and bending strength was also calculated and was found to be R^2=0.59. Thus, by application of the new grading method, a considerable increase of R^2 was achieved. The improvement was of the same order as the one observed by Bacher (2008), see section 3.2, when R^2 was based on an IP combination of axial dynamic MOE and X-ray scanned knot measures rather than on the basis of axial dynamic MOE as single IP.

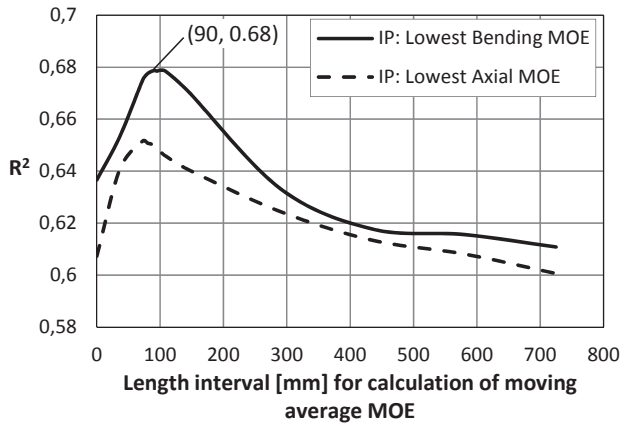

Figure 27. Relationship between length interval for calculation of moving average MOE (x-axis) and R^2 between bending strength and the lowest moving average MOE (y-axis) for planks of dimension 45×145×3600 mm (see Paper III).

For the sample of side boards, the IP application results are exhibited in Figure 28. In spite of the fact that the boards were tested in tension, the strongest relationship (R^2=0.77) between the IPs and strength was found for the lowest *bending* MOE determined as a moving average over a length

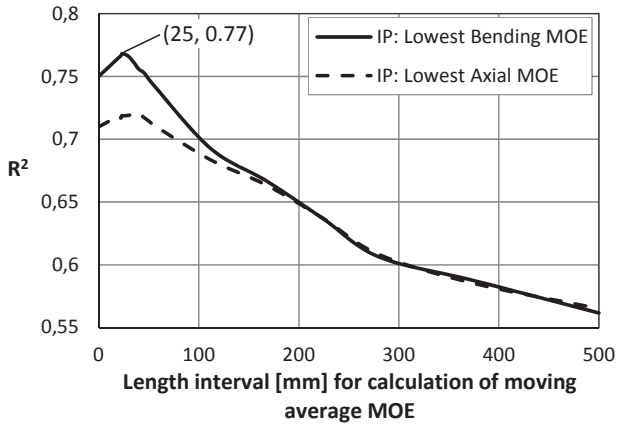

Figure 28. Relationship between length interval for calculation of moving average MOE (x-axis) and R^2 between tensile strength and the lowest moving average MOE (y-axis) for side boards of dimension 25×56×3000 mm (see Paper III) .

interval of about 25 mm, *i.e.* an interval of about half the board width. The reason why the largest R^2 was achieved for the IP based on *bending* stiffness, although the boards were tested in tension, is probably the fact that edge knots cause an uneven stress distribution over the cross-section resulting in edgewise displacements, as discussed in the last paragraph of section 4.1.2.3 and shown in Figure 25c for one of the boards in the sample. The coefficient of determination between tensile strength and axial *dynamic* MOE was found to be R^2=0.52 (see Paper VI in which the side board sample was applied for the purpose of investigating the possibility of grading narrow boards in a wet state by means of axial dynamic excitation).

In Figure 29, the edgewise bending MOE determined by means of the new strength grading method is shown for the entire length of side board no. 28B, *i.e.* the same board the mid part of which is shown in Figure 25a. Detail 1 in Figure 29a shows scanned fibre directions around the knot at the critical section located about 1 meter from the root end of the board. Corresponding longitudinal MOE variation is displayed in Detail 2, in which the reduction of longitudinal MOE in the knot and in the vicinity of the same is clearly visualized. The edgewise bending MOE variation exhibited in Figure 29b was calculated for a moving average length interval of 25 mm, *i.e.* the optimum length interval according to Figure 28. The strong correspondence between the positions of knots and distinct dips in the graph should be noted. It also deserves to be mentioned that the failure of board no. 28B did not occur at the critical section, but at the second deepest dip in the MOE graph, *i.e.* at the two knots located about two meters from the root end. The actual failure is shown in Figure 25a. It should also be noted that the horizontal line at MOE level of

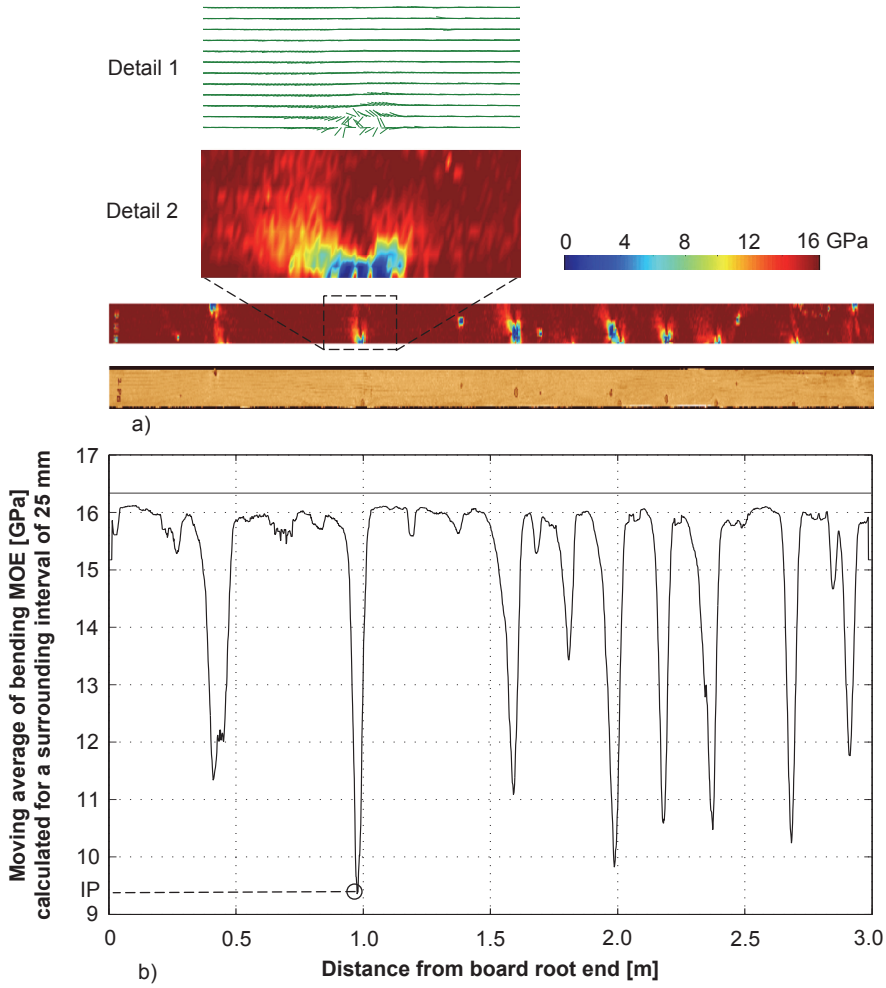

Figure 29. a) Image of flatwise surface of board no. 28B and contour plot of calculated longitudinal MOE variation (exaggerated width in both image and contour plot). Detail 1: Scanned fibre directions at critical section. Detail 2: Longitudinal MOE variation at critical section. b) Variation of moving average of edgewise bending MOE, determined over a moving average length interval of 25 mm, and indicated value (about 9.4 GPa) of the indicating property.

about 16.3 GPa in Figure 29b represents the MOE that would have been achieved if all the fibres had been oriented in the longitudinal board direction.

4.1.4.4 Application of the new strength grading method on a larger mixed sample

The graph presented in Figure 27 shows that the strongest relationship between bending strength for the investigated plank sample (dimension 45×145×3600 mm) and the new IP for edgewise bending was obtained for a moving average MOE calculated over a length interval of about 90 mm. A similar result has recently been achieved within the scope of an ongoing research project carried out in co-operation between Linnæus University, the SP Technical Research Institute of Sweden, two machine manufacturers and three sawmilling companies. The research concerns a timber sample consisting of three subsamples from different parts of Sweden, each including timber of different dimensions.

The total number of investigated boards is about 450 and the dimensions are typical for structural timber. The boards were planed at one of the participating sawmill's planer mill, and the first axial resonance frequency of each board was determined using a Precigrader (Figure 15) installed in the same mill. Fibre angle scanning was then performed at Linnæus University, Växjö, using a WoodEye scanner, model v5 (Figure 30). On the basis of the results from scanning and Precigrader excitation, IP values based on edgewise bending were calculated on the basis of the new strength grading method. The boards were finally tested according to EN 408 in SP's laboratory in Borås.

At the time of writing, analysis of the test results is ongoing and what has been found so far indicates that the largest R^2 values are obtained, more or less irrespective of the investigated board dimensions, for moving average IPs calculated over a length interval of somewhat less than 100 mm. This measure is of similar order as the extension in longitudinal board direction of typical knot clusters of Norway spruce.

Figure 30. WoodEye scanner model v5.

4.2 EWP development using side board laminations

4.2.1 Properties of side boards

Already in the last paragraph of section 1.1, it was mentioned that glulam is a product that combines the EWP concept of gluing with strength grading of solid timber members. Since 2006, Linnæus University and the SP Technical Research Institute of Sweden have conducted research regarding development and manufacturing of wet glued glulam beams made up of laminations of Norway spruce side boards, *i.e.* boards of narrow dimensions cut from the outer parts of a log. The research has been carried out in close co-operation with the Södra Timber AB, which is one of the leading sawmill companies in Sweden.

For a typical Norway spruce sawmill in the south of Sweden, side boards account for about 30 % of the volume of sawn timber. The combination of large production volumes and small dimensions result in large numbers of pieces that have to be handled in the sawmill process. Another consequence of the small dimensions is that side boards are unsuitable for structural applications. Instead, they are used as raw material for low value products such as tongued and grooved boards and loading pallets. Large volumes and low value imply that side board production results in poor profitability. However, in section 2.2.1 it was mentioned that the value of several structural properties such as stiffness and density increase considerably in the direction from pith to bark. The main purpose of the research introduced in the previous paragraph was to utilize the properties of side board for development of wet glued glulam beams with high performance. Issues that have been investigated are *e.g.* properties of bond lines and finger joints, respectively, and structural performance of glued beams. A summary of the research results are presented in Papers IV-VI. Further details about the findings have been presented by Serrano *et al.* (2011) and Sterley (2012).

4.2.2 Wet gluing of side boards

Wet gluing of side boards is expected to result in a more cost efficient production process compared with the one that is applied when the boards are dried before gluing. The differences between the two processes are visualized in Figure 31. When, as in the dry gluing process, boards are dried their cross-section will enter a cup shape, which means that planing is needed before flat gluing into beams. Due to the narrow board dimensions, such planing will cause a considerable reduction of the sawing yield. Furthermore, board end cracks will appear due to the fast drying in the fibre direction at board ends. Thus, trimming is required, which results in further reduction of the yield.

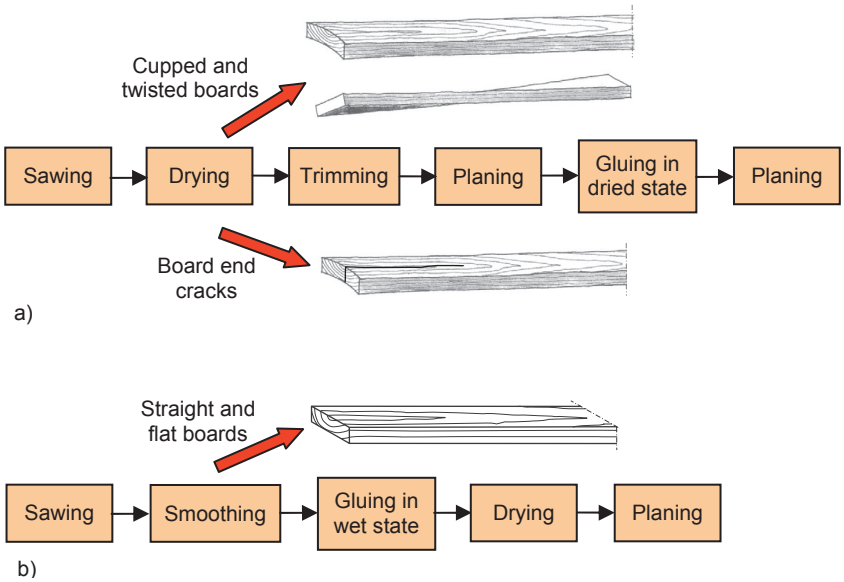

Figure 31. Processes for manufacturing of glulam beams made up of side board laminations. a) "Dry gluing" – gluing after drying, and b) "Wet gluing" – gluing before drying (Serrano et al. 2011).

The process of wet gluing is based on straight and flat boards for which only smoothing is needed, *i.e.* the flat surfaces of a board are rendered plane-parallel by "light" planing. However, the material loss caused by such machining is much less compared with the loss that planing of cupped boards will produce. Another important benefit of wet gluing of side boards is that the gluing of narrow laminations into beams early in the process will reduce the number of individual pieces that have to be handled through the entire sawmill production. Wet gluing can also imply energy savings, since it can be performed at room temperature, whereas dry gluing requires pre-heating or warm-pressing. Drawbacks of wet gluing is that the lead time between cutting of logs and gluing of boards must be short, since the surfaces that are to be glued must not be allowed to dry. Another obstacle is that investments in new production plants are needed since, as shown in Figure 31, the logistics of wet gluing and dry gluing, respectively, are very different.

4.2.3 Strength grading of wet side boards

As described in the last paragraph of section 1.1, products of glulam combine the concepts of EWPs and strength grading of solid timber members. The latter is used to optimize the utilization of the raw material such that laminations with high stiffness are used in the outer parts of the cross-section of glulam members, whereas laminations with limited performance are placed

in the inner zone, closer to the neutral layer. However, strength grading has traditionally been carried out after drying, *i.e.* for timber members with a moisture content typically varying between 12-20 % MC. However, for undried Norway spruce timber, the MC varies from the fibre saturation point of about 30 % MC up to moisture contents over 150 %. Since the described research concerned wet gluing of side boards, the issue of strength grading in a wet state was raised. The purpose of the investigation presented in Paper IV was to evaluate the possibility of grading undried narrow side boards by means of the grading technique based on axial dynamic excitation. It was concluded that strength grading in a wet state was just as reliable as grading carried out after drying, provided that the actual wet board density was regarded when the axial dynamic MOE was determined. It should be noted that the investigation on which Paper IV is based was carried out already in 2009. Since then, several strength grading machines have been approved for strength grading of wet timber members.

4.2.4 Performance of wet glued beams

In Paper V, results from testing of more than 100 beams manufactured by face gluing of side board lamination is presented. The laminations were 21-25 mm thick and 120-125 mm wide. The beams were glued using a one-component moisture curing polyurethane adhesive approved for manufacturing of structural wood members glued in a dried state. After gluing, the beams were split, dried and planed to final cross-sectional dimension 50×300 mm. A typical beam lay-up is found in the introduction of Paper VI. Beams composed of ungraded as well as graded laminations were investigated and compared. The grading criteria were fairly simple. Beams made up of graded laminations consisted of 15 laminations, and for the outermost three laminations at each edge, it was required that the axial dynamic MOE should be larger than 12000 MPa and that the maximum wide face knot size should be less than 25 mm. For the remaining nine inner laminations, no criterion was set on the maximum knot size, whereas the axial dynamic MOE was set to be between 7000 and 12000 MPa. Here, it should be noted that the MOE requirements referred to laminations in a wet state, *i.e.* with MC above the fibre saturation point. Since there is negative relationship between MC and MOE for MC below the fibre saturation point (Dinwoodie 2000), the MOE of the laminations increased during kiln drying.

Bending tests based on EN 408 of beams with lay-up in accordance with the described grading scheme showed that high structural performance can be achieved. The tests gave as result a bending strength with a 5-percentile characteristic value of 40.1 MPa, combined with a mean local MOE of 14360 MPa. A further observation was that the strength variation in terms of coefficient of variation of the beams was considerably reduced when graded laminations were introduced.

4.2.5 Optimized finger jointing of side board laminations

To improve the structural properties of the wet-glued beams even further, the issue of defect elimination in outer laminations was raised. The strength of such narrow laminations as those used in the split beams described above is even more dependent on the occurrence of large knots than what is the case for structural timber of dimensions representative for centre yield. Support for such a statement can be obtained by a comparison of strength and stiffness properties of the second (105 boards of plank dimension 45×145×3600 mm) and third (116 split boards of dimension 25×56×3000 mm) samples described in section 1.4, even if, firstly, the sampling of the two samples were not coordinated and, secondly, the applied strength tests differed between them. The results exhibited in Table 6 indicate that the strength of the boards was considerably lower and more scattered than for the planks. As regards average axial dynamic MOE, the results in the two investigations were similar.

Table 6. Mean values, standard deviations and coefficients of variation for axial dynamic MOE and strength of the second (105 planks of dimension 45×145×3600 mm) and third (116 split boards of dimension 25×56×3000 mm) timber samples described in section 1.4.

Sample	Axial dynamic MOE			Strength		
	Mean [GPa]	Stand.dev. [GPa]	CoV [%]	Mean [MPa]	Stand.dev. [MPa]	CoV [%]
Boards, (25×56×3000)	13.04	2.93	22.5	24.8[1]	13.5	54.4
Planks, (45×145×3600)	12.4	2.6	21	38.4[2]	12.9	33.6

1. Tensile strength according to EN 408.
2. Bending strength according to EN 408.

If large knots in narrow side boards are eliminated by means of finger jointing, a considerable improvement of the strength may reasonably be expected. For the purpose of verification of this assumption, the investigation described in Paper VI was carried out. The fourth sample described in section 1.4 was utilized. Initially, it included 51 side boards of dimension 25×125×4800 mm. Each of these were split into two boards, one randomly assigned to a group of boards for which defects were to be eliminated by means of finger jointing, and the other one assigned to a reference group of non-jointed boards. The number of joints to be inserted was determined on the basis of an assessment of sawmill costs incurred by such processing. Here it was decided that an average distance of 2.4 m between the joints was reasonable, implying that a total of 102 finger joints were to be distributed along the boards selected for jointing. The defects to be removed were identified using profiles of edgewise bending determined on the basis of the new strength grading method described in Paper II and summarized in section

4.1.4.2. After finger jointing, all 102 boards were planed and cross-cut to dimension 21×57×3885 mm and finally tested in tension in accordance with EN 408. It was found that the average strength of the finger jointed boards was about 36 % higher than the corresponding strength of the boards in the reference group, whereas the increase of local tensile MOE was about 6 %.

4.3 Conclusions

The primary purpose of this doctoral candidate project was to initiate a development towards more accurate methods for machine strength grading of structural timber. The research has included application of different measurement techniques, analysis of structural behaviour of timber pieces on both local and global level, strength tests in both bending and tension, development of algorithms for a new strength grading method, verification of the usefulness of the new method as regards different board dimensions, and development of EWPs on the basis of machine strength grading and optimized defect elimination of laminations. The most important conclusions can be summarized as follows:

- The contact-free deformation measurement technique based on digital image correlation provides researchers with a tool by which the behaviour of wood pieces subjected to loading can be analyzed on both a global and a very local level. Such analyses provide substantial information about the structural behaviour of wood and knowledge about strains occurring at and around knots. The technique is an excellent means to be used for verification and calibration of finite element models.
- Stiffness variations along timber pieces can be determined on the basis of dot laser scanning of local fibre angles projected on board surfaces. In combination with board density and average axial dynamic MOE, such information can be utilized for calculation of local MOE variation in longitudinal board direction with a resolution that corresponds to scanned fibre angles.
- Strength grading results that are more accurate than those achieved by grading machines of today can be obtained by application of a new strength grading method based on the relationship between stiffness determined on a very local scale and strength. Preliminary results indicate that optimum accuracy is reached for stiffness measures determined as moving average values calculated over length intervals of similar order as length of knot clusters.
- By means of wet gluing of side board laminations, glulam beams with high performance can be achieved from sawn products that are traditionally considered to be of low value. To be able to optimize the use of the lamination material, the possibility of grading side boards

in a wet state by means of axial dynamic excitation and weighing was investigated. It was found that such grading gives just as accurate results as grading carried out after drying.

- To improve the strength of side board laminations to be used in the wet glued glulam beams, algorithms of the new strength grading method described above can be applied for identification of weak sections to be eliminated by means of finger jointing. Such measures will have a significant effect on the performance of the laminations.

4.4 Future work

The starting point of this doctoral candidate project was the rather poor relationships between indicating properties and strength on which today's strength grading methods are based. As a consequence, many timber pieces are downgraded into strength classes with characteristic bending strength that is much lower than the actual strength of the pieces. It is the hope of this author that some of the findings presented in this thesis will be of benefit for the wood working industry. However, there are a number of issues related to the presented research that deserves to be further investigated.

Possibilities of developing the new strength grading method presented in Paper II should be considered. There are at least three measures that may contribute to improvement. The first one concerns the tracheid effect scanning of fibre angles. Currently, the new method utilizes two dimensional fibre angles that are obtained on board surfaces as a result of the projection of three-dimensional fibre directions. It can be assumed that knowledge about and application of the diving angle, *i.e.* the angle between the plane of the board surface and the 3D fibre direction, will considerably improve both the accuracy of calculated local stiffness and, consequently, also the relationship between this stiffness and board strength. The possibility of identifying the diving angle by means of optical laser scanning is therefore an interesting research task to address. The second measure also relates to dot laser scanning. The scanning that has been applied in this doctoral project has been made with a resolution, *i.e.* distance between laser dots, of about four mm in the lateral direction of scanned pieces. The effect that a doubled lateral resolution would have on the relationship between locally determined stiffness and board strength would be interesting to examine, for boards of narrow dimension in particular. The third conceivable improvement concerns the applied beam model based on Bernoulli-Euler beam theory. According to research presented by Hu (2013), this model can properly predict the beam stiffness at knot clusters in which the knots are located closely together in the longitudinal direction of the board, whereas predictions regarding clusters in which the knots are spread out are rather poor. Thus, development and

application of alternative models would be an interesting research task for the future.

The opportunities of utilizing the new strength grading method for development and optimization of high strength engineered wood products are deemed to be of great interest. Since the new method provides high resolution information about stiffness variation along timber members, it is, as shown in Paper VI, highly appropriate for optimization of defect elimination by means of finger jointing of timber pieces, narrow glulam laminations in particular. The obvious next step is to investigate to what extent defect elimination of such laminations will influence the strength and stiffness of glulam beams. Another possibility to evaluate is if defect elimination based on localized stiffness information can be applied for upgrading rejects to C-classed timber.

There are several further possibilities of using the information obtained from optical fibre angle scanning for industrial purposes. One such area to probe into is to what extent such information can be of use for detection of serious defects such as top ruptures.

An objective to be aimed at in a long-term perspective is development of strength grading methods based on the actual fracture behaviour of individual timber pieces. The research idea is basically that the strength of a board can be accurately predicted by means of finite element analyses using models designed on the basis of scanned fibre angle information, relevant timber properties and fracture mechanics.

5 REFERENCES

5.1 Standards and other normative documents

ALS (2010), *American Softwood Lumber Standard*. Voluntary Product Standard PS 20-10, US Department of Commerce, Washington, DC.

Anon (1981) *Instruktioner för sortering och märkning av T-virke (Instructions for grading and marking of T-timber)*. Board of the T-timber Association (in Swedish).

Anon (2012) *Guidelines for sampling a growth area for deriving machine settings.* 5th DRAFT, 30 May. European Committee for Standardization / TC 124 / TG1.

Anon (2014a) *Timber structures – Strength graded timber – Test methods for structural properties.* International Standard, Final draft, ref. no. ISO/FDIS 13910:2014(E). International Organization for Standardization.

Anon (2014b) *List of approved machines*. American Lumber Standard Committee, Germantown, MD. http://www.alsc.org/untreated_machinegraded_mod.htm. (12 March 2014).

DIN 4074-1 (2012) *Sortierung von Holz nach der Tragfähigkeit – Teil 1: Nadelschnittholz (Strength grading of wood – Part 1: Coniferous sawn timber)*. DIN – Deutsches Institut für Normung.

BS 4978 (2007) *Visual strength grading of softwood – Specification*. British Standards Institution.

EN 338 (2009) *Structural timber – Strength classes*. European Committee for Standardization.

EN 384 (2010) *Structural timber – Determination of characteristic values of mechanical properties and density*. European Committee for Standardization.

EN 408 (2010) + A1 (2012) *Timber structures – Structural timber and glued laminated timber – Determination of some physical and mechanical properties*. European Committee for Standardization.

EN 1611-1 (1999) + A1 (2002) *Sawn Timber – Appearance grading of softwoods – Part 1: European spruces, firs, pines and Douglas firs*. European Committee for Standardization.

EN 1912 (2012) *Structural Timber – Strength classes – Assignment of visual grades and species*. European Committee for Standardization.

EN 1995-1-1 (2004) + A1 (2008) *Eurocode 5: Design of timber structures – Part 1-1: General – Common rules and rules for buildings*. European Committee for Standardization.

EN 14081-1 (2005) + A1 (2011) *Timber Structures – Strength graded structural timber with rectangular cross section – Part 1: General requirements*. European Committee for Standardization.

EN 14081-2 (2010) + A1 (2012) *Timber structures – Strength graded structural timber with rectangular cross section – Part 2: Machine grading; additional requirements for initial type testing*. European Committee for Standardization.

EN 14081-3 (2012) *Timber structures – Strength graded structural timber with rectangular cross section – Part 3: Machine grading; additional requirements for factory production control*. European Committee for Standardization.

EN 14081-4 (2009) *Timber structures – Strength graded structural timber with rectangular cross section – Part 4: Machine grading – Grading machine settings for machine controlled systems*. European Committee for Standardization.

Innovativ Vision (2014) *A method and device for evaluating a wooden board (Förfarande och anordning för utvärdering av en bräda av trä)*. Swedish Patent, Patent No.: 536623, 2014-04-08.

INSTA 142 / SS 230120 (2010) *Nordic visual strength grading rules for timber.* Inter-Nordic standardization, Swedish Standards Institute (in Swedish).

5.2 Scientific publications and books

Aichholzer, A., Arthaber, H., Schuberth, C., Mayer, H. (2013) *Non-destructive evaluation of grain angle, moisture content and density of spruce with microwaves*. European Journal of Wood and Wood Products, 71:779-786.

Bacher, M. (2008) *Comparison of different machine strength grading principles*. In: Proceedings of 2nd Conference of COST Action E53 – Quality control for wood and wood products, Delft, the Netherlands, October 29-30.

Baumann, R. (1922) *Die bisherigen Ergebnisse der Holzprüfungen in der Materialprüfungsanstalt an der Technichen Hochschule Stuttgart (Available wood testing results achieved at the Materials Testing Institution, Technical College, Stuttgart)*. Forschungsarbeiten auf dem Gebiete des Ingenieurwesens, Heft 231, Berlin, Germany (in German).

Beall, F. C. (2002) *Overview of the use of ultrasonic technologies in research on wood properties.* Wood Science and Technology, 36:197-212.

Bechtel, F. K., Allen, J. R. (1987) *Methods of implementing grain angle measurements in the machine stress rating process.* In: Proceedings of the 6th Nondestructive Testing of Wood Symposium, Washington State University, Pullman, WA, USA, September 14-16, pp. 303-353.

Betzhold, D. (1999*) Maschinelle Festigkeitssortierung. Einfluss der Hochtemperatur-trocknung auf die elastomechanischen Eigenschaften des Schnittholzes (Machine strength grading. Influence of high-temperature drying on elastomechanical properties of sawn timber)*. Diplomarbeit, Fachhochschule Eberswalde, Germany (in German).

Blass, H. J., Gard, W. (1994) *Machine strength grading of timber*. In: Proceedings of the Pacific Timber Engineering Conference, Gold Coast, Australia, July 11-15.

Blass, H. J., Frese, M. (2004) *Sortierverfahren für die kombinierte maschinelle und visuelle Festigkeitssortierung* (*Combined visual and machine strength grading*). Holz als Roh- und Werkstoff, 62:325-334 (in German with abstract in English).

Blom, G. (1970) *Statistikteori med tillämpningar (Statistics theory with applications)*. ISBN 91-44-05591-9, Studentlitteratur, Lund, Sweden, p.13/25 (in Swedish).

Boström, L. (1999) *Determination of the modulus of elasticity in bending of structural timber – comparison of two methods*. Holz als Roh- und Werkstoff, 57:145-149.

Boughton, G. (1994) *Superior sorting of timber using localised stiffness on edge*. In: Proceedings of the Pacific Timber Engineering Conference, Gold Coast, Australia, July 11-15.

Brundin, J. (2011) SP Technical Research Institute of Sweden, Stockholm, Sweden. Personal communication.

Brännström, M. (2009) *Integrated strength grading*. Doctoral thesis, ISBN 978-91-86233-12-9, Division of Wood Technology, Skellefteå Campus, Luleå University of Technology, Sweden.

Corder, S. E. (1965) *Localized deflection related to bending strength of lumber*. In: Proceedings of the Second Symposium on Nondestructive Testing of Wood, Spokane, WA, USA, pp. 461-473.

Côté, W. A., Day, A. C., Kutscha, N. P., Timell, T. E. (1967) *Studies on compression wood. V. Nature of the compression wood formed in the early springwood of conifers*. Holzforschung – International Journal of the Biology, Chemistry, Physics and Technology of Wood, 21(6):180-186.

Dahlblom, O., Persson, K., Petersson, H., Ormarsson, S. (1999) *Investigation of variation of engineering properties of spruce*. In: Proceedings of 6th International IUFRO Wood Drying Conference, Stellenbosch, South Africa, January 25-28, pp. 253-262.

Denzler, J. K., Koppensteiner, J., Arthaber, H. (2013) *Grain angle detection on local scale using microwave transmission*. International Wood Products Journal, 4(2):68-74.

Denzler, J. K., Weidenhiller, A. (2014) *New perspectives in machine strength grading: Or how to identify a top rupture*. In: S. Aicher *et al.* (eds.), *Materials and joints in timber structures*, RILEM Bookseries 9, DOI: 10.1007/978-94-007-7811-5_68, RILEM 2014.

Dinwoodie, J. M. (2000) *Timber: Its nature and behaviour*. Second edition, E & FN Spon, London, UK.

Eliasson, L. (2005) *Automatisk egenskapsidentifiering av trä (Automatic identification of wood properties)*. Reports, no 18, School of Technology and Design, Växjö University, Växjö, Sweden (in Swedish with abstract in English).

Fewell, A. R. (1982) *Machine stress grading of timber in the United Kingdom*. Holz als Roh- und Werkstoff, 40:455-459.

Foley, C. (2003) *Modeling the effect of knots in structural timber*. Doctoral thesis, Division of Structural Engineering, Report TVBK-1027, Lund Institute of Technology, Lund, Sweden.

Foschi, R. O. (1987) *A procedure for the determination of localized modulus of elasticity*. Holz als Roh- und Werkstoff, 45(6):257-260.

Foslie, M. (1971) *Norsk granvirkes styrkeegenskaper. Del 3 – Styrkeegenskaper for små, feilfrie prøver (Strength properties of Norwegian spruce (Picea abies karst). Part 3 – Strength properties of small, clear specimens)*. Report No. 42. The Norwegian Institute of Wood Working and Wood Technology (in Norwegian).

Galligan, W. L., McDonald, K. A. (2000) *Machine grading of lumber – Practical Concerns for lumber producers.* Forest Products Laboratory, General Technical Report FPL-GTR-7, Madison, WI, USA.

Glos, P. (1995) *Strength grading.* STEP1, Lecture A6, Centrum Hout, The Netherlands.

Glos, P., Heimeshoff, B. (1982) *Möglichkeiten und Grenzen der Festigkeitssortierung von Brettlamellen für den Holzleimbau (Possibilities and limitations regarding strength grading of board laminations for glulam construction).* Ingenieurholzbau in Forschung und Praxis (Ehlbeck und Steck). Bruderverlag, Karlsruhe, Germany (in German).

Görlacher, R. (1990) *Klassifizierung von Brettschichtholzlamellen durch Messung von Longitudinalschwingungen (Classification of glulam laminations by measurement of longitudinal vibrations.* 4. Folge – Heft 21. Dissertation.Versuchsanstalt für Stahl, Holz und Steine der Universität Fridericiana in Karlsruhe, Germany (in German).

Hankinson, R. L. (1921) *Investigation of crushing strength of spruce at varying angles of grain*. Air Service Information Circular, 3(259), Material Section Report No 130, US Air Service, USA.

Hansson, M. (2014) SP Technical Research Institute of Sweden, Borås, Sweden. Personal communication.

Hatayama, Y. (1984) *A new estimation of structural lumber considering the slope of the grain around knots.* Bulletin of the Forestry and Forest Products Research Institute, Japan, No 326, pp 69-167 (in Japanese).

Hearmon, R. F. S. (1966) *Vibration testing of wood*. Forest Products Journal, 16(8):29-40.

Herman, M., Dutilleul, P., Avella-Shaw, T. (1998) *Growth rate effects on temporal trajectories of ring width, wood density, and mean tracheid length in Norway spruce (Picea abies (L.) Karst.).* Wood and Fiber Science, 30(1):6-17.

Hoffmeyer, P. (1984) *Om konstruktionstræs styrke og styrkesortering (About strength and strength grading of structural timber)*. I Skovteknologi. Et historisk og perspektivisk strejftog. Dansk Skovforening, pp.34-46 (in Danish).

Hoffmeyer, P. (1990) *Failure of wood as influenced by moisture and duration of load.* Doctoral thesis, State University of New York, College of Environmental Science and Forestry, Syracuse, New York, USA.

Hoffmeyer, P. (ed.) (1995) *Styrkesortering ger mervärde, Del 2 – Tillgængelig teknik (Strength grading adds value, Part 2 – Available technique).* Laboratoriet for Bygningsmaterialer, Danmarks Tekniske Universitet, Teknisk Rapport 335-1995, ISSN 0908-3871 (in Danish, Norwegian and Swedish).

Hu, M., Johansson, M., Olsson, A., Enquist, B. (2013) *Comparison of local variation of modulus of elasticity determined on basis of scanned fiber angles and full strain field measurements.* In: Proceedings of the 18th International Nondestructive Testing and Evaluation of Wood Symposium, Madison, WI, USA, September 24-27, pp. 356-363.

Huang, C.-L., Lindström, H., Nakada, R., Ralston, J. (2003) *Cell wall structure and wood properties determined by acoustics – a selective review.* Holz als Roh- und Werkstoff, 61:321-335.

Högberg, K.-A., Hallingbäck, H. R., Säll, H., Johansson, M., Jansson, G. (2014) *The potential for the genetic improvement of sawn timber traits in Picea abies*. Canadian Journal of Forest Research, 44(4):273-280.

Isaksson, T. (1999) *Modelling the variability of bending strength in structural timber – Length and load configuration effects*. Doctoral thesis, Division of Structural Engineering, Report TVBK-1015, Lund Institute of Technology, Lund, Sweden.

Johansson, C.-J. (1976) *Draghållfasthet hos limträlameller – Kvistars inverkan på draghållfastheten parallellt med fibrerna hos limträlameller av granvirke (Tensile strength of glulam laminations – The effect of knots on tensile strength parallel to the grain in glulam laminations of Norway spruce)*. Internal report no S 76:18. Chalmers University of Technology, Gothenburg, Sweden (in Swedish).

Johansson, C.-J. (2003) *Grading of timber with respect to mechanical properties.* In: Thelandersson, S. and Larsen, H. J. (eds.) *Timber Engineering*, John Wiley & Sons Ltd, Chichester, England, pp. 23-43.

Johansson, C.-J., Brundin, J., Gruber, R. (1992) *Stress grading of Swedish and German timber – A comparison of machine stress grading and three visual grading systems*. SP Swedish National Testing and Research Institute, SP REPORT 1992:23.

Johansson, C.-J., Boström, L., Bräuner, L., Hoffmeyer, P., Holmqvist, C., Solli, K. H. (1998) *Laminations for glued laminated timber – Establishment of strength classes for visual strength grades and machine settings for glulam laminations of Nordic origin*. SP Swedish National Testing and Research Institute, SP REPORT 1998:38.

Johansson, J., Hagman, O., Fjellner, B.-A. (2003) *Predicting moisture content and density distribution of Scots pine by microwave scanning of sawn timber*. Journal of Wood Science, 49:312-316.

Kliger, I. R., Perstorper, M., Johansson, G., Pellicane, P. J. (1995) *Quality of timber products from Norway spruce. Part 3. Influence of spatial position and growth characteristics on bending stiffness and strength*. Wood Science and Technology, 29:397-410.

Kliger, R., Johansson, M., Bäckström, M. (2003) *Dynamisk mätning av elasticitetsmodul på stockar – en möjlig sorteringsmetod? (Dynamic measurement of modulus of elasticity of logs – a possible grading method?).* Division of Structural Engineering, Report No. 03:5, Chalmers University of Technology, Gothenburg, Sweden (in Swedish).

Kollman, F. F. P., Côté, W. A. (1968) *Principles of wood science and technology*. Springer Verlag, Berlin Heidelberg, Germany.

Kurle, T. (2013) Metriguard Inc., Pullman, WA, USA. Personal communication.

Kurle, T. (2014) Metriguard Inc., Pullman, WA, USA. Personal communication.

Källsner, B., Oja, J., Grundberg, S. (2002) *Prediction of timber strength by industrial X-ray scanning of Pinus sylvestris saw logs.* In: Proceedings of the 7th World Conference on Timber Engineering, Shah Alam, Malaysia, August 12-15.

Källsner, B., Ormarsson, S. (1999) *Measurement of modulus of elasticity in bending of structural timber*. In: Proceedings of 1st RILEM Symposium on Timber Engineering, Stockholm, Sweden, September 13-15, pp 639-648.

Lackner, R., Foslie, M. (1988) *Gran fra Vestlandet – Styrke og sortering (Spruce from Western Norway – Strength, stiffness and grading)*. The Norwegian Institute of Wood Technology, Report no. 74 (in Norwegian).

Lam, F., Prion, H. G. L. (2003) *Engineered Wood Products for structural purposes.* In: Thelandersson, S. and Larsen, H. J. (eds.) *Timber Engineering*, John Wiley & Sons, Ltd, Chichester, England, pp. 81-102.

Lam, F., Barrett, J. D., Nakajima, S. (2004) *Influence of knot area ratio based grading rules on the engineering properties of Hem-fir used in Japanese post and beam housing*. Wood Science and Technology, 38:83-92.

Larsson, D., Ohlsson, S., Perstorper, M., Brundin, J. (1998) *Mechanical properties of sawn timber from Norway spruce*. Holz als Roh- und Werkstoff, 56:331-338.

Lundgren, N., Brännström, M., Hagman, O., Oja, J. (2007) *Predicting the strength of Norway spruce by microwave scanning: A comparison with other scanning techniques.* Wood and Fiber Science, 39(1):167-172.

Lycken, A., Oja, J., Lundahl, C. G. (2009) *Kundanpassad optimering i såglinjen – Virkeskvalitet On-line (Customised optimisation in the saw line – Wood quality On-line)*. SP Technical Research Institute of Sweden, SP Report 2009:05 (in Swedish with abstract in English).

Madsen, B. (1992) *Structural behavior of timber.* Timber Engineering Ltd, North Vancouver, British Columbia, Canada, ISBN 0-9696162-0-1.

McGovern, M., Senalik, A., Chen, G., Beall, F. C., Reis, H. (2010) *Detection and assessment of wood decay using X-ray computer tomography*. In: Tomizuka, M. *et al.* (eds.) *Sensors and Smart Structures Technologies for Civil, Mechanical and Aerospace Systems 2010*. Proceedings of SPIE Vol. 7647, pp. 76474B-1 – 76474B-12. DOI: 10.1117/12.843709.

Metzler, B. (1997) *Quantitative assessment of fungal colonization in Norway spruce after green pruning*. European Journal of Forest Pathology, 27:1-11.

Montgomery, D. C. (2009) *Design and Analysis of Experiments*. John Wiley & Sons, Inc., Hoboken, NJ, USA. ISBN 978-0-470-39882-1, 7th Edition.

Müller, P. H. (1968) *Mechanical stress-grading of structural timber in Europe, North America and Australia*. Wood Science and Technology, 2:43-72.

Mäkinen, H., Hein, S. (2006) *Effect of wide spacing on increment and branch properties of young Norway spruce*. European Journal of Forest Research, 125(3):239-248.

Nagai, H., Murata, K., Nakano, T. (2011) *Strain analysis of lumber containing a knot during tensile failure.* Journal of Wood Science, 57:114-118.

Nylinder, M., Fryk, H. (2011) *Timmer (Timber)*. Swedish University of Agricultural Sciences, Department of Forest Products, Uppsala, Sweden (in Swedish), ISBN 978-91-576-9030-2.

Nyström, J. (2002) *Automatic measurement of compression wood and spiral grain for the prediction of distortion in sawn wood products*. Doctoral thesis, Division of wood technology, Publication 2002:37, Luleå University of Technology, Luleå, Sweden.

Nyström, J. (2003) *Automatic measurement of fibre orientation in softwoods by using the tracheid effect.* Computers and Electronics in Agriculture, 41:91-99.

Ohlsson, S., Perstorper, M. (1992) *Elastic wood properties from dynamic tests and computer modeling*. Journal of Structural Engineering, 118(10):2677-2690.

Oja, J., Källsner, B., Grundberg, S. (2005) *Predicting the strength of sawn wood products: A comparison between x-ray scanning of logs and machine strength grading of lumber.* Forest Products Journal, 55(9):55-60.

Olsson, A., Oscarsson, J., Johansson, M., Källsner, B. (2012) *Prediction of timber bending strength on basis of bending stiffness and material homogeneity assessed from dynamic excitation.* Wood Science and Technology, 46(4):667-683.

Ormarsson, S. (1999) *Numerical analysis of moisture-related distortions in sawn timber*. Doctoral thesis, Department of Structural Mechanics, Publication 99:7, Chalmers University of Technology, Gothenburg, Sweden.

Pellerin, R. F. (1965) *A vibrational approach to nondestructive testing of structural lumber*. Forest Products Journal, 15(3):93-101.

Perstorper, M., Pellicane, P. J., Kliger, I. R., Johansson, G. (1995) *Quality of timber products from Norway spruce. Part 1. Optimization, key variables and experimental study.* Wood Science and Technology, 29:157-170.

Petersson, H. (2010) *Use of optical and laser scanning techniques as tools for obtaining improved FE-input data for strength and shape stability analysis of wood and timber.* In: Proceedings of V European Conference on Computational Mechanics, Paris, France, May 16-21.

Rais, A., Pretzsch, H., van de Kuilen, J.-W. G. (2014) *Roundwood pre-grading with longitudinal acoustic waves for production of structural boards.* European Journal of Wood and Wood Products, 72:87-98.

Råberg, U., Edlund, M.-L., Terziev, N., Land, C. J. (2005) *Testing and evaluation of natural durability of wood in above ground conditions in Europe – an overview*. Journal of Wood Science, 51:429-440.

Sandoz, J. L. (1996) *Ultrasonic solid wood evaluation in industrial applications.* In: Proceedings of the 10th International Symposium on Nondestructive Testing of Wood, Lausanne, Switzerland, September 26-28, pp. 147-153.

Schajer, G. S. (2001) *Lumber strength grading using X-ray scanning*. Forest Products Journal, 51(1):43-50.

Schajer, G. S., Bahar Orhan, F. (2006) *Measurement of wood grain angle, moisture content and density using microwaves.* Holz als Roh- und Werkstoff, 64(6):483-490.

Serrano, E., Blixt, J., Enquist, B., Källsner, B., Oscarsson, J. (ed.), Petersson, H., Sterley, M. (2011) *Wet glued laminated beams using side boards of Norway spruce.* Report No 5, School of Engineering, Linnæus University, Växjö, Sweden.

Skog, J., Vikberg, T., Oja, J. (2010) *Sapwood moisture-content measurements in Pinus sylvestris sawlogs combining X-ray and three-dimensional scanning*. Wood Material Science and Engineering, 5:91-96.

Skog, J., Lundgren, N., Oja, J. (2011) *Detecting top rupture in Pinus sylvestris sawlogs.* In: Proceedings of the 20th International Wood Machining Seminar, Skellefteå, Sweden, June 7-10, pp. 132-140.

Skog, J. (2013) *New forest industry production systems based on high-speed CT scanning*. WoodWisdom-Net Research Project, Final report.

Stapel, P., van de Kuilen, J.-W. G. (2014) *Efficiency of visual strength grading of timber with respect to origin, species, cross section, and grading rules: a critical evaluation of common standards*. Holzforschung, 68(2):203-216.

Steffen, A., Johansson, C.-J., Wormuth, E.-W. (1997) *Study of the relationship between flatwise and edgewise moduli of elasticity of sawn timber as a means to improve mechanical strength grading technology.* Holz als Roh- und Werkstoff, 55:245-253.

Stenman, B. (2012) SP Technical Research Institute of Sweden, Borås, Sweden. Personal communication.

Sterley, M. (2012) *Characterisation of green-glued wood adhesive bonds*. Doctoral dissertation No 85/2012, School of engineering, Linnæus University.

Svensson, A. (2012) Vida Vislanda AB, Vislanda, Sweden. Personal communication.

Säll, H. (2002) *Spiral grain in Norway spruce*. Doctoral Thesis, Acta Wexionensia No 22/2002, Växjö University Press, Växjö University, Växjö, Sweden.

Thaler, N., Lesar, B., Humar, M. (2012) *Correlation between brown rot decay and Pilodyn measurements*. European Journal of Wood and Wood Products, 70:893-895.

Thörnqvist, T. (2011) Linnaeus University, Växjö, Sweden. Personal communication.

Wang, X., Carter, P., Ross, R. J., Brashaw, B. K. (2007a) *Acoustic assessment of wood quality of raw forest materials – A path to increased profitability*. Forest Products Journal, 57(5):6-14.

Wang, X., Ross, R. J., Carter, P. (2007b) *Acoustic evaluation of wood quality in standing trees. Part I. Acoustic wave behavior.* Wood and Fiber Science, 39(1):28-38.

Wang, X., Verrill, S., Lowell, E., Ross, R. J., Herian, V. L. (2013) *Acoustic sorting models for improved log segregation.* Wood and Fiber Science, 45(4):343-352.

Wimmer, R., Johansson, M. (2014) *Effects of reaction wood on the performance of wood and wood-based products*. In: B. Gardiner *et al*. (eds.) *The Biology of Reaction Wood*, Springer Series in Wood Science, DOI 10.1007/978-3-642-10814-3_8, Springer-Verlag, Berlin Heidelberg.

Wormuth, E.-W. (1993) *Untersuchung des Verhältnisses von flachkant zu hochkant ermitteltem Elastizitätsmodul von Schnittholz zur Verbesserung der maschinellen Festigkeitssortierung (Study of the relationship between flatwise and edgewise moduli of elasticity of sawn timber for the purpose of improving machine strength grading technology)*. Master's thesis. Department of Wood Technology, University of Hamburg, Germany (in German).

Xu, P., Walker, J. C. F. (2004) *Stiffness gradients in radiata pine trees.* Wood Science and Technology, 38:1-9.

Ziethén, R. (2006) *Proof loading – a new principle for machine strength grading of timber*. Licentiate thesis, School of Technology and Design, Reports, No. 33, Växjö University, Växjö, Sweden.

Ziethén, R. (2012) SP Technical Research Institute of Sweden, Borås, Sweden. Personal communication.

I

Wood Sci Technol (2012) 46:593–610
DOI 10.1007/s00226-011-0429-8

ORIGINAL

Strain fields around knots in Norway spruce specimens exposed to tensile forces

Jan Oscarsson · Anders Olsson · Bertil Enquist

Received: 10 June 2010 / Published online: 27 May 2011

Abstract Two-dimensional strain fields around knots in two Norway spruce specimens subjected to tension loading were detected using a contact-free measuring technique based on white-light digital image correlation. The first specimen included a traversing Edge knot, and the second one, a Centric knot. The development of strain fields as a function of load level was measured by consecutive cyclic load tests where one side of the specimen was studied during each test. The objectives were to examine to what extent the strain fields could be detected, to investigate the correlation between strain fields measured on different sides of a specimen and to analyse the strain distributions around the knots. The results show that the applied technique is useful for catching both overall and detailed information about the behaviour of knots in wood members exposed to loading. Clear wood defects that could not have been detected by neither visual inspection nor scanning were observed, and conclusions could be drawn regarding the release of internal stresses. The correlations between strain fields on different sides of the specimens were excellent, and the correspondence between measurement results and comparative finite element calculations was surprisingly good considering the fact that the employed FE models were fairly simple.

Introduction

Strength grading of structural timber means that strength, modulus of elasticity and density of individual timber members are predicted or measured by visual

J. Oscarsson (✉)
SP Technical Research Institute of Sweden, Videum Science Park, 351 96 Växjö, Sweden
e-mail: jan.oscarsson@sp.se

A. Olsson · B. Enquist
Linnæus University, 351 95 Växjö, Sweden

inspection or non-destructive machine testing. The market is, today, dominated by machine grading techniques that involve the determination of either flat-wise bending stiffness or dynamic stiffness in axial direction of a board. From previous research carried out by, *inter alia*, Johansson et al. (1992) and Larsson (1997), it is well known that the mentioned stiffnesses are, to a certain degree, correlated with the bending strength of a board. These relations are used to predict the latter property.

Present-day methods for machine grading result in a maximum characteristic strength of 40–45 MPa, but there are boards that in fact have a strength that exceeds 80 MPa. The reason why structural timber with characteristic strength higher than 45 MPa is not graded is that the prediction of a board's load-bearing capacity by the use of any available technique is not particularly good due to the somewhat limited correlation between stiffness and strength. Thus, to be able to utilize the potential of high strength timber, better grading methods are needed.

Mechanical properties of timber are, to a large extent, dependent on the occurrence of defects in the wood material. The degree of importance that different defects have on strength and stiffness has been investigated by, *inter alia*, Johansson et al. (1998) and Johansson (2003). It was found that knots were by far the type of defects that had the largest influence on visual grading and that the major cause of fracture was the presence of knots. Hence, it follows that a thorough knowledge and understanding of the behaviour of knots and the surrounding wood fibres in timber members exposed to loading is of great importance for the development of more accurate strength grading methods. Studies have been carried out concerning the effect of knots on the mechanical behaviour and mechanical properties of branch junctions. In an investigation carried out by Müller et al. (2006), it was found that the strain distribution of a mechanically loaded Norway spruce branch junction was very homogeneous, due to a combination of naturally optimized shape and optimized mechanical properties in the junction area. Jungnikl et al. (2009) measured the microfibril angle and density distribution at branch junctions of pine using computer tomography and X-rays, respectively, and found that the material properties vary locally as a response to different mechanical demands.

For studying the effect of knots on the strain distribution, techniques for contact-free deformation and strain measurement on surfaces of timber members could be useful. One such method, today widely used in, for example, the vehicle and aviation industries, is based on white-light digital image correlation (DIC). The use of DIC techniques in connection with wood or wood-based products is, however, rather limited. A review of research carried out up to the year 2005 is found in Serrano and Enquist (2005) where results from an investigation into strain distribution along wood adhesive bonds using DIC technique are presented. In recent years, the technique has been used for the measurements of, for example, strain in steel-to-timber dowel joints (Sjödin et al. 2006), strain in bi-axially loaded sheathing-to-framing connections (Vessby et al. 2008), strain distribution in timber subjected to four-point bending tests (Murata et al. 2005), strain-softening behaviour of wood under tension perpendicular to the grain (Miyauchi and Murata 2007) and tensile properties of early wood and late wood of loblolly pine (Young Jeong et al. 2009).

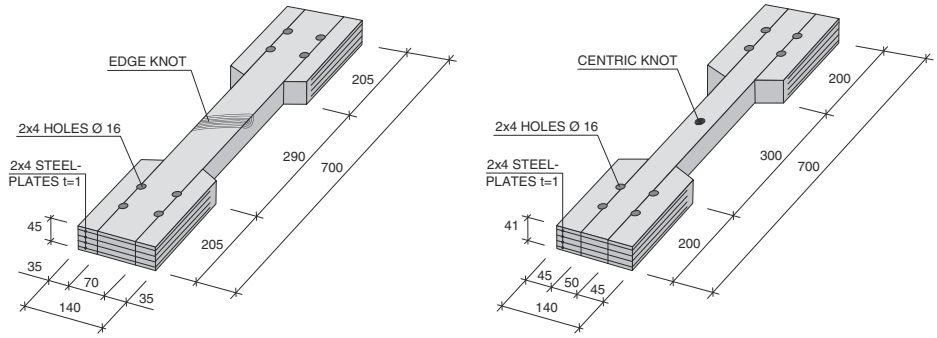

Fig. 1 Test specimens with Edge knot (*left*) and Centric knot (*right*)

Aim and scope

In this paper, findings from an investigation into two-dimensional strain fields around knots in wood members subjected to tensile forces are presented. Two test specimens of Norway spruce, one with a traversing Edge knot (henceforth denoted *Edge knot*) and one with a Centric knot (see Fig. 1), were studied using a non-contact optical 3D deformation measurement system of white-light DIC type. The aims were to examine 1. to what extent the strain fields could be detected, 2. the correlation between the strain fields measured on different sides of a specimen, and 3. the strain distribution around the knots. The development of strain fields was followed and measured by consecutive cyclic load tests consisting of both loading and unloading. Only one side of a specimen was studied during each test. Except for an initial test in which a crack in the Edge knot specimen widened and propagated, the loading was kept within the elastic range. Thus, the strain fields as a function of load level were detected in a comparable manner on all four sides of each specimen, even though only one side was studied during each test. The experimental results were also compared with those obtained from finite element (FE) simulations.

Test set-up and measurement equipment

The test set-up that was used for the experiments is shown in Fig. 2. The test specimens were fixed in a material testing machine of fabricate MTS with a 322 test frame, a control system of type FT60 and a maximum force capacity of ± 100 kN. The cyclic load that was applied during each test ranged from 0 to 30 kN, except for one test in which the maximum load was 40 kN. The load developed by the MTS machine was transferred to the test specimens by pin-ended steel yokes, each connected to the specimens by four steel dowels.

The two-dimensional strain fields in longitudinal and lateral directions and in shear occurring on the surfaces of the test specimens were detected using the measuring system ARAMIS^{TM}. It includes two charge-coupled device (CCD) cameras, in this case with a resolution of 2,048 $\times$ 2,048 pixels, placed in front of the specimen at angles and distances in accordance with a calibration procedure

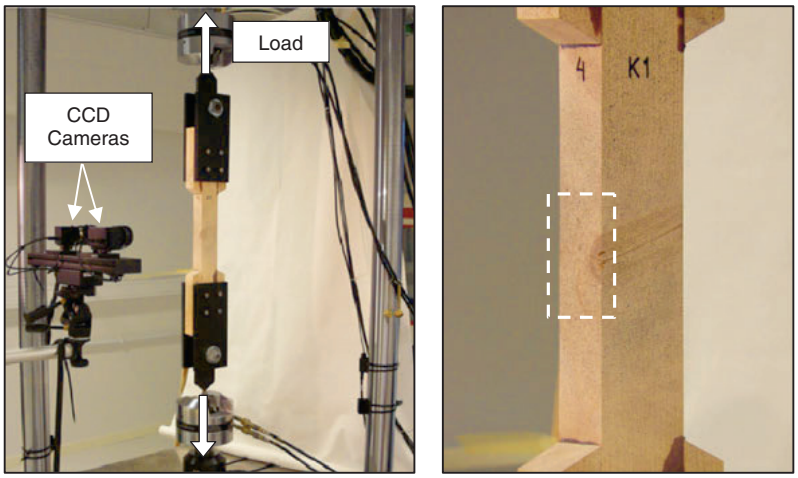

Fig. 2 Test set-up for the measurement of strain fields on one side of the Edge knot specimen (*left*) and corresponding measurement area (*right*)

carried out prior to the tests. With this equipment, strains in the range of 0.01–200% could be measured with an accuracy of up to 0.01% strain (GOM 2007).

During loading, the surface deformations and displacements are measured and recorded by pictures taken simultaneously, but from different angles, by the two cameras at fixed time intervals during the entire load test. Stereoscopic images are obtained from each pair of pictures, and current 3D-coordinates for a large number of points on the distorted surface are calculated relative to a coordinate system defined through the calibration procedure. In this research, pairs of pictures were taken at a time interval of 2 s, corresponding with a load increment of 400 N. Thus, each pair of pictures represents a unique load stage.

To be able to determine the displacements of a distinct point on the surface, each picture is divided into partially overlapping square or rectangular image subpictures, so-called facets. The size in pixels of both facets and overlap could be adjusted and chosen due to the spatial resolution and measurement accuracy needed for the test in question. In this case, the system's default settings, which are square 15 × 15 pixel facets and two pixel overlapping areas along the border of adjacent facets, see Fig. 3 (left), were chosen. This resulted in a facet step of 13 pixels, corresponding to a spatial resolution of about 0.67 mm. The default values are chosen as a compromise between measurement accuracy and computational time (GOM 2007). During a load test, each facet is identified for every subsequent stereoscopic image in the recording. This requires that the surface of the test object has an identifiable pattern, in this case a random speckled pattern of sprayed paint, see Fig. 3 (middle and right). During a test, the pattern deforms along with surface distortions, see Fig. 3 (right), and by the use of correlation algorithms, the 3D facet coordinates are calculated as the mean value of the coordinates of the facet corners. In Fig. 4, the coordinates of nine facets are shown as red and blue dots. These coordinates also define and coincide with the measuring point of the facet. Displacements of facet coordinates in a 3 × 3 facet mesh are used to calculate the strains in the measuring

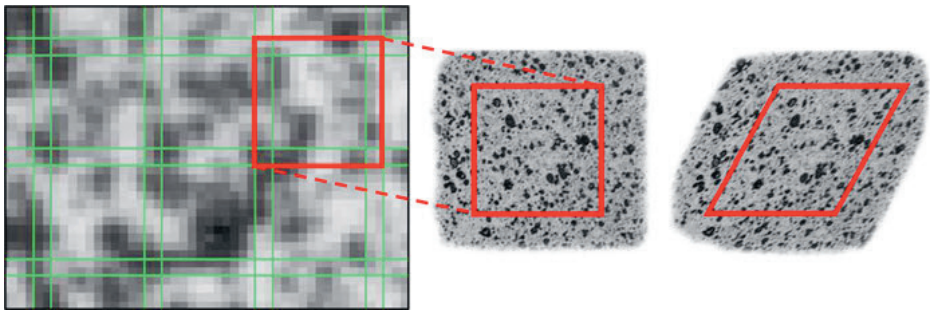

Fig. 3 Pixel facets of size 15 × 15 pixels with a two pixel overlap (*left*, GOM 2007), and random speckled pattern of a facet before loading (*middle*) and under loading (*right*)

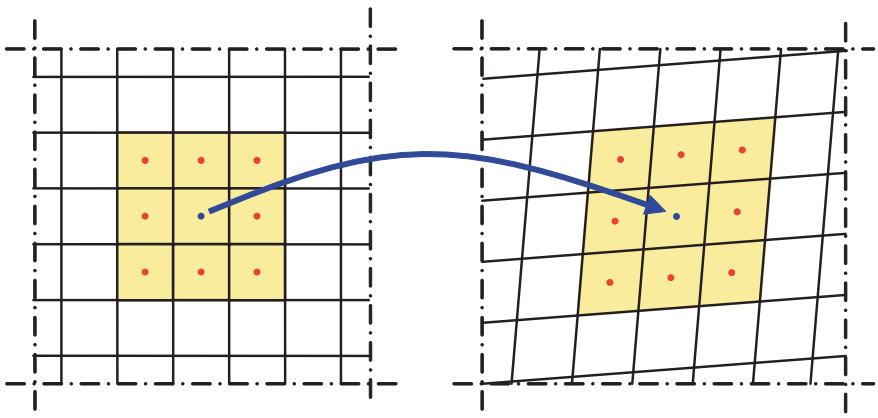

Fig. 4 Facet mesh before loading (*left*) and distorted facet mesh under loading (*right*)

point (blue dot in Fig. 4) of the centre facet of the mesh. By following the position changes of a large number of facets, the strain field as a function of load level can be determined and visualized.

Test specimens and loading

Drawings of the test specimens are shown in Fig. 1, and the dimensions and positions of the Edge knot and the Centric knot, respectively, are shown in Figs. 5 and 6. The experimental part of the research was divided into two test series, one for each test specimen. The Edge knot specimen was exposed to five load tests, numbered A0–A4, and the Centric knot specimen was exposed to four tests, numbered B1–B4.

In order to keep the stresses and strains within the elastic range, a maximum tension load of 30 kN was chosen for the Centric knot specimen, equal to an average tensile stress of about 15 MPa. For the Edge knot specimen, a higher load level was selected as the cross-section area of this specimen was more than 50% larger than the corresponding area of the Centric knot specimen. Since the presence

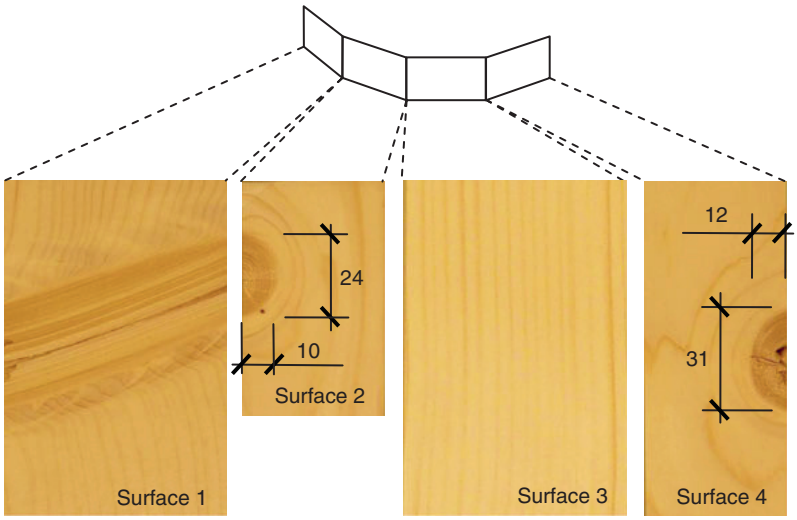

Fig. 5 Knot dimensions (mm) in Edge knot specimen

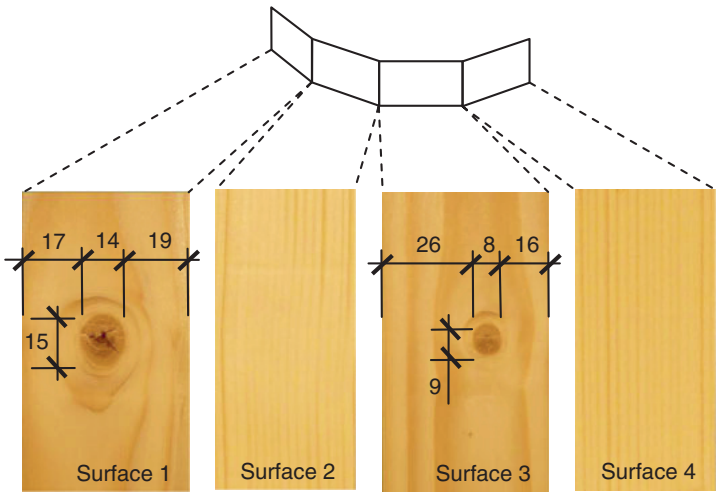

Fig. 6 Knot dimensions (mm) in Centric knot specimen

of the Edge knot caused a load eccentricity e of about 5.5 mm in the section through the knot, see Fig. 7 (left), the increase in the load level was limited to 10 kN resulting in a tension load of 40 kN for the Edge knot specimen. However, during the first load test (no. A0), an initial crack at the pith of the Edge knot expanded and propagated to the full depth of the knot, see Fig. 7 (left). Because of this, the load level was reduced to 30 kN, a load for which the strains on the surfaces of the Edge knot specimen were measured in tests A1–A4.

The load application in all tests was force-controlled, i.e., the load was both applied and detached with a constant load rate, in this case 200 Newton/s. The load–time relations for the different tests are shown in Fig. 7 (right).

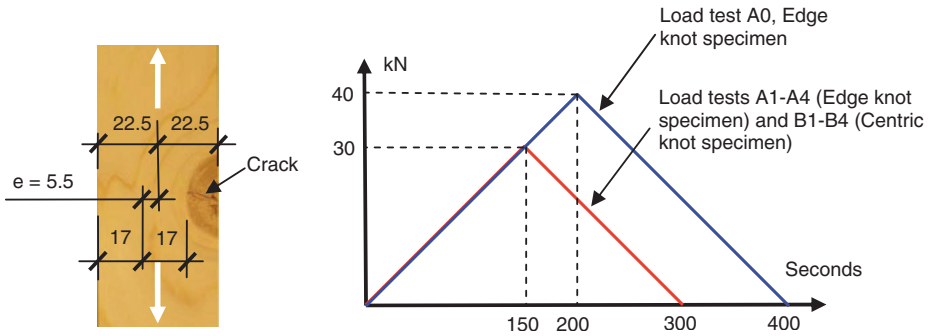

Fig. 7 Load eccentricity *e* (mm) in Edge knot specimen (*left*), and load–time relations for performed load tests (*right*)

Test results and evaluation

Two ARAMIS^{TM} post-processing tools, contour plots and section diagrams, were used to visualize the strain measuring results. By the first tool, a camera image of a measured surface is overlaid with coloured strain contour plots showing the strain distribution, for a defined load stage, over the measured surface. Such plots offer a qualitative and easily conceivable impression of the specimen's behaviour under loading. To obtain quantitative information with a higher degree of accuracy, sections can be defined in surface camera images and the strain variation along such sections can be shown in section diagrams. The position of a section is denoted in a local *xyz*-coordinate system defined in the camera image of each specimen surface. The results that are presented below concern the in-plane (*xy*-plane) strains that occurred on the surfaces of the test specimens. To be able to relate the four different coordinate systems on a specimen to each other, small marks of ink were applied on each surface. Since all marks were located at the same position in the longitudinal direction of a specimen and since the origin for each local coordinate system was located at such a mark, the measurement results for different surfaces of a specimen could easily be related to each other.

Load test no. A0: Edge knot specimen, load 40 kN

As described under the heading *Test specimens and loading* above, a tension load of 40 kN was chosen for this test where the strains on the specimen surface that shows a split section of the knot were measured, i.e. Surface 1 in Fig. 5.

Longitudinal strains (ε_y) for certain load stages are presented in Fig. 8. Stages 0–4 represent the undeformed and unloaded reference state, and the specified load level of 0.10 kN is considered as measuring noise. The load application started at stage 5 for which, at a load level of 0.59 kN, the widening of the initial crack in the pith of the knot is clearly visible.

Load stages 102–105 (see Fig. 8) illustrate the strain field just before and after the maximum load level of 40.1 kN was reached at stage 103. At this load, the crack had propagated and widened to such an extent that it was no longer possible to

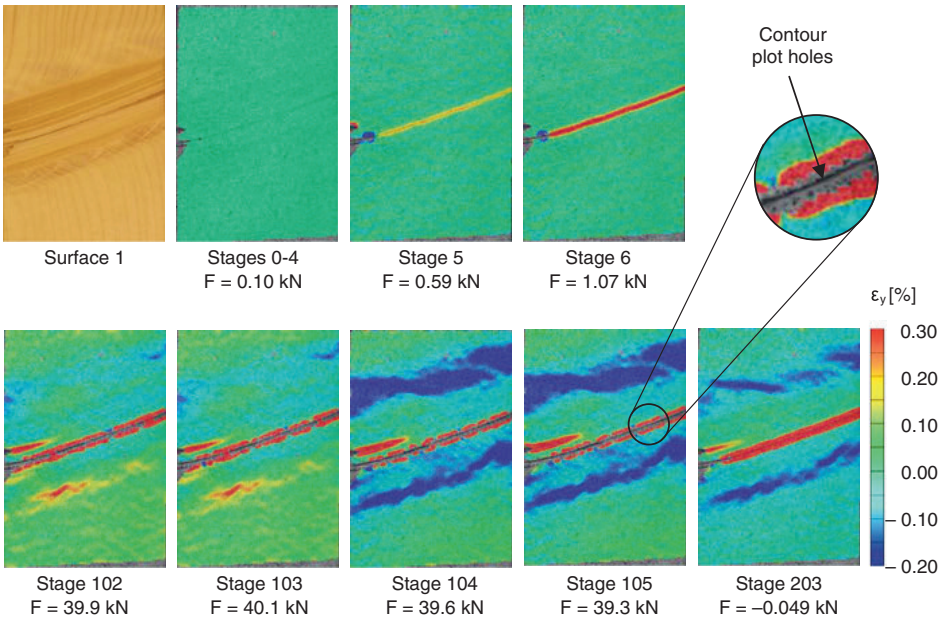

Fig. 8 Contour plots for longitudinal strains (ε_y) on surface 1, Edge knot specimen, load test no. A0, load stages no. 0–6, 102–105 and 203

identify displacements and deformations of facets in the crack area by means of the surface pattern of sprayed paint. Surface points that were not possible to identify are shown as holes in the contour plots, see detail in Fig. 8. During the unloading phase, the crack was gradually closed and the pattern restored to a degree where the facet displacements across the crack area were again possible to measure. However, considerable deformations, caused by crack propagation, remained in the crack after completed unloading at load stage 203. These deformations were represented by the ARAMIS^{TM} system as remaining longitudinal strains across the crack area, and they are shown as a thick red stripe in the contour plot for load stage 203, see Fig. 8.

In addition to the described crack deformations, large remaining negative (compressive) strains appeared in the wood fibres close to the knot. In general, strain changes measured by the ARAMIS^{TM} system from one load stage to another are rather small and more or less foreseeable, but in this test, the negative strains along the knot appeared instantly, at load stage 104, immediately after the maximum load of 40.1 kN was reached. During the 2 s that elapsed between the moments when pictures of load stages 103 and 104 were taken, the strain field was completely changed and areas of considerable negative strains emerged. A large portion of these remained after unloading, see load stage 203. A reasonable explanation for the sudden strain field changes is that crack growth during the test led to the release of internal stresses. After the test, the specimen was carefully examined and by using a pocket lens, two longitudinal clear wood cracks along the curvature of the fibre direction around the knot and one crack at the edge of the knot were discernible on Surfaces 2 and 4. The cracks are highlighted in the section diagrams of Figs. 9 and

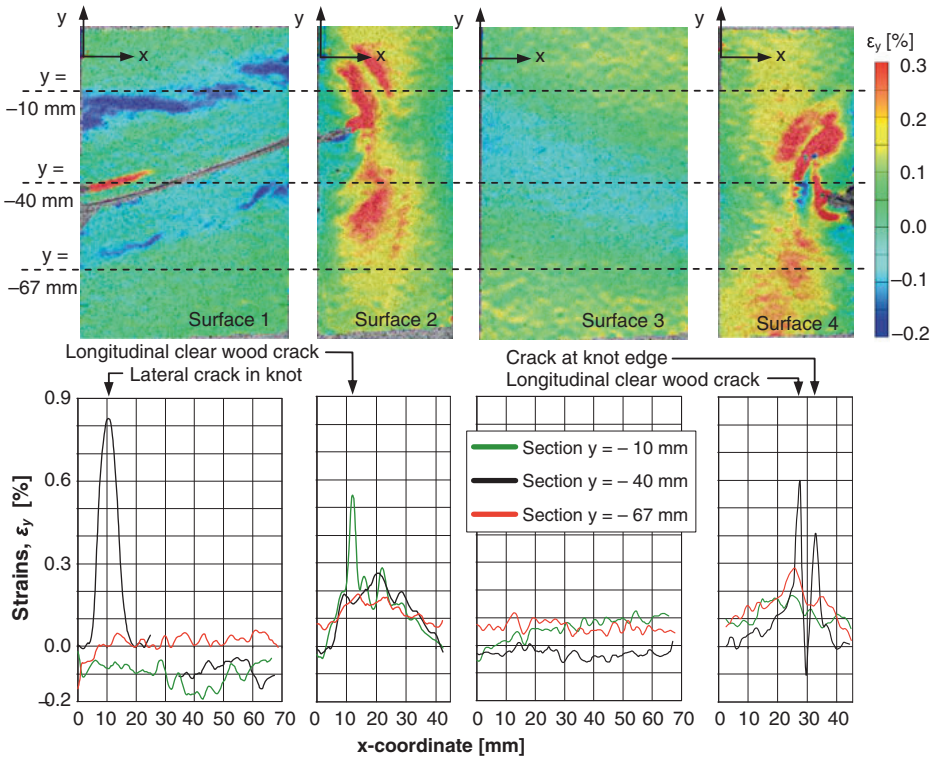

Fig. 9 Longitudinal strains (ε_y), Edge knot specimen, maximum load 30 kN, load tests A1–A4. *Top row* contour plots. *Bottom row* section strain diagrams for defined sections (*dashed lines*)

10. It should also be noted that the stress release occurred between the load stages 103 and 104, i.e. just *after* the maximum load level was reached. This indicates that the release was, to some extent, triggered by the change of sign of the load–time graph derivative, see Fig. 7 (right).

Load test no. A1–A4: Edge knot specimen, load 30 kN

In Load tests A1–A4, where the final strain stage of Load test A0 was used as unloaded reference stage (stage 0), the Edge knot specimen was exposed to a tension load of 30 kN for which the entire specimen displayed an elastic behaviour. Strain contour plots and section diagrams referring to the load stages for which the maximum load of 30 kN was reached are shown in Figs. 9 and 10.

The longitudinal strains (ε_y) are exhibited in Fig. 9. In spite of the fact that the specimen was exposed to tension loads, longitudinal negative strains were visible on Surfaces 1 and 3. The negative strains on Surface 1, measured during Load test A1, appeared in the same fibres as those where internal stresses were released in Load test A0. The appearance of these negative strains during Load test A1 was confirmed by a numerical analysis based on a 3D linear elastic model, see description under the heading "Numerical analyses" below. A possible explanation

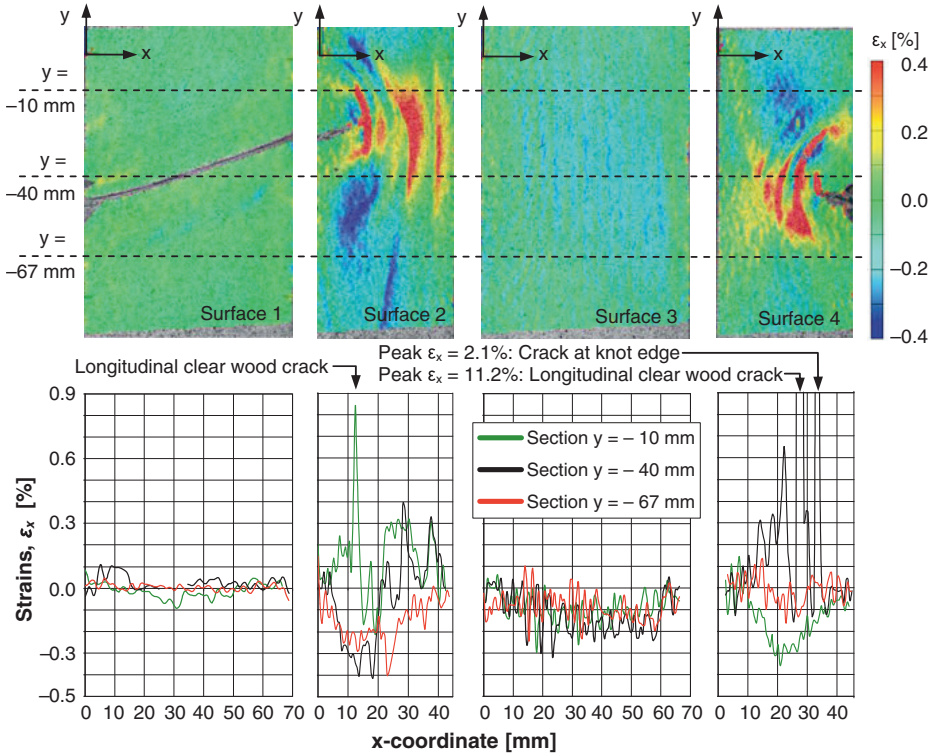

Fig. 10 Lateral strains (ε_x), Edge knot specimen, maximum load 30 kN, load tests A1–A4. *Top row* contour plots. *Bottom row* section strain diagrams for defined sections (*dashed lines*)

for this phenomenon is related to the behaviour of stress flow lines, i.e. imaginary lines showing how load is transferred between neighbouring material points. Such lines could be thought of as occurring in the vicinity of defects in specimens exposed to loading (Karihaloo 1995), and they create a biaxial stress and strain state. This effect is enhanced by deviating fibre directions around knots in timber members. The stress flow lines in the Edge knot specimen under tensile loading are exhibited in Fig. 11. The flow lines that develop under limited loading are shown as continuous lines. When the load increases, the eccentricity e shown in Fig. 7 creates a lateral deformation of the specimen that straightens the flow lines to the shapes represented by the dashed lines. From Fig. 11, the negative longitudinal strains occurring close to the knot on Surface 1 could be understood by studying the distances denoted a and b, measured between the tips of two lines drawn perpendicular to the flow line closest to the knot. The distance is reduced ($a > b$) when the line is straightened, and this may explain the negative strains in the clear wood fibres closest to the knot. The lateral deformation of the specimen, caused by the load eccentricity e, also explains the minor longitudinal negative strains in Section $y = -40$ mm on Surface 3, see Fig. 9.

The contour plots for Surfaces 2 and 4 in Fig. 9 exhibit large longitudinal tensile strains close to the knot. These strains are, like the strains discussed in the previous paragraph, related to the eccentricity e. Since hardly any stresses in the longitudinal

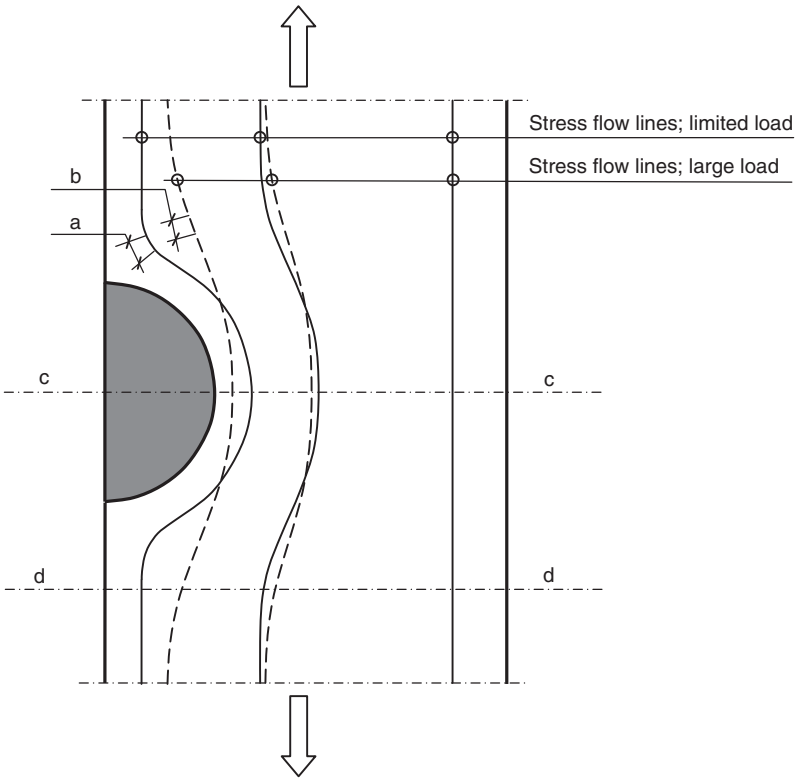

Fig. 11 Edge knot specimen under loading: straightening of imaginary stress flow lines

direction could be transferred through the knot, equilibrium requires higher longitudinal stresses and strains close to the knot than on the edge opposite to the knot. Furthermore, the fibre direction in the vicinity of the knot deviates considerably from the loading direction, and this difference probably contributes to increasing longitudinal tensile strains close to the knot.

The three strain peaks ($\varepsilon_y \geq 0.4\%$) in the section diagrams for Surfaces 2 and 4 in Fig. 9 are related to the previously described cracks that were observed by using a pocket lens. What is represented as surface strain peaks are, in fact, displacements caused by gradual widening of the cracks as load is applied.

A local tensile strain of about 0.82% was registered at Section $y = -40$ mm on Surface 1. As for the three strain peaks on Surfaces 2 and 4, this large strain value was also caused by the widening of a crack, in this case located within the knot and shown as a red stripe in the contour plot.

The lateral strains (ε_x) are presented in Fig. 10. They were insignificant on Surface 1, since the clear wood contraction was prevented by the presence of the knot. From a comparison of the contour plot of Surface 3 in Fig. 10 and the corresponding surface photo in Fig. 5, a correlation between the annual ring width and the wave-like pattern of the plot can be observed. This indicates a difference

between the Poisson's ratios of early wood and late wood of Norway spruce. Such a difference has been observed for loblolly pine by Young Jeong et al. (2009).

On Surfaces 2 and 4, lateral tensile strains developed beside the knot and compressive (negative) strains emerged in areas above and below the knot. As for the previously discussed longitudinal compressive strain shown on Surface 1, these lateral strains could also be understood from a study of the behaviour of the stress flow lines shown in Fig. 11. In section *c*, the lateral distance between the two flow lines that bend around the knot increases with increasing load and this indicates tensile strains in lateral direction. In section *d*, the lateral distance between the bending flow lines decreases corresponding to a lateral contraction. The huge apparent strains that coincide with the previously described cracks highlighted in the section diagrams in Fig. 10 are in fact lateral displacements caused by widening of the cracks.

Load tests no. B1–B4: Centric knot specimen, load 30 kN

Measurement results from tests carried out on the Centric knot specimen are shown in Fig. 12 (longitudinal strains, ε_y) and Fig. 13 (lateral strains, ε_x). All contour plots and section diagrams refer to the load stage for which the maximum load 30 kN was reached.

The contour plots for Surfaces 1 and 3 show large local strains, both longitudinal and lateral, in the vicinity of the knot. In the longitudinal direction (see Fig. 12), they could possibly and in a similar way as for the Edge knot be explained by a combination of stress flow line concentrations and deviation between fibre and loading directions. Regarding the strains in lateral direction, see Fig. 13, the expected contraction due to longitudinal tension loading is visible on both sides of the knot. The concentrations of large negative (compressive) lateral strains close to the knot are most likely caused by the curvature in the fibre directions and stress flow lines around the knot. The areas of tensile lateral strains visible above and below the knot on Surfaces 1 and 3 in Fig. 13 are similarly explained by an opposite curvature in fibres and stress flow lines.

From the lateral strain contour plots of Surfaces 2 and 4 in Fig. 13 and the photographs of the same surfaces shown in Fig. 6, the difference in Poisson's ratios between early wood and late wood is once again observed.

The contour plots and section diagrams in Fig. 12 reveal a concentration of longitudinal tensile strains in a section 20 mm below the local x-axis on Surface 4. According to the corresponding section diagram, there are strains as large as 0.95%, which is highly improbable. From the contour plots in Figs. 12 and 14 (left), it should be noted that just above the area where the large longitudinal strains occur, there are two zones where the longitudinal strains are approximately zero. In the same section as the large longitudinal strains appear on Surface 4, there are also, on an even more local scale, extreme contractions and expansions measured in the lateral direction of that surface, see Figs. 13 and 14 (right). A microscopic picture of the relevant area is shown in Fig. 14 (middle) where grain disturbances along a line on the surface are displayed. What is actually seen is the free edge of a surface chip and the concentration of large apparent strains described above are caused by

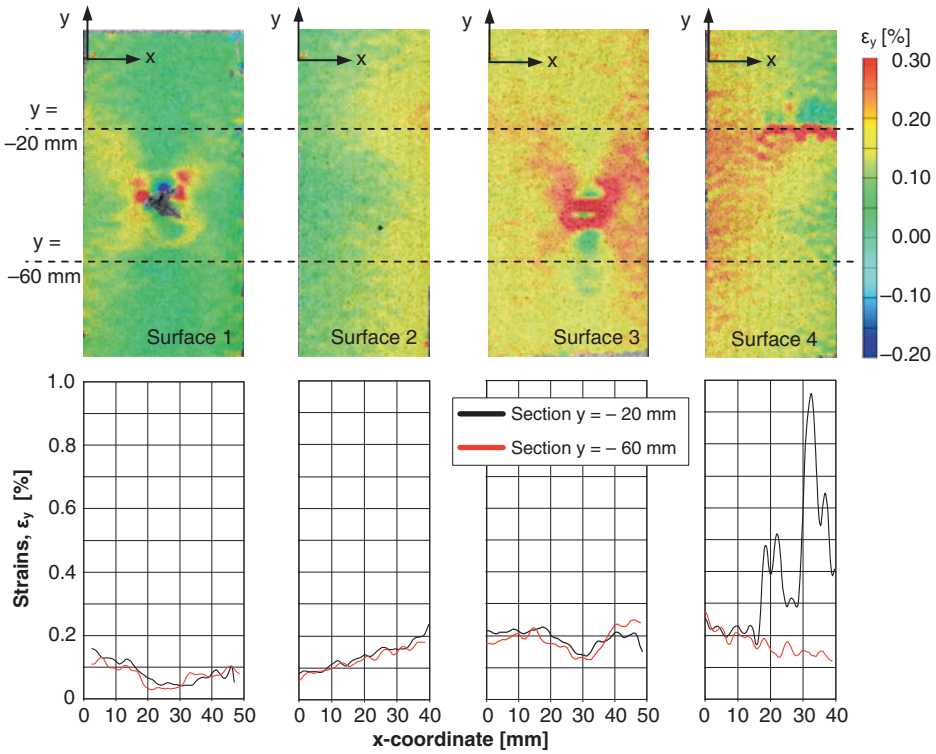

Fig. 12 Longitudinal strains (ε_y), Centric knot specimen, maximum load 30 kN, load tests B1–B4. *Top row* contour plots. *Bottom row* section strain diagrams for defined sections (*dashed lines*)

longitudinal and lateral translation of this edge. The presence of a chip clarifies why large apparent longitudinal strains are measured along a line on Surface 4 at the same time as there are large differences between the strains measured in areas on opposite sides of that line. The zero tensile strains in the area above the line are due to a rigid body translation of the chip.

Two more observations from Figs. 12 and 13 require comments. The first one concerns the fact that strains on both sides of a test specimen corner generally do not offer a perfect match. Computation of 3D coordinates and strain values for the measuring point of a facet requires that the previously described stochastic pattern of sprayed paint covers the entire area of the facet and that the entire pattern within the facet is visible from both the left and the right cameras. These requirements are not fulfilled for square facets that cover a corner of a test specimen. Consequently, on each side of a specimen corner, there are narrow areas where no strains could be calculated. However, with the exception of the corners themselves, the strain match between adjacent surfaces is very good considering the fact that they were established during different load tests. The second observation is that small areas of large lateral strains, both contraction and expansion, are found on the right-hand side of the contour plot of Surface 1 in Fig. 13. On this part of the specimen, the surface is rough due to minor maltreatment. According to the user manual for the

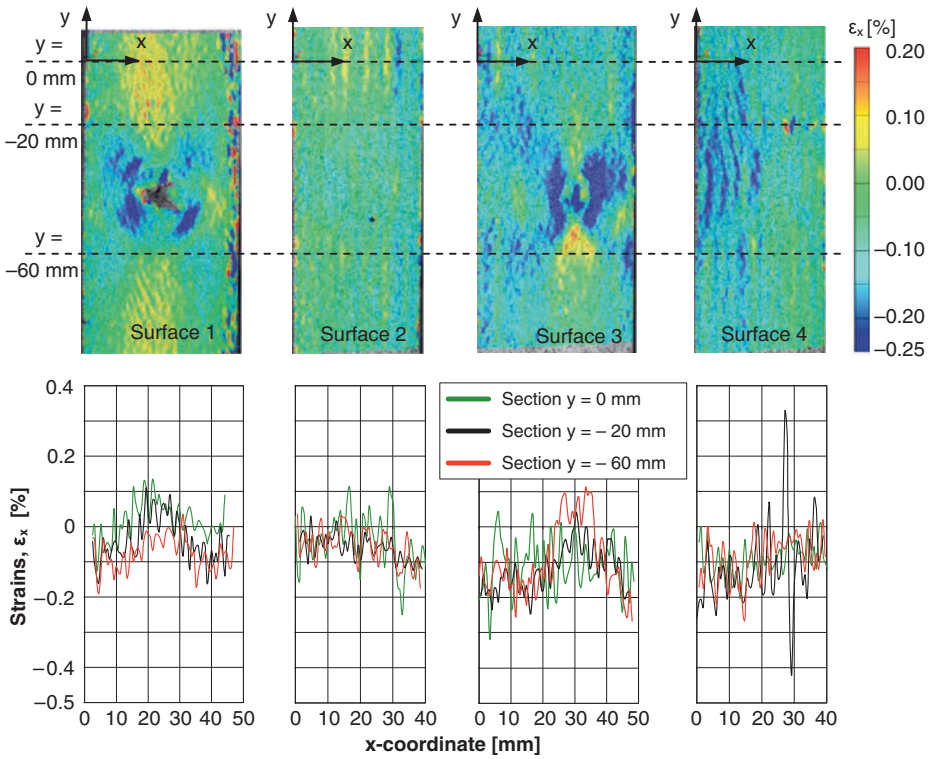

Fig. 13 Lateral strains (ε_x), Centric knot specimen, maximum load 30 kN, load tests B1–B4. *Top row* contour plots. *Bottom row* section strain diagrams for defined section (*dashed lines*)

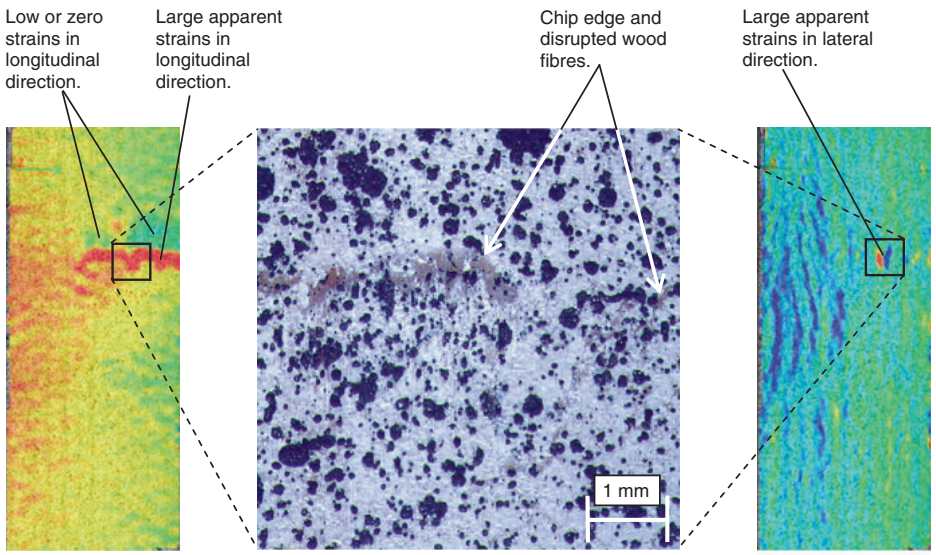

Fig. 14 Surface 4, Centric knot specimen: longitudinal strains (*left*), lateral strains (*right*) and microscopic picture showing disrupted wood fibres and chip edge (*middle*)

ARAMIS system (GOM 2007), an optimum specimen surface is smooth since highly structured surfaces may cause problems in facet identification and 3D point computation. Thus, the large strains identified on the rough part of the specimen surface are caused by incorrect measurement results and calculations.

Numerical analyses

The results of the experiments were compared with those obtained from FE simulations using the software ABAQUS (ABAQUS Inc. 2008). In the FE calculations, 3D linear elastic models of the test specimen's behaviour under loading were used. The model of the Edge knot specimen comprised about 113,000 2nd order elements and 483,000 nodes resulting in 1,449,000 degrees of freedom. Corresponding numbers for the Centric knot specimen model were 33,300 2nd order elements, 146,100 nodes and 438,200 degrees of freedom. In all simulations, a tension load of 30 kN was applied as a distributed load over the end surfaces of the specimens.

The material data needed for the numerical calculations, expressed in terms of elastic constants for spruce with a moisture ratio of 12%, were obtained from literature (Kollman and Côté 1968). The constants used for both clear wood and knots were $E_L = 13{,}500$, $E_R = 893$, $E_T = 481$, $G_{LR} = 716$, $G_{LT} = 500$ and $G_{RT} = 29$ MPa for the moduli of elasticity and the shear moduli and $\upsilon_{LR} = 0.43$, $\upsilon_{LT} = 0.53$ and $\upsilon_{RT} = 0.42$ for Poisson's ratios. The indices L, R and T refer to the longitudinal, radial and tangential directions, respectively, of the modelled orthotropic wood material. The longitudinal direction of the clear wood was oriented parallel to the longitudinal direction of the specimens, whereas the longitudinal direction of the knots was oriented perpendicular to the mentioned clear wood direction.

The applied FE models were fairly simple. The crack that widened and propagated in the pith of the Edge knot during load test no. A0 was included, but the material orientation deviations that always occur in clear wood close to knots were not regarded. Nevertheless, the simulation results presented in Figs. 15, 16 and 17 show, on an overall and qualitative level, a degree of correspondence with the experimental results shown in Figs. 9 and 10 and Figs. 12 and 13 that is surprisingly good. In terms of strain features on a closer level, several similarities deserve attention. For Surface 1 of the Centric knot specimen, calculated and measured strain fields in the vicinity of the knot strongly resemble one another, see Figs. 12, 13 and 15. This resemblance remains even if the knot is replaced by a hole, see Fig. 15, which is in accordance with assumptions made in, for example, the Nordic visual strength grading rules for timber, INSTA 142 (1998), namely that knots in structural timber should be equalized with holes (personal communication, Jan Brundin, SP Technical Research Institute of Sweden, 2008). INSTA 142 is referred to in the European Standard EN 1912 (2008) where nationally applied visual strength grades for visual grading of structural timber are assigned to common European strength classes established in the European Standard EN 338 (2003).

For the Edge knot specimen, the longitudinal negative strains measured on Surfaces 1 and 3, see contour plots in Fig. 9, could also be found in the

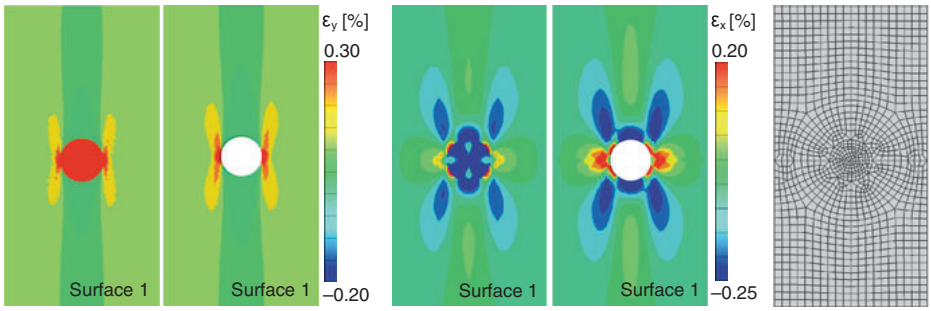

Fig. 15 Results from FE simulations, Centric knot specimen: longitudinal strains with and without knot (*left*), lateral strains with and without knot (*middle*) and FE mesh (*right*)

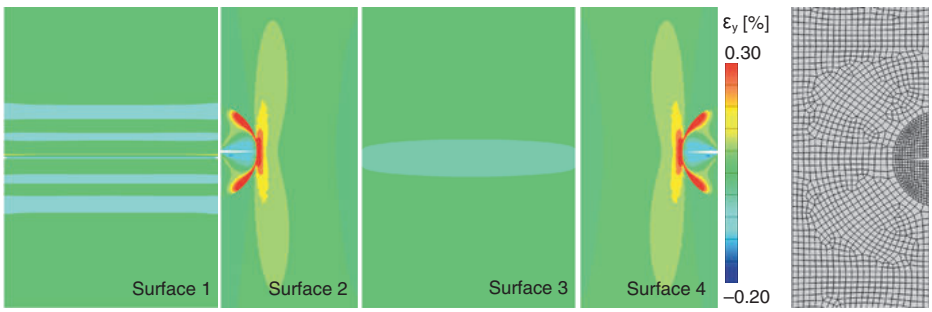

Fig. 16 Results from FE simulation, Edge knot specimen: longitudinal strains and FE mesh

corresponding plots in Fig. 16 and the areas of lateral compressive and tensile strains measured by the ARAMIS^{TM} system were also verified, see Fig. 17. However, the lateral strains are less evident in the FE simulations than in the ARAMIS^{TM} contour plots. The reason for this is probably that the curvature in the fibre direction around the knots increases the lateral strains measured on the surfaces of the test specimens, whereas no such effect is found in the FE calculations, since fibre curvatures are not included in the models.

The most conspicuous difference between measured and calculated strains concerns the large apparent tensile strains, both longitudinal and lateral, that occurred close to the knot in the Edge knot specimen. These apparent strains, which in fact were displacements caused by the cracks that were identified by using a pocket lens, could not be seen in the results of the simulations since these cracks were not included in the model.

Conclusion and future work

The objectives of this research were to investigate to what extent strain fields around knots could be detected by the use of DIC technique, to analyse the strain distribution around the investigated knots and to examine the correlation between

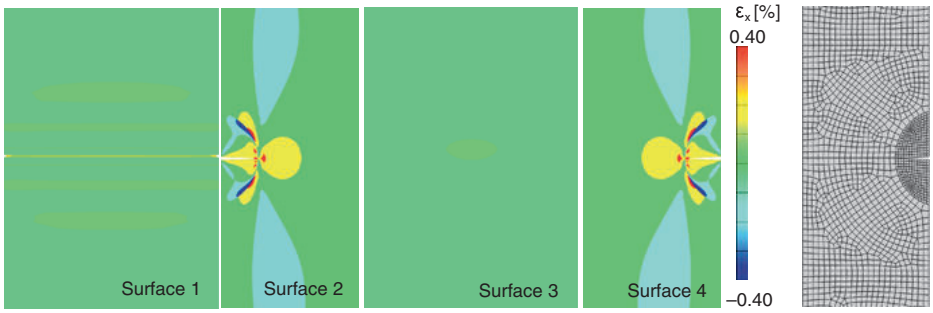

Fig. 17 Results from FE simulation, Edge knot specimen: lateral strains and FE mesh

the strain fields measured on different sides of a test specimen. Regarding the two first objectives, it could be concluded that the DIC technique is a useful tool for catching both qualitative and quantitative information about the behaviour of knots in wood members exposed to loading. The observation of release of internal stresses close to the knot in the Edge knot specimen must be considered as rather interesting. The graphical representations of the strain measuring results by the use of contour plots and section diagrams for different load stages in a load test provide valuable information about the strain distribution and development around knots. It is also possible to detect clear wood defects that are difficult to identify otherwise. For example, the chip on Surface 4 of the Centric knot specimen and the three cracks on Surfaces 2 and 4 of the Edge knot specimen could not have been detected neither by scanning nor by visual inspection. It is very likely that the discovered cracks will serve as indications of fracture and in the plans for future work, fracture tests are included. In such tests, the progress of fracture of the two specimens will be measured and documented by the use of the ARAMIS^{TM} system.

With reference to the objective concerning correlation between strain fields on different specimen surfaces, it has been demonstrated that the strain match between adjacent sides is very good, taken into account that only one specimen surface was measured during each load test.

Finally, the correspondence between the measurement results and the FE simulations is, indeed, promising, especially considering the fact that the applied models were rather simple. The DIC technique used in this research will, with a high degree of probability, be of great interest for the calibration of finite element models for, for instance, the analyses of fracture mechanical behaviour of knots in wood members. Such models would be of great importance for the development of more accurate strength grading methods based on scanned information concerning the occurrence of knots liable to initiate fractures in wood members to be graded.

Acknowledgments This research was made possible by the financial support from The Knowledge Foundation and The Swedish Research Council for Environment, Agricultural Sciences and Spatial Planning.

References

ABAQUS Inc. (2008) ABAQUS/Standard and ABAQUS/CAE version 6.8, User's manuals

European Standard EN 1912:2004+A2 (2008) Structural timber—strength classes—assignment of visual grades and species

European Standard EN 338 (2003) Structural timber—strength classes

GOM mbH (2007) ARAMIS User Manual—Software, aramis_v6_1st_en_rev-c, 25 April 2007

Inter-nordic standardisation INSTA 142/SS 23 01 20 (1998) Nordic visual strength grading rules for timber (in Swedish)

Johansson C-J (2003) Grading of timber with respect to mechanical properties. In: Thelandersson S, Larsen HJ (eds) Timber engineering. Wiley, Chichester, pp 23–43

Johansson C-J, Brundin J, Gruber R (1992) Stress grading of Swedish and German timber—a comparison of machine stress grading and three visual grading systems. SP Swedish National Testing and Research Institute, SP REPORT 1992:23

Johansson C-J, Boström L, Bräuner L, Hoffmeyer P, Holmqvist C, Solli KH (1998) Laminations for glued laminated timber—establishment of strength classes for visual strength grades and machine settings for glulam laminations of Nordic origin. SP Swedish National Testing and Research Institute, SP REPORT 1998:38

Jungnikl K, Goebbels J, Burgert I, Fratzl P (2009) The role of material properties for the mechanical adaptation at branch junctions. Trees 23(3):605–610

Karihaloo BL (1995) Fracture mechanics & structural concrete. Longman Group Ltd, Harlow

Kollman FFP, Côté WA (1968) Principles of wood science and technology. Springer, Berlin

Larsson D (1997) Mechanical characterization of engineering materials by modal testing. Dissertation D97:4, Chalmers University of Technology, Gothenburg

Miyauchi K, Murata K (2007) Strain-softening behaviour of wood under tension perpendicular to the grain. J Wood Sci 53(6):463–469

Müller U, Gindl W, Jeronimidis G (2006) Biomechanics of a branch-stem junction in softwood. Trees 20(5):643–648

Murata K, Masuda M, Ukyo S (2005) Analysis of strain distribution of wood using digital image correlation method—four-point bend test of timber including knots. Trans Visual Soc Jpn 25(9):57–63

Serrano E, Enquist B (2005) Contact-free measurement and non-linear finite element analyses of strain distribution along wood adhesive bonds. Holzforschung 59:641–646

Sjödin J, Serrano E, Enquist B (2006) Contact-free measurements and numerical analyses of the strain distribution in the joint area of steel-to-timber dowel joints. Holz Roh Werkst 64:497–506

Vessby J, Olsson A, Enquist B (2008) Contact-free strain measurement of bi-axially loaded sheathing-to-framing connection. In: Proceedings (CD) of the 10th world conference on timber engineering, Miyazaki, Japan

Young Jeong G, Zink-Sharp A, Hindman DP (2009) Tensile properties of earlywood and latewood from Loblolly Pine (Pinus Taeda) using Digital Image Correlation. Wood Fibre Sci 41(1):51–63

II

Eur. J. Wood Prod. (2013) 71:319–333
DOI 10.1007/s00107-013-0684-5

ORIGINALS ORIGINALARBEITEN

Prediction of timber bending strength and in-member cross-sectional stiffness variation on the basis of local wood fibre orientation

Anders Olsson · Jan Oscarsson · Erik Serrano · Bo Källsner · Marie Johansson · Bertil Enquist

Received: 29 November 2012 / Published online: 21 March 2013

Abstract Machine strength grading of structural timber is based upon relationships between so called indicating properties (IPs) and bending strength. However, such relationships applied on the market today are rather poor. In this paper, new IPs and a new grading method resulting in more precise strength predictions are presented. The local fibre orientation on face and edge surfaces of wooden boards was identified using high resolution laser scanning. In combination with knowledge regarding basic wood material properties for each investigated board, the grain angle information enabled a calculation of the variation of the local MOE in the longitudinal direction of the boards. By integration over cross-sections along the board, an edgewise bending stiffness profile and a longitudinal stiffness profile, respectively, were calculated. A new IP was defined as the lowest bending stiffness determined along the board. For a sample of 105 boards of Norway spruce of dimension 45 × 145 × 3,600 mm^3, a coefficient of determination as high as 0.68–0.71 was achieved between this new IP and bending strength. For the same sample, the coefficient of determination between global MOE, based on the first longitudinal resonance frequency and the board density, and strength was only 0.59. Furthermore, it is shown that improved accuracy when determining the stiffness profiles of boards will lead to even better predictions of bending strength. The results thus motivate both an industrial implementation of the suggested method and further research aiming at more accurately determined board stiffness profiles.

A. Olsson (✉) · E. Serrano · B. Källsner · M. Johansson · B. Enquist
Faculty of Technology, Linnaeus University, 351 95 Växjö, Sweden
e-mail: anders.olsson@lnu.se

J. Oscarsson
SP Technical Research Institute of Sweden, Vidéum Science Park, 351 96 Växjö, Sweden

Bestimmung der Biegefestigkeit von Schnittholz und der Variation der Biegesteifigkeit in Brettlängsrichtung in Abhängigkeit des lokalen Faserverlaufs

Zusammenfassung Maschinelle Festigkeitssortierung von Bauholz basiert auf dem Verhältnis zwischen Sortierparametern, den sogenannten IPs, und der Biegefestigkeit. Allerdings sind die heute gebräuchlichen Parameter eher schwach korreliert. In dieser Studie werden neue Sortierparameter sowie ein neues Sortierverfahren für eine genauere Festigkeitsbestimmung vorgestellt. Der lokale Faserverlauf auf den Schmal- und Breitseiten der Bretter wurde mittels hochauflösendem Laserscanning ermittelt. Bei bekannten generellen Materialeigenschaften eines Brettes konnte anhand der Faserwinkelangaben die Variation des lokalen Elastizitätsmoduls in Längsrichtung dieses Brettes berechnet werden. Durch Integration über Querschnitte entlang des Brettes wurde ein Steifigkeitsprofil für Hochkant-Biegebeanspruchung über die gesamte Bretlänge berechnet. Als neuer Sortierparameter (IP) wurde die niedrigste Biegesteifigkeit entlang des Brettes definiert. An einer Stichprobe aus 105 Fichtenbrettern mit den Abmessungen 45 × 145 × 3,600 mm^3 wurde für die Beziehung zwischen diesem neuen IP und der Biegefestigkeit ein Bestimmtheitsmaß von 0,68–0,71 ermittelt. Bei derselben Stichprobe ergab sich für die Beziehung zwischen dem globalen Elastizitätsmodul, berechnet aus der Eigenfrequenz einer Längsschwingung und der Brettrohdichte, und der Festigkeit ein Bestimmtheitsmaß von nur 0,59. Des Weiteren wurde gezeigt, dass eine höhere Genauigkeit bei der Bestimmung des Steifigkeitsprofils von Brettern zu

einer noch besseren Bestimmung der Biegefestigkeit führt. Die Ergebnisse rechtfertigen sowohl eine industrielle Anwendung des vorgestellten Verfahrens als auch weitere Forschungsbemühungen, um die Steifigkeitsprofile von Brettern noch genauer bestimmen zu können.

List of symbols

σ_m	Bending strength
E_m	Local MOE based on measured deflections in static bending
$E_{m,g}$	Global MOE based on measured deflections in static bending
ρ	Board (average) density
f_{a1}	Resonance frequency of first longitudinal mode of vibration
E_{a1}	MOE calculated on basis of f_{a1} and ρ
$E_{a,min}$	MOE calc. for longitudinal direction in the weakest section, based on fibre orientation and f_{a1}
$E_{b,min}$	MOE calc. for bending of the weakest section, based on fibre orientation and f_{a1}
$E_{b,min,\delta}$	MOE calc. for bending of the weakest δ mm long part of the beam
$E_{b,min,\delta,w}$	MOE calc. for bending of the weakest δ mm long part of the beam in relation to a weight function w
R^2	Coefficient of determination

1 Introduction

Structural timber is classified into specific strength grades using various methods available on the market. A brief description of the most important ones is given below. However, the statistical relationships being utilized today between the indicating properties (IP) and the target bending strength are rather weak. In commercially available machine strength grading systems, the coefficient of determination, R^2, between the IPs and the bending strength typically lies in the range of 0.5–0.6 for Norway spruce. With the most advanced systems known to the market, using a multitude of sensors and measurement principles, values above $R^2 = 0.7$ can be achieved but such systems are rarely used in practice. Improvements of the coefficient of determination between the IPs and the bending strength have a considerable commercial potential as higher accuracy would make it possible to efficiently grade timber into higher strength classes than what can be done today, and a better yield would be achieved in the more common strength classes.

The basic principle for machine strength grading of structural timber is generally to determine a modulus of elasticity (MOE) of a board and to use this property as an IP for prediction of bending strength. Dynamic excitation can, in combination with density and board length, be used to determine a global, longitudinal MOE directly, see e.g. Larsson (1997). This method is frequently applied using relatively inexpensive machines. It could also be utilized without determination of the actual board density. In such cases, an average density of the graded wood species is used.

A literature review carried out by Olsson et al. (2011) showed that the bending stiffness correlates better with bending strength than what the longitudinal stiffness does. Olsson et al. (2011) also showed that a set of resonance frequencies corresponding to higher modes of vibration can be used for assessing the homogeneity of a board. A measure of inhomogeneity (MOI), corresponding to the variation of stiffness along a board, was suggested as a complementary IP, i.e., to be used in combination with the MOE, for prediction of bending strength.

Flatwise bending machines have been used since the 1960s and are still available on the market. Over a span of about one metre, and moving along the board, the bending stiffness is measured and on this basis a MOE valid for *flatwise* bending representing a certain part of the board is calculated. Thus, such machines give some information regarding the stiffness variation along the board.

The sizes and locations of knots can be detected with rather high precision using X-ray techniques. The benefit of such detection is underlined by the fact that fracture testing of a sample of about 1,000 pieces of timber has shown that more than 90 % of the failures were caused by knots (Johansson 2003). Schajer (2001) was able to make better predictions using an X-ray technique than what could be done using a bending machine in a comparative study. There are grading machines on the market today that combine X-ray techniques with either flat-wise bending or measurement of the dynamic longitudinal stiffness. The information added by the X-ray technique compared to the other techniques is a high resolution in measuring the variation of the density within a board.

The orientation of wood fibres in timber has a large effect on stiffness and strength and there are techniques to identify the fibre orientation locally on the surface or within wooden members. An early attempt to utilize such information for strength grading purposes was presented by Bechtel and Allen (1987). The fact that the dielectric constant is higher in the fibre direction or actually in the direction of fibres projected on a surface than across the fibres was utilized. Fibre angles were identified over the two face surfaces of boards and it was shown that the detected grain field could be used for identifying knots. Three different methods aiming at actually calculating the crack path and the tensile strength of boards were also

suggested. The methods were based on the Hankinson formula by which the local tensile strength in the direction of the board was expressed as a function of the tensile strength in the fibre direction and the local fibre angle. For a small sample consisting of 24 specimens it was shown that a coefficient of determination between calculated and true tensile strength exceeding 0.8 could be reached. However, the coefficient of determination between global MOE and true tensile strength was for the same sample 0.77, which is very high compared with what has been presented in other studies and also compared with what is reached in grading utilizing global MOE as indicating property to strength. Two possible explanations for the high R^2 values were offered. First, the tensile test was carried out over a short span (70 cm) and, second, usual statistical procedures for material sampling were not followed. Recently Moore and Baldwin (2011) discussed the method suggested by Bechtel and Allen and concluded that nowadays it is possible to identify the grain angle field on the basis of the dielectric constant in a speed corresponding to the production speed at sawmills. They also suggested an improved version of one of the methods suggested by Bechtel and Allan, but it was only verified on a very small sample consisting of nine planed fir boards two of which had to be excluded because of twist causing difficulties when applying the dielectric method.

Laser techniques utilizing the so-called tracheid effect for detecting fibre orientation are available and have been implemented in high speed, high resolution wood-scanners already on the market. However, the technique is not yet utilized for strength grading purposes in a sophisticated way. Petersson (2010) showed that size and location of knots can be determined on the basis of the grain-angle distribution detected using this technique. In addition, he presented research which was aimed at accurately predicting the stiffness on the basis of end scanning, including information about pith location and annual ring width.

In a study by Jehl et al. (2011), the influence of fibre angles on the prediction of both MOE and tensile strength was evaluated. The fibre angle fields were examined over the face surfaces of 350 boards. Also the diving angle, i.e. the angle between the board surface and the wood fibres, was evaluated by examining the shape of the elliptic laser dot, which due to the tracheid effect is stretched in the direction of the projected fibre angle. The authors claim that the diving angle can be determined in this way but they also say that the results achieved are rather uncertain. Furthermore, it was assumed that the MOE is an affine function of the density. Thus, a map of the local board density, averaged through the thickness of each board, was obtained from an optical scanner equipped with an X-ray source. From such maps, the fraction of the thickness occupied by a knot was computed on pixel level and the corresponding clear wood area ratio (CWAR) was determined. To take the effect of fibre angle fields into account, local CWAR values were modified using Hankinson's formula. Finally, a board's MOE was determined either from axial dynamic excitation or as the product of modified CWAR and the clear wood's MOE. The tensile strength was similarly estimated as the product of modified CWAR and clear wood tensile strength. By application of the described method it was possible to predict tension strength with very high accuracy, at best with a coefficient of determination of 0.78.

As previous research has pointed out, high resolution information regarding fibre angles has a very interesting potential for strength grading purposes. However, whereas the research referred to above is based mainly upon empirical relationships, a theoretically sound base for the relationship between wood material properties, fibre orientation in timber and local MOE in the direction of the board is presented in this paper. A suitable IP to bending strength is also defined and the potential for further improvements of the concept of utilizing local stiffness for strength grading purposes is evaluated. A patent application has recently been filed for an invention corresponding to the method presented herein.

2 Sampling of material for evaluation

The sampling of timber for the investigation took place in Långasjö, Sweden, on December 11-12, 2007, at a sawmill owned by the company Södra Timber. The timber consisted of sawn boards of Norway spruce (*Picea abies*) of nominal dimensions 50×150 mm^2 and of length 3,900 mm or 4,500 mm. In the sampling it was aimed for a sample with large variation in strength. Thus, boards with high and low expected strength were included. For this purpose a grading machine of type Dynagrade® was employed with settings for grading of timber to be used for roof trusses (strength class TR26) on the UK market. Both boards fulfilling (61 pieces) and boards not fulfilling the requirements (44 pieces) were selected for further investigation. A visual assessment was performed in order to identify the weakest section of each board according to instructions in the European standard EN 384 (CEN 2010a). This standard prescribes that the weakest section should be located in the maximum bending moment zone, i.e. between the two point loads in a four point bending test, and that the tension edge shall be selected at random after the weakest section has been chosen.

All the boards were planed to dimension 45×145 mm^2 immediately after selection. Then the boards were cut to a length of 3,600 mm and placed in a climate room holding a temperature of 20 °C and 65 % relative humidity (RH).

Small pieces of wood were also saved and stored in the climate room for assessment of the moisture content.

3 Methods and measurements

The research involves laboratory testing including laser scanning, dynamic excitation and static loading. Quantities measured in the laboratory were the weight and dimensions of the boards, high resolution fibre orientation fields on the surfaces of the boards, resonance frequencies corresponding to longitudinal modes of vibration, static edgewise bending stiffness (determined in two different ways, giving a local and a global measure, respectively) and the bending strength. The arrangements and performance of the scanning and dynamic and static tests are described below.

In addition to the laboratory work, the research also involves analytical and numerical calculations and common regression analysis using the software Matlab®.

3.1 Scanning for detection of fibre angles on surfaces

A WoodEye scanner (from Innovativ Vision AB) equipped with four sets of multi-sensor cameras, dot and line lasers and conveyor belts for feeding boards in the longitudinal direction through the scanner was used for face and edge scanning. Figure 1 shows the WoodEye-scanner (left) and an overview of the WoodEye system with lasers, light and multi-sensor cameras (right). The notation "IN" marks the cross section of a scanned board. The laser scanning makes use of the so-called tracheid effect where one of the principal axes of the light intensity distribution around a laser dot is oriented in the direction of the wood fibres (Nyström 2003). This provides a practical method for measuring variations in grain angle on a wood surface. Figure 2 shows a piece of wood including a knot (left), an image showing how the light from the dot lasers spread on the wood surface (middle) and the fibre orientation on the wood surface (right) calculated by identifying the major principal axis of each light spot using image analysis. Within knots, where the shape of the light spots is close to circular, the calculation of the fibre direction becomes uncertain. This is indicated in Fig. 2 (right) by the dotted lines drawn for the calculated fibre orientations corresponding to such laser dots.

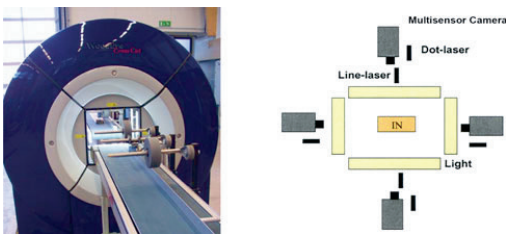

Fig. 1 WoodEye-scanner (*left*) and overview of the WoodEye system with lasers, light and multisensor cameras (*right*). The notation "IN" marks the cross-section of a scanned board [Images originate from Petersson (2010).]

Abb. 1 WoodEye-Scanner (links) und Darstellung des WoodEye-Systems mit Lasern, Licht und Multisensorkameras (rechts). „IN" gibt den Querschnitt des gescannten Brettes an (aus Petersson 2010)

The resolution employed for scanning of the boards, i.e. the distance between laser dots on the surfaces, was 0.8 mm in the longitudinal direction of the board and 3.6 mm in the lateral board direction. It should be noted that the grain angle detected actually represents the fibre orientation projected on the surface. Consequently, the so called diving angle is not assessed here.

3.2 Determination of dynamic stiffness

Determination of the lowest longitudinal resonance frequency of each board, which in combination with the board density is used for calculating an average board MOE, was performed using an MTG hand-held timber grader. The MTG grader is a wireless measuring instrument for strength grading of structural timber (Brookhuis Micro-Electronics 2009). It is approved as machine grading system with settings listed in EN 14081-4 (CEN 2009). The frequency measurement is carried out simultaneously as the board is supported by a balance from which the weight is determined. The resonance frequencies of the boards included in this study were also assessed using a more advanced laboratory setup in which free–free boundary conditions were resembled by suspending the boards in rubber bands. In this test setup the board was hit with an impulse hammer at one end of the board and the vibration content was measured using an accelerometer fastened at the other end. The coefficient of determination between the lowest longitudinal resonance frequencies measured using the two different sets of equipment was as high as $R^2 = 0.999$.

3.3 Static four-point bending test

The local and global static bending stiffness and the bending strength of the boards were determined using a four point bending test according to the European standard EN 408 (CEN 2010b). The total span was 2,610 mm long (corresponding to eighteen times the depth of the board) and the two point loads were applied 870 mm apart, each of them 870 mm from the nearest support. For such a load case, the mid-span is subjected to a constant bending moment and no shear force. The predicted weakest part of

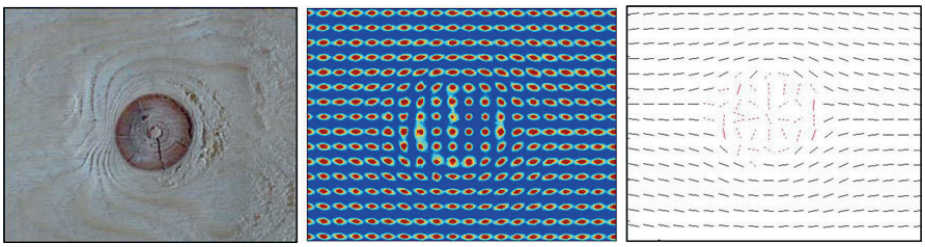

Fig. 2 A piece of wood including a knot (*left*), an image showing how the light from dot lasers spread on the wood surface (*middle*) and the fibre orientation on the wood surface (*right*) calculated by identifying the major principal axis of each light spot using image analysis [Images originate from Petersson (2010).]

Abb. 2 Holzprobe mit Ast (links); Bild, das zeigt, wie sich das Licht der Punktlaser auf der Holzoberfläche ausbreitet (Mitte); Faserverlauf auf der Holzoberfläche (rechts) berechnet mittels Bildanalyse auf Basis der bestimmten Hauptachse jedes Lichtpunktes (Petersson (2010))

each board, selected by means of visual inspection, was located within the zone with constant bending moment, i.e. between the two point loads, and was randomly located with respect to the position of the tension side of the board.

4 Calculation of stiffness on the basis of fibre angles

It is well known that wood is a strongly orthotropic material having very high stiffness and strength in the fibre direction but low stiffness and strength in other directions. In a stem or wooden board, most fibres are close to parallel with the longitudinal stem or board direction, but also small deviations in fibre direction have a significant effect on the board properties. Locally, in particular within and in the close surrounding of knots, the fibre direction may deviate strongly from the longitudinal direction of the stem or board, see Fig. 2 (right), and this is crucial for the structural properties of timber.

Figure 3 shows a drawing of a part of a stem and a drawing of a board that could have been cut out from it. Two different coordinate systems are displayed, one global with axes parallel to the sides of the board and one local relating to the main directions of the wood material in a position in the stem. From an engineering point of view one needs to describe the structural properties in relation to a coordinate system where one axis (x) is parallel to the longitudinal direction of the board and the other two axes (y and z) are oriented parallel to the thickness direction and depth direction, respectively. Knowing the fibre orientation locally in relation to the board direction, material transformations can be carried out giving the local material properties corresponding to the principal directions of the board, i.e. the global coordinate system. Assuming that (**l**, **r**, **t**) and (**i**, **j**, **k**) are the unit vectors along the l-r-t system and the x-y-z system, respectively, one can write

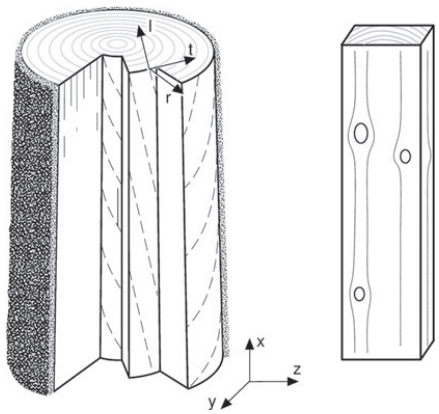

Fig. 3 Drawing of a part of a stem and of a board that could have been cut out from it. Two different coordinate systems are displayed, one global with axes parallel to the sides of the board and one local relating to the main directions of the wood material in a position in the stem [The *left drawing* originates from Ormarsson (1999).]
Abb. 3 Teil eines Stammes und ein daraus entnommenes Brett. Zwei verschiedene Koordinatensysteme sind dargestellt, ein globales mit Achsen parallel zu den Seiten des Brettes sowie ein lokales entsprechend den Hauptrichtungen der Holzstruktur im Stamm (linke Zeichnung aus Ormarsson 1999)

$$\begin{bmatrix} \mathbf{l} \\ \mathbf{r} \\ \mathbf{t} \end{bmatrix} = \mathbf{A}^{\mathbf{T}} \begin{bmatrix} \mathbf{i} \\ \mathbf{j} \\ \mathbf{k} \end{bmatrix} \tag{1}$$

where

$$\mathbf{A} = \begin{bmatrix} a_l^x & a_r^x & a_t^x \\ a_l^y & a_r^y & a_t^y \\ a_l^z & a_r^z & a_t^z \end{bmatrix} \tag{2}$$

where a denotes cosine for the two axes indicated by the subscript and the superscript, respectively, for instance, a_l^x denotes cosine for the angle between the l- and x-axes.

The wood material properties relating to local directions can be stored in the compliance matrix $\bar{\mathbf{C}}$ as (the symbol $\bar{}$ is used in notations whenever a quantity is expressed in the local coordinate system and omitted when the quantity is expressed in the global coordinate system)

$$\bar{\mathbf{C}} = \begin{bmatrix} \frac{1}{E_l} & -\frac{\nu_{rl}}{E_r} & -\frac{\nu_{tl}}{E_t} & 0 & 0 & 0 \\ -\frac{\nu_{lr}}{E_l} & \frac{1}{E_r} & -\frac{\nu_{tr}}{E_t} & 0 & 0 & 0 \\ -\frac{\nu_{lt}}{E_l} & -\frac{\nu_{rt}}{E_r} & \frac{1}{E_t} & 0 & 0 & 0 \\ 0 & 0 & 0 & \frac{1}{G_{lr}} & 0 & 0 \\ 0 & 0 & 0 & 0 & \frac{1}{G_{lt}} & 0 \\ 0 & 0 & 0 & 0 & 0 & \frac{1}{G_{rt}} \end{bmatrix} \quad (3)$$

where E_l, E_r, E_t are the moduli of elasticity in the orthotropic directions, G_{lr}, G_{lt}, G_{rt} are the shear moduli in the respective orthotropic planes, and the parameters ν_{lr}, ν_{rl}, ν_{lt}, ν_{tl}, ν_{rt} and ν_{tr} are Poisson's ratios. Note that the relations $\nu_{rl} = \mathrm{E}_r/\mathrm{E}_l \times \nu_{lr}$, $\nu_{tl} = \mathrm{E}_t/\mathrm{E}_l \times \nu_{lt}$ and $\nu_{tr} = \mathrm{E}_t/\mathrm{E}_r \times \nu_{rt}$ hold which means that $\bar{\mathbf{C}}$ only contains nine independent material parameters.

The material matrix $\bar{\mathbf{D}} = \bar{\mathbf{C}}^{-1}$ (relating to the l-r-t system, i.e. the local coordinate system) may be used to express a linear elastic constitutive relation between stresses and strains as

$$\bar{\boldsymbol{\sigma}} = \mathbf{D}\varepsilon \quad (4)$$

where strain and stress components are stored in $\bar{\boldsymbol{\varepsilon}}$ and $\bar{\boldsymbol{\sigma}}$, respectively, as $\bar{\boldsymbol{\varepsilon}} = [\,\varepsilon_l \quad \varepsilon_r \quad \varepsilon_t \quad \gamma_{lr} \quad \gamma_{lt} \quad \gamma_{rt}\,]^{\mathrm{T}}$ and $\bar{\boldsymbol{\sigma}} = [\,\sigma_l \quad \sigma_r \quad \sigma_t \quad \tau_{lr} \quad \tau_{lt} \quad \tau_{rt}\,]^{\mathrm{T}}$. Strains and stresses may be transformed between the l-r-t system and the x-y-z system using a transformation matrix $\mathbf{G}$ as

$$\bar{\boldsymbol{\varepsilon}} = \mathbf{G}\varepsilon \quad (5)$$

and

$$\boldsymbol{\sigma} = \mathbf{G}^{\mathbf{T}}\bar{\boldsymbol{\sigma}} \quad (6)$$

respectively, where the transformation matrix

$$\mathbf{G} = \begin{bmatrix} a_l^x a_l^x & a_l^y a_l^y & a_l^z a_l^z & a_l^x a_l^y & a_l^z a_l^x & a_l^y a_l^z \\ a_r^x a_r^x & a_r^y a_r^y & a_r^z a_r^z & a_r^x a_r^y & a_r^z a_r^x & a_r^y a_r^z \\ a_t^x a_t^x & a_t^y a_t^y & a_t^z a_t^z & a_t^x a_t^y & a_t^z a_t^x & a_t^y a_t^z \\ 2a_l^x a_r^x & 2a_l^y a_r^y & 2a_l^z a_r^z & a_l^x a_r^y + a_l^y a_r^x & a_l^z a_r^x + a_l^x a_r^z & a_l^y a_r^z + a_l^z a_r^y \\ 2a_t^x a_l^x & 2a_t^y a_l^y & 2a_t^z a_l^z & a_t^x a_l^y + a_t^y a_l^x & a_t^z a_l^x + a_t^x a_l^z & a_t^y a_l^z + a_t^z a_l^y \\ 2a_r^x a_t^x & 2a_r^y a_t^y & 2a_r^z a_t^z & a_r^x a_t^y + a_r^y a_t^x & a_r^z a_t^x + a_r^x a_t^z & a_r^y a_t^z + a_r^z a_t^y \end{bmatrix} \quad (7)$$

is based on the components of $\mathbf{A}$ defined in Eq. (2) (Ormarsson 1999). By premultiplication of Eq. (4) by $\mathbf{G}^{\mathbf{T}}$and considering Eqs. (5–6) it follows that the material matrix relating to the x-y-z system can be expressed as

$$\mathbf{D} = \mathbf{G}^{\mathbf{T}}\bar{\mathbf{D}}\mathbf{G} \quad (8)$$

Of particular interest for the following is that $c_{1,1}^{-1}$, i.e. the inverse of the component stored in the first row and first column of the globally oriented compliance matrix $\mathbf{C} = \mathbf{D}^{-1}$, is now equal to $E_x(x,y,z)$, i.e. the local MOE valid in the longitudinal direction of the board.

4.1 Modulus of elasticity calculated on board surfaces

The description above concerning how to calculate local MOE in the longitudinal board direction is presented in general terms. In practice, however, certain assumptions have to be made as the knowledge regarding true fibre angle orientation is not complete. It is now assumed that the projected fibre angles on the lateral board surfaces (a lateral board surface is a surface with a normal direction perpendicular to the longitudinal direction of the board) detected by means of scanning represent the true, three-dimensional fibre orientation on these surfaces. It is also assumed that the normal direction of each lateral board surface is parallel with the radial direction of the wood material, i.e. that each lateral surface is oriented in the longitudinal-tangential plane. If the basic wood material parameters, i.e. the parameters involved in the locally oriented compliance matrix $\bar{\mathbf{C}}$ (Eq. 3 above), are known the MOE on the lateral board surfaces in the longitudinal board direction can be calculated. The issue of how to determine the basic wood material parameters valid for an individual board is addressed in a separate section below, but it is suitable for the purposes of this study to show, already at this stage, an example of calculation results, with high spatial resolution, regarding MOE on lateral board surfaces. Figure 4 (left) shows photographs of all four sides of one board (denoted board number 74) and MOE in longitudinal board direction over the board surfaces (right) calculated on the basis of the local fibre angles (or rather on their projections on the wood surface). The x-axis starts at the root end of the board. Red colour indicates a high MOE, found in areas where the orientation of the wood fibres coincide with the longitudinal direction of the board, and blue colour indicates a particularly low MOE corresponding to a local fibre direction diverging substantially from the longitudinal board direction. Note that areas occupied by knots typically have a fibre orientation substantially diverging from the longitudinal board direction. The absolute level of the MOE in the individual board depends on the basic material parameters, of which the MOE in the fibre direction is the most important one. The centre parts of Fig. 4 shows photographs, projected fibre angle field and calculated MOE in the longitudinal board direction of a small part of the board. The topmost centre part of Fig. 4 shows an enlargement of the fibre angle field at a single large knot in the board.

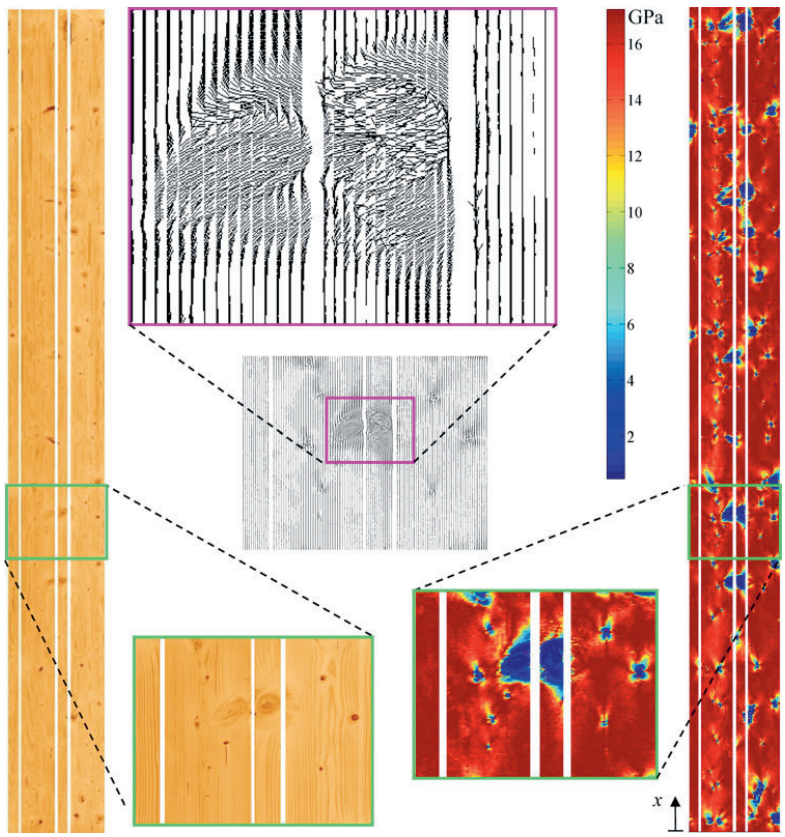

Fig. 4 Photographs of all four sides of one board (*left*) and calculated MOE in longitudinal board direction over the entire board surface (*right*). The x-axis starts at the root end of the board. Red colour indicates a high MOE, found in areas where the orientation of the wood fibres coincide with the longitudinal direction of the board, and blue colour indicates a particularly low MOE corresponding to a local fibre direction diverging substantially from the longitudinal board direction. The *centre parts* show photographs, projected fibre angle field and calculated MOE in a small part of the board. The *topmost centre* part shows an enlargement of the projected fibre angle field at a single large knot in the board

Abb. 4 Aufnahmen aller vier Brettseiten (links) und berechneter Elastizitätsmodul in Brettlängsrichtung über die gesamte Brettfläche (rechts). Die x-Achse beginnt am Fußende des Brettes. Rote Farbe gibt einen hohen E-Modul an in Bereichen, in denen der Faserverlauf mit der Brettlängsrichtung übereinstimmt, und blaue Farbe zeigt einen besonders niedrigen E-Modul bei einem lokalen Faserverlauf, der wesentlich von der Brettlängsrichtung abweicht. In der Mitte sind ein projiziertes Faserwinkelfeld und der E-Modul-Verlauf eines kleinen Brettabschnitts abgebildet. Ganz oben in der Mitte ist eine Vergrößerung des projizierten Faserwinkelfeldes im Bereich eines großen Astes zu sehen

5 Integration of cross-sectional stiffness properties

Now follows a more general description and it is assumed that the MOE valid in the longitudinal direction of the board is known in every position within it, i.e. $E_x = E_x\,(x, y, z)$ is known for $0 \le x \le L$, $-t/2 \le y \le t/2$ and $-d/2 \le z \le d/2$, where L, t and d is the length, thickness and depth of the board, respectively. Furthermore, a coordinate system with its origin at one end of the board and in the geometrical centre of the cross-section is introduced. Considering the wooden board as a beam, the position of the neutral axis (i.e. the position (y, z) within the board cross-section where, according to traditional beam theory, zero normal stress is obtai ned when the beam is exposed to pure bending around the y-axis and the z-axis, respectively) can be calculated as

$$\bar{y}(x) = \frac{\iint E_x \cdot y\, dydz}{\iint E_x\, dydz} \tag{9}$$

and

$$\bar{z}(x) = \frac{\iint E_x \cdot z \, dydz}{\iint E_x \, dydz} \tag{10}$$

respectively. The bending stiffness along the beam with respect to bending around the y- and z-axis can then be calculated as

$$EI_y(x) = \iint E_x \cdot (z - \bar{z})^2 dydz \tag{11}$$

and

$$EI_z(x) = \iint E_x \cdot (y - \bar{y})^2 dydz \tag{12}$$

respectively (One may note that these axes are not actually principal axes.). The longitudinal board stiffness can be calculated as

$$EA(x) = \iint E_x dydz \tag{13}$$

5.1 Calculation of cross-sectional stiffness properties under certain assumptions

Knowing the spatial distribution of the material orientation and the stiffness properties of the material everywhere within the board it is thus possible to calculate the stiffness in the longitudinal direction of the board and, by integration, to calculate the stiffness properties on the cross-sectional level. However, with limited information regarding the material orientation within the boards, certain assumptions have to be made before the cross-sectional stiffness properties can actually be calculated. In addition to the assumptions declared above when calculating the MOE in the longitudinal board direction on the lateral board surfaces it is also assumed that the detected fibre directions are representative for the material to a certain depth in the board in direction perpendicular to the surfaces. Figure 5 illustrates a suggested way to represent the fibre angle field and MOE within the board. The drawing on the left shows the cross-section divided into small strips, each with one side coinciding with one side of the board. One such strip is highlighted in grey. The drawing on the right shows a small segment of length dx in the longitudinal direction of the board and projected fibre angles, φ, on one surface of this segment. Fibre angles are detected with a certain resolution which is illustrated by the size of the strips drawn. The MOE in the longitudinal direction of the board is calculated for each fibre angle sampling point and this MOE is considered as being representative for a certain wood volume, i.e. the volume given by the area dA times the distance dx, cf. Fig. 5. A numerical integration is then executed in accordance with Eqs. (9–13) giving, as functions of x, the position of the neutral axis, the cross-sectional bending stiffness in the strong and weak direction of the board, respectively, and the longitudinal board stiffness. The distance a shown in Fig. 5 is set to

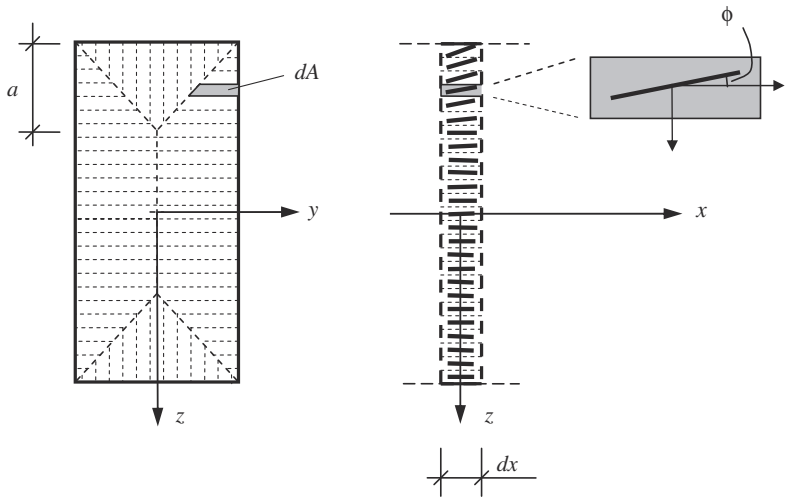

Fig. 5 A suggested way to represent the fibre angle field and MOE within the board. The drawing on the *left* shows the cross-section divided into small strips, each with one side coinciding with one side of the board. One strip is highlighted in *grey*. The drawing on the *right* shows a small segment of length dx in the longitudinal direction of the board and detected fibre angles on one surface of this segment

Abb. 5 Vorschlag zur Darstellung des Faserwinkelfeldes und des E-Moduls in einem Brett. Links: Brettquerschnitt unterteilt in kleine Streifen, ausgerichtet zu den Brettseiten. Ein Streifen ist grau markiert. Rechts: Kleiner Abschnitt in Brettlängsrichtung dx mit ermitteltem Faserwinkel auf einer Brettseite dieses Abschnittes

35 mm when performing the integration herein. More advanced integration schemes, possibly taking into account pith location and the general pattern for three dimensional grain flows around knots would be an interesting subject for further research.

Examples of graphs displaying the position of the neutral axis in the *xy*-plane (in relation to the geometric centre axis) and the edgewise bending stiffness profile, respectively, are shown in Fig. 6 for one board, here denoted board number 74 (the same board is shown in Fig. 4). The calculations are performed using the assumptions and integration scheme described above and results are shown for two different resolutions in the board direction. The two diagrams at the top of Fig. 6 show graphs corresponding to the maximum resolution achieved from scanning, i.e. with values determined at a distance of 0.8 mm apart along the board. The two diagrams at the bottom show graphs where the value at each position (i.e. at each x coordinate) is the average value of the surrounding 80 mm along the board, i.e. along 40 mm on each side of the *x*-coordinate in question. The root end of the board has *x*-coordinate equal to zero.

6 Material parameters and calibration of cross-sectional stiffness properties

The procedure described above for calculating cross-sectional stiffness properties along boards requires that the wood material properties are known, i.e. that they are known in relation to a local coordinate system with axes coinciding with the longitudinal, radial and tangential directions, respectively. Though average values for material properties valid for different species can be found in literature, the properties may differ substantially between boards originating from different trees and stands. Even *within* a tree, some properties may vary considerably, particularly in the direction from pith to bark (e.g. Wormuth 1993). The modulus of elasticity in the fibre direction, E_l, is by far the material parameter with the highest influence on the MOE in the board direction. Therefore it is important to assess a value for this parameter valid for each single board. Table 1 shows nominal values, $E_{l,0}$, $E_{r,0}$, $E_{t,0}$, $G_{lr,0}$, $G_{lt,0}$, $G_{rt,0}$, ν_{lr}, ν_{lt}, and ν_{rt}, originating from Dinwoodie (2000), for the wood material parameters used in this study. The material parameters are then adjusted for each individual board by considering an experimentally determined resonance frequency as described below. The parameters are adjusted in such a way that the relations between the different calibrated parameters, E_l, E_r, E_t, G_{lr}, G_{lt}, G_{rt}, are preserved, i.e. they are identical with the corresponding relations for the nominal parameters. The Poisson's ratios, ν_{lr}, ν_{lt} and ν_{rt} are kept constant. This means that a locally oriented compliance matrix, Eq. (3), determined for a particular board only differs compared to the nominal compliance matrices (i.e., a compliance matrix having nominal values for all material parameters involved) by a constant factor. Variations of material parameters within boards are ignored herein, i.e. the locally oriented compliance matrix valid for a particular board is not a function of position within the board.

As described in a previous section the resonance frequency corresponding to the first longitudinal mode of vibration can be determined experimentally. On the basis of such an experiment, an average MOE valid for the longitudinal direction of the board can be calculated as

$$E_{a1} = 4 \cdot \rho \cdot f_{a1}^2 \cdot L^2 \tag{14}$$

where ρ is the average board density, f_{a1} is the measured resonance frequency and L is the board length.

The material parameters representing a particular board should be such that an eigenfrequency analysis on a computational model based on these material parameters should give the same resonance frequency as the one determined experimentally. Therefore a simple one dimensional finite element model of each board is established which resembles the longitudinal stiffness profile calculated using Eq. (13) on the basis of nominal values for material parameters. The stiffness of each finite element in the model represents a short distance, Δx (approximately one centimetre), of the total board length and the axial stiffness of the pth element is calculated by averaging the axial stiffness obtained from Eq. (13) over the element length

$$k_p = \frac{\int_{(p-1)\Delta x}^{p\Delta x} EA(x)dx}{\Delta x^2} \tag{15}$$

In the FE model the mass of the board is assumed to be uniformly distributed in the longitudinal direction and a resonance frequency denoted $\hat{f}_{a1}$ is calculated by performing eigenvalue analysis on this FE model. The reason for calculating $\hat{f}_{a1}$ is thus to compare it with f_{a1} and to adjust the value employed for material parameters accordingly. Starting with the nominal values for all the material parameters the final values are adjusted in relation to the quota of the two resonance frequencies in square, e.g.

$$E_l = E_{l,0} \frac{f_{a1}^2}{\hat{f}_{a1}^2} \tag{16}$$

The final board stiffness profiles, $EA\ (x,)\ EI_y\ (x)$ and $EI_z\ (x)$ that may be utilized for strength grading purposes are thus based on material parameters assessed individually for each board after calibration to an experimentally determined resonance frequency. This means, of course, that the calculation results displayed in Figs. 4 and 6 are

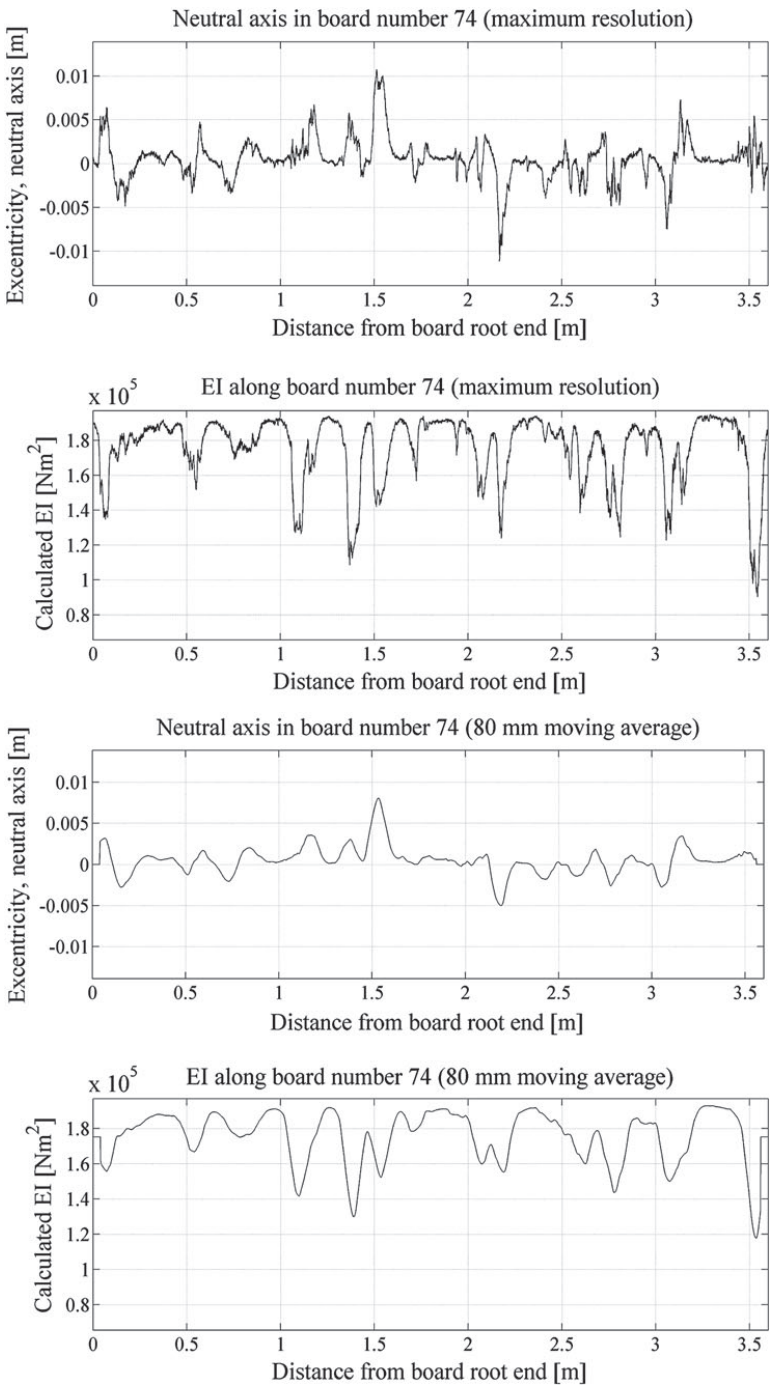

Fig. 6 Calculated position of neutral axis and local bending stiffness of board number 74. The two diagrams at the *top* show graphs corresponding to maximum resolution in the board direction, i.e. with values determined at a distance of 0.8 mm apart along the board. The two diagrams at the *bottom* show graphs where the value at each position is the average value of the surrounding 80 mm along the board

Abb. 6 Berechnete Lage der neutralen Achse und lokale Biegesteifigkeit des Brettes Nummer 74. Die beiden oberen Diagramme zeigen Graphen mit der maximalen Auflösung in Brettlängsrichtung, d.h. mit Werten, die in einem Abstand von 0,8 mm bestimmt wurden. Die beiden unteren Diagramme zeigen Graphen, bei denen die Werte über eine Länge von 80 mm gemittelt wurden

Table 1 Nominal material parameters employed (Norway spruce)
Tab. 1 Verwendete Materialkenngrößen (Fichtenholz)

$E_{l,0}$	10,700 MPa
$E_{r,0}$	710 MPa
$E_{t,0}$	430 MPa
$G_{lr,0}$	500 MPa
$G_{lt,0}$	620 MPa
$G_{rt,0}$	24 MPa
ν_{lr}	0.38
ν_{lt}	0.51
ν_{rt}	0.51

not actually achieved until this part of the calculation process is performed.

7 Definition and assessment of indicating properties

Below, novel IPs are defined on the basis of the cross sectional stiffness profiles calculated as described above. However, in order to evaluate the competitiveness of those IPs, comparisons must be made with IPs that are commonly employed in grading methods of today or within research. Thus also IPs to be employed for comparisons are defined below.

7.1 Common IPs to be used for comparison

In EN 408 it is defined how to determine a *local* MOE and a *global* MOE, denoted E_m and $E_{m,g}$, respectively, using four point bending tests. The local MOE is calculated on the basis of the local deflection measured within the constant moment zone and over a distance of five times the depth of the board, here 725 mm containing what is supposed to be the weakest part of the board. The global MOE is based on the mid-span deflection of the board. A thorough definition of E_m and $E_{m,g}$ is also given by Olsson et al. (2011).

In addition to E_m and $E_{m,g}$, the dynamic MOE calculated on the basis of the resonance frequency corresponding to the first longitudinal mode of vibration, i.e. E_{a1} according to Eq. (14), and the average board density, ρ, are used as comparative IPs in the result section below.

7.2 Novel IPs based on board stiffness profiles on cross-sectional level

The MOE defined by the lowest edgewise bending stiffness along the board, calculated using Eq. (11) and with calibration according to Eq. (16), can be expressed (if edgewise bending is bending around the y-axis) as

$$E_{b,min} = \min_{0 \le x \le L} \big(EI_y(x)\big)/I_{y0} \tag{17}$$

where $I_{y0} = td^3/12$. The bending stiffness $E_{b,min}$ is here evaluated as a possible IP to bending strength. It should be noted that the employed spatial resolution when calculating $EI_y(x)$ is very high, the bending stiffness being assessed every 0.8 mm along the board, and it is likely that an average stiffness value over a certain distance, δ, along the board, would give a better IP to bending strength. Therefore a more general expression for possible IPs is defined as

$$E_{b,min,\delta} = \min_{\delta/2 \le \bar{x} \le L-\delta/2} \left(\frac{1}{\delta} \int_{x=\bar{x}-\delta/2}^{\bar{x}+\delta/2} EI_y(x)\, dx \right) / I_{y0} \tag{18}$$

Considering the fact that large knots or groups of knots in spruce have an extension of typically 60–100 mm it is reasonable to assume that the average bending stiffness over such a distance can give a suitable IP to bending strength. Therefore $E_{b,min,60}$, $E_{b,min,80}$ and $E_{b,min,100}$, i.e. IPs defined according to Eq. (18) with $\delta = 60$, 80 and 100 mm, respectively, have been assessed.

The stiffness profile gives information not only about the lowest stiffness value and the extension of the weak zones in the longitudinal direction of the board but also about their position, see the graphs shown in Fig. 6. Furthermore, structural timber is rarely exposed to large bending moments close to the ends and in a four point bending test, carried out in accordance with EN 408, only a distance of six times the depth of the board is exposed to the maximum bending moment. In any case, the parts of the boards closer to the ends than about $7d$ cannot be exposed to maximum bending moment when assessed according to the standard. Therefore it is reasonable to evaluate an IP defined as

$$E_{b,min,\delta,w} = \min_{d+\delta/2 \le \bar{x} \le L-d-\delta/2} \left(\frac{1}{\delta} \int_{x=\bar{x}-\delta/2}^{\bar{x}+\delta/2} EI_y(x) \cdot w(x) dx \right) / I_{y0} \tag{19}$$

where the weight function $w(x)$ is defined as

$$w(x) = \begin{cases} 6\mathrm{d}/(x-d), & d < x < 7d \\ 1, & 7d \le x \le L-7d \\ 6\mathrm{d}/(L-d-x), & L-7d < x < L-d \end{cases} \tag{20}$$

This gives a weighting of the stiffness profile in correspondence with a load case were the bending moment distribution is such that no bending occurs at a distance d from each end of the beam, a linear increase in bending moment then occurs from d to $7d$ from each end and a constant, maximum bending moment occurs in the middle part of the beam.

Though it can be expected that the calculated cross sectional stiffness profile $EA(x)$ is less useful for defining efficient IPs to bending strength than what $EI_y(x)$ is, it may be interesting for comparison to evaluate how well the bending strength may be predicted using an IP defined as

$$E_{a,min} = \min_{0 \le x \le L} (EA(x))/(t \times d) \quad (21)$$

8 Results and discussion

The results and discussion presented below is divided into two parts. In the first, statistical results for the measured and calculated properties defined above, which are of general interest for strength grading purposes, are presented and discussed. In the second part additional results and observations regarding the particular test series comprising 105 boards are presented and discussed. These results give indications regarding the potential for further development of the method.

8.1 Statistical relations for common board properties and novel IPs to bending strength

Table 2 shows mean values and standard deviations for the bending strength, the local and global MOE, respectively, the dynamic longitudinal MOE, the board density and the novel IPs defined above. It is observed that the novel IP candidates $E_{b,min}$, $E_{b,min,80}$, $E_{b,min,80,w}$ and $E_{a,min}$ are considerably lower than the mean values for E_m, $E_{m,g}$, and E_{a1}. For the lowest MOE calculated for a section along a beam, $E_{b,min}$, the mean value is as low as 7.1 GPa, i.e. only 57 % of the mean value of E_{a1}. The mean value of $E_{b,min,80}$ is 9.4 MPa, i.e. 76 % of the mean value of E_{a1}. This gives an indication of how much lower the bending stiffness is on a local level compared to the average board stiffness.

Table 3 shows coefficients of determination between the same properties as those included in Table 2. Of particular interest are the coefficients of determination between IPs and bending strength (printed in bold face in Table 3). The axial dynamic stiffness E_{a1} is often used as an IP in commercial grading and for the boards assessed here it gives a coefficient of determination to the bending strength of 0.59. The IP $E_{b,min}$ gives a better result, $R^2 = 0.64$, but an additional improvement was reached using the minimum bending stiffness over a distance of 80 mm, rather than using the lowest value in a single section of the beam. For $E_{b,min,80}$ the coefficient of determination to bending strength was 0.68. Attempts were made for shorter and longer distances, i.e. with other values of δ in $E_{b,min,\delta,w}$, but 80 mm gave the highest coefficient of determination. By considering that the outer parts of the boards, closer to the ends than $7d$ cannot be subjected to maximum bending moment in a test according to EN 408, the correlation between the IP and the bending strength was even further improved. $E_{b,min,80,w}$ gave a coefficient of determination as high as 0.71. In practical grading, $E_{b,min,80,w}$ should not be used as an IP as parts from different boards may be joined together by a finger joint and a weak part close to the end of one original graded board may end up in a critical position of an assembled board, but it is presented herein in order to illustrate the ability of the suggested method. In practise, $E_{b,min,80}$ is a more suitable IP. Figure 7 shows scatter plots, coefficients of determination and equations for regression lines between E_{a1}, and σ_m and between $E_{b,min,80,w}$ and σ_m, respectively.

8.2 Additional results and observations

For the 105 boards investigated the part of each board including the worst defect, i.e. the knot or group of knots that was supposed to cause failure, was if possible positioned in the maximum bending moment zone when bending strength was determined according to EN 408. If

Table 2 Mean values and standard deviations for different properties of the 105 boards
Tab. 2 Mittelwerte und Standardabweichungen verschiedener Eigenschaften der 105 Bretter

	Mean value	SD
σ_m	38.4 MPa	12.9 MPa
E_m	11.0 GPa	2.8 GPa
$E_{m,g}$	10.6 GPa	2.3 GPa
E_{a1}	12.4 GPa	2.6 GPa
ρ	472 kg/m^3	52 kg/m^3
$E_{b,min}$	7.1 GPa	2.7 GPa
$E_{b,min,80}$	9.4 GPa	2.9 GPa
$E_{b,min,80,w}$	9.7 GPa	2.9 GPa
$E_{a,min}$	8.4 GPa	2.5 GPa

Table 3 Coefficients of determination, R^2, between different properties of the 105 boards
Tab. 3 Bestimmtheitsmaße R^2 für die Beziehung zwischen verschiedenen Materialeigenschaften der 105 Bretter

R^2	σ_m	E_{a1}	ρ	$E_{b,min}$	$E_{b,min,80}$	$E_{b,min,80,w}$	$E_{a,min}$
σ_m	1	**0.59**	**0.27**	**0.64**	**0.68**	**0.71**	**0.61**
E_{a1}	**0.59**	1	0.65	0.80	0.89	0.88	0.88
ρ	**0.27**	0.65	1	0.41	0.47	0.43	0.49
$E_{b,min}$	**0.64**	0.80	0.41	1	0.95	0.92	0.90
$E_{b,min,80}$	**0.68**	0.89	0.47	0.95	1	0.97	0.92
$E_{b,min,80,w}$	**0.71**	0.88	0.43	0.92	0.97	1	0.90
$E_{a,min}$	**0.61**	0.88	0.49	0.90	0.92	0.90	1

Bold values indicate coefficients of determination between bending strength and other properties are particularly interesting

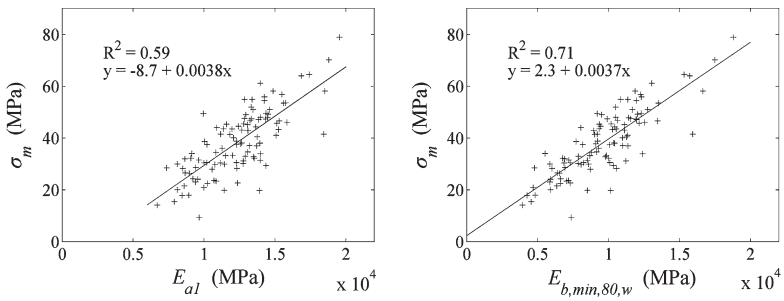

Fig. 7 Scatter plots, coefficients of determination and equations for the regression lines between (*left*) E_{a1} and σ_m and (*right*) $E_{b,min,80,w}$ and σ_m
Abb. 7 Streudiagramme, Bestimmtheitsmaße und Gleichungen der Regressionsgeraden zwischen (links) E_{a1} und σ_m sowie (rechts) $E_{b,min,80,w}$ und σ_m

this part was so close to the end that it could not be positioned within this zone the second worst defect was placed in the maximum bending moment zone and so on. For all the boards it was documented where the supports and point loads were positioned and thereby it is known what part of each board that was subjected to maximum bending moment. Furthermore, for each board the location of the failure initialization was documented, although in some cases it was difficult to identify this position accurately in the broken board.

With knowledge regarding how each board was positioned in the testing machine and with a calculated bending stiffness profile for each individual board, it was possible to establish a finite element (FE) model for the part of each board that was actually subjected to bending and to simulate the load case of four point bending. The FE model employed here consists of a series of beam elements, each approximately 2 cm long. On the basis of the displacements obtained in the FE-calculation, MOEs, here denoted $E_{m,c}$ and $E_{m,g,c}$, respectively, were then calculated in analogy with E_m and $E_{m,g}$ obtained from the measured deflections during testing. Table 4 shows coefficients of determination between these different MOEs, based on measurements during testing and based on FE-calculations, respectively, but representing the same timber, i.e. the same $18d = 2{,}610$ mm long parts of the boards in four point bending. The coefficients of determination between these MOEs and the bending strength are also shown in Table 4. The MOEs based on measured deflections, E_m and $E_{m,g}$, correlate considerably better with the bending strength ($R^2 = 0.74$ and 0.72 respectively) than what the MOEs based on calculated deflections, $E_{m,c}$ and $E_{m,g,c}$, do ($R^2 = 0.61$ for both cases). There is, however, a rather strong correlation between MOEs based on measured and calculated deflections, the coefficients of determination being 0.85 both between E_m and $E_{m,c}$ and between $E_{m,g}$ and $E_{m,g,c}$.

As both MOEs based on measured and calculated deflections represent the same physical parts of the timber, any differences between E_m and $E_{m,c}$, or between $E_{m,g}$ and $E_{m,g,c}$, reveals a certain lack of precision when trying to calculate the true bending stiffness profile on the basis of projected fibre angles, employed integration scheme and longitudinal dynamic excitation. The suggested approach seems to be accurate enough to give a very good correlation between suggested IPs and bending strength, but the results presented in Table 4 indicate that there is a considerable potential to improve the correlation further. If the high resolution of the bending stiffness profiles (which can be calculated rapidly on the basis of results from scanning) can reach the accuracy of the measured edgewise bending stiffness (i.e. measured on a more or less global level during four-point bending) it is likely that a coefficient of determination between a single IP and the bending strength may approach or even exceed $R^2 = 0.80$. To what degree the present differences between E_m and $E_{m,c}$, and between $E_{m,g}$ and $E_{m,g,c}$ depend (1) on the fact that projected fibre angles on surfaces are utilized rather than the true, three dimensional fibre angle field within the wooden member, (2) on the simplifying assumption that the wood material parameters relating to the l-r-t system are constant within a wooden member, (3) on the assumption that the stiffness can be captured accurately enough using a beam model, or on some other conditions should be investigated through further research.

A final observation concerns the position along each beam where failure actually was initialized in relation to

Table 4 Coefficients of determination, R^2, between bending strength and MOEs based on measurements and calculations, respectively
Tab. 4 Bestimmtheitsmaße R^2 für die Beziehung zwischen Biegefestigkeit und E-Modul basierend auf Messungen und Berechnungen

R^2	σ_m	E_m	$E_{m,g}$	$E_{m,c}$	$E_{m,g,c}$
σ_m	1	**0.74**	**0.72**	**0.61**	**0.61**
E_m	**0.74**	1	0.92	0.85	0.85
$E_{m,g}$	**0.72**	0.92	1	0.89	0.91
$E_{m,c}$	**0.61**	0.85	0.89	1	0.99
$E_{m,g,c}$	**0.61**	0.85	0.91	0.99	1

Bold values indicate coefficients of determination between bending strength and other properties are particularly interesting

where it was expected to occur, i.e. where the calculated bending stiffness was at its lowest in relation to the applied bending moment. In 70 % of the boards the distance between the actual position of failure and the predicted position was less than 5 cm and for 78 % of the boards the distance was less than 10 cm. This indicates a high probability for failure to take place within a close surrounding of the section with the lowest bending stiffness. It may be noted, however, that many boards have a second weak section, and maybe even a third, with calculated bending stiffness almost as low as the weakest one.

9 Conclusion

High resolution information regarding local fibre orientation on face and edge surfaces of wooden boards can nowadays be sampled in a speed corresponding to the production speed at a sawmill. By utilizing such information in order to calculate the variation in bending stiffness along an individual board very accurate indicating properties with respect to bending strength can be defined. However, information regarding basic wood material properties, in particular MOE in the fibre direction, needs to be available for each individual board. One way to obtain such information is to measure the first longitudinal resonance frequency and the board density which in combination with fibre orientation information can be used to calculate an average MOE in the fibre direction.

For a sample consisting of 105 spruce boards of dimension 45 × 145 × 3,600 mm^3 it is shown that an IP defined as the edgewise bending stiffness of the weakest (least stiff) 80 mm part along each board gave a coefficient of determination to bending strength of 0.68. If it is considered that sections close to the ends of the boards cannot be subjected to large bending moments when tested the coefficient of determination increases to 0.71. For the same boards the coefficient of determination between global MOE based on the first resonance frequency and the board density is only 0.59.

The theory of how the local stiffness in the direction of a board can be calculated on the basis of basic wood parameters and three dimensional fibre directions is presented independently of the simplifying assumptions that need to be introduced when actually calculating the stiffness profiles, indicating properties and coefficients of determination. It is also shown that higher accuracy when determining these properties, i.e. if errors originating from simplifying assumptions can be avoided, an even stronger correlation would be achieved between a local bending stiffness and bending strength. Thus, along with the development of commercial grading procedures on the basis of the research results already presented herein, further development towards even more accurate calculations of bending stiffness profiles of boards is encouraged.

To obtain optimum IPs, the distance δ over which the average bending stiffness is calculated may depend on the dimensions of the wooden boards assessed. Some tests and calculations performed on batches of timber of other dimensions than 45 × 145 mm^2 suggest that a distance of about half the depth of the timber member (rather than a constant distance of 80 mm) would give a suitable IP, but further tests and calculations on different dimensions of wooden boards need to be carried out in order to confirm this.

Finally, it should be noted that the calculated stiffness profiles could also be of use in a material efficient production of engineered wood products where the significance of weak sections may depend on their location or when it is suitable to eliminate weak sections before assembling.

References

Bechtel FK, Allen JR (1987) Methods of implementing grain angle measurements in the machine stress rating process. In: 6th Nondestructive testing of wood symposium, Sept 1987, Washington State University, Pullman

Brookhuis Micro-Electronics BV (2009) Timber grader MTG—operating Instructions. MTG Manual GB 12062009-C

CEN (2009) EN 14081-4 Timber structures: strength graded structural timber with rectangular cross section, Part 4: machine grading—Grading machine settings for machine controlled systems

CEN (2010a) EN 384 Structural timber: determination of characteristic values of mechanical properties and density. European Committee for Standardization, CEN/TC124

CEN (2010b) EN 408 Timber structures: structural timber and glued laminated timber—determination of some physical and mechanical properties. European Committee for Standardization, CEN/TC124

Dinwoodie JM (2000) Timber: Its nature and behaviour. E & FN Spon, New Fetter Lane, London

Jehl A, Bléron L, Meriaudeau F, Collet R (2011) Contribution of Slope of Grain Information in Lumber Strength Grading. In: 17th international nondestructive testing and evaluation of wood symposium, Sept 2011, University of West Hungary, Sopron

Johansson C-J (2003) Grading of timber with respect to mechanical properties. In: Thelandersson S, Larsen HJ (eds) Timber engineering. Wiley, Chichester, UK

Larsson D (1997) Mechanical Characterization of Engineering Materials by Modal Testing. Doctoral thesis, Chalmers University of Technology, Gothenburg

Moore HE, Baldwin RD (2011) Structural grading of lumber using grain angle in a production environment. In: 17th International nondestructive testing and evaluation of wood symposium, Sept 2011, University of West Hungary, Sopron

Nyström J (2003) Automatic measurement of fiber orientation in softwoods by using the tracheid effect. Computers and Electronics in Agriculture, 41(1):91–99

Olsson A, Oscarsson J, Johansson M, Källsner B (2011) Prediction of timber bending strength on basis of bending stiffness and material homogeneity assessed from dynamic excitation. Wood Sci Technol 46(4):667–683

Ormarsson S (1999) Numerical analysis of moisture-related distorsions in sawn timber. Doctoral thesis, Chalmers University of Technology, Gothenburg

Petersson H (2010) Use of optical and laser scanning techniques as tools for obtaining improved fe-input data for strength and shape stability analysis of wood and timber. IV European Conference on Computational Mechanics, May 2010, Paris

Schajer GS (2001) Lumber strength grading using x-ray scanning, Forest Products Journal 51(1), 43–50

Wormuth E-W (1993) Study of the relation between flatwise and edgewise modulus of elasticity of sawn timber for the purpose of improving mechanical stress methods. Diploma work, University of Hamburg, Hamburg

III

LOCALIZED MODULUS OF ELASTICITY IN TIMBER AND ITS SIGNIFICANCE FOR THE ACCURACY OF MACHINE STRENGTH GRADING

Jan Oscarsson
SP Wood Technology, SP Technical Research Institute of Sweden, Växjö, Sweden, jan.oscarsson@sp.se

Anders Olsson
Department of Building and Energy Technology, Linnæus University, Växjö, Sweden, anders.olsson@lnu.se

Bertil Enquist
Department of Building and Energy Technology, Linnæus University, Växjö, Sweden, bertil.enquist@lnu.se

ABSTRACT

Machine strength grading is normally based on rather poor statistical relationships between bending strength and modulus of elasticity (MOE). The latter is often determined as flatwise bending MOE or axial dynamic MOE. Furthermore, European Standards stipulate that local MOE shall be determined at a critical section and over a length of five times the depth of the timber member. However, strain fields determined on side board surfaces using contact-free measurement technique showed that stiffness reduction at critical sections is much more localized than what standard requirements indicate. This fact was recently utilized in the development of a grading method in which the indicating property (IP) is defined as the lowest local edgewise bending MOE and determined on the basis of scanned fibre directions. In the investigation presented below, the relationship between grading accuracy, in terms of coefficient of determination (R^2), and the degree of localization of reduced stiffness was investigated for two samples. Maximum R^2 values, which were as high as 0.68 and 0.77, respectively, were obtained for IPs determined over lengths corresponding to about half the depth of the investigated members. Consequently, application of a highly localized bending MOE as IP will result in grading that is very competitive.

Keywords: fibre angle, indicating property, laser scanning, machine strength grading, modulus of elasticity, strain fields

INTRODUCTION

Machine strength grading of structural timber is based on statistical relationships between strength and various non-destructively measured wood characteristics such as density, annual ring width, stiffness in terms of modulus of elasticity (MOE) and occurrence of knots. Structural properties of timber are also influenced by, *inter alia*, reaction wood, top ruptures, fibre angle and fibre disturbances. From previous research (eg Hoffmeyer 1995) it is well known that the best single indicating property (IP) of strength in both bending and tension is the MOE which can be measured in different ways. The majority of commercial grading machines are based on either flatwise bending or axial dynamic excitation. In the first case, a bending test is carried out continuously as a timber member is passing through a machine. For most such machines, the bending is obtained by a three-point loading test. The length of span varies, typically between 600 and 1200 mm, depending on the make of the machine. The relationship between load P and deflection δ is registered and local static MOE (E_{flat}) is determined as

$$E_{flat} = \frac{Pl^3}{48 I_{flat} \delta} \tag{1}$$

where l is the span length and I_{flat} is the second moment of inertia in the flatwise direction. In connection with an axial dynamic excitation a timber member is set into vibration by means of a hammer blow at one end. The resonance frequency of the first axial mode of vibration is determined on the basis of the impulse response captured by either a microphone or a laser vibrometer. The global (ie average) axial dynamic MOE ($E_{a,1}$) is calculated as

$$E_{a,1} = 4\rho(f_{a,1}L)^2 \tag{2}$$

where ρ is the board's mass density, $f_{a,1}$ is the determined resonance frequency and L is the board length.

Another global MOE can be determined on the basis of resonance frequencies corresponding to edgewise (transversal) bending modes excited by a hammer blow on the board edge (Olsson et al 2012). Accurate calculation of edgewise bending MOE may be somewhat complicated, since bending vibrations include shear. However, shear deformations have a limited influence on resonance frequencies of lower bending modes. According to Bernoulli-Euler beam theory, in which shear deformations are disregarded, a bending MOE ($E_{b,1}$) corresponding to the resonance frequency ($f_{b,1}$) of the first edgewise bending mode can be estimated using

$$E_{b,1} = \frac{0.96\rho L^4 f_{b,1}^2}{h^2} \tag{3}$$

where h is the depth of the measured timber member (Fig 1). An approximation in accordance with eq. (3) will result in an underestimation of dynamic edgewise bending MOE by a few percent. A few makes of grading machines based on transversal bending excitation, flatwise and/or edgewise, are approved for application on the European and North American market, respectively, (Lanvin et al 2012; American Lumber Standard Committee 2013) but their share of each market is very limited.

The European Standard EN 408 specifies a test method for determination of strength and local as well as global static MOE in edgewise bending. A test set-up based on the standard is shown in Fig 1. The critical section, which according to EN 384 is defined as the section at which failure is expected to occur, shall be in a position between the two point loads. The local static edgewise MOE ($E_{m,loc}$) is calculated as

$$E_{m,loc} = \frac{a l_1^2 (F_2 - F_1)}{16 I_e (v_2 - v_1)} \tag{4}$$

where $a = 6h$ is the distance between one of the point loads and the nearest support, h is the depth of the timber member, l_1 is the length equal to $5h$ over which the local deformation v is measured, I_e is the edgewise second moment of inertia, $F_2 - F_1$ is an increment of the sum of the two point loads and $v_2 - v_1$ is the corresponding increment of local deformation. The global static edgewise MOE ($E_{m,glob}$) is obtained from

$$E_{m,glob} = \frac{L_b^3 (F_2 - F_1)}{b h^3 (w_2 - w_1)} \left[\left(\frac{3a}{4L_b} \right) - \left(\frac{a}{L_b} \right)^3 \right] \tag{5}$$

where b is the member thickness, $L_b = 18h$ is the span in bending and $w_2 - w_1$ is the increment of global deformation.

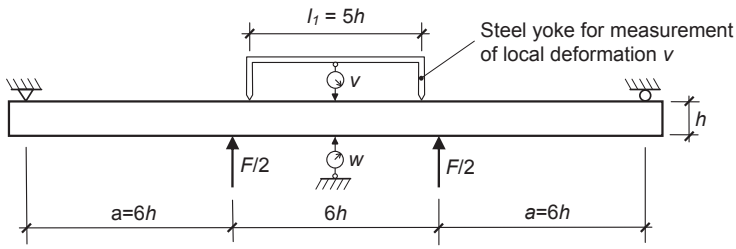

Figure 1—Test set-up based on EN 408 for determination of bending strength (σ_m), and static edgewise bending MOE, local ($E_{m,loc}$) as well as global ($E_{m,glob}$).

The standard EN 408 also includes a test method for determination of both strength ($\sigma_{t,0}$) and local static MOE ($E_{t,0}$) in tension parallel to the grain, the latter determined at the critical section as

$$E_{t,0} = \frac{l_1(F_2 - F_1)}{A(w_2 - w_1)} \tag{6}$$

where A is the cross-sectional area, F_2-F_1 is a load increment and w_2-w_1 is the corresponding increment of local deformation measured over a length (l_1) equal to five times the width (Fig 2, right).

In recent research (Olsson et al 2012; Oscarsson 2012) the MOE measures presented in eqs. (1)-(5) were determined for a sample of 105 strength graded Norway spruce planks of nominal dimensions 45×145×3600 mm, sampled at Södra Timber's sawmill in Långasjö, Sweden. At the time of testing, the mean moisture content (MC) was 13%. The results presented in Table 1 show that the strongest relationship in terms of coefficient of determination (R^2) between bending strength and MOE was achieved for local static MOE in edgewise bending ($E_{m,loc}$), determined in accordance with the test set-up shown in Fig 1. This relationship (R^2=0.73) was considerably stronger than those obtained for $E_{a,1}$, $E_{b,1}$ and E_{flat}, respectively, which, as described previously, are applied in commercial strength grading. Thus, the results in Table 1 indicate that more accurate strength grading would be achieved if grading methods based on IPs reflecting localized edgewise MOE were available.

Several previous research works have shown that short-span MOE is a better indicating property of strength than long-span MOE. For example, the relationship between tension strength and flatwise bending MOE of Southern pine (*Pinus spp.*) timber of different strength classes was investigated by Gerhards (1972) who found that R^2 was improved by 0.05 when the span length applied for determination of the bending MOE was reduced from ~4570 mm (15 ft.) to ~1220 mm (4 ft.). Orosz (1976), who

Table 1—Mean value, standard deviation (SD), relationship in terms of R^2 to bending strength (σ_m), and standard error of the estimate of σ_m (SEE) for five different MOE measures, see eqs (1)-(5), obtained from investigating 105 planks of Norway spruce of nominal dimensions 45×145×3600 mm (Olsson et al 2012; Oscarsson 2012). Reported values are based on actual dimensions of 104 planks (one plank disregarded due to a major crack).

Method for assessment of MOE	Symbol	Mean [GPa]	SD [GPa]	R^2 between MOE and σ_m	SEE [MPa]
Local static edgewise bending (EN 408)	$E_{m,loc}$	11.0	2.8	0.73	6.8
Global static edgewise bending (EN 408)	$E_{m,glob}$	10.9	2.3	0.72	7.0
Axial dynamic excitation	$E_{a,1}$	12.4	2.6	0.60	8.3
Edgewise dynamic excitation	$E_{b,1}$	12.3	2.5	0.67	7.6
Local static flatwise bending	E_{flat}	9.7	1.9	0.62	8.1

examined structural timber of West coast hemlock (*Tsuga heterophylla*), obtained optimum R^2 between tension strength and flatwise bending MOE when the latter was determined over a gage length of ~406 mm (16 in.)

Over the years, extensive research resources have been allocated to investigations concerning the possibility of determining MOE on a scale that is even more local than the one applied in EN 408. According to Bechtel et al (2006), the determination of MOE over a bending span, such as the one applied in the determination of local MOE according to EN 408 or in grading machines based on three-point flatwise bending (author's remark), is a smoothing operation which may mask the effect of knots and other local characteristics affecting structural value. The bending MOE, determined on the basis of applied bending forces and measured deflections over the span, is a composite result which represents the intrinsic MOE values at points along the length segment of the board coinciding with the bending span. Thus, the MOE value determined over such a span is a smoothed version of the underlying point-wise MOE values. Kass (1975) meant that a timber member exposed to bending may be considered as being composed of discrete regions, each with a distinct and individual (localized) bending stiffness. According to eg Foschi (1987) it is known that the correlation between strength and the smoothed MOE is improved if this MOE is replaced by the minimum localized MOE found within the measured span. The possibility of actually measuring the localized MOE over lengths that are much shorter than those applied in either EN 408 or in grading machines based on flatwise bending has been commented upon by eg Kass (1975), Foschi (1987), Pope and Matthews (1995), and Aicher et al (2002). In these works it was emphasized that determination of local bending MOE over very short spans is a task that is associated with difficulties such as uncertainties related to the accurate measuring of small deformations obtained over such spans. Another highlighted problem concerns occurrence of excessive stresses due to beam bending or local crushing, the latter appearing at supports and load application points.

Other techniques developed in order to estimate bending MOE on a localized level have been presented. Boughton (1994) determined bending MOE in timber members using an edgewise four-point bending machine. The MOE obtained on the basis of deformations measured over a span of 1200 mm was interpreted as an apparent MOE determined as a weighted moving average of the local stiffness properties within the span. The effects of this averaging were minimized using an algorithm by which the apparent MOE distribution along a member was used to calculate the corresponding localized edgewise MOE distribution. Application of an IP defined as the calculated minimum localized MOE found along a member resulted in predictions of strength in tension and edgewise bending, respectively, that were more accurate than what was obtained using apparent MOE as IP. It was also shown that edgewise bending MOE was a better predictor of strength than flatwise bending MOE when both values were determined over the same span length.

The possibility of obtaining the true high-resolution distribution of MOE along timber members was also investigated by Bechtel (1985) and Foschi (1987), respectively. It was assumed that the relationship between MOE and strength would be improved if the former was a true localized measure rather than an average value measured over a certain span. An approach, which was originally presented by Bechtel (1985), was developed for application together with apparent MOE distributions determined by means of grading machines based on three-point flatwise bending. Basic features of the approach were the Fourier transform and weighting functions, the latter describing the fact that local MOE values near the centre of a measurement span have a stronger influence on the measurement results than values at span ends. On the basis of the apparent MOE distribution and the weighting functions, the corresponding localized flatwise MOE distribution was to be calculated using the Fourier transform. In order to test the approach, Foschi (1987) assumed three MOE distributions with different degrees of localization, determined the corresponding apparent distributions, and then reconstructed the localized distributions using the Fourier transform. It was found that both value and position of the true minimum MOE could be accurately predicted and that the apparent MOE distributions resulted in considerable overestimation of the

minimum MOE. The latter characteristic was also observed by Kass (1975). However, Foschi (1987) also found that determination of MOE distribution on the basis of deflections and loads related to short spans may be biased by measurement noise and numerical errors. Further investigation of this problem (Lam et al 1993) showed that the described approach would provide a limited improvement of the correlation between strength and MOE compared with grading methods based on apparent MOE. Similar results were obtained by Pope and Matthews (1995).

Methods for stochastic modeling of localized MOE have also been developed. For example, Kline et al (1986) presented a model by which lengthwise variability in flatwise MOE could be generated with a resolution of 30-inch (762 mm) for two dimensions and two grades of Southern pine (*Pinus spp*), and Taylor and Bender (1991) modeled localized flatwise MOE, with a resolution of 2-ft (617mm), for two grades and one dimension of Douglas fir (*Pseudotsuga menziesii*). The need for further research concerning eg improved measurement resolution and modeling of other species, grades and board dimensions was pointed out in the investigations.

The purpose of the present research is to show how new measurement methods may be utilized for determination of local MOE with high resolution and to identify suitable levels of localization of MOE when employed as IP to bending strength. By means of laser scanning it is today possible to determine local fibre orientation on wood surfaces with a resolution in the order of 1 mm along a timber member, in a speed corresponding to the production speed at a sawmill. In turn, knowledge of the fibre orientation enables the calculation of local MOE in the direction of the timber member and, by integration over the cross-section, also the bending stiffness or longitudinal stiffness on the corresponding scale along the member. Olsson et al (2013) suggested a novel IP to bending strength based on this approach. In the research presented below, it is investigated to what extent R^2 between strength and local MOE is dependent on the length over which the MOE is determined, and for which such length optimum relationship in terms of R^2 is achieved. In addition, it is shown how a contact-free measurement technique based on white-light digital image correlation (DIC) can be used to gain valuable information concerning stiffness variation along the length of timber members. Thereby assumptions regarding the magnitude and significance of MOE in the close surroundings of knots, made by other researchers as described in the survey above, are here both verified and utilized in a new way.

MATERIALS AND METHODS

Materials

Test results obtained from two samples of timber, one of boards and one of planks, were utilized in this research. Both samples have been applied in previous but different investigations. The plank sample is described above and referred to in Table 1. The board sample consisted initially of 58 Norway spruce side boards of nominal dimensions 25×120×3900 mm. The boards, which were of sawfalling quality and sampled in a wet state, were planed and delivered to Linnæus University from the sawmill company Södra Timber, subsequently split and cut to nominal dimensions 25×56×3000 mm, and then used in an investigation concerning the possibility of grading narrow glulam laminations of Norway spruce side boards in a wet state using axial dynamic excitation (Oscarsson et al 2011). In that investigation, global axial dynamic MOE ($E_{a,1}$) and density (ρ) was determined both in a wet state and after drying to a MC of 12-14%. Local static MOE in tension ($E_{t,0}$) and tensile strength ($\sigma_{t,0}$) were determined in accordance with EN 408 after the dried boards had been stored at standard climate 20°C/65% relative humidity for seven months. The tensile test set-up is shown in Figs 2-3 and the relationships between stiffness measures and tensile strength are shown in Table 2. As for the plank sample, the largest R^2 was achieved for the locally determined static MOE.

Table 2—Mean value, standard deviation (SD), relationship in terms of R^2 to tension strength ($\sigma_{t,0}$), and standard error of the estimate of σ_m (SEE) for three different MOE measures, see eqs (2) and (6), obtained from investigating 116 side boards of Norway spruce of nominal dimensions 25×56×3000 mm (Oscarsson et al 2011). Reported values are based on actual dimensions.

Method for assessment of MOE	Symbol	Mean [GPa]	SD [GPa]	R^2 between MOE and $\sigma_{t,0}$	SEE [MPa]
Local static tension (EN 408)[1]	$E_{t,0}$	9.6	3.4	0.68	7.7
Axial dynamic excitation, wet state[2]	$E_{a,1,wet}$	10.8	2.6	0.55	9.1
Axial dynamic excitation, dried state[2]	$E_{a,1,dried}$	13.0	2.9	0.52	9.4

1. Ten boards disregarded due to rot (eight) and damage (two).
2. Eight boards disregarded due to rot.

Tensile tests and strain field determination of narrow boards

For nine of the split boards included in the board sample, two-dimensional strain fields occurring on one of the flatwise surfaces during the tensile strength tests were determined on the basis of deformations measured by two contact-free measurement systems based on DIC technique and connected in a master-slave fashion (Fig 2, left). The set-up for the tensile tests and simultaneous DIC measurements is shown in Figs 2-3. The testing machine was of make MFL with a hydraulic force generation, 2.0 m length of stroke and a 3.0 MN load cell. The distance between the wedge type grips was ~1500 mm and the load was applied with a constant loading rate of 7-8 kN/minute. To ensure high measurement resolution of the long and narrow surface to be measured (56×~1500 mm), two identical DIC ARAMIS systems from GOM, Germany, were used. Each system, including two cameras, separately measured deformations occurring on slightly more than half the visible board length (Fig 3). Prior to the tests, two 3D coordinate systems, one for each DIC system, were defined through a calibration procedure carried out for each system and based on the cameras being positioned at angles and distances that depend on the size of the object to be measured. The difference in angle meant that stereoscopic pictures of the measured surface were obtained from each system. The master-slave application implied that pictures were taken simultaneously by both pair of cameras at an interval of three seconds during a load test. Each such double pair of pictures represented a *load stage* to which unique strain fields corresponded. Based on the stereoscopic pictures, 3D positions (ie coordinates) of a large number of measurement points on the surface were determined for every load stage. The strains at each such point were calculated, using the ARAMIS software. The distance between measurement points was set to 3.6 mm in longitudinal board direction and 1.8 mm in lateral direction. Regarding the ARAMIS system, a more detailed description is found in Oscarsson et al (2012).

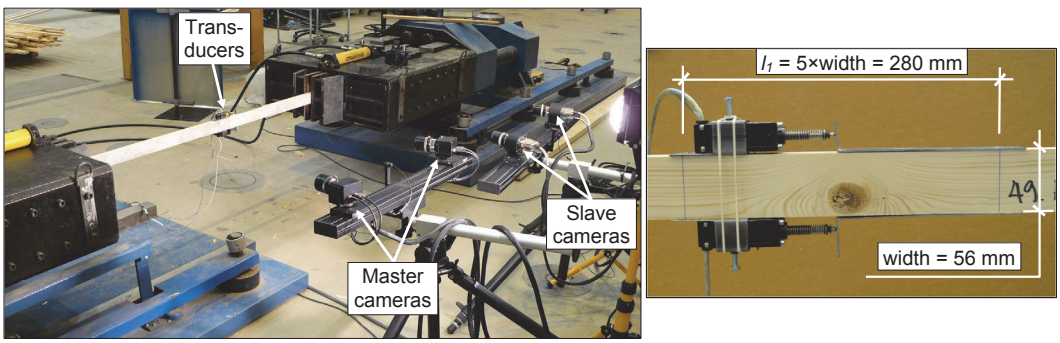

Figure 2—Set-up for tension tests according to EN 408 and for DIC measurements (left), and transducers for deformation measurements at assumed critical board section (right).

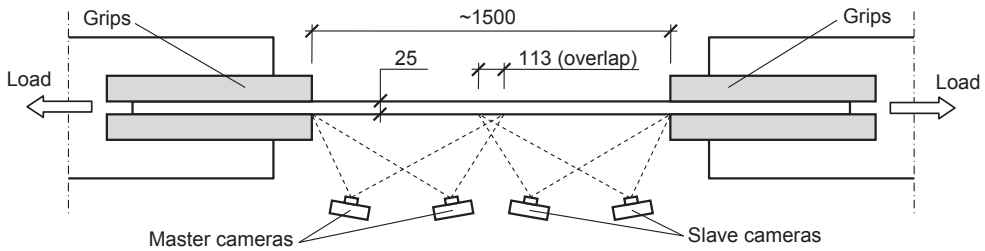

Figure 3—Camera set-up (plan) for DIC measurements.

To be able to evaluate and visualize strains along the entire board length jointly and simultaneously, a third coordinate system to which the other two could be transformed was needed. For this purpose, yet another GOM measurement system called TRITOP was used. A set-up (Fig 4, left) including orientation crosses, a scale bar and 27 reference point markers fixed to a metal sheet, was arranged. On the basis of digital pictures of the set-up taken from several angles using a photogrammetric camera, the third 3D coordinate system was defined using TRITOP software. This implied that the markers on the sheet shared a fixed TRITOP coordinate relationship, a characteristic that was utilized for the coordinate transformation. When a master-slave measurement was prepared, the sheet was put behind the board (Fig 4, right). As the pictures of the first load-stage were taken, the markers were also caught and their positions in each ARAMIS coordinate system determined. By that, a relationship between TRITOP coordinates and ARAMIS coordinates was established and the transformation could be carried out accordingly. The transformed measurement results from the two ARAMIS systems were subsequently combined and jointly visualized (Figs 6b-c).

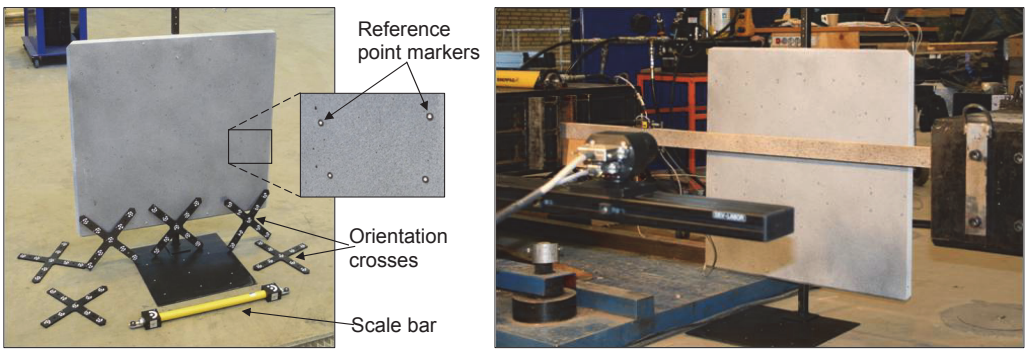

Figure 4—Set-up for determination of TRITOP coordinate system (left) and set-up for establishment of relationship between ARAMIS coordinates and TRITOP coordinates.

Determination of bending MOE profiles and local IP

In the research referred to in Tables 1-2, the highest R^2 between strength and stiffness was achieved for edgewise and longitudinal MOE, respectively, determined locally on the basis of test set-ups described in EN 408. As described in the *Introduction*, it is known that more accurate grading will be achieved if grading methods based on locally determined edgewise IPs were available, and that such a method has recently been presented (Olsson et al 2013). In this new method, a commercial optical scanner of make WoodEye is applied for lengthwise dot laser scanning of timber surfaces. By means of the tracheid effect, high-resolution information about the angle φ between local fibre direction and the member's longitudinal direction is obtained (Fig 5a). Even small angles will cause considerable reduction of the structural

properties, since wood is a strongly orthotropic material with superior structural performance in the longitudinal fibre direction. Information about φ provides a basis for transformation of material properties related to the fibre direction to local material properties referring to the member's longitudinal direction. Local MOE in the latter direction (Fig 5c) provides data for integration of MOE profiles valid for either edgewise bending or in the longitudinal direction of the member. According to Olsson et al (2013), the IP for a certain member is defined as the lowest *edgewise bending* MOE found along the member. Important assumptions utilized in the method presented by Olsson et al (2013) are that

- the Bernoulli-Euler beam theory is applicable,
- the density (ρ) and the MOE in the fibre direction (E_l) are constant within a member,
- an initial value of the MOE in the fibre direction ($E_{l,in}$) is assumed,
- other stiffness parameters are linear functions of E_l,
- fibre directions measured on the wood surface (Fig 5a) are located in the longitudinal-tangential plane,
- the fibre direction coincide with the wood surface, ie the diving angle is set to zero, and
- the fibre direction measured on a surface is valid to a certain depth. This means that the fibre angle φ highlighted in Fig 5a, and the corresponding local longitudinal MOE, is assumed to be valid within the volume defined by the area dA (Fig 5b) times the length dx (Figs 5a and 5d).

The only property, apart from ρ, that has to be determined individually for each member is E_l. To do this, the resonance frequency of the first axial mode of vibration ($f_{a,1}$) is measured and applied. The parameter E_l is determined such that an axial eigen value analysis of a simple one dimensional finite element model of the member, including an axial stiffness profile with the same shape as the one determined using the initially assumed value of $E_{l,in}$, results in the same longitudinal resonance frequency as the one determined experimentally.

The scanning resolution in longitudinal direction, *i.e.* the distance between dot laser measurements, is dependent on the speed with which the members are fed through the scanner. In this research, in which the method presented by Olsson et al (2013) was applied, the feed speed was set to 60 m/minute, resulting in a longitudinal scanning resolution of 0.8 mm. The resolution in the lateral direction is dependent on the configuration of the laser source. In this case, a source resulting in a lateral resolution of 4 mm was chosen.

RESULTS AND DISCUSSION

DIC measurements

Results of DIC measurements can be exhibited using *contour plots* and *section diagrams*. A *contour plot* means that the strain distribution in longitudinal or lateral board direction or in shear is visualized for a certain load stage, on the basis of a defined colour scaling. *Sections* are defined in camera images as lines on the measured surface. Strains and displacements along such lines can be plotted in corresponding *diagrams*. An example (board no. 28B) of typically achieved results for the nine investigated boards is shown in Fig 6. The exhibited strains refer to a load stage at which the tensile stress had reached a value of 26.4 MPa, equivalent with 76% of the failure stress. This load stage is displayed since the contour plots for subsequent stages were disturbed by occurring cracks. An image of the measured surface is shown in Fig 6a. Contour plots showing longitudinal tensile strains (ε_x) achieved separately by the two DIC systems, are exhibited in Fig 6b. The combination of these plots is visualized in Fig 6c which also includes the position of three defined sections and of the origin of the TRITOP coordinate system. Lateral (edgewise) displacements (Δy) along the defined sections are shown in Fig 6d and longitudinal tensile strains (ε_x) along two of the sections are displayed in Fig 6e.

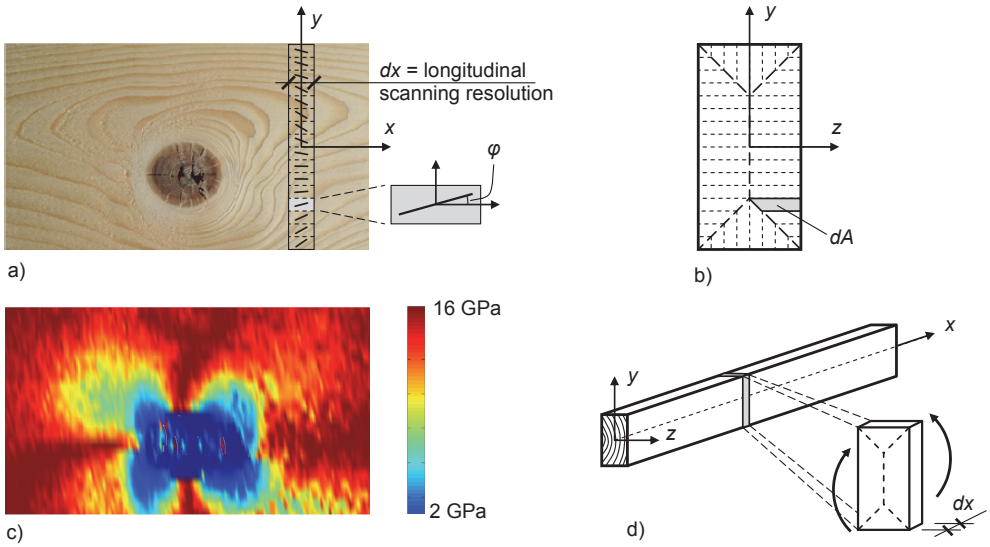

Figure 5—a) local fibre directions scanned on a member's surface by means of a row of laser dots, b) cross-section divided into sub-areas implying that the exhibited angle φ and corresponding MOE in the member's longitudinal direction is valid within the volume $dA \times dx$, c) distribution of longitudinal MOE around the exhibited knot, and d) segment of length dx. The edgewise bending MOE of this segment is calculated by stiffness integration over the segment's cross-section.

The most important result of the DIC measurements is that the reduction of MOE at critical knots occurs very locally. It was found that the length of such reduction, indicated in Fig 6e by the increase of longitudinal strain at TRITOP x-coordinates -650 mm and 350 mm, roughly corresponded to the board's width. This measure is just 20% of the length that according to EN 408 shall be applied for determination of local MOE in tension, see eq. (6). Thus, on the basis of the displayed results, it can be concluded that the method of EN 408 will result in an overestimation of local tensile MOE at critical knots, since the stipulated measurement length of 280 mm (Fig 2, right) will include clear wood parts in which the stiffness is unaffected by the presence of knots. In this context, knots are of particular importance, since failures in timber members are very often related to such defects (Johansson 2003). The described overestimation of localized MOE was also observed by Foschi (1987), who noted that determination of an apparent flatwise bending MOE over a span length of 910 mm would result in an overestimation of the true minimum MOE, and by Kass (1975) who found that the edgewise MOE of a defect zone is overestimated by an amount that is dependent on the length of this zone, the span length over which deformations are measured, and the ratio of MOE of the defect region to the MOE of surrounding clear wood material.

Another observation that can be made from the DIC measurements is that considerable displacements in the edgewise board direction, ie perpendicular to the load direction, occur (Fig 6d). Since displacement peaks coincide with major edge knots, a reasonable explanation is that these displacements can be attributed to uneven stress distribution over the cross-section.

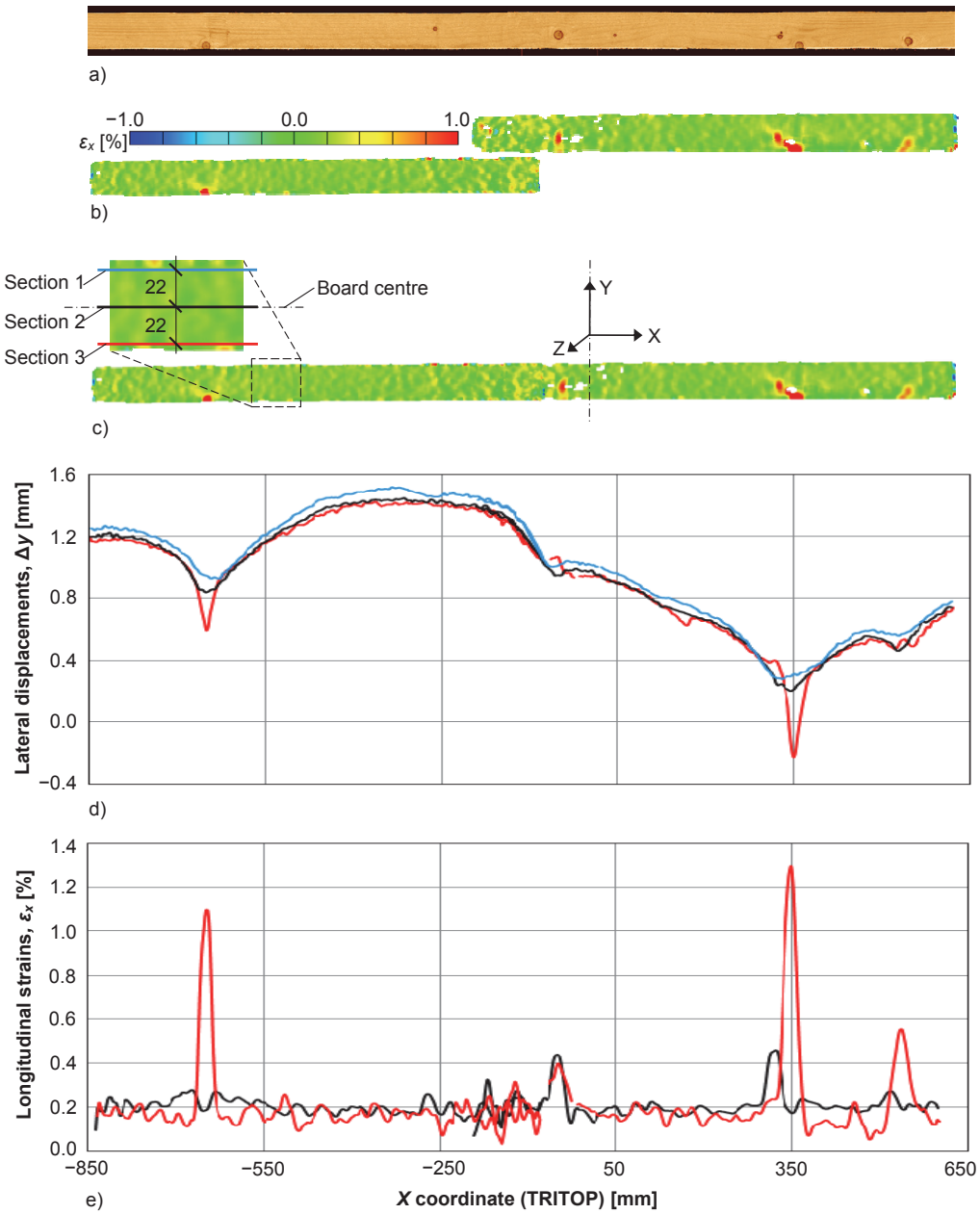

Figure 6—DIC measurement results for board no. 28B at a tensile stress of 26.4 MPa: a) flatwise board surface, b) contour plots of longitudinal strains, ε_x, determined by master system (left) and slave system (right), c) combined contour plot, positions of defined sections (left detail), and position of TRITOP coordinate system (right detail), d) displacements, Δy, in edgewise board direction along Sections 1-3, and e) longitudinal strains, ε_x, along Sections 2-3.

Bending MOE profiles and relationship between IP and bending strength

Typical edgewise bending MOE profiles obtained for one of the members in the investigated plank sample are shown in Fig 7. The left profile exhibits a bending MOE profile calculated for maximum resolution, ie a resolution equal to the scanning resolution. The right profile displays a moving average MOE calculated over an interval equal to half the depth of the member. The latter means that each MOE value along the profile is calculated as the average value of the surrounding 72 mm, ie along 36 mm on each side of the longitudinal position in question. A comparison of the two graphs shows that the IP's dependency on the length of the moving average interval is strong. The IP corresponding to full resolution was 5.5 GPa, whereas a higher value (IP=7.6 GPa) was reached for the moving average profile. The relationship between IP and length interval of moving average was studied in more detail. Of particular interest was the IP achieved for the interval of 725 mm, equal to five times the depth, ie the length over which local MOE in both bending and tension is determined according to EN 408. This IP was as high as 12.0 GPa, whereas the actual local edgewise bending MOE according to EN 408 was 10.6 GPa. The results are in accordance with research referred to in the *Introduction* as regards the overestimation of point-wise MOE values due to smoothing effects when MOE is averaged over a span of certain length. Of particular interest is the considerable difference between the point-wise MOE=5.5 GPa obtained at maximum scanning resolution (Fig 7, left), and the corresponding local MOE=10.6 GPa achieved on the basis of EN 408.

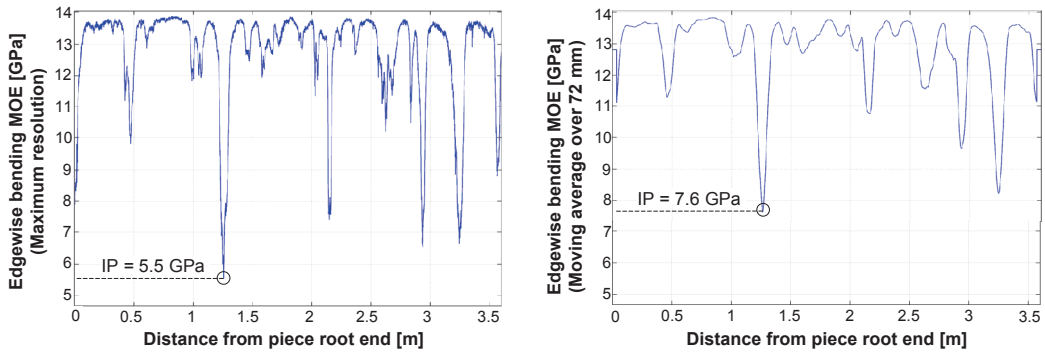

Figure 7— Bending MOE profiles for plank no. 34 corresponding to maximum scanning resolution (left) and to a moving average calculated over a length interval of half the depth of the plank (right), respectively.

For the board sample, profiles of both bending and axial MOE were studied and corresponding IPs in terms of lowest MOE along each board determined. As for the planks, the IP's dependency on the length of the moving average interval was noted. Consequently, it was also interesting to investigate to what extent the variation of length interval influenced the R^2 between IP and strength. For both samples, MOE profiles of bending and axial MOE, respectively, were calculated for different length intervals and corresponding IPs were determined. The results presented in Fig 8 show that, for both samples, higher R^2 was achieved for IPs based on bending. For the board sample, which was tested in tension, this may seem surprising, but an explanation may be that edge knots cause uneven stress distribution over the cross-section resulting in edgewise deformations, as discussed above in connection with the edgewise deformations exhibited in Fig 6d. The results in Fig 8 also show that maximum R^2 values were, for the planks loaded in bending, achieved for an IP determined over a length interval of about 90 mm and, for the boards loaded in tension, for an IP determined over a length interval of about 25 mm. These lengths correspond to about half the depth of each type of member. They also correspond to the typical length of clusters of knots or to the diameter of individual critical knots, respectively, at the sections where failure occurs in each type of members. A comparison between these R^2 values and those presented in Tables 1-2

reveals interesting facts, partly discussed in Olsson et al (2013). The maximum R^2=0.68 for the plank sample (Fig 8, left) is higher than those referring to $E_{a,1}$, $E_{b,1}$ and E_{flat} in Table 1, implying that the new grading method can provide a grading accuracy that exceeds what is achieved by common methods on the market. However, R^2 determined on the basis of static edgewise bending MOEs according to EN 408 ($E_{m,loc}$ and $E_{m,glob}$ in Table 1) are stronger than 0.68. Since the MOEs determined on the basis of the standard reflect "real" MOEs, it can be concluded that there is a potential for improvement as regards the assumptions on which the new strength grading method is based. For example, it is very likely that inclusion of the diving angle would improve the performance of the new method. Analysis of results from contact-free deformation measurements has also shown that local deformations occurring within knot clusters cannot be properly described by means of beam theory. Yet, the maximum R^2=0.77 for the board sample (Fig 8, right) is remarkably strong compared to those presented in Table 2, which is probably due to the fact that the strength of narrow pieces is much dependent on the occurrence of single large knots and that this characteristic is properly caught by means of the new method.

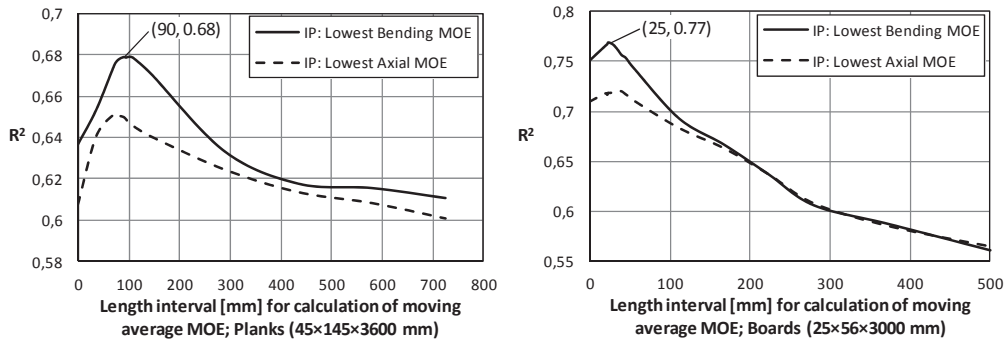

Figure 8—Relationship between length interval for calculation of moving average MOE and R^2 between strength and IP (IPs determined as lowest edgewise bending MOE and lowest axial MOE, respectively).

CONCLUSIONS

The research presented in this paper clearly shows and quantifies what has been assumed but only partly verified by other researcher, namely that determination of local MOE on the basis of EN 408 hides the effect of localized defect zones and, consequently, results in an overestimation of local MOE on the scale most relevant for prediction of strength. By application of a new strength grading method (Olsson et al 2013) in which MOE profiles are applied for IP determination, it is shown that maximum R^2 between strength, in bending as well as in tension, and IP is achieved for IPs determined as moving average *bending* MOE calculated over a length interval of approximately half the depth of investigated timber members. The application of fibre orientation information obtained by means of fast dot laser scanning for calculation of MOE on a closer scale is still quite new and further development of the approach towards even more accurate predictions of stiffness and strength can be foreseen.

REFERENCES

Anon (2013) List of approved machines. American Lumber Standard Committee, Germantown, MD. http://www.alsc.org/untreated_machinegraded_mod.htm. (21 November 2013).

EN 384 (2010) Structural timber – Determination of characteristic values of mechanical properties and density. European Committee for Standardization, Brussels, Belgium.

EN 408 (2010) Timber structures – Structural timber and glued laminated timber – Determination of some physical and mechanical properties. European Committee for Standardization, Brussels, Belgium.

Aicher S, Höfflin L, Behrens W (2002) Determination of local and global modulus of elasticity in wooden boards. Otto-Graf-Journal 13:183-198.

Bechtel FK (1985) Beam stiffness as a function of pointwise E, with application to machine stress rating. In Proc International Symposium on Forest Products Research, CSIR, Pretoria, South Africa.

Bechtel FK, Hsu CS, Wang N, Hanshaw TC (2006) Method for estimating compliance at points along a beam from bending measurements. United States Patent, Patent No.: US 7.047.156 B1.

Boughton G (1994) Superior sorting of timber using localised stiffness on edge. Pages 510-515 *in* Proc Pacific Timber Engineering Conference, 11-15 July 1994, Gold Coast, Australia.

Foschi RO (1987) A procedure for the determination of localized modulus of elasticity. Holz Roh-Werkst 45(6):257-260.

Gerhards CC (1972) Relationship of tensile strength of Southern pine dimension lumber to inherent characteristics. Research paper, FPL 174, USDA For Serv Forest Products Laboratory, Madison, WI.

Hoffmeyer P, ed (1995) Strength grading adds value, Part 2 – Available technique. Technical University of Denmark, Lyngby, Denmark. Technical Report 335-1995. In Danish, Norwegian and Swedish.

Johansson C-J (2003) Grading of timber with respect to mechanical properties. Pages 23-43 *in* S Thelandersson and HJ Larsen, eds Timber Engineering, John Wiley & Sons, Ltd, Chichester, UK.

Kass AJ (1975) Middle ordinate method measures stiffness variation within pieces of lumber. Forest Prod J 25(3):33-41.

Kline DE, Woeste FE, Bendtsen BA (1986) Stochastic model for modulus of elasticity of lumber. Wood Fiber Sci 18(29):228-238.

Lam F, Foschi RO, Barrett JD, He QY (1993) Modified algorithm to determine localized modulus of elasticity of lumber. Wood Sci Technol 27(2):81-94.

Lanvin J-D, Reuling D, Rouger F (2012) Machines for classification of wood according to strength: Presentation of different measurement techniques for grading French species (document updated 1 November 2012). FCBA Institut Technologique, Paris, France. In French.

Olsson A, Oscarsson J, Johansson M, Källsner B (2012) Prediction of timber bending strength on basis of bending stiffness and material homogeneity assessed from dynamic excitation. Wood Sci Technol 46(4):667-683.

Olsson A, Oscarsson J, Serrano E, Källsner B, Johansson M, Enquist B (2013) Prediction of timber bending strength and in-member cross-sectional stiffness variation on the basis of local wood fibre orientation. Eur J Wood Products 71(3):319-333.

Orosz I (1976) Relationship between apparent modulus of elasticity, gage length, and tensile strength of lumber. Wood Sci Technol 10(4), 273-291.

Oscarsson J, Olsson A, Johansson M, Enquist B, Serrano E (2011) Strength grading of narrow dimension Norway spruce side boards in the wet state using first axial resonance frequency. International Wood Products Journal 2(2):108-114.

Oscarsson J, Olsson A, Enquist B (2012) Strain fields around knots in Norway spruce specimens exposed to tensile forces. Wood Sci Technol 46(4):593-610.

Oscarsson J (2012) Strength grading of structural timber and EWP laminations of Norway spruce – Development potentials. Licentiate thesis, Report No. 15, School of Engineering, Linnæus University, Växjö, Sweden. 131 pp.

Pope DJ, Matthews FW (1995) A comparison of deconvolution techniques to improve MOR estimation from stress grading machine output. Wood Sci Technol 29(6):431-439.

Taylor SE, Bender DA (1991) Stochastic model for localized tensile strength and modulus of elasticity in lumber. Wood Fiber Sci 23(4):501-519.

IV

Strength grading of narrow dimension Norway spruce side boards in the wet state using first axial resonance frequency

J. Oscarsson*[1], A. Olsson[2], M. Johansson[2], B. Enquist[2] and E. Serrano[2]

Strength grading of Norway spruce [*Picea abies* (L.) Karst.] side boards in the wet state was investigated. For a sample of 58 boards, density and dynamic modulus of elasticity in the axial direction (MOE_{dyn}) were determined in the wet state. The boards were then split into two parts and the procedure of determining MOE_{dyn} was repeated both before and after the boards were dried to a target moisture content of 12%. Finally, tensile strength of the split boards was measured and its relationship to MOE_{dyn} for both wet and dried split boards was determined. The investigation also included an evaluation of a so called reversed lamination effect on the stiffness caused by the splitting of boards into two parts. The results show that strength grading of split boards in the wet state can give just as good results as grading performed after drying. The reversed lamination effect on the stiffness of split boards was found to be of lower order.

Keywords: Strength grading, Axial stiffness, Side boards, Wet state, Green state

Introduction

Approximately 30% of the volume of sawn timber produced at a typical Swedish sawmill consists of side boards, i.e. boards of narrow dimensions sawn from the outer parts of a log. Large production volumes and small dimensions imply that considerable numbers of side board pieces have to be handled in the sawmilling process and the costs for production, storage and sales are, in many cases, not met by the selling price on the market.

Previous research has shown that several wood characteristics that influence the structural properties of sawn timber vary considerably in the radial direction, i.e. from pith to bark. For example, the modulus of elasticity (MOE) in softwood trees increases significantly from the pith and outwards (Wormuth 1993) and similar behaviour has also been found for density of Norway spruce (Steffen *et al.* 1997; Dahlblom *et al.* 1999). Accordingly, side boards possess excellent structural properties but due to their small dimensions, they are very seldom used for load bearing purposes. Since 2005, Växjö University (from 1 January 2010 named Linnæus University) and SP Technical Research Institute of Sweden have conducted research regarding the development of high-value products utilising softwood side boards. The research carried out by the University and the Institute concerns the possibility to use undried Norway spruce [*Picea abies* (L.) Karst.] side boards as laminations in wet-glued laminated beams for load-bearing applications. The beams consist of flatwise glued wet boards with cross-section dimensions of 25×120 mm. For wet boards, the moisture content (MC) could vary from the fibre saturation point, which for Norway spruce occurs at $\sim$30%, to $\sim$150% (Boutelje and Rydell 1995). After gluing, each beam is split, dried and planed into two new beams with a width of 50 mm (*see* Fig. 1).

Structural properties of these split beams have been measured and analysed, and the results obtained so far are promising (Petersson *et al.* 2009; Serrano *et al.* 2010). Despite the fact that the beams have been produced from batches of un-graded boards, their stiffness and strength properties are consistent with both glued laminated timber of strength class GL32h, as defined in EN1194 (CEN 1999), and structural timber of strength class C35, as defined in EN338 (CEN 2009). Furthermore, by gluing boards in the wet state, directly after sawing, a higher yield and a much more cost-efficient handling in the sawmill production process would be obtained.

To improve the structural properties of the beams even further, defect elimination by finger jointing and strength grading of the wet side boards before gluing has been proposed. Grading of structural timber into different strength classes means that the grade-determining properties (namely bending strength, MOE and density of timber members) are predicted or measured by visual inspection or non-destructive machine testing. The market is, today, dominated by machine strength grading based on the relationship between a determined MOE value, which is used as the indicating property, and the other two grade-determining properties. One such approach is based upon dynamic excitation and measurement of the first resonance frequency f_{A1} (Hz) in

[1]SP Technical Research Institute of Sweden, Videum Science Park, SE-351 96 Växjö, Sweden
[2]School of Engineering, Linnæus University, SE-351 95 Växjö, Sweden

*Corresponding author, email jan.oscarsson@sp.se

Received 31 October 2010; accepted 27 August 2011
DOI 10.1179/2042645311Y.0000000015

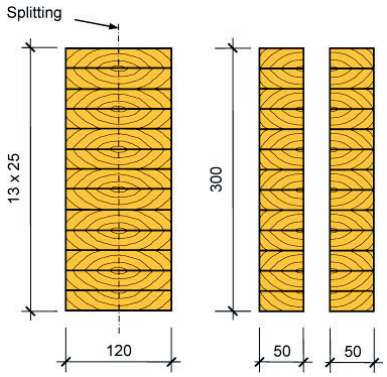

1 Wet-glued beams before (left) and after (right) splitting, drying and planing (Petersson *et al.* 2009; Serrano *et al.* 2010)

the axial direction. The relationship between this frequency and the board length L (m), density ρ (kg m^{-3}) and dynamic modulus of elasticity E_{An} (Pa) in the axial direction is expressed by equation (1) (e.g. Ohlsson and Perstorper 1992)

$$E_{An} = 4\rho\left(\frac{f_{An}L}{n}\right)^2 \quad (1)$$

where n denotes the mode number used to evaluate MOE. Thus, from equation (1), it is made clear that MOE could also be evaluated on the basis of resonance frequencies of higher modes. However, the research reported in this paper is based upon measurement and application of the first resonance frequency. This is due to the fact that industrially applied strength grading techniques that are based upon axial dynamic excitation and listed in EN14081-4 (CEN 2009) utilise only one resonance frequency, i.e. the first resonance frequency, for assignment of timber to strength classes defined in EN338 (CEN 2009). In such industrial applications, the E_{A1} value obtained from equation (1) is used to predict the board's bending strength. This prediction also decides to which strength class the board is graded. Other relevant strength properties such as tensile strength are either defined in the strength class, or calculated in accordance with EN384 (CEN 2010) from the bending strength determined for a sample, or determined from tests described in EN408 (CEN 2010). In this context, it should be noted that MOE is a material property that varies along the length of a board. Thus, the axial dynamic MOE, determined using either f_{A1} or a resonance frequency corresponding with a higher mode, is an apparent MOE that reflects an average MOE value in a board.

The approach described above is generally used for strength grading of structural timber in the dried state, i.e. typically timber with an MC of about 16–18%, but recently grading systems based on axial excitation have also been approved for wet state grading of structural timber (e.g. Initial type testing report; CEN 2010). In previous research carried out by Glos and Burger (1998), similar yields were found when structural timber with thickness >50 mm was graded in both the green state and after kiln-drying to ~12%MC using a bending and radiation type machine. Unterwieser and Schickhofer (2007) investigated the possibility of grading sawn timber, both centre-cuts and side boards with thickness >41 mm, in the wet state. They found that the axial dynamic MOE showed no dependence on the MC above the fibre saturation point and that the relationship in terms of coefficient of determination R^2 between wet and dried axial dynamic MOE was as strong as R^2=0·96.

In this paper, the results from a study to investigate the possibility to grade narrow dimension side boards in the wet state by axial dynamic excitation are presented. For a sample of boards, E_{A1} was determined by dynamic excitation under both wet and dried conditions. Subsequently, tensile strength and local static MOE in tension were measured in the dried state and the correlation between results in wet and dried states was analysed. The reason why the tests were carried out in tension was that laminations in outer parts of the type of split beam that is shown in Fig. 1 are mainly loaded in this mode and, subsequently, the tension properties of such laminations are in most cases determinant for the bending strength of a beam.

In the context of wet-glued laminated split beams made of narrow side boards, the issue of a so called reversed lamination effect on the stiffness of split boards was also raised. The effect concerns to what extent the stiffness of such boards of narrow dimensions is reduced due to the splitting, relative to the stiffness of the corresponding un-split board. This paper includes an evaluation of such an effect.

Methods and materials

A sample consisting of 58 wet Norway spruce side boards of dimensions 25 × 120 × 3900 mm was used in this project. The length of the boards was reduced to 3000 mm by removing 450 mm from each end and a small specimen of 100 mm length was cut from one of the sections removed from each board. The MC of these specimens was determined according to the oven dry method described in EN13183-1 (CEN 2002). Boards and specimens were marked in corresponding consecutive orders from no. 1 to 58.

The first axial resonance frequency f_{A1} was then measured for each board using a Timber Grader MTG which is a handheld and wireless measuring instrument for strength grading of structural timber (Brookhuis Micro-Electronics BV 2009). A grading set includes grader, balance and computer software and hardware. When measuring f_{A1}, the Grader is held against one of the board ends and longitudinal modes of vibration are excited by the blow of a metal piston incorporated in the Grader. Vibration data are measured by a sensor in the Grader and sent via a Bluetooth connection to the PC. From installed software, several axial resonance frequencies could be obtained, but only the first one is employed for determining the dynamic axial MOE. The Grader is approved as a machine grading system with settings listed in EN14081-4 (CEN 2009) and the approval concerns timber with mean MC between 10 and 25%. In this investigation, a board's weight and f_{A1} were obtained from the balance and the Grader respectively. Density and E_{A1} were calculated manually: the latter parameter from equation (1).

In the next step, each board was split in the longitudinal direction into two parts. One of them, randomly

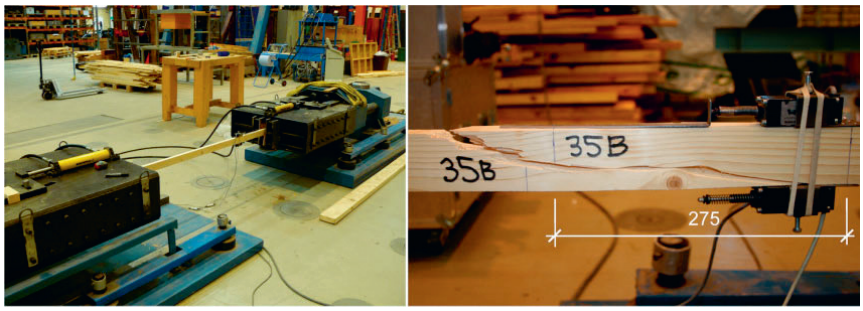

2 Test set-up for tension tests (left) and transducers and measurement length (275 mm) for elongation measurement (right)

chosen, was marked with an 'A' and the other one with a 'B' to supplement the marking from the previous step. The procedure for determination of resonance frequency, density and E_{A1} was then repeated for each split board. After drying to an MC varying between 12 and 14%, the measurement procedure was carried out once again.

Finally, after the boards had been stored at standard climate 20°C/65% relative humidity for ~7 months, tensile strength and local static MOE in tension were measured in accordance with procedures described in EN408 (CEN 2010). The test set-up is shown in Fig. 2 (left). The testing machine was of make MFL with hydraulic force generation, maximum load 3·0 MN and 2000 mm length of stroke. Wedge type grips were used, which prevented rotation of the board ends, and the distance between the grips was 1500 mm. The load

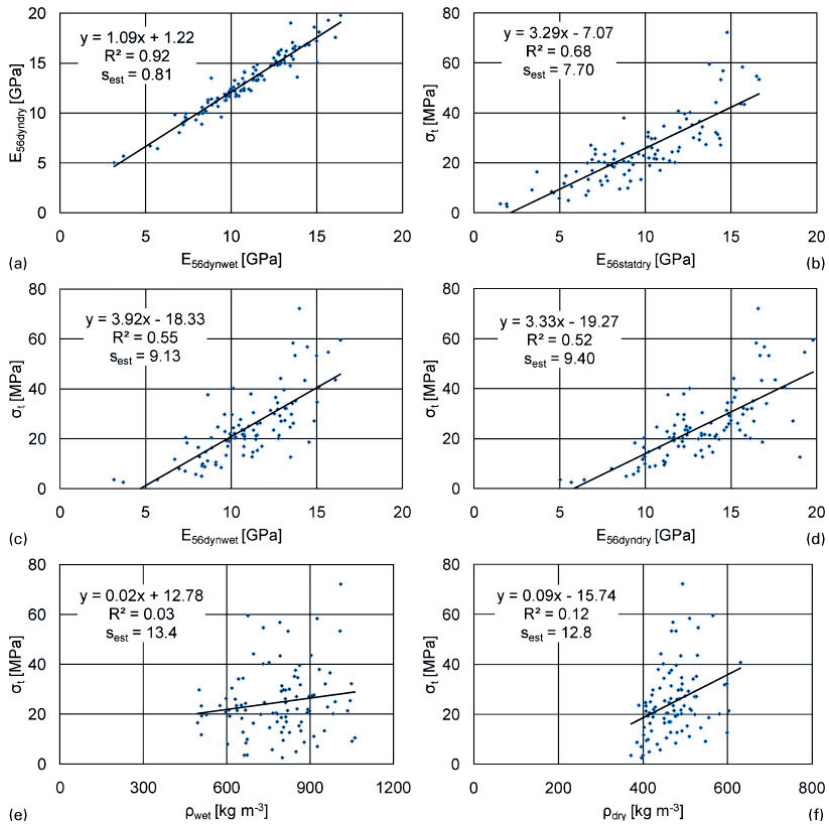

3 Relationship between *a* $E_{56dynwet}$ and $E_{56dyndry}$, *b* $E_{56statdry}$ and σ_t, *c* $E_{56dynwet}$ and σ_t, *d* $E_{56dyndry}$ and σ_t, *e* ρ_{wet} and σ_t and *f* ρ_{dry} and σ_t

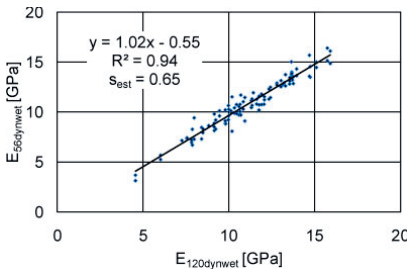

4 Relationship between $E_{120dynwet}$ and $E_{56dynwet}$

application was force controlled with a constant loading rate of 7–8 kN min^{-1} and the average time to failure for the tested boards was 304 s.

The local static MOE was determined from the elongation, measured by two transducers, between two points 275 mm apart, corresponding to a length of five times the width of the boards. The transducers were placed on opposite narrow board edges [*see* Fig. 2 (right)], at the worst defect, i.e. at the board section where the fracture was expected to occur. This critical section was, in most boards, chosen as the one including the largest single knot. For boards that contained traversing edge knots or several potential critical knots of similar size, the grain disturbances around the knots were also considered.

The measurement results were analysed using simple linear regression. To evaluate the possibility of grading wet boards, the following relationships in terms of coefficients of determination R^2 between different material parameters were calculated (indices '56' and '120' refer to the average widths of split boards and un-split boards respectively):

(i) axial dynamic MOE measured for split boards in the wet state, denoted $E_{56dynwet}$, in relation to axial dynamic MOE for split boards in the dried state (12–14%MC), denoted $E_{56dyndry}$ (Fig. 3*a*)
(ii) local static MOE measured for split boards in the dried state $E_{56statdry}$ in relation to the tensile strength for split boards in the dried state σ_t (Fig. 3*b*)
(iii) $E_{56dynwet}$ and $E_{56dyndry}$ respectively, in relation to σ_t (Fig. 3*c* and *d*)
(iv) density before drying ρ_{wet} in relation to σ_t (Fig. 3*e*)
(v) density after drying ρ_{dry} in relation to σ_t (Fig. 3*f*).

Table 2 Coefficients of determination R^2 of different properties of investigated boards

R^2	$E_{56dynwet}$	$E_{56dyndry}$	$E_{56statdry}$	σ_t	ρ_{wet}	ρ_{dry}
$E_{56dynwet}$	1	0·92	0·62	0·55	0·05	0·37
$E_{56dyndry}$		1	0·62	0·52	0·03	0·46
$E_{56statdry}$			1	0·68	0·01	0·14
σ_t				1	0·03	0·12
ρ_{wet}					1	0·06
ρ_{dry}						1

The reversed lamination effect was assessed on the basis of the relationship between $E_{56dyndry}$, as defined above, and $E_{120dynwet}$, i.e. axial dynamic MOE determined for un-split wet boards (Fig. 4).

In addition to the R^2 values presented in the figures referred to above, standard errors of the estimate s_{est} and equation of the regression lines y are also given in the same figures.

Results and discussion

Grading of wet side boards

A number of seven out of the 58 un-split boards and eight out of the 116 split board appeared to contain rot and were eliminated from the subsequent analysis (*see* explanatory notes in Table 1). The MC of the remaining 51 un-split boards in their green state varied considerably, from a minimum value of 28% to a maximum of 180%. The mean MC value was 93% with a standard deviation of 43%.

Mean values and standard deviations of determined parameters defined in the section on 'Methods and materials' are shown in Table 1. Relevant scatter plots are exhibited in Fig. 3*a–f* and the R^2 values for selected interrelationships are presented in Table 2. The mean value of $E_{56dynwet}$ was ~17% lower than $E_{56dyndry}$, which corresponds fairly well with results referred to in Dinwoodie (2000), and the mean value of $E_{56statdry}$ is 26% lower than $E_{56dyndry}$. The last observation is partly explained by the fact that the dynamically measured MOE of a board is related to an average MOE value of the entire board, whereas the local static MOE is measured locally, at the section where the worst defect is located. The difference is also related to the fact that the dynamically measured MOE of a board is, in general, larger than the corresponding statically measured MOE (Larsson *et al.* 1998).

There was a strong relationship between dynamic MOEs measured for split boards in wet and dried states (R^2=0·92, *see* Fig. 3*a*), similar to the one that was found

Table 1 Mean values and standard deviations of different properties of investigated boards

	Unit	Mean value	Standard deviation	Number of boards
$E_{120dynwet}$	GPa	11·10	2·57	50*
$E_{56dynwet}$	GPa	10·84	2·58	108†
$E_{56dyndry}$	GPa	13·04	2·93	108†
$E_{56statdry}$	GPa	9·59	3·40	106‡
σ_t	MPa	24·8	13·5	96§
ρ_{wet}	kg m^{-3}	785	141	108†
ρ_{dry}	kg m^{-3}	471	53	108†

*Eight boards disregarded due to rot (seven) and measurement error (one).
†Eight boards disregarded due to rot.
‡Ten boards disregarded due to rot (eight) and damage (two).
§Twenty boards disregarded due to rot (eight), damage (two) and failure in grips (ten).

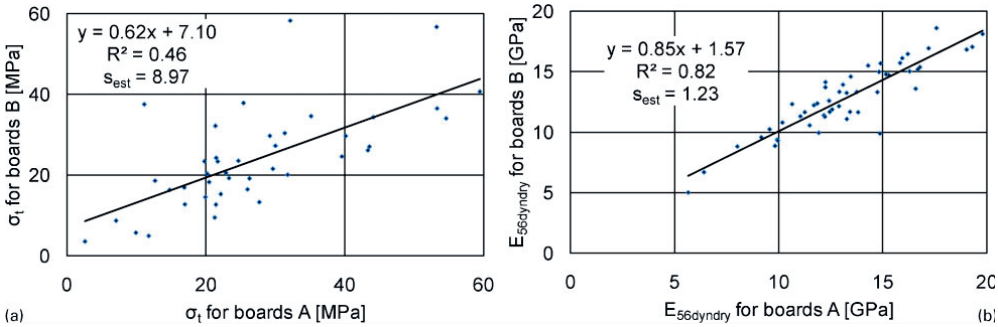

5 Relationship between *a* σ_t for pairs of split boards A and B and *b* $E_{56dyndry}$ for pairs of split boards A and B

by Unterwieser and Schickhofer (2007) for centre-cuts and side boards with thickness >41 mm.

A comparison of Fig. 3*c* and *d* shows that the relationship between dynamic MOE in wet condition and tensile strength was of similar strength as the corresponding relationship between dynamic MOE in dried condition and tensile strength (R^2=0·55 in wet state and R^2=0·52 in dried state). The coefficient of determination for the latter relationship increased to R^2=0·58 when the dried state density was included as a second prediction variable in a multiple linear regression analysis. The relationship between local static MOE, measured in the dried state at the assumed weakest board section, and tensile strength was stronger (R^2=0·68, *see* Fig. 3*b*) than the relationships between tensile strength and dynamic MOE in wet and dried conditions respectively (*see* Fig. 3*c* and *d*). This is presumably due to the fact that the local static MOE is measured at the board section where the fracture is expected to occur, whereas the dynamic MOEs reflect average values for the entire board.

There was a weak relationship between tensile strength and density in the dried state (R^2=0·12, *see* Fig. 3*f*), whereas no such relationship was established between density in the wet state and the tensile strength (R^2=0·03, *see* Fig. 3*e*). It was not surprising that the latter relationship was found to be even weaker than the former, since the density measured in the dried state is a good measure of the amount of wood cell material, whereas in the wet state at variable MC, it is not. Furthermore, the level of significance in terms of p values was calculated for the relationships between densities and tensile strength. The relationship in the dried state was found to be statistically significant (p<0·001), whereas the p value for R^2 between wet state density and strength was, as expected, considerably higher (p=0·12).

The results obtained in this study indicate that it is possible to grade split side boards in the wet state using axial dynamic excitation since, first, the dynamic MOE values measured in wet and dried states are strongly related and, second, the tensile strength is as strongly related to axial dynamic MOE measured in the wet state as it is to axial dynamic MOE measured in the dried state. However, the presented coefficients of determination require that the actual densities in wet and dried states respectively, are regarded when axial dynamic MOEs are calculated.

The idea of grading side boards in the wet state originates from ongoing research concerning wet-glued laminated split beams. For such beams, strength grading of laminations has to be carried out for un-split boards. Thus, the relationship between axial dynamic MOE measured for un-split wet boards $E_{120dynwet}$ and σ_t for dried split boards was also determined and it was found to be R^2=0·45 for the entire sample. However, since $E_{120dynwet}$ is related to σ_t of two split boards, each split board observation is not truly independent. From Fig. 5*a*, it is clear that σ_t of A boards and B boards are correlated to a certain degree. Because of this, the relationships between $E_{120dynwet}$ and σ_t of A and B boards respectively, were determined. For A boards only, the relationship between σ_t and $E_{120dynwet}$ was R^2=0·53 and for B boards it was R^2=0·39. From the calculated coefficients of determination, it could be concluded that the relationship between $E_{120dynwet}$ and σ_t for dried split boards was, as expected, slightly weaker than the relationship between $E_{56dynwet}$ and σ_t (R^2=0·55, *see* Fig. 3*c*).

In some of the split boards, there were knots larger than half the width of the board [*see* Fig. 6 (left and middle)], and in such cases strength values as low as 2·6 MPa were found. The strength of the strongest

6 Fracture in two of weakest split boards (left and middle) and in strongest split board (right)

board was 72·1 MPa [*see* Fig. 6 (right)]. Furthermore, there was a considerable amount of variation in σ_t for boards split from the same original board (R^2=0·46, *see* Fig. 5*a*). The strength of this relationship, together with the mean value and the standard deviation for σ_t given in Table 1, indicates that the scattering of measured strength values for the split boards could be considered as rather large, compared with other investigations of laminations for glued laminated timber (Johansson *et al.* 1998). This is not surprising as the boards examined here are of very narrow dimensions. In comparison, there was a much stronger relationship between values of $E_{56dyndry}$ for boards split from the same original board (R^2=0·82, *see* Fig. 5*b*).

Even if the strength of many of the boards was very low due to the occurrence of knots, this does not necessarily reflect the behaviour of the boards when they are used as flatwise glued laminations in the type of glulam beams shown in Fig. 1. For example, large deformations, both longitudinal and lateral, in flexible sections of a lamination are restrained by adjacent laminations, and tensile forces in weak laminations could, to a certain degree, be transferred via bond lines to other laminations. This, in combination with the fact that the beams consisted of side board laminations, explains why high performance wet-glued beams could be achieved from un-graded batches of split Norway spruce side boards.

Reversed lamination effect

From Table 1, the mean value and standard deviation of the stiffnesses, in the wet state, of split and un-split boards ($E_{56dynwet}$ and $E_{120dynwet}$) used in this investigation could be compared and the relationship between $E_{56dynwet}$ and $E_{120dynwet}$ is shown in Fig. 4. According to the obtained results, the mean value was 2% lower after splitting, the standard deviations were almost the same and the relationship was very strong (R^2=0·94). The two variables, before splitting ($E_{120dynwet}$) and after splitting ($E_{56dynwet}$), were compared with a paired *t*-test and the difference in MOE, although small, was found to be statistically significant ($p<0·01$). In the analysis, the value for an un-split board was compared with values for both split boards. Consequently, the $E_{56dynwet}$ observations are not truly independent, as the stiffnesses of A boards and B boards are correlated (*see* Fig. 5*b*). However, the effect is small. For the A boards only, the relationship between $E_{56dynwet}$ and $E_{120dynwet}$ was R^2=0·94, and for the B boards it was R^2=0·93, i.e. almost exactly the same R^2 values as was obtained for the entire sample of split boards.

Conclusions and future work

The objectives of this research were to investigate the possibility to grade Norway spruce side boards of narrow dimensions in the wet state using axial dynamic excitation, and to evaluate a possible reversed lamination effect on the stiffness caused by splitting wet boards longitudinally into two parts. According to the results, strength grading in the wet state using axial dynamic MOE as indicating property is just as reliable as grading carried out correspondingly after drying, provided that actual board density in both wet and dried states are measured and regarded when MOE values are determined. The relationship between axial dynamic MOE for split boards in the wet and dried states, $E_{56dynwet}$ and $E_{56dyndry}$, was found to be as high as R^2=0·92.

The results also show that the difference in strength between two split boards originating from the same un-split board could be considerable. However, the difference would most likely be reduced by implementation of defect elimination such as finger jointing of un-split side boards, since such a measure would result in a reduction in the inhomogeneity of material properties in both split and un-split boards. This is an issue to be addressed in future work.

Regarding the reversed lamination effect on the stiffness of split boards, it was in this investigation found to be of lower order.

Acknowledgements

This research was made possible by financial support from The Knowledge Foundation, The Swedish Research Council for Environment, Agricultural Science and Spatial Planning and CBBT – Centre for Building and Living with Wood.

References

Boutelje, J. B., and Rydell, R. 1995. Wood facts – 44 wood species in text and illustrations (in Swedish). Trätek – Swedish Institute for Wood Technology Research, Stockholm, Sweden. Publ. no. 8604028.

Brookhuis Micro-Electronics BV. 2009. Timber Grader MTG – operating instructions. Enschede: Brookhuis Micro-Electronics BV. MTG Manual GB 12062009-C.

CEN. 1999. EN1194 Glued laminated timber – strength classes and determination of characteristic values. European Committee for Standardization, Brussels, Belgium. CEN/TC124.

CEN. 2002. EN13183-1 Moisture content of a piece of sawn timber – Part 1: determination by oven dry method. European Committee for Standardization, Brussels, Belgium. CEN/TC175.

CEN. 2009. EN338 Structural timber – strength classes. European Committee for Standardization, Brussels, Belgium. CEN/TC124.

CEN. 2009. EN14081-4 Timber structures – strength graded structural timber with rectangular cross section – Part 4: machine grading – grading machine settings for machine controlled systems. European Committee for Standardization, Brussels, Belgium. CEN/TC124.

CEN. 2010. EN384 Structural timber – determination of characteristic values of mechanical properties and density. European Committee for Standardization, Brussels, Belgium. CEN/TC124.

CEN. 2010. EN408 Timber structures – structural timber and glued laminated timber – determination of some physical and mechanical properties. European Committee for Standardization, Brussels, Belgium. CEN/TC124.

CEN. 2010. Initial type testing report no. ITT/36/20/03. European Committee for Standardization, Brussels, Belgium. CEN/TC124/TG1.

Dahlblom, O., Persson, K., Petersson, H., and Ormarsson, S. 1999. Investigation of variation of engineering properties of spruce. Proc. 6th Int. IUFRO Wood Drying Conf. Stellenbosch, South Africa, January 1999. IUFRO. Pages 253–262.

Dinwoodie, J. M. 2000. Timber: its nature and behaviour. London: Second Edition, E & FN Spon.

Glos, P., and Burger, N. 1998. Maschinelle Sortierung von frisch eingeschnittenem Schnittholz (in German). Holz. Roh. Werkst. 56(5): 319–329.

Johansson, C.-J., Boström, L., Bräuner, L., Hoffmeyer, P., Holmqvist, C., and Sollie, K. H. 1998. Laminations for glued laminated timber – establishment of strength classes for visual strength grades and machine settings for glulam laminations of Nordic origin. SP Swedish National Testing and Research Institute, Sweden. SP report 1998:38.

Larsson, D., Ohlsson, S., Perstorper, M., and Brundin, J. 1998. Mechanical properties of sawn timber from Norway spruce. Holz. Roh. Werkst. 56(5): 331–338.

Ohlsson, S., and Perstorper, M. 1992. Elastic wood properties from dynamic tests and computer modeling. J. Struct. Eng. 118(10): 2677–2690.

Petersson, H., Bengtsson, T., Blixt, J., Enquist, B., Källsner, B., Oscarsson, J. (ed.), Serrano, E., and Sterley, M. 2009. Increased value yield by wet and dry gluing of sawn side boards into

property optimized wood products for the construction market (in Swedish). School of Technology and Design, Växjö University, Sweden. Reports no. 53.

Serrano, E., Oscarsson, J., Enquist, B., Sterley, M., Petersson, H., and Källsner, B. 2010. Green-glued laminated beams – high performance and added value. Proc. (Poster session) 11th World Conf. on Timber Engineering, Riva del Garda, Italy, June 2010. Trees and Timber Institute. Pages 829–830.

Steffen, A., Johansson, C.-J., and Wormuth, E.-W. 1997. Study of the relationship between flatwise and edgewise moduli of elasticity of sawn timber as a means to improve mechanical strength grading technology. Holz. Roh. Werkst. 55(2–4): 245–253.

Unterwieser, H., and Schickhofer, G. 2007. Pre-grading of sawn timber in green condition. Proc. 1st Conf. of COST Action E53 – quality control for wood and wood products. Warzaw, Poland, October 2007. European Science Foundation.

Wormuth, E.-W. 1993. Untersuchung des Verhältnisses von flachkant zu hochkant ermitteltem Elastizitätsmodul von Schnittholz zur Verbesserung der maschinellen Festigkeitssortierung (in German). Master's dissertation. University of Hamburg, Germany.

V

Green-glued Products for Structural Applications [1]

Erik Serrano[1,2], Jan Oscarsson[2], Magdalena Sterley[2] and Bertil Enquist[1]

[1]Linnaeus University, Department of Building and Energy Technology

[2]SP Technical Research Institute of Sweden

Abstract The results from bending tests on 107 laminated, green-glued, beams manufactured from Norway spruce side boards are presented. The beams were made by face gluing 21-25 mm thick boards using a commercial one-component moisture curing polyurethane adhesive. In addition to the bending test results, results from shape stability measurements after climatic cycling and bond line strength and durability test results are also presented. The results from the bending tests show that, by applying very simple grading rules, it is possible to obtain beams with high bending strength (with a 5%-percentile characteristic value of 40,1 MPa) and substantial stiffness (mean value of 14360 MPa). Also the shape stability of the beams and the strength and the durability of the interlaminar bonds were found to be satisfactory.

Introduction

For a typical south-Swedish saw mill, approximately 30% of the produced volume consists of so-called side boards (here we focus on saw mills producing spruce timber, *Picea abies*). Such side boards are of rather narrow dimensions, 18-25 mm in thickness, and are not of major interest for structural applications. At the same time, the huge number of narrow-dimension boards to be dealt with increases considerably the costs for internal logistics at the saw mills.

The side boards are cut from the logs at a relatively large distance from the pith and it is well known (see e.g. Steffen et al. 1997) that basic mechanical properties, such as the modulus of elasticity along grain, are positively correlated to the distance from pith. Thus, the narrow-dimension side boards are of great interest if it would be possible to use them in structural applications.

[1] This is the manuscript of a paper published in: S. Aicher *et al.* (eds.) *Materials and Joints in Timber Structures*, RILEM Bookseries 9, DOI:10.1007/978-94-007-7811-5_4, © RILEM 2014. The manuscript is presented here, since one of the figures was not correctly reproduced in the publication referred to.

With the above in mind, an obvious approach would be to produce large-dimension products from the side boards, similar to how traditional glued laminated timber (glulam) production is done. However, in traditional glulam production, the laminations have to be dried to approximately 12% moisture content (MC), and, in addition, laminations have to be planed within a short period of time prior to gluing. If kiln-dried thin side boards are used, such planing would cause a substantial waste. If instead the laminations could be face-glued already in the wet state, with a minimum of planing (or no planing at all) much would be gained. This is the basic idea behind the research presented here and thus the approach has been to investigate the mechanical properties of green-glued laminated products, produced from freshly sawn spruce side boards.

The research presented herein relates to three research projects running at Linnaeus University from 2006 to 2013. Only the main results in terms of mechanical behaviour (stiffness and strength) from beam bending tests are reported in detail here. In addition, investigations on the shape stability of beams exposed to varying climates, on the durability and strength of adhesive bond lines, on the fracture mechanical behaviour of bond lines and on the performance of green-glued finger joints have been performed. Only some results from these investigations are briefly mentioned here, but further details can be found in e.g. Serrano *et al.* (2010), Serrano *et al.* (2011) and Sterley (2012).

Materials and methods

Material selection and manufacturing methods

Wood raw material, grading and adhesives

All wood material used is Norway spruce (*Picea abies*). The material was taken from ordinary production at the saw mills, and was not graded before delivery to the production facilities were the laminated beams were manufactured.

In two out of a total of three test series, the laminations were used as is, i.e. in the saw falling quality delivered to the production facility, although with some rejects due to vane. In the third series an effort was done to produce cross sections with high quality outer laminations. In that test series it was decided to use two grading criteria in order to classify the boards into inner laminations, outer laminations and rejects. First, a visual grading was performed, in which maximum knot size was checked. For outer laminations, the maximum wide face knot size was set to 25 mm. No criterion on maximum knot size was set for inner laminations. Following the visual grading, a hand-held grader (Timber Grader MTG, Brookhuis Brookhuis Micro-Electronics) was used in order to determine the dynamic modu-

lus of elasticity (MOE) along the board direction of each lamination. For outer laminations the MOE-criterion was 12 000 MPa, boards with MOE-values between 7 000 and 12 000 MPa were used as inner laminations and boards with MOE less than 7 000 MPa were rejected. Thus, laminations with MOE > 12 000 MPa, but with maximum knot size being > 25 mm were rejected.

In all tests, the laminations were delivered at an MC close to the fibre saturation point, or considerably above that. The same adhesive was used in all test series – a commercial one-component, moisture curing polyurethane. The adhesive is not specifically designed for green gluing, but is in fact an approved structural wood adhesive for load bearing applications according to the European standardisation and approval system – when used in traditional "dry gluing".

Beam lay-ups and manufacturing

The original test plans included a total of 128 beams in three main series with different variations. The variations included the annual ring orientation of the laminations, grading of the laminations, and various climatic cycling schemes. The various beam test series are denoted series I-III, with letters a-d denoting the variations within each series.

Lamination lay-ups that were discussed in the planning phase are shown in Fig. 1. Note that beam lay-ups B and C rely on the laminations being split to their final width before gluing the laminations together to form the beam cross-section. Beam lay-ups A and D can be manufactured by splitting the beam after gluing the laminations together. Splitting the beam after gluing has the advantage of minimising waste, since only two sides have to be planed and since the waste from the saw cut in general is less than the waste from planing.

It was decided, based on the results from simple finite element analyses, to investigate orientations type A, B and D in the various test series. Lay-ups A and D were chosen since these are the most practical in production and lay-up B was chosen since the finite element analyses showed that orientation B would lead to less distortion of the cross-section.

Two different approaches in manufacturing of the beams from the laminations were thus used. In series I (comprising lay-up A) and in series II (comprising lay-up D) the beams were manufactured with 120 mm wide laminations and the beams were split into two halves of approximately 60 mm width after curing. Thus, each such pair of beam halves comprises two beams with a good match of the lamination properties.

In test series III annual ring orientations B and D were used, orientation D being used for reference to test series II. By comparing the distortion between orientations B and D for pairs of beams with *matched* laminations the variability could be kept at a minimum. The matching procedure was realised by first splitting 120 mm wide boards into two halves, one such half being used as a type D-lamination in a type D-beam, the other half being used as a type B-lamination at the same position in the corresponding type B-beam. Consequently, test series III

included pairs of beams, each pair being one type B-orientation beam and one type D-orientation beam. Each lamination in a type B-beam was thus matched as close as possible with the lamination at the corresponding position of the type D-beam. Before gluing the laminations in series III, the laminations were also graded, as described below. This meant that not all laminations could be used, since there was a constraint that both halves should be placed at the same position in corresponding beams. Thus, if one half was graded (based on either stiffness or knot size) as being an outer lamination and the other as an inner lamination, both halves had to be rejected. The somewhat complicated procedure used in series III was used in order to minimise variability, and thereby simplify the evaluation of the results. In production, clearly this approach cannot be used, for practical reasons.

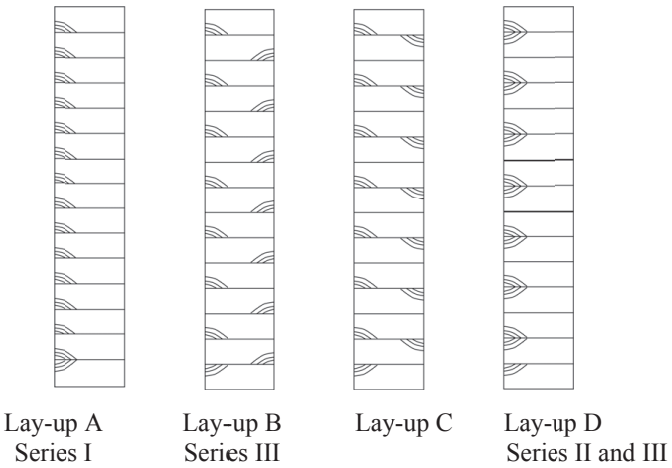

Fig. 1. Lamination lay-ups used in the various test series.

All beams were manufactured with full length laminations, thus no finger joints were used. The beam gluing was done in semi-industrial scale beam presses. A new pressing equipment was developed for use in series II and III due to insufficient performance of the equipment used in series I. The nominal clamping pressure was around 0,5 MPa in series I and 0,9 – 1,0 MPa in series II and III. The press time varied slightly between the various series, but was in general 45 - 60 minutes. The nominal spread rates used in applying the adhesive was 250 g/m^2 in series I and 200 g/m^2 in series II and III.

After curing, and in relevant cases after splitting of the beam into two halves, the beams were kiln dried together with structural timber of similar dimensions (thickness). Finally, planing to target dimensions was done after kiln drying. All test specimens manufactured for the three series are specified in Table 1. After delivery to the laboratory, the beams to be tested without climatic cycling were in all cases stored under controlled climate (20°C/50%RH or 20°C/65%RH) for at least 3 months before testing. The beams to be exposed to climatic cycling were stored for 3-7 months in the various climates.

Table 1. Beam series and parameter variation in manufacturing and climatic conditioning. Laminations marked with * were split to half their width (giving two matched lamination halves) *prior* to assembly of the beam.

Test series	Number of beams	Lay-up	Laminations thickness×width× length (mm^3)	Grading of laminations	Beams Width×depth (mm^2)	Gluing conditions	Climates, RH (%).
Ia	15	A	21×120×4900	No	50×300	Dry	50[1]
Ib	12	A	21×120×4900	No	50×300	Green	50[1]
Ic	13	A	21×120×4900	No	50×300	Green	50-90-50[1]
IIa	16	A	25×120×5400	No	50×300	Green	65[2]
IIb	16	A	25×120×5400	No	50×300	Green	65-35-65[2]
IIc	16	D	25×120×5400	No	50×300	Green	65[2]
IId	16	D	25×120×5400	No	50×300	Green	65-35-65[2]
IIIa	5	B	21,5×120×5400*	Yes	50×300	Green	65[2]
IIIb	7	B	21,5×120×5400*	Yes	50×300	Green	65-35-90-65[2]
IIIc	5	D	21,5×120×5400*	Yes	50×300	Green	65[2]
IIId	7	D	21,5×120×5400*	Yes	50×300	Green	65- 35-90-65[2]

[1] Beams were to be tested after conditioning at climate 20°C/50%RH.
[2] Beams were to be tested after conditioning at climate 20°C/65%RH.

Beam bending tests

The bending stiffness and the bending strength of the beams were evaluated. The tests were all performed in 4-point bending, as is prescribed in EN 408. Due to the limited length of the beams in series 1, the standard 18 times beam depth for the total span was not possible to use. Instead, approximately 15,3 times the beam depth was used in series I and 16,7 times the beam depth was used in series II and III. The minimum requirement according to the standard is 16 times the beam depth. The distance between the loads was, however, always 6 times the nominal beam depth. The test set-up used is depicted schematically in Fig. 2 for the case of 16 times the beam depth.

Two different types of deflection measurements were used, denoted v and w in the figure. The local deformation, v, includes the deformation due to bending only, since there is no shear force in the mid span. The deformation denoted w includes deformation due to shear but also due to local effect at supports. Therefore, the most relevant stiffness to report is the one calculated using the deformation v. This stiffness is also known as local modulus of elasticity (local MOE). All tests were performed in displacement control with the loading speed set such that failure was reached within 5-10 minutes.

Prior to testing to failure, the stiffness was determined by calculating the deformation between two load levels within the elastic domain. All test results in terms of strength have been evaluated in relation to EN 14358, and EN 14080, as-

suming a lognormal distribution of bending strength with unknown standard deviation. The characteristic values are determined as 5-percentiles at 75% confidence level. The size correction factor according to EN 1194 has been used, and such corrected strength values are thus representative for a 600 mm deep and 150 mm wide beam. Since the beams in fact were approximately 300 mm in depth, the actual strength of the beams in testing was approximately 13% higher than the reported values.

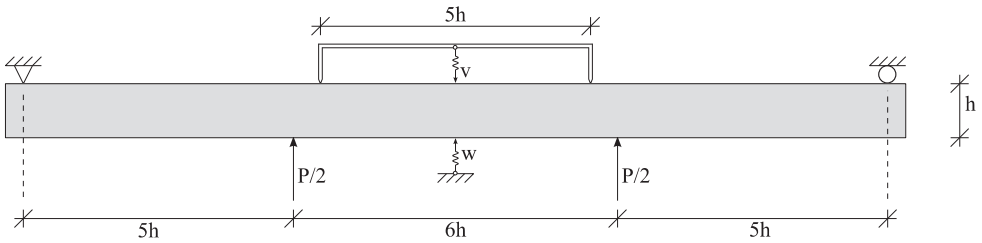

Fig. 2. Test set-up used in beam bending tests.

Shape stability, bond line shear strength and durability

The shape of the beams was measured at delivery to the University and after completing the different climatic cycles. In those measurements a special rig making it possible to measure twist, cup, bow, crook and cross-sectional distortion (meaning deviation from 90° angle at the corners). Here, twist, bow and crook were measured over a length of 3,72 m while cup was measured over a 270 mm length in the height direction of the cross section.

For assessment of the adhesive bonds in the beams, shear strength and wood failure percentage (WFP) were determined according to the European standards EN 392 and EN 386, respectively. The delamination of the bonds according to EN 391 was also measured. In a first test series, specimens for shear and for delamination tests were taken from four beams from series II (two with a annual ring orientation of type A and two of type D) that had been tested in bending (without climatic cycling). In total 48+48 bonds from the type A beams and 24+24 bonds from the type D beams were tested for shear strength and delamination, respectively. A second test series was performed by taking additional specimens from two type A that were manufactured especially for the shear and delamination tests and thus had not been tested in bending or been exposed to climatic cycling. These beams had two different spread rates: 150 and 200 g/m^2. Here in total 24+24 bonds for each spread rate were tested for shear strength and delamination, respectively. A third test series was realized by cutting specimens from beams that had been tested in bending after being exposed to climatic cycling. These specimens were used only for delamination tests.

Results

Beam bending tests

The results from all tests performed are summarised in Table 2 and Table 3. The characteristic strength values of Table 3 correspond to the 5%-percentile estimates calculated according to the provisions of EN 14358. Size-effect corrected values are calculated according to EN 1194. Bending MOE values are based on *local* MOE, cf. Fig. 2. Note that in manufacturing the test specimens according to the schedule in Table 1, there was at one occasion a malfunction of the pressing equipment, and thus three of the planned tests of Series III could not be performed. In addition, cracks running from the end of the beams had developed during kiln drying in three specimens, such that at testing of these beams failure was due to shear along that same pre-existing crack. Such specimens have been excluded from the evaluation. Thus, out of the planned 128 beams, only 122 are evaluated.

Table 3 gives the results statistics for various combinations of beam lay-ups (cf. Table 1). Most of the variations studied seem to have a relatively small influence on average bending strength, except combination D (graded laminations) which gives a higher strength, and also a lower COV, resulting in a considerably higher characteristic bending strength. The MOE variation was in all cases small, both within the test series and between test series.

Table 2. Bending strength, f_m, MOE, density and MC. k_h is the size factor according to EN 1194. Density and MC (only measured in one series) refer to beam mass/beam volume at the time of testing, after conditioning in 20°C/50%RH or 20°C/65%RH, cf. Table 1.

Series	N	f_m		$f_m \cdot k_h$	MOE		Density	MC
		Mean [MPa]	COV [%]	Mean [MPa]	Mean [MPa]	COV [%]	Mean [kg/m^3]	Mean [%]
Ia	15	43,9	9,1	38,8	14210	4.2	495	-
Ib	12	44,8	9,3	39,6	13860	6.2	498	-
Ic	12	42,6	12,6	37,6	13750	5.6	504	-
IIa	16	45,5	10,0	40,2	13680	4.7	495	~14-16
IIb	16	45,5	14,8	40,1	13800	6.6	492	~13-14
IIc	16	46,8	12,1	41,3	14030	5.5	507	~14-16
IId	16	50,4	7,1	44,4	14510	6.8	504	~13-14
IIIa	2	48,7	-	43,0	13880	-	500	-
IIIb	7	52,5	5,7	46,3	14690	3.8	495	-
IIIc	3	51,8	-	45,7	13830	-	493	-
IIId	7	49,8	5,1	44,0	14380	4.6	493	-

Table 3. Test results, combinations of test series. k_h is the size factor according to EN 1194.

Series	N	f_m			$f_m \cdot k_h$		MOE	
		Mean [MPa]	COV [%]	Char [MPa]	Mean [MPa]	Char [MPa]	Mean [MPa]	COV [%]
A: Series Ib+Ic+II+III	107	47,0	11,2	36,9	41,5	32,6	14020	5.9
B: Series II+III	83	48,0	10,7	37,9	42,3	33,5	14080	5.9
C: Series II	64	47,1	11,5	36,5	41,5	32,2	14000	6.3
D: Series III	19	51,0	5,2	45,4	45,0	40,1	14360	4.3

Shape stability, bond line durability and strength

An example of results from the shape stability measurements are given in Fig. 3, showing the twist of the beams (measured over a length of 3,72 m) of Series III after the various climatic conditioning schemes.

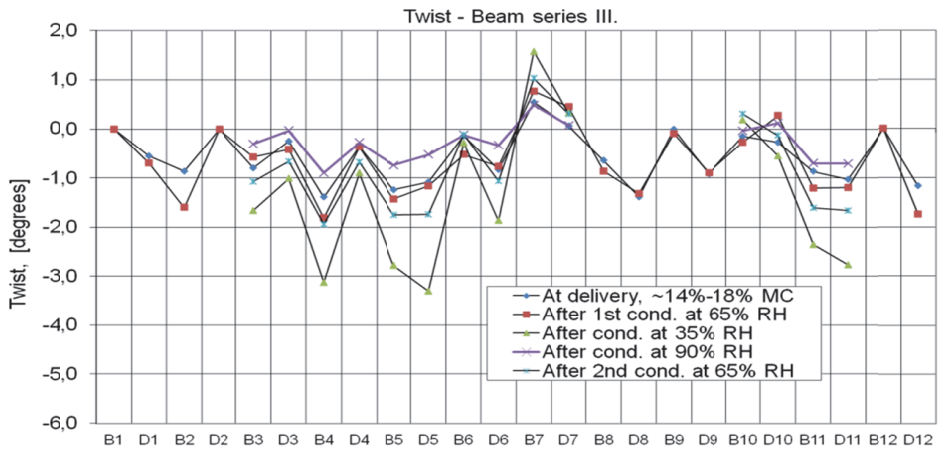

Fig. 3. Measured twist after various climatic conditioning schemes for series III.

Results from the bond line durability and shear strength tests are presented in Table 4. The results fulfil on average the strength versus wood failure percentage requirements of EN 386. Individual specimens do however, for one of the test series, not fulfil the requirements: Using only 150 g/m^2 adhesive spread rate, *two* individual tests (out of 24 tests) failed to comply with the strength requirements of EN 386 (for structures in service class 3). For the delamination tests on bonds that had *not* been subjected to climatic variations a 3,0-5,2 % delamination was obtained. On average this meets the requirements and the spread rate 200 g/m^2 appears to be

enough to obtain both sufficient mechanical strength and to obtain adequate resistance to delamination (note that some of the delamination tests were done on specimens taken from tested beams). The test series showing highest delamination values (see Table 4) are tests performed on specimens subjected both to bending tests and climatic cycling.

Table 4. Results from tests of adhesive bonds. Standard deviations in parenthesis.

Lay-up and specimen type	Mean shear strength (MPa)	Mean wood failure (%)	Delamination (%)
A. (200 g/m^2, after bending test, no climatic cycling)	9,3 (1,4)	94 (12)	3,4
D. (200 g/m^2, after bending test, no climatic cycling)	10,3 (1,4)	91 (13)	5,1
A(150 g/m^2, no bending test, no climatic cycling)	9,5 (1.9)	86 (13)	5,2
A (200 g/m^2 no bending test, no climatic cycling)	9,9 (1.2)	93 (10)	3,3
A (200 g/m^2 after bending test, climatic cycling)	-	-	19 (9) Min 1 Max 34
D (200 g/m^2 after bending test, climatic cycling)	-	-	17 (7) Min 3 Max 26
Requirements for *average* according to EN386	6 8 ≥11	Min. 90 Min. 72 Min. 45	Max 5

Discussion and concluding remarks

With the approach presented here it was possible to obtain laminated beams with strength corresponding to GL36h (according to EN 1194) and almost matching the MOE requirement (14360/14700=97,7%) of that same glulam grade. Using very simple visual grading rules and MOE-measurements based on axial excitation, it was possible to obtain a characteristic beam bending strength of 40,1 MPa.

In terms of shape stability (distortion of cross section and shape changes due to moisture variations) it was found that the influence of lamination lay-up is only of minor importance. In general, distortions (cup, twist, bow and crook) were very small. The interlaminar bond line strength, achieved with reasonable amounts of adhesive spread rate (200 g/m^2) and moderate clamping pressure (0,5-1,0 MPa) fulfil the requirements of the EN standards for glued laminated timber to be used in service class 2 (on average the strength requirements for service class 3 are also fulfilled). For some of the delamination tests series performed the requirements of the EN-standards were also fulfilled, but for other test series this was not the case. Since the specimens used in some of the delamination tests had been subjected to climatic changes already before the delamination test it is difficult to assess whether they would have passed the requirements if the tests had been performed

on specimens cut from "virgin" beams – which is assumed to be the case in the standard. However, for the only series performed with a normal adhesive spread rate and virgin material specimens, the requirements were fulfilled.

On-going research (see e.g. Sterley 2012) has shown that finger-joints made in the green state, show a good potential in terms of creating close-contact and homogeneous bonds with high strength. It is believed that including such finger-joints in combination with defect elimination in the laminations even better beam performance can be expected.

In order for the timber industry to be able to take full advantage of the green gluing technology in timber engineering applications, there is a need for standardisation and/or approval procedures. Today's EN standards do not include the possibility of producing e.g. CE-marked green glued laminated beams. A CUAP procedure for the type of product presented here is under development, with the aim of having this approved during 2013.

Acknowledgments This research was possible thanks to the financial support from The Knowledge foundation, Linnaeus University and CBBT (Centre for building and living with wood). The authors gratefully acknowledge this support.

Keywords: green gluing, glulam, bond line shear strength, durability, adhesive bonds

References

EN 386:2003. Glued laminated timber – Performance requirements and minimum production requirements.

EN 391:2003. Glued laminated timber – Delamination test of glue lines

EN 392:1995. Glued laminated timber – Shear test of glue lines.

EN 1194:1999. Glued laminated timber –Strength classes and determination of characteristic values.

EN 14080:2005. Timber structures – Glued laminated timber – Requirements.

EN 14358:2006. Timber structures – Calculation of characteristic 5-percentile values and acceptance criteria for a sample.

Anon. (2011). THE SWEDISH FOREST INDUSTRIES Facts and figures 2011. Swedish Forest Industry Federation . Available via http://www.forestindustries.se/. Accessed 14 May 2013.

Serrano, E, Blixt, J, Enquist, B, Källsner, B, Oscarsson, J, Petersson, H, Sterley, M. (2011). Wet glued laminated beams using side boards of Norway spruce, Linnaeus University, School of Engineering, Report No 5, ISBN: 978-91-86491-79-6

Serrano, E, Oscarsson, J, Enquist, B, Sterley, M, Petersson, H, Källsner, B (2010). Green-glued laminated beams – High performance and added value. In proc of World Conference on Timber Engineering, WCTE2010, Riva del Garda, Italy.

Steffen, A, Johansson, C-J and Wormuth, E-W. (1997). Study of the relationship between flatwise and edgewise moduli of elasticity of sawn timber as a means to improve mechanical strength grading technology. Holz als Roh und Werkstoff, 55:245–253.

Sterley, M, (2012). Characterisation of green-glued wood adhesive bonds. Dissertation, Linnaeus University press. ISBN: 978-91-86983-57-4.

VI

Improving Strength of Glulam Laminations of Norway Spruce Side Boards by Removal of Weak Sections Using Optimized Finger Jointing

Jan Oscarsson[1], Anders Olsson[2], and Bertil Enquist[2]

[1] SP Technical Research Institute of Sweden, Växjö, Sweden
jan.oscarsson@sp.se
[2] Linnæus University, Växjö, Sweden

Abstract. Recent research has shown that glulam laminations of Norway spruce side boards possess excellent structural properties. This investigation concerns the possibility of improving the performance of such laminations through elimination of weak board sections by means of finger jointing. Sections to be removed were identified using profiles of edgewise bending stiffness determined on the basis of scanned fibre angle fields on board surfaces. The difference in average tension strength and average tension stiffness, respectively, between a group of finger jointed boards and a reference group of non-jointed boards was evaluated. Joints were inserted in the first group with an average distance of 2.4 m. It was found that the finger jointing gave a considerable increase of strength (36 %), whereas the stiffness improvement was not as evident. Based upon the results, it can be assumed that application of finger jointed side board laminations will result in glulam beams with very high strength.

Keywords: Dot laser, finger jointing, glulam, scanning, side boards.

1 Introduction

Side boards, *i.e.* boards of narrow dimensions cut from the outer parts of a log, are in most cases regarded as products of poor profitability owing to low value and costly handling. Their main outlets are *e.g.* loading pallets and formwork timber. However, their structural properties are, in general, excellent (*e.g.* Steffen *et al.* 1997) which indicates that utilization of side boards as laminations in engineered wood products will result in load bearing components with high structural performance. As a consequence, considerable increase of board value could be expected.

Research concerning the application of Norway spruce (*Picea abies*) side boards as laminations in wet-glued glulam beams has been jointly conducted by the SP Technical Research Institute of Sweden, Linnæus University, and the

S. Aicher et al. (eds.), *Materials and Joints in Timber Structures*, RILEM Bookseries 9,
DOI: 10.1007/978-94-007-7811-5_71, © RILEM 2014

sawmilling company Södra Timber. The principal lay-up of investigated beams is shown in Fig. 1. After gluing (Fig. 1, left) the beams were split, dried and planed (Fig. 1, right) whereupon modulus of elasticity (MOE) and bending strength was determined on the basis of testing procedures laid down in the European Standard EN 408. In two initial test series, the beams were produced from ungraded side boards, but in a third series, the three outermost laminations at both beam edges were selected on the basis of strength grading criteria concerning maximum knot size and minimum global axial dynamic board MOE. The results were very promising (Serrano *et al.* 2011). High performance and low variability in terms of strength and stiffness was achieved, particularly for beams with graded boards.

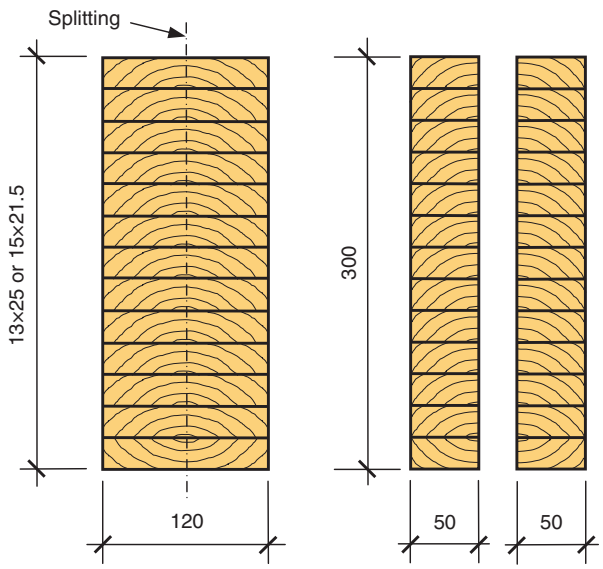

Fig. 1 Wet-glued beams before (left) and after (right) splitting, drying and planing

This paper concerns the possibility of improving structural properties of graded side board laminations even further by removal of weak sections using optimized finger jointing. Previous research (*e.g.* Hoffmeyer 1995) has shown that strong indicating properties (IPs) of strength can be defined on the basis of stiffness measures determined locally, at so called critical sections in timber pieces. According to EN 384, such a section is defined as the position at which failure is expected to occur. To what extent elimination of critical sections will contribute to increased strength and stiffness has been investigated by comparing the difference in average tension strength, average local static tension MOE, and average global axial dynamic MOE, respectively, between a group of finger jointed (FJ) boards and a reference group of non-jointed (NJ) boards. Sections to be removed has been identified on the basis of the relationship between strength and critical sections, the latter defined as local dips in edgewise bending MOE profiles determined

along the boards. The method applied for calculation of such profiles has recently been presented by Olsson *et al.* (2013).

2 Sampling of Material

A number of 51 side boards of nominal dimensions 25×125×4800 mm were sampled from a batch of 360 boards of sawfalling quality delivered from Södra Timber's sawmill in Torsås, Kalmar County. Before delivery, the boards were dried to a target moisture content (MC) of 16 %. The sampling was aimed at achieving a large variation of strength between sampled boards. Boards in which the amount of compression wood exceeded 10 % of the cross-sectional area were rejected. This requirement, evaluated on the basis of visual inspection, is in accordance with the acceptance criteria for strength classes C18 to C30 laid down in the Nordic visual strength grading rules INSTA 142. After ten months storage in a standard climate of 20 °C and 65 % relative humidity (RH), MC equilibrium had been reached. Each sampled board was then split longitudinally into two parts, one randomly assigned to the FJ board group and the remaining one to the NJ group.

3 Methods and Measurements

The laboratory work included determination of global axial dynamic MOE, laser scanning, finger jointing and static tensile loading. Board quantities and properties measured or determined were dimensions, weight, resonance frequency of the first axial mode of vibration, fibre direction fields determined on board surfaces on the basis of dot laser illumination and tracheid effect scanning, static tensile strength, and local static tensile MOE. In addition, the research also comprised application of beam theory, finite element modeling, and development and application of optimization algorithms for identification of critical sections to be removed by finger jointing. The software Matlab® was used for these purposes.

3.1 Global Axial Dynamic MOE

The global axial dynamic MOE, E_{dyn} [Pa], was determined for each split board as

$$E_{\mathrm{dyn}} = 4\,\rho\,(f_{1,\mathrm{a}}\,L)^2 \tag{1}$$

where ρ is the density [kg/m^3] calculated on the basis of measured weight and dimensions, $f_{\mathrm{a},1}$ is the axial resonance frequency [Hz] that corresponds to the first mode of vibration, and L is the board length [m]. The value of $f_{\mathrm{a},1}$ was measured using a Timber Grader MTG, which is a handheld wireless measuring device certified for commercial strength grading of structural timber.

3.2 *Fibre Direction Fields on Board Surfaces Based on Laser Scanning*

By application of the tracheid effect, fibre direction fields on both flat and edge surfaces of the split boards were measured using an optical scanner of make WoodEye, see Fig. 2 (left). The mentioned effect, resulting in laser dots entering an elliptic shape when they illuminate a board surface, is due to the fact that laser light is more easily spread in the fibre direction than in other directions, see Fig. 2 (middle). As a board is transported length-wise through the scanner, flat and edge surfaces are scanned simultaneously using four sets of laser sources and multisensor cameras. Each laser source provides a row of laser dots which is oriented perpendicular to the longitudinal board direction. The boards were fed through the scanner with a feed speed of about 60 m.p.s. In combination with the sampling frequency of the cameras, this resulted in a longitudinal scanning resolution of 1.2 mm. Corresponding resolution in lateral direction was 3.9 mm. The total number of fibre direction measurement points was approximately 180000 on each board. A typical fibre direction field scanned around a traversing face knot is shown in Fig. 2 (right).

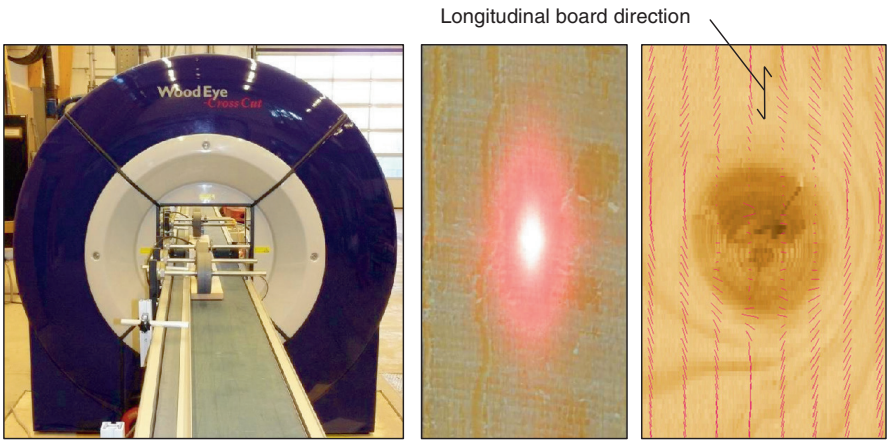

Fig. 2 WoodEye scanner (left), tracheid effect (middle), and scanned fibre direction field around a traversing face knot (right)

3.3 *Identification of Critical Board Sections*

As mentioned in the *Introduction*, edgewise bending MOE profiles were applied in order to identify critical board sections to be removed by means of finger jointing. A brief description of the procedures by which such profiles are determined follows below, whereas a more detailed account is found in Olsson *et al.* (2013). An important novelty is the application of fibre direction fields

described above. Such fields provide information about the angle φ between local fibre direction and lengthwise board direction, see Fig. 3 (left). Since wood is an orthotropic material with the highest structural performance in the longitudinal fibre direction, even small deviations between fibre direction and lengthwise board direction result in a considerable impairment of structural board properties.

Transformations taking material properties in different directions into account serve as a basis for calculation of local material stiffness in the board direction, which in turn provides data for integration of an MOE profile valid for edgewise bending. Important assumptions in the method are that

- the MOE in the longitudinal fibre direction, E_l, and density, ρ, are constant within a board,
- other stiffness parameters are linear functions of E_l,
- fibre directions measured on board surfaces are located in the longitudinal-tangential plane,
- the fibre direction coincide with the wood surface, *i.e.* the so called diving angle is set to zero, and
- the fibre direction measured on a surface is representative for the fibre direction to a certain depth within the board. Thus, the fibre angle φ shown in Fig. 3 (left) is assumed to be valid within the volume defined by the area dA (see Fig. 3 middle) times the length dx (see Fig. 3 left).

Thus, except from ρ, the only parameter that has to be determined individually for each board is E_l. This parameter is determined such that an eigen value analysis on a one dimensional finite element model of a board result in the same resonance frequency as the one determined experimentally.

According to Olsson *et al.* (2013), calculated MOE profiles can also be utilized for strength grading of structural timber. The IP for a certain board is defined as the lowest edgewise bending MOE found along its length. In the research referred to it was found that the relationship between this IP and strength was dependent on the local scale on which the IP was determined. It could be determined with a maximum resolution corresponding with the longitudinal scanning resolution of 1.2 mm, see Fig. 3 (left). However, since critical knots have a certain extension in this direction, it was found that the strongest relationship between IP and strength was obtained for IPs determined on the basis of MOE profiles representing a moving average MOE calculated over an interval of about half the board depth. Consequently, the research presented here was based on edgewise bending MOE profiles calculated over intervals of about 30 mm. The reason why bending profiles was applied, although the boards were loaded in axial direction, was due to the fact that an IP based on bending MOE correlates better to tensile strength than what an IP based on profiles representing axial MOE does (Oscarsson 2012).

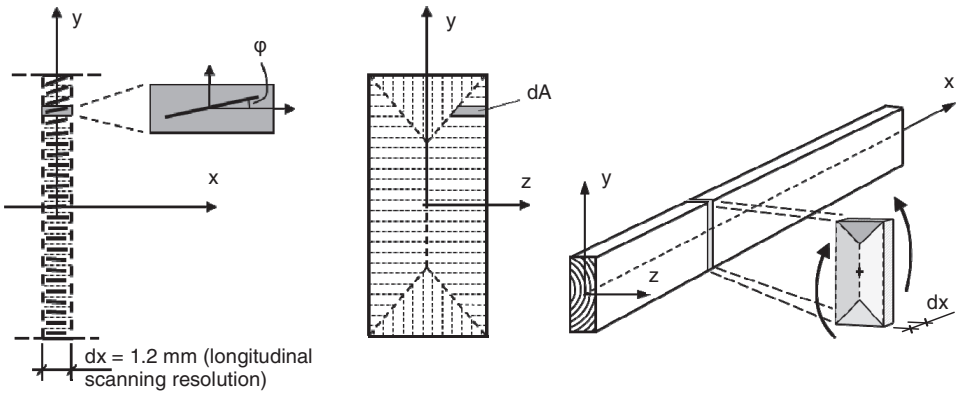

Fig. 3 Fibre directions measured on a board's flat surface (left), cross-section divided into sub-areas (middle) implying that the highlighted angle φ is valid within the volume given by $dA \times dx$, and board segment of length dx (right) the edgewise bending MOE of which is calculated by stiffness integration over the segment's volume

3.4 Critical Sections to Be Removed; Optimization Algorithms

Critical sections to be removed in the FJ boards were identified by means of algorithms designed to optimize the average tensile strength and stiffness, respectively, of the FJ group. It was assumed that the tensile strength is directly proportional to the lowest local bending MOE. As a result, the application of the algorithms resulted in different number of joints in different boards.

The benefit of finger jointing in terms of improved structural properties had to be put in relation to the costs incurred by such processing. This issue was discussed with representatives of Södra Timber resulting in a decision implying that joints were to be inserted with an average distance of 2.4 m over the total FJ board length of 245 m. Thus, a total number of 102 joints, *i.e.* on average two joints per FJ board, were to be inserted.

Elimination of a critical section meant that the length of the board in question was reduced with about 120 mm (see under heading *Finger jointing* below). Consequently, for those boards in which several joints were inserted, the length was considerably reduced. Since the strength of timber is dependent on the length of tested pieces (Isaksson 1999), it was necessary that all boards, both FJ- and NJ boards, were strength tested at the same length, determined by the FJ board with the largest number of inserted joints. For all other boards, cross cutting was necessary, although this implied that board information was lost. To confine such loss, the maximum number of joints inserted into a board was limited to six.

By means of the optimization algorithms, the six deepest dips in the MOE profile of each FJ board were identified as possible sections to be removed. Such dips coincided with significant knots. As an example, identified dips, denoted D1 to D6, in board no. FJ25 are shown in Fig. 4. For each FJ board, the IP improvement per section selected for possible removal was calculated. The equations applied for such calculations varied depending on the number of

sections assumed to be selected simultaneously. When only the deepest dip (D1) was considered, the potential IP improvement was calculated as the difference between the second deepest dip (D2) and D1. When the *two* deepest dips were considered simultaneously, the potential improvement per section was calculated as the difference between D3 and D1 divided by 2, *i.e.* (D3-D1)/2, and so on. Thus, when six sections were considered at the same time, the potential improvement per section was calculated as (D7-D1)/6. The described calculation procedure was carried out for each FJ board and all potential improvement values were subsequently assembled into a matrix the principle of which is exhibited in Table 1. Highlighted potential improvement values for board no. FJ25 show that the largest increase of the IP value of this board was achieved when five sections were selected at the same time.

It should be noted that MOE dips with a distance shorter than 200 mm was considered as one single dip, since the minimum length of pieces possible to joint in the applied finger jointing machine, see under heading *Finger jointing* below, was of this length.

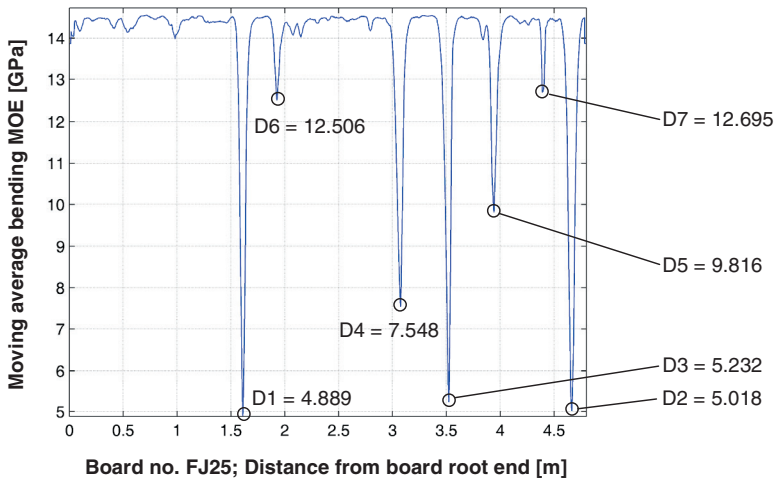

Fig. 4 MOE profile of board no. FJ25 and possible sections, defined by MOE dips D1-D6, to be removed

Table 1 IP improvement matrix for selection of sections to be removed by finger jointing

FJ board number	Potential IP improvement per selected section[1] [MPa]					
	1	2	3	4	5	6
01	D2-D1	(D3-D1)/2	(D4-D1)/3	(D5-D1)/4	(D6-D1)/5	(D7-D1)/6
:	:	:	:	:	:	:
25	129	172	886	1231	1523	1301
:	:	:	:	:	:	:
51	D2-D1	(D3-D1)/2	(D4-D1)/3	(D5-D1)/4	(D6-D1)/5	(D7-D1)/6

1. Figures 1-6 refer to the number of sections simultaneously selected for removal.

The selection of board sections to be actually removed was carried out using the matrix exhibited in Table 1 and the following algorithm loop:

1. The matrix element with the largest value was identified.
2. The section (or sections), *i.e.* the MOE dip (or dips), to which this element referred was selected for finger jointing.
3. The identified matrix element and possible elements in the same row to the left of this element were deleted.
4. Possible remaining elements in the same row were renumbered D1, D2, etc. and new IP improvement values were calculated accordingly.
5. Loop iteration.

The loop was reiterated until 102 sections were selected.

3.5 Finger Jointing

Finger jointing of the FJ boards was carried out using a compact jointing machine of make Ersson EKS 160, see Fig. 5 (left), with finger cutting tools of dimensions 15×3.8×0.42 mm according to EN 385. A melamine-formaldehyde adhesive, Casco Adhesives 1250, was used together with a hardener, Casco Adhesives 2550. This adhesive-hardener combination is approved for use in load-bearing structures in service classes 1, 2 and 3. The fingers were visible on the flat board surfaces and the applied nominal end pressure was 7.7 MPa.

The length of eliminated defect zones was determined on the basis of the length over which fibre directions were disturbed due to the presence of the defect, *i.e.* a knot or a cluster of knots. It was found that elimination of a board length of 120 mm, *i.e.* a length of about twice the board depth, was appropriate, although this meant that EN 385 requirements concerning distance between cross cut and removed knot were occasionally violated. In some cases, the eliminated length was increased due to requirements in EN 385 regarding distance between finger joint and adjacent knots.

Since the application of the optimization algorithms resulted in different number of joints in different boards, the length of the jointed FJ boards varied from 3885 mm to 4800 mm. As mentioned before, all boards (both FJ- and NJ boards) were then cross cut in the board's root end to 3885 mm length. After subsequent planing to cross-sectional dimensions 21×57 mm, tracheid effect scanning and determination of global axial dynamic MOE, respectively, was carried out once again.

3.6 Tension Testing

Tension strength and local static MOE, respectively, of both FJ- and NJ boards were determined in tension parallel to the grain in accordance with EN 408. The testing machine was of make MFL, see Fig. 5 (right), with a hydraulic force generation, 2.0 m length of stroke and a load cell with a capacity of 3.0 MN. The grips were of wedge type and the gripping length at actual testing was

estimated to 735 mm, which means that the board length between the grips was 2415 mm. The load was applied in force control mode with a constant loading rate of 8 kN/minute and the average time to failure was 283 seconds. Pairs of corresponding load-deformation values were sampled at a frequency of 2 Hz.

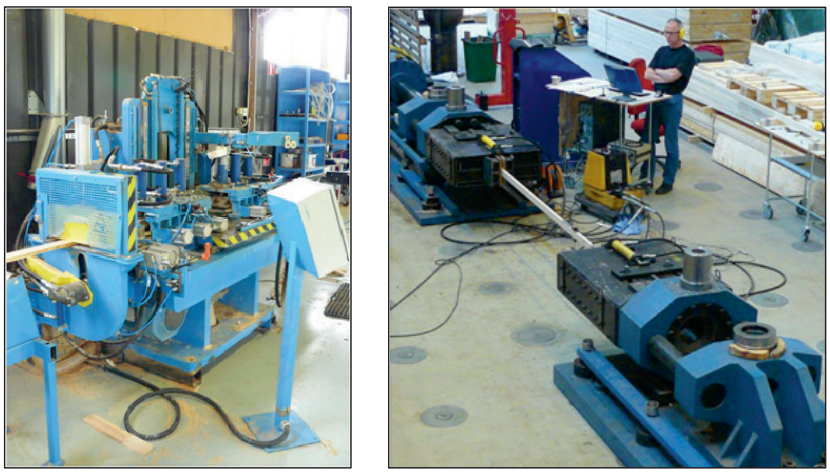

Fig. 5 Finger jointing machine Ersson EKS 160 (left), and tension testing machine MFL (right)

4 Results and Conclusions

Application of the optimization algorithms resulted in a large variation of the number of joints allocated to different boards. For example, nine boards were not allotted any joints at all, see example in Figure 6 (left), whereas two boards were given the maximum number of six joints each, see example in Figure 6 (right).

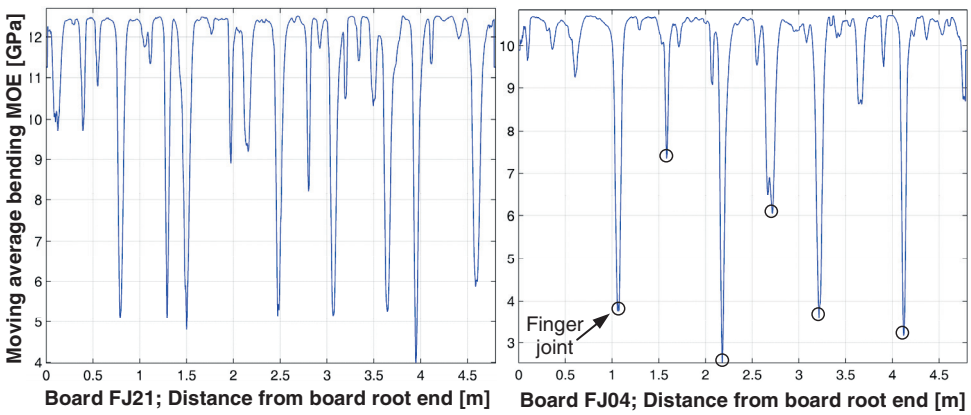

Fig. 6 MOE profiles; board with zero (left) and board with six sections to be jointed (right), respectively

The results from the tensile strength tests and from the determinations of global axial dynamic MOE, respectively, are presented in Table 2. By means of finger jointing, the mean tensile strength was increased from 24.2 MPa to 32.9 MPa, an improvement of no less than 36 %. The strength variation in terms of coefficient of variation was simultaneously reduced with 10 %, whereas the standard deviation was somewhat increased. The latter could not be considered as very surprising, given the considerable increase of strength achieved by the finger jointing. It was also observed that the number of boards with strength higher than 40 MPa was 12 in the FJ group, but only 4 in the reference group. As regards the MOE values, the finger jointing resulted in limited improvements of both mean value and spread.

It should be mentioned that the results from the tensile tests using the MFL machine were based on evaluation of 46 pairs of boards since 5 pairs had to be rejected due to tensile board failure within the grips of the machine.

The conclusions that can be drawn from the results are that finger jointing of narrow side boards based on dips in MOE profiles is an efficient means for increasing mean strength and reducing strength variation, whereas such treatment has a limited effect on the board stiffness in terms of MOE. Thus, to investigate to what extent the strength of laminated beams exhibited in Fig. 1 could be improved by finger jointing of outer laminations is a very interesting research issue to be probed into further. The larger number of boards with high strength (> 40 MPa) in the FJ group indicates that other optimization criteria than average strength of selected samples should be interesting to investigate thoroughly.

Table 2 Mean value, standard deviation (Std.) and coefficient of variation (CoV) for tension strength, local static tension MOE and global axial dynamic MOE for investigated boards

Board group	Tension strength			Loc. stat. tens. MOE			Glob. ax. dyn. MOE		
	Mean [MPa]	Std. [MPa]	CoV [%]	Mean [MPa]	Std. [MPa]	CoV [%]	Mean [MPa]	Std. [MPa]	CoV [%]
Non-jointed (NJ) boards	24.2	12.7	52.6	13674	2010	15.4	14240	2130	14.9
Jointed (FJ) boards	32.9	14.1	42.9	14520	2120	14.6	14710	2062	14.0

References

EN 384. Structural timber – Determination of characteristic values of mechanical properties and density. CEN (2010)

EN 385. Finger jointed structural timber – Performance requirements and minimum production requirements. CEN (2003)

EN 408. Timber structures – Structural timber and glued laminated timber – Determination of some physical and mechanical properties. CEN (2010)

INSTA 142 / SS230120. Nordic visual strength grading rules for timber. Inter-Nordic standardization, Swedish Standards Institute (2010) (in Swedish)

Hoffmeyer, P. (ed.): Strength grading adds value, Part 2 – Available technique. Technical University of Denmark, Technical Report 335-1995 (1995) (in Danish, Norwegian and Swedish)

Isaksson, T.: Modelling the variability of bending strength in structural timber – Length and load configuration effects. Doctoral thesis, Lund Institute of Technology, Report TVBK-1015, Lund, Sweden (1999)

Olsson, A., Oscarsson, J., Serrano, E., Källsner, B., Johansson, M., Enquist, B.: Prediction of timber bending strength and in-member cross-sectional stiffness variation on basis of local wood fibre orientation. European Journal of Wood and Wood Products 71(3), 319–333 (2013)

Oscarsson, J.: Strength grading of structural timber and EWP laminations of Norway spruce – Development potentials. Licentiate thesis, School of Eng., Linnæus University (2012)

Serrano, E., Blixt, J., Enquist, B., Källsner, B., Oscarsson, J., Petersson, H., Sterley, M., Petersson, H., Sterley, M. (ed.): Wet glued laminated beams using side boards of Norway spruce. Report No 5, School of Engineering, Linnæus University, Växjö, Sweden (2011)

Steffen, A., Johansson, C.-J., Wormuth, E.-W.: Study of the relationship between flatwise and edgewise moduli of elasticity of sawn timber as a means to improve mechanical strength grading technology. Holz als Roh- und Werkstoff 55, 245–253 (1997)

Linnaeus University Dissertations

Below please find a list of recent publications in the series Linnaeus University Dissertations. For a full list and more information: Lnu.se

120. Erik Rosell, 2013. *Entreprenörskap som kommunikativ handling – skapande av interaktion, uppmärksamhet och manifestationer* (företagsekonomi/business administration) ISBN: 978-91-87427-09-1.

121. Karl-Johan Persson, 2013. *Influence of cyanobacterial blooms on coastal fish recruitment* (akvatisk ekologi/aquatic ecology) ISBN: 978-91-87427-11-4.

122. Hongzhen Wang, 2013. *Studies on the expression of enzymes related to the artemisinin biosynthesis in Artemisia annua L.* (biokemi/biochemistry) ISBN: 978-91-87427-12-1.

123. Linda Fälth, 2013. *The use of interventions for promoting reading development among struggling readers* (pedagogik/education) ISBN: 978-91-87427-13-8.

124. Minh-Dao Duong-Thi, 2013. *Introducing weak affinity chromatography to drug discovery with focus on fragment screening* (biokemi/biochemistry) ISBN: 978-91-87427-14-5.

125. Einat Karpenstam, 2013. *Causes and consequences of niche differentiation between color morphs of pygmy grasshoppers* (biologi/biology) ISBN: 978-91-87427-15-2.

126. Judy Chow, 2013. *Vårdandets symfoni – fenomenet vårdrelation i skenet av två världsbilder* (vårdvetenskap/caring science) ISBN: 978-91-87427-17-6.

127. Nayani K. Vidyarathna, 2013. *Influence of Human-induced Environmental Changes on the Physiology of the Harmful Benthic Marine Microalga Ostreopsis ovata* (akvatisk ekologi/aquatic ecology) ISBN: 978-91-87427-19-0.

128. Anna Callenholm, 2013. *Erinnerte Erfahrung der Shoah in den Werken von Ruth Klüger und Cordelia Edvardson* (tyska/german) ISBN: 978-91-87427-20-6.

129. Chantal Albépart Ottesen, 2013. *L'auto-reformulation corrective : une stratégie dans la production orale de FLE* (franska/french) ISBN: 978-91-87427-21-3.

130. Hanna Palmér, 2013. *To become - or not to become - a primary school mathematics teacher. A study of novice teachers' professional identity development* (matematikdidaktik/mathematics education) ISBN: 978-91-87427-22-0.

131. Yvonne Kahlin, 2013. *Physical activity and self-related health in Swedish high school students* (vårdvetenskap/caring science) ISBN: 978-91-87427-23-7.

132. Elisabet Ekman, 2013. *Pharmacovigilance – spontaneous reporting in healthcare* (biomedicinsk vetenskap/biomedical sciences) ISBN: 978-91-87427-24-4.

133. Tobias Gutzmann, 2013. *Benchmarking Points-to Analysis* (datavetenskap/computer science) ISBN: 978-91-87427-25-1.

134. Malin Persson, 2013. *Characterization and optimization of the in vitro motility assay for fundamental studies of myosin II* (biomedicinsk vetenskap/biomedical sciences) ISBN: 978-91-87427-26-8.

135. Sawanya Laohaprapanon, 2013. *Wastewater generated by the wooden floor industry: Treatability investigation applying individual and coupled technologies* (miljövetenskap/environmental science) ISBN: 978-91-87427-28-2.

136. Birgitta Semark, 2013. *Patient characteristics, perceived health and drug prescription in primary care* (biomedicinsk vetenskap/biomedical sciences) ISBN: 978-91-87427-29-9.

137. Thomas Sandstedt, 2013. *Om rekrytering i akademin – exemplen prefekter och forskarstuderande* (pedagogik/education) ISBN: 978-91-87427-31-2.

138. Elinor Meiby, 2013. *Progress of Weak Affinity Chromatography as a Tool in Drug Development* (biomedicinsk vetenskap/biomedical sciences) ISBN: 978-91-87427-33-6.

139. Neelam Akram, 2013. *From genes to ecological function in marine bacteria* (mikrobiologi/microbiology) ISBN: 978-91-87427-34-3.

140. Ekaterina Yurova Axelsson, 2013. *P-adic dynamical systems and van der Put basis technique* (matematik/mathematics) ISBN: 978-91-87427-37-4.

141. Vahid Azimi Mousolou, 2013. *Quantum Holonomy for Many-Body Systems and Quantum Computation* (fysik/physics) ISBN: 978-91-87427-38-1.

142. Eva Kumar, 2013. *Removal of Inorganic Anionic Pollutants from Water Using Adsorption Technology* (miljövetenskap/environmental science) ISBN: 978-91-87427-39-8.

143. Miranda Kajtazi, 2013. *Assessing Escalation of Commitment as an Antecedent of Noncompliance with Information Security Policy* (informatik/informatics) ISBN: 978-91-87427-44-2.

144. Lasse Ten Siethoff, 2013. *Towards Myosin Powered Lab-on-a-chip Devices* (biomedicinsk vetenskap/biomedical sciences) ISBN: 978-91-87427-45-9.

145. Stina Alriksson, 2013. *Environmental preferences among steel stakeholders* (mijövetenskap/environmental science) ISBN: 978-91-87427-46-6.

146. Andreas Mångs, 2013. *Self-employment in Sweden: A gender perspective* (nationaleknomi/economics) ISBN: 978-91-87427-47-3.

147. Ulf Pettersson, 2013. *Textmedierade virtuella världar. Narration, perception och kognition* (litteraturvetenskap/comparative literature) ISBN: 978-91-87427-49-7.

148. Stefan Stenudd, 2013. *Colour Response in Drying of Nordic Hardwood* (skogsindustriella produktionssystem/forest industry production systems) ISBN: 978-91-87427-52-7.

149. Pernilla Söderberg, 2013. *Towards Novel Applications for Biomolecular Interactions at Surfaces.* (kemi/chemistry) ISBN: 978-91-87427-53-4.

150. Leteng Lin, 2013. *Char conversion kinetics and aerosol characterization in biomass gasification.* (/bioenergiteknik/bioenergy technology) ISBN: 978-91-87427-56-5.

151. Osama Mansour, 2013. *The Bureaucracy of Social Media – An Empirical Account in Organizations.* (informatik/informatics) ISBN: 978-91-87427-57-2.

152. Carl-Henrik Adolfsson, 2013. *Kunskapsfrågan - En läroplansteoretisk studie av den svenska gymnasieskolans reformer mellan 1960-talet och 2010-talet* (pedagogik/education) ISBN: 978-91-87427-59-6.

153. Kristina Schildmeijer, 2013. *Aspects of retrospective record review - A matter of patient safety* (vårdvetenskap/caring science) ISBN: 978-91-87427-60-2.

154. Angelika Thelin, 2013. *Åldersfattigdom: Ekonomisk utsatthet i yngre åldrespensionärers vardag* (socialt arbete/social work) ISBN: 978-91-87427-61-9.

155. Qiao-Yu Cui, 2013. *Fire history in the hemiboreal zone of southern Sweden during 11000 years: relationships with past vegetation composition and human activities and implications for biodiversity issues* (miljövetenskap/environmental science) ISBN: 978-91-87427-62-6.

156. Jan Berggren, 2013. *Engelskundervisning i gymnasieskolan för mobilisering av ungdomars livschanser* (pedagogik/education) ISBN: 978-91-87427-64-0.

157. Ann-Christin Karlsson, 2013. *Att vara vaken under operation i regional anestesi. Från patienters upplevelser till en vårdande modell* (vårdvetenskap/caring science) ISBN: 978-91-87427-65-7.

158. Camilla Mohlin, 2013. *Neural progenitor cell-derived neurotrophic support for the degenerating retina: an in vitro study* (biomedicinsk vetenskap/biomedical sciences) ISBN: 978-91-87427-67-1.

159. David Oersted Mirera, 2014. *Capture-based mud crab (Scylla serrata) aquaculture and artisanal fishery in East Africa* (biologi/biology) ISBN: 978-91-87427-70-1.

160. Muhammad Asim Ibrahim, 2014. *Risk of spontaneous fires at temporary storages sites for organic material, waste fuels and recyclables - Quantification and mitigation* (miljövetenskap/environmental sciences) ISBN: 978-91-87427-71-8.

161. Esther Mufunda 2014. *Diabetes Pandemic. The Influence of Beliefs about Health and Illness and Knowledge on Self-care Practices in Zimbabweans with Diabetes* (vårdvetenskap/caring science) ISBN: 978-91-87427-72-5.

162. Farvid, Seyed Mojtaba 2014. *Essays on Inventory Theory* (skog- och träteknik/forestry and wood technology) ISBN: 978-91-87427-76-3.

163. Bengtsson, Elina 2014. *Cooperativity in muscle proteins: a study of actin filaments and myosin II* (biomedicin/biomedical sciences) ISBN: 978-91-87427-77-0.

164. Hultqvist, Sara 2014. *Att göra aktivitetsersättning. Om målförskjutning och icke-kontakt vid förtidspension för unga* (socialt arbete/social work) ISBN: 978-91-87427-78-7.

165. Shoravi, Siamak 2014. *Towards Rational Molecularly Imprinted Polymer Design Using Molecular Dynamics-based Strategies* (kemi/chemistry) ISBN: 978-91-87427-79-4.

166. Truong, Nguyen Le 2014. *District heat production under different environmental and social cost scenarios* (byggteknik/building technology) ISBN: 978-91-87427-80-0.

167. Scaramuzzino, Gabriella 2014. *Sexsäljares och sexköpares kollektiva handlande på internet: En svensk "fuckförening"?* (socialt arbete/social work) ISBN: 978-91-87427-81-7.

168. Lundby, Erika 2014. *Consuming for friendship. Children's perceptions of relational consumption* (socialt arbete/social work) ISBN: 978-91-87427-82-4.

169. Griekspoor Berglund, Petra 2014. *Exploring the epidemiology and population structure of Campylobacter jejuni in humans, broilers and wild birds* (mikrobiologi/micro biology) ISBN: 978-91-87427-83-1.

170. Oscarsson, Jan 2014. *Strength grading of structural timber and EWP laminations of Norway spruce – development potentials and industrial applications* (byggteknik/building technology) ISBN: 978-91-87427-84-8.

Lnu.se
ISBN: 978-91-87427-84-8

Linnéuniversitetet